Department of Pharmacology

Vascularization of connective-lung tissues in Organ-on-Chip

Δημιουργία αιμοφόρων αγγείων σε συνδετικό ιστό σε πλατφόρμα «όργανο μέσα σε τσίπ»

ΔΙΔΑΚΤΟΡΙΚΗ ΔΙΑΤΡΙΒΗ

Antonio Varone

This thesis is presented for the degree of Doctor of Philosophy in Medicine

July 2021

ACKNOWLEDGMENTS

This dissertation would not have been possible without the help of several individuals who contributed to the preparation and completion of this study at the Department of Pharmacology School of Medicine, University of Crete, and the Institute of Molecular Biology and Biotechnology, Foundation of Research and Technology-Hellas (IMBB-FoRTH).

First and foremost, I want to express my deepest gratitude to my supervisors Professor Achilleas Gravanis and Professor Katia Catherine Karalis for the constant support and encouragement. They inspired me all these years and changed my way of thinking in both research and non-research areas. I am particularly thankful for their teaching and scientific inputs which helped me complete my studies. I acknowledge that most of my scientific achievements would not have been completed without their encouragement and support!

Yet, my sincere thanks go to the member of my supervising committee for their feedbacks and their valuable comments on my work.

I am very thankful to my dear friends and respected colleagues, Norman Wen, Sonalee Barthakur, Debora Petropolis, Lian Leng, David Conegliano, Sifis Pediadikatis and Tzeranis Dimitris for their support and patience all of these years as well as for co-operating and for the good times we had together. I really appreciate all your assistance.

More personally, I would like to extend my appreciation to my close friends, Riccardo Barrile and Magdalena Kasendra, Justin Nguyen and Carolina Lucchesi for their understanding and comedic relief, after a hard day and to handling my anxiety, disappointment and despairs during the fulfillment of my Ph.D., eventually, all of them turned to my very good friend in personal life.

I would also like to give my special thanks to Geraldine Hamilton and James Coon, whose help and support strengthened me at critical moments, which I will never forget.

Special thanks to my family who stood by me in a very unique way providing anything I needed from time to time, last but not least, I am truly grateful to my parents Romeo Varone and Raffaela Fasulo and my brother Ivano Varone who have always been supportive of my academic and professional goals and for standing by me through this experience and for their economical and moral support. All my efforts and choices were accompanied by their love and understanding, which made everything look easier.

You all supported me with everything you had. Either through nature or nurture, I could not have done this work without your support – Thank you!

Table of Abbreviation

2D: Two-dimensional
3D: Three-dimensional
AAT: Alpha-1 antitrypsin (deficiency)
ALI: Air-liquid interface
ATI: Alveolar type I
ATII: Alveolar type II
BME: Basement membrane extract
BSC: Biological safety cabinet
cAMP: Cyclic adenosine monophosphate
CD41: Cluster of differentiation 41 (Integrin alpha-2b)
CD133: Cluster of differentiation 133 (prominin-1)
COPD: Chronic obstructive pulmonary disease
DNA: Deoxyribonucleic acid
E-cad: Epithelial cadherin
ECM: Extracellular matrix
EIA: Enzyme immunoassay
ESC: Embryonic stem cell
ELISA: Enzyme-linked immunosorbent assay
FAK: Focal adhesion kinase
FBS: Fetal bovine serum
FCS: Fetal calf serum
FITC: Fluorescein isothiocyanate
hrEGF: Human recombinant epidermal growth factor
hrKGF (FGF-7): Human recombinant keratinocyte growth factor (fibroblast growth factor 7)
IBMX: 3-Isobutyl-1-methylxanthine
ICAM-1: Intercellular Adhesion Molecule 1 (CD54)
IL-6: Interleukin 6
IL-8: Interleukin 8
ILDs: Interstitial lung diseases
ISH: In situ hybridization
IPF: Idiopathic pulmonary fibrosis
iPS: Induced pluripotent stem cell
LPS: Lipopolysaccharides
LSEC: Liver sinusoidal endothelial cell
LDH: Lactate dehydrogenase
OOC: Organ-on-a-chip
MMP: Matrix metallopeptidases, also known as matrix metalloproteinase
NQO1: NAD(P)H Quinone Dehydrogenase 1
Nrf2: Nuclear factor erythroid 2–related factor 2
H3K9ac: histone H3 lysine 9 acetylation
Oct-4: octamer-binding transcription factor 4
PCTS: Precision-cut tissue explants
PECAM-1: Platelet endothelial cell adhesion molecule-1 (CD31)

ROS: Reactive oxygen species
SOX2: SRY-Box Transcription Factor 2
SRXN1: Sulfiredoxin 1
TGF-β1: Transforming growth factor beta 1
VALI: Ventilator-Associated lung injury
VE-Cad: Vascular endothelial cadherin
VWF: Von Willebrand Factor

Thesis overview

Cultures of primary human cells provide more ethical and potentially more effective alternative to animal models for drug testing. Recent studies also evidenced that culturing together two or more cell types in a three-dimensional (3D) microenvironment that mimicries the native tissue architecture improves cell viability, polarization, and differentiation in vitro. Among all 3D cell-culture models in vitro, the one known as Organ-on-a-Chip has recently gained momentum because it managed to promote levels of cellular differentiation and tissue organization not possible in conventional two-dimensional (2D) culture systems.

Dr. Dongeun Dan Huh, who is considered the inventor of Organ-on-a-Chip technology, demonstrated in his famous Science paper: "Reconstituting organ-level lung functions on a chip" that replicating organ architecture is necessary to restore its functions. Element such as delivery of oxygen, spatiotemporal gradients of nutrients, cellular components of the local microenvironment, geometry of the tissue-tissue interface (e.g. between epithelium and vascular endothelium), and mechanical forces acting on cells (e.g. mechanical stretch, air flow on the alveolar epithelium and fluid flow on endothelium) play a crucial role on cell behavior and on our capacity to restore their native functions.

Therefore, advancement in biomaterials and tissue engineering will be required to better replicate in a controlled microenvironment the specific aspects of human physiology and to advance the field of tissue engineering and regenerative medicine. Unfortunately, despite the level of sophistication achieved by Dr. Huh with his Lung-on-a-Chip, the model is still failing to reconstitute an essential element of the human living alveolar wall architecture, such as the stroma, which makes the Organ-on-a-Chip model of the lung not fully mature yet, but more a 2D culture on a three-dimensional (3D) artificial surface resembling the natural interface between the tissues that compose the lung.

In our efforts to address this limitation, we developed a more comprehensive 3D model of the alveolus by combining the advantages offered by Organ-on-a-Chip technology, we have just described, with the advantages offered by organotypic cultures, which are three-dimensional culture systems where cells are grown using scaffolds made of natural extracellular matrix (ECM) to preserve part of the stroma-epithelium architecture and most of the cellular interactions within the cultured organ. Specifically, by leveraging microfabrication technologies derived from the microchip industry, we manufactured a microfluidic chip that integrates the alveolus stroma with the physical component of the chip; it replicates most of the structural elements of the alveolar wall cross-section and recapitulates the mechanical forces normally acting on the alveolar microenvironments such as mechanical stretch and fluidic shear.

An in vitro model of the human alveolus that provides an adequate mimicry of the lung microenvironment could facilitate drug discovery and give new insight on lung disease mechanisms of chronic obstructive pulmonary disease (COPD), asthma, and idiopathic pulmonary fibrosis (IPF) or acute injury such as ventilator-associated lung injury (VALI) for which are not available comprehensive models. Most of the existing alveolus models lack the biological architecture, the cellular complexity and the microenvironment mechanical stimuli necessary to recapitulate the disease mechanisms.

Here, we describe the development of a tridimensional breathing human “Alveolus-Chip” that incorporates an interstitial compartment populated with lung fibroblasts lined with alveolar and microvascular pulmonary endothelial cells on opposite sides. The interstitial compartment provides structural and functional support to the alveolar epithelium and promotes maturation of tissue-specific markers. We show for the first time that primary human alveolar cells co-cultured together with primary human lung fibroblasts and microvascular endothelial cells, exposed to air and breathing motions, express tissue specific markers and secrete soluble surfactant proteins. Co-culture models that use human primary epithelial, mesenchymal and endothelial cells are particularly important in the contest of drug discovery and drug testing because drug metabolism is a species-specific process and failure in accurately recapitulating the biological, chemical and physical alveolar niche can easily results in cellular in vitro response non predictive of the in vivo response.

The Alveolus-Chip model was used to recapitulate some of the key aspects of acute and chronic lung injury caused by oxidative stress, including loss of air-liquid interface, release of pro-inflammatory cytokines, and formation of platelet clots. We demonstrate that vascular administration of therapeutic compounds targeting the Nrf2 pathway protect the Alveolus-Chip from oxidative stress acute injury and reduce inflammatory response. Our study provides a proof of principle of the validity of our biomimetic system by using an organ-chip that reconstitutes alveolar organ-level functions for modeling lung injury, and for testing anti-inflammatory compounds targeting the Nrf2 pathway.

Our approach based on better mimicking the native human organ microenvironment enhanced alveolar cell differentiation and partially restored the functions of the alveolus. The encouraging results obtained on Alveolus-Chip model, let us believe that this technology could help improving the functionality of other organ models, help replicating the systemic response of the human body by linking together multiple organ-chip models through an integrated microfluidic circulatory system to serve as replacements for animals in drug testing.

ΠΕΡΙΛΗΨΗ

Οι καλλιέργειες κυττάρων in vitro έχουν αποδειχθεί πολύτιμο εργαλείο για την προώθηση της κατανόησης της λειτουργείας και των βιολογικών μηχανισμών που διέπουν την κυτταρική συμπεριφορά in vivo και να αποκρυπτογραφήσουν τους μηχανισμούς που ενέχονται στην νόσο. Για παράδειγμα, οι διδιαστατες (2D) κυτταρικές καλλιέργειες έχουν χρησιμοποιηθεί στην ανακάλυψη φαρμάκων για τη μελέτη των κυτταρικών αποκρίσεων σε βιοφυσικές και βιοχημικές διεγέρσεις για πάνω από έναν αιώνα. Ωστόσο, παρά το γεγονός ότι είναι καλά αποδεκτά και έχουν συμβάλει σημαντικά στην προώθηση της κατανόησής μας για την κυτταρική βιολογία, αυξανόμενες ενδείξεις δείχνουν ότι η κυτταρική συμπεριφορά σε συστήματα 2D αποκλίνει σημαντικά από το in vivo και προβλέπουν τη φυσική κυτταρική απόκριση μόνο υπό συγκεκριμένες συνθήκες.

Λόγω αυτών των περιορισμών, έχει γίνει προσπάθεια διερεύνησης εναλλακτικών τρόπων καλλιέργειας και παρατήρησης των βιολογικών ιστών. Ωστόσο, η αναδημιουργία των συνθηκών για την μίμηση βιολογικών λειτουργιών σε επίπεδο οργάνου ή η αναπαραγωγή της φυσικής και παθοφυσιολογικής απόκρισης in vitro είναι δύσκολη, εν μέρει λόγω της περιορισμένης κατανόησης της πολυπλοκότητας του βιολογικού μικροπεριβάλλοντος και της συνολικής μικροαρχιτεκτονικής του ιστού, αλλά και λόγω της περιορισμένης ικανότητάς μας να αναπαράγουμε το συγκεκριμένο όργανο-ιστό ex vivo.

Ως αποτέλεσμα, χρησιμοποιούνται συνήθως τα ζωικά μοντέλα για την ανάλυση συστημικού επιπέδου σε μελέτες για τους μηχανισμούς της ανθρώπινης νόσου. Τα ζωικά μοντέλα έχουν συμβάλει σε σημαντικά ευρήματα και ανακαλύψεις στην κατανόηση των υποκείμενων μηχανισμών διαφόρων ασθενειών, ωστόσο η προγνωστική τους αξία είναι συχνά χαμηλή, οδηγώντας σε μεταφραστική στον άνθρωπο αποτυχία, εκτός από το ότι είναι κοστοβόρα και εγείρουν πολλά ζητήματα βιοηθικής Είναι πλέον γνωστό ότι περισσότερο από το 90% των φαρμάκων που εισέρχονται σε κλινικές δοκιμές αποτυγχάνουν, παρά τα θετικά αποτελέσματα σε προκλινικές δοκιμές σε πειραματοζώα. Η αποτυχία στην ανάπτυξη νέων θεραπευτικών έχει δείξει επανειλημμένα ότι τα ζωικά μοντέλα δεν μιμούνται με ακρίβεια τις ανθρώπινες φυσιολογικές αποκρίσεις ή δεν προβλέπουν με ακρίβεια την αποτελεσματικότητα και την τοξικότητα του φαρμάκου στον άνθρωπο λόγω των εγγενών βιολογικών διαφορών που υπάρχουν μεταξύ των διαφόρων ειδών σε γενετικό και ανατομικό επίπεδο.

Πρόσφατες μελέτες έδειξαν ότι η τρισδιάστατη βιομιμητική καλλιέργεια που προσομοιώνει το φυσικό κυτταρικό μικροπεριβάλλον μπορεί να πετύχει τα κύτταρα να συμπεριφέρονται φυσιολογικά και ως εκ τούτου να χρησιμοποιηθεί για τη βελτίωση της προκλινικής αποτελεσματικότητας και τοξικότητας των φαρμάκων καθώς και της δοκιμής αποτελεσματικότητας in vitro, προσφέροντας μια εναλλακτική λύση στη χρήση ζωικών μοντέλων.

Στοιχεία της φυσικής αρχιτεκτονικής μικροπεριβάλλοντος, συμπεριλαμβανομένων της κυτταρικής και διακυτταρικης σύνθεσης και τοπογραφίας του ιστού, η τριών διαστατική δομική γεωμετρία του καθώς και οι μηχανικές δυνάμεις όπως η διακυτταρικη τάση η κυτταρικη διάταση αντιπροσωπεύουν βασικά συστατικά για την προσομοίωση των φυσιολογικών και παθολογικών λειτουργιών των οργάνων. Τα τρισδιάστατα συστήματα κυτταροκαλλιέργειας που επιτρέπουν την προσομοίωση της in vivo πολυπλοκότητας θα μπορούσαν να γεφυρώσουν το χάσμα μεταξύ πειραματοζώων και ανθρώπων στις προκλινικές μελέτες. Μεταξύ όλων των μοντέλων in vitro οι 3D κυτταροκαλλιέργειας, που είναι γνωστές ως Organ-on-a-Chip κέρδισαν πρόσφατα δυναμική επειδή κατάφεραν να προσομοιάσουν τα επίπεδα της κυτταρικής διαφοροποίησης και της οργάνωσης των ιστών που δεν επιτυγχάνεται σε συμβατικά συστήματα δύο διαστάσεων (2D) ή τρισδιάστατων (3D) καλλιεργειών. Ο Δρ Dongeun Dan Huh, ο οποίος θεωρείται ο εφευρέτης της τεχνολογίας Organ-on-a-Chip, ανέφερε στη περίφημη δημοσίευση του: «Η ανασύσταση των λειτουργιών των πνευμόνων σε επίπεδο οργάνου σε ένα τσιπ» ότι η αναπαραγωγή της αρχιτεκτονικής των οργάνων είναι απαραίτητη για την προσομοίωση των λειτουργιών των ιστών. Στοιχεία όπως παροχή οξυγόνου, χωροχρονικές βιολογικές αποκρίσεις, τα θρεπτικά συστατικά, τα κυτταρικά συστατικά του τοπικού μικροπεριβάλλοντος, η γεωμετρία της διεπαφής μεταξύ των διαφόρων ιστών (π.χ. μεταξύ επιθηλίου και αγγειακού ενδοθηλίου) και οι μηχανικές δυνάμεις που δρουν στα κύτταρα (π.χ. μηχανικές ιστιδικης διάτασης, ροή αέρα στο κυψελιδικό επιθήλιο και ροή υγρού στο ενδοθήλιο) παίζουν καθοριστικό ρόλο στη συμπεριφορά των κυττάρων και στην ικανότητα να εκφράζουν τις φυσικές τους λειτουργίες.

Επομένως, απαιτείται πρόοδος στα βιοϋλικά και την μηχανική των ιστών για την ακριβέστερη προσομοίωση των ανθρωπίνων ιστών σε ένα ελεγχόμενο μικροπεριβάλλον συγκεκριμένων πτυχών της ανθρώπινης φυσιολογίας και για την προώθηση του τομέα της μηχανικής των ανθρωπίνων ιστών και της αναγεννητικής ιατρικής. Η προσομοίωση υγιών ή ασθενών πρωτογενών κυψελιδικών φυσιολογικών ανθρώπινων κυττάρων in vitro είναι πολύ περίπλοκη και υπήρξε ιστορικά ανεπιτυχής διότι τα πρωτογενή ανθρώπινα κυψελιδικά κύτταρα είναι πολύ ευαίσθητα στο μικροπεριβάλλον και δεν έχουμε γνώση σχετικά με τις συγκεκριμένες οδούς σηματοδότησης που συμβάλλουν κυρίως στην κυτταρική επιβίωση, διαφοροποίηση και ωρίμανση στο κυψελιδικό μικροπεριβάλλον. Μια κατάσταση που έχει εκ των πραγμάτων περιορίσει έντονα την ικανότητά μας να κατασκευάσουμε in vitro μοντέλα κυψελίδων στα οποία τα πρωτογενή ανθρώπινα κυψελιδικά κύτταρα διατηρούν φαινοτύπους διαφοροποιημένους για ενήλικες, κυτταρικές λειτουργίες και συνθέτουν πρωτεΐνη επιφανειοδραστικού παράγοντα C. Κατά συνέπεια, οι παραδοσιακές in vitro 2D και 3D κυψελιδικές μέθοδοι καλλιέργειας απέτυχαν πλήρως να αναπαραγάγουν τη δομική και λειτουργική φυσιογνωμία του φυσικού κυψελιδικού ιστού και κατέληξαν σε ένα υπερ-απλουστευμένο μοντέλο του ανθρώπινου πνεύμονα, όπου τα περισσότερα από τα βασικά στοιχεία του φυσικού περιβάλλοντος είναι απόντα.

Στις προσπάθειές μας να αντιμετωπίσουμε αυτόν τον περιορισμό, αναπτύξαμε μια πιο ολοκληρωμένη πλατφόρμα για την καλλιέργεια τρισδιάστατων μοντέλων ανθρώπινου επιθήλιου συνδυάζοντας τα πλεονεκτήματα που προσφέρει η τεχνολογία Organ-on-a-Chip με

πλεονεκτήματα που προσφέρονται από οργανοτυπικές καλλιέργειες, οι οποίες είναι τρισδιάστατα συστήματα καλλιέργειας όπου τα κύτταρα αναπτύσσονται χρησιμοποιώντας ικριώματα κατασκευασμένα από φυσική εξωκυτταρική μήτρα (ECM) για τη διατήρηση μέρους της αρχιτεκτονικής στρώματος-επιθηλίου και των περισσότερων κυτταρικών αλληλεπιδράσεων εντός του καλλιεργημένου οργάνου. Συγκεκριμένα, αξιοποιώντας τεχνολογίες μικροκατασκευής που προέρχονται από τη βιομηχανία των μικροτσίπ, κατασκευάσαμε ένα μικρορευστό τσιπ που ενσωματώνει μια υδρογέλη με το φυσικό συστατικό του τσιπ. Αναπαράγει τα περισσότερα από τα δομικά στοιχεία της διατομής του κυψελιδικού τοιχώματος και προσομοιώνει τις μηχανικές δυνάμεις που συνήθως δρουν στα κυψελιδικά μικροπεριβάλλοντα όπως μηχανική έκταση. Ένα in vitro μοντέλο του ανθρώπινου αναπνευστικού επιθηλίου που παρέχει επαρκή μίμηση του μικροπεριβάλλοντος του πνεύμονα θα μπορούσε να διευκολύνει την ανακάλυψη φαρμάκων και να δώσει νέα εικόνα σχετικά με τους μηχανισμούς της πνευμονικής νόσου της χρόνιας αποφρακτικής πνευμονικής νόσου (ΧΑΠ), του άσθματος και της ιδιοπαθούς πνευμονικής ίνωσης (IPF) ή οξύς τραυματισμός όπως πνευμονική βλάβη που σχετίζεται με αναπνευστήρα (VALI) για την οποία δεν υπάρχουν διαθέσιμα ολοκληρωμένα μοντέλα.

Τα περισσότερα από τα υπάρχοντα μοντέλα κυψελίδων δεν διαθέτουν τη βιολογική αρχιτεκτονική, την κυτταρική πολυπλοκότητα και τα μηχανικά ερεθίσματα του μικροπεριβάλλοντος που είναι απαραίτητα για την προσομοίωση των μηχανισμών της νόσου. Στην ερευνητική μας εργασία περιγράφουμε την ανάπτυξη ενός τρισδιάστατου ανθρώπινου αναπνευστικού «Alveolus-Chip» που ενσωματώνει ένα διάμεσο διαμέρισμα περιέχον

ινοβλάστες πνευμόνων επενδυμένους με επιθηκθακα πνευμονικά κύτταρα και μικροαγγειακά πνευμονικά ενδοθηλιακά κύτταρα. Το διάμεσο διαμέρισμα παρέχει δομική και λειτουργική υποστήριξη στο κυψελιδικό επιθήλιο και προάγει την ωρίμανση των ειδικών για τον ιστό βιοδείκτες. Δείχνουμε για πρώτη φορά ότι πρωτογενή ανθρώπινα κυψελιδικά κύτταρα συν-καλλιεργούμενα με πρωτογενείς ανθρώπινους πνευμονικούς ινοβλάστες και μικροαγγειακά ενδοθηλιακά κύτταρα, εκτεθειμένα σε κινήσεις αέρα και αναπνοής, εκφράζουν συγκεκριμένους βιοδείκτες του ιστού και εκκρίνουν τις σχετικές διαλυτές επιφανειοδραστικές πρωτεΐνες. Τα μοντέλα συν-καλλιέργειας που χρησιμοποιούν ανθρώπινα πρωτογενή επιθηλιακά, μεσεγχυματικά και ενδοθηλιακά κύτταρα είναι ιδιαίτερα σημαντικά στην προσπάθεια της ανακάλυψης φαρμάκων και της δοκιμής φαρμάκων, επειδή ο μεταβολισμός φαρμάκων είναι μια ειδική για κάθε είδος διαδικασία. Το μοντέλο Alveolus-Chip χρησιμοποιήθηκε για να προσομοιώσει μερικές από τις βασικές πτυχές της οξείας και χρόνιας πνευμονικής βλάβης που προκαλείται από οξειδωτικό στρες, συμπεριλαμβανομένης της απώλειας διεπαφής αέρα-υγρού, απελευθέρωση προφλεγμονωδών κυτοκινών και σχηματισμός θρόμβων αιμοπεταλίων. Δείχνουμε ότι η αγγειακή χορήγηση θεραπευτικών ενώσεων με στόχευση της οδού Nrf2 προστατεύει το Alveolus-Chip από οξείες βλάβες οξειδωτικού στρες και μειώνει τη φλεγμονώδη απόκριση. Η προσέγγισή μας βασίστηκε στην καλύτερη μίμηση του φυσικού μικροπεριβάλλοντος των ανθρώπινων πνευμονικών ιστών που υποστήριξε τη διαφοροποίηση των κυψελιδικών κυττάρων και εν μέρει τις λειτουργίες του κυψελίδας. Το μοντέλο Alveolus-Chip, θα μπορούσε να συμβάλει στη βελτίωση της λειτουργικότητας και άλλων μοντέλων οργάνων, να βοηθήσει στην προσομοίωση της συστημικής απόκρισης του ανθρώπινου

σώματος, συνδυάζοντας και συνδέοντας πολλαπλά μοντέλα τσιπ οργάνων μέσω ενός ολοκληρωμένου μικρορευστικού κυκλοφορικού συστήματος που θα χρησίμευε στο μέλλον στην αντικατάσταση των πειραματόζωων.

1. INTRODUCTION

Introduction

The traditional pharmaceutical research and the drug development process is burdened by high cost and lengthy process, not including the fact that systemic adverse effects that can only be identified later in the clinical trial such as lack of in vivo efficacy, poor pharmaceutical properties (e.g. low potency or unacceptable toxicity) and marketing reasons, prevent most of the therapeutics from reaching the market(Atkinson et al. 2007)(Seyhan 2019)(Atkinson et al. 2007).

Tufts Center for the Study of Drug Development published in the Journal of Health Economics that the average cost to gain market approval for new drugs in 2017 was about $2.6 billion with drug entering clinical development approved for marketing barely reaching 12 percent(Mohs and Greig 2017).

In one hand, the necessity for new drug discovery exists for many diseases or medical needs for which existing therapies are inadequate or completely absent (Regulatory Framework for Drugs for Rare Diseases - Rare Diseases and Orphan Products). Drug developers, due to ethical or economic reasons, are eagerly seeking new therapeutics for treating diseases for which no cure or better treatment exists, including neurodegenerative disease (i.e Alzheimer and Parkinson's disease(Bulck et al. 2019)), gastro intestinal syndromes (i.e. Chrohn or inflammatory bowel disease (IBD)), cancer, and (auto)immune disorders such as arthritis and psoriasis, or genetic diseases (i.e. multiple sclerosis, amyotrophic lateral sclerosis(Durães, Pinto, and Sousa 2018)). On other hand, they are often very skeptical about the fact that new findings reported in the scientific literature could be a target of interest for new drug discovery because existing pre-clinical 2D and 3D culture models often failed to predict human clinical responses or identify targets of clinical relevance in vivo(Hughes et al. 2011).

Current models still fail to fully recapitulate the human organ physiognomy in part due to the poorly understood complexity of the biological microenvironment and its overall architecture, in part due to our limited ability to replicate organ specific makeup and mechano-chemical signaling, which seem (or, at least, it is currently believed) to limit the cellular ability to replicate the natural physiological and pathophysiological response in vitro(Warrick, Murphy, and Beebe 2008). As a result, animal models are commonly used to perform systemic-level analysis in studies on human disease mechanisms. This practice, besides being expensive, has raised many ethical issues(Singh et al. 2016). Moreover, it has repeatedly been shown that animal models do not accurately predict human drug efficacy and toxicity(Shanks, Greek, and Greek 2009).

In the last decades, scientists came out with new methods for culturing tissues in an effort to enhance tissue viability and functionality in vitro, including precision cut tissue-slice(I. A. M. de Graaf, Groothuis, and Olinga 2007a), 3D culture organotypic culture, micro-patterned culture, organoids, various biomimetic microfluidic devices and bioreactors(Théry 2010)(Shanks, Greek, and Greek 2009). However, despite the fact that all of these options support increased tissue viability or improve marker expression and tissue functionality to some extent, only the biomimetic microfluidic device, called Organ-on-a-Chip(Huh 2015), exhaustingly addressed the matter of mechanical forces, which are known to directly affect cell behavior, including adhesion, migration, shape, proliferation, differentiation, intracellular signal transduction, and matrix turnover, in vivo(I. A. M. de Graaf, Groothuis, and Olinga 2007a) .

Before moving further into my studies, I believe it is important to contextualize where the Open-top Chip technology comes from to better understand where this technology stands at in the realm of 3D culture system. Therefore, I will make a brief digression on the evolution of in vitro biology taking a quick look at 2D culture, 3D culture such as precision-cut tissue explants, organotypic culture and organoids-spheroids, and microfluidic devices. In my opinion, those represent pivotal moments or major turning points in biology. A look to the past should assist the reader in putting in prospective the limitations and the potentials that each methodology has in replicating tissue functionality and help to better appreciate the work that has been done to overcome many disadvantages from previous models.

2D culture

Two-dimensional culture refers to a technique in which cells are removed from an organism (either animal or plant) by enzymatic or mechanical means and placed in an artificial environment favorable to their growth(Anton et al. 2015). Under proper conditions, cells proliferate, a process characterized by cell division (mitosis), or differentiate, a process during which cells change phenotype, and start expressing markers specific of the tissue or exhibiting functions analogous to those of the organ cells are derived from(Jedrzejczak-Silicka 2017).

The practice of culture cells was initiated in 1907 at Yale University laboratory by Ross Harrison who managed to remove nerves from frogs and maintain them in a salt solution for several days(Jedrzejczak-Silicka 2017). Few years later in 1915, Richard Goldschmidt, a visiting scientist at Harrison's laboratory, reported the successful attempt to culture spermatocytes from Cecropia moth in vitro. Goldschmidt was the first to recognize the utility of in vitro culture for the study of biology(Resh and Cardé 2009)(Jedrzejczak-Silicka 2017). However, insect cell cultures became very popular only when Thomas D. C. Grace managed to establish four cell lines from the Emperor Gum Moth, Antheraea eucalypti capable of continuous growth in vitro(Jedrzejczak-Silicka 2017). Those insect cell lines became very popular because they could be stored and sub-cultured and thank to these properties they became also widely used for studying the pathogenesis of viruses that have potential application as biological pest control agents(Resh and Cardé 2009). During this time, human cell culture method remained mostly limited to hanging drop and plasma clot explant fed by salt solution or animal extract in glass flask and Petri dishes(Jedrzejczak-Silicka 2017)(Resh and Cardé 2009).

In the mid-1950s, there was a great impulse to the development of in vitro human biology thanks to a series of breakthroughs such as the establishment of the mouse “L” cell-line (1943) and human “HeLa” cell-line (1951)(Bairoch 2018), as well as the successful large scale manufacturing of the inactivated poliovirus vaccine (IPV) at the Connaught Medical Research Laboratories in Toronto (April 1954) by the virologist Jonas Salk who managed to replicate the Polio virus in monkey kidney cell suspension cultured in vitro using one of the world’s first purely synthetic nutrient medium(Rutty 1996), the famous M199 medium, which was developed by the researcher Raymond Parker and biochemists Joseph Morgan and Helen Morton in the 1940(Bairoch 2018)(Rutty 1996). The success of M199 in culturing cell for producing vaccines greatly boosted investments into in vitro biology because it evidenced for the first time the great value that synthetic biology has for improving people lives, for enhancing the progress of humanity as well as the great potential it has as business activity(Rutty 1996).

At the time, most primary cells had difficulty to attach in culture, specifically on the glass substrates commonly used to culture them(Jedrzejczak-Silicka 2017). This apparently minor technical limitation impacted strongly on the widespread and adoption of in vitro technologies, until George Gey in 1956 figured out that coating glass surfaces with rat tail collagen dramatically improves cell attachment and growth(Bairoch 2018)(Rooke 2013). Glass surfaces for cultures (vessels, flasks, or Petri dishes) had also another critical disadvantage, specifically, they required tedious and cautious cleaning procedures to avoid contaminations of the cells with detergent residues. In response to the complication associated with handling culture on glass surfaces, researchers began experimenting the use of disposable plastics as culturing substrates(Satyada 2016)(Bairoch 2018). Among all the plastic materials tested, polystyrene became very popular because easy to mold, sterilizable by irradiation but most important because of its excellent optical clarity(Curtis et al. 1983)(Rooke 2013).

Despite its versatility, initially polystyrene had a significant weakness, specifically absence of functional groups, which reduced the capacity of cells to attach to it(Curtis et al. 1983). The problem of cell attachment was solved few years later when manufacturers introduced highly energetic gas ions process (corona discharge or gas-plasma under vacuum) to oxidize the polystyrene surface. These oxidative treatments introduced chemical functional groups (amine, carboxyl, hydroxyl, etc.) onto the polystyrene material surface dramatically improving cell attachment(Raey et al. 1984)(Curtis et al. 1983). This simple manufacturing improvement combined with the concomitant establishment of in vitro 2D culture methods for the clonal expansion and maintenance of primary epithelial cells by James Rheinwald and Howard Green (1975) had a huge impact on the worldwide spread of adherent cultures(Rheinwatd and Green 1975)(Raey et al. 1984)(Jedrzejczak-Silicka 2017).

Adherent cultures on artificial substrate, as polystyrene, immediately showed important limitations such as the loss of cellular differentiation and the appearance of alterations of the karyotype(Rheinwatd and Green 1975)(Jedrzejczak-Silicka 2017). Those anomalies were particularly dramatic in primary cells cultured in serum-free media. The appearance of an abnormal cell phenotype was lately correlated to the aberrant activation of focal adhesion kinase (FAK) pathways when cells attached to unnatural ligands(Schlaepfer, Hauck, and Sieg 1999). Anomalous FAK-mediated signal transduction causes abnormal cell division which ultimately induces aneuploidy or other genetic anomalies as well as abnormal gene encoding which severely alters cellular marker expression(Schlaepfer, Hauck, and Sieg 1999)(Schlaepfer, Hauck, and Sieg 1999). The issue of abnormal cellular phenotype induced by culturing cells on artificial substrates was partially overcome when studies on purified basement membrane extracts (BME) and native extracellular matrix (ECM) evidenced that the coating of artificial materials with biologically active proteins extracted from the tissues where cells were derived from, could partially restore the innate regenerative potential of those cells, improve cell survival and reestablish normal cell functions by regulating important aspects of cell behavior such as apical-basal polarization, proliferation and differentiation, as well as significantly improve both cell attachment and performance(Reid and Rojkind 1979). As a result of these studies, a variety of biological materials including collagens (type I and type IV), laminins and fibronectins, as well as heparin sulfate, hyaluronic acid, chondroitin sulfate and elastin emerged and were tested to better understand their roles in cell attachment, in cell migration and in the restoration of native cellular functions(Reid and Rojkind 1979) (Wong et al. 2019)(Edmondson et al. 2014).

Surface functionalization with natural ECM proteins greatly enhanced performance of 2D cultures, however, the lack of the third dimension impeded the full restoration of natural cell functions and

stimulated abnormal cell behaviors. The disturbance generated by the unnatural interactions among cells and extracellular matrix proteins in 2D results in anomalies of the cell morphology, polarity, proliferation rate, migration and often generate an abnormal response to drug and toxic compounds(Reid and Rojkind 1979)(Edmondson et al. 2014). Due to these limitations, it was clear that to create models more predictive of the in vivo response there was the necessity to replicate more accurately the conditions present in vivo in the natural organ microenvironment(Edmondson et al. 2014)(Rheinwatd and Green 1975)(Rijal and Li 2018).

In recent years, 3D cell cultures have received more and more attention from scientists, part due to the increased ethical concerns of the public opinion around the use of animals for drug testing and part because pre-clinical studies conducted on animal and 2D models have proven to be poorly predictive of the cellular response to drug and chemicals in humans(Edmondson et al. 2014)(Chaicharoenaudomrung, Kunhorm, and Noisa 2019). In addition, animal studies have been often criticized for their high cost, lack of reproducibility, labor-intensiveness, and lack of control over physiological parameters. All these factors gave rise to the exigence to develop 3D cultures more controllable and adapt for preclinical studies, which also ideally predict more accurately the human biological response, and fit the standards of scale and reproducibility(Chaicharoenaudomrung, Kunhorm, and Noisa 2019)(Rijal and Li 2018).

3D culture methods

3D culture refers to a series of primary human, cell lines or patient-derived cell culture techniques, which, as the name suggests, aim to reproduce in vitro a three-dimensional miniaturized version of the organ niche from which cells derive from(Langhans 2018)(Edmondson et al. 2014). Advances in the fields includes:

Precision-cut tissue explants

Precision-cut tissue slice (PCTS) is an ex vivo culture method used to study metabolism and toxicity effect of xenobiotics in organ slices which represent a miniaturized model of the organ they derive from(Nardini 2014). Thin slices in the range of 100 to 1000µm are commonly prepared from fresh tissue biopsies embedded in cylinders of agarose which are cut using a vibratome or a specially engineered tissue slicer(Y. Liu, Gill, and Huang 2017)(Y. Liu, Gill, and Huang 2017). In this type of culture, tissues viability varies greatly depending of the tissue and can range from about 24h for intestine specimens going up to 96 hours in the case of liver biopsy slices when incubated under very specific culturing conditions(R. O. N. De Graaf, Have, and Van Dorsselaer 2010)(Y. Liu, Gill, and Huang 2017).

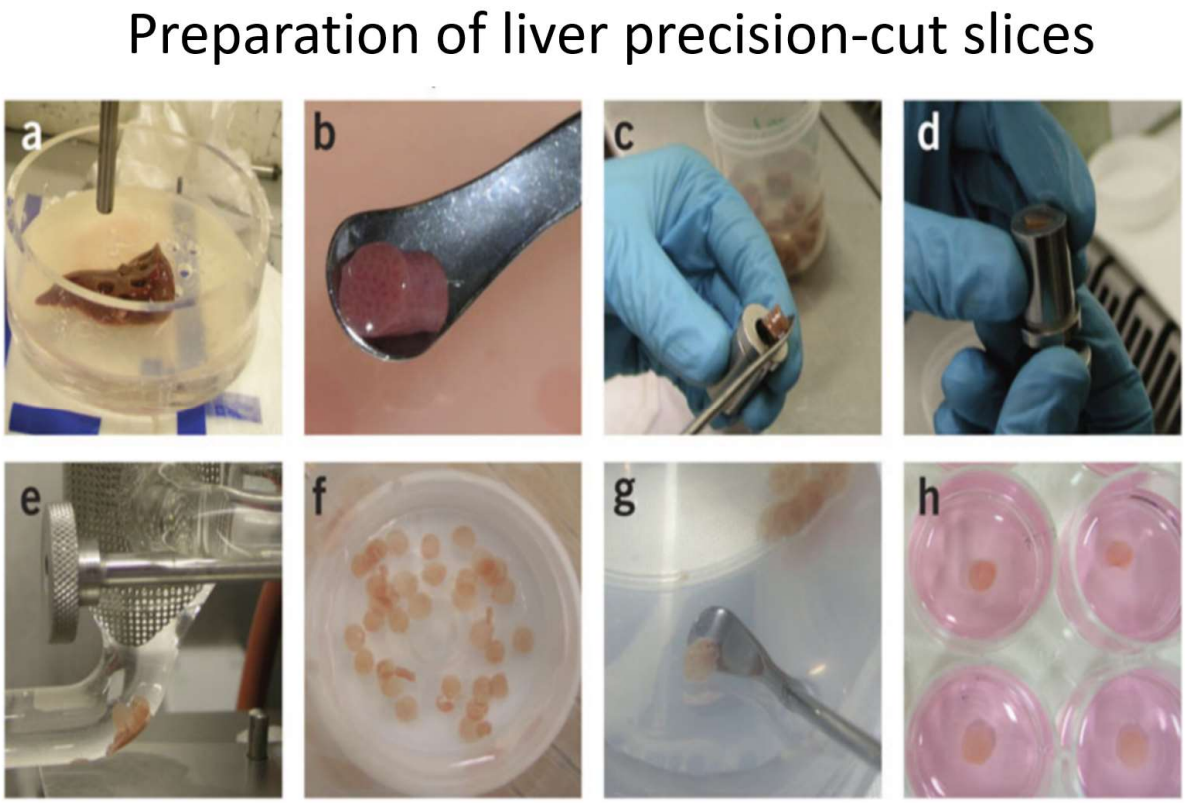

Image courtesy of Inge A M de Graaf et al., Nature Protocols 2010; (DOI: 10.1038/nprot.2010.111).

Figure 1.0: Preparation of liver precision-cut slices: photographs show zoomed images of (a) drilling with a hollow bit of liver specimen, (b) cylindrical liver core, (c) insertion of the cylindrical core liver into chamber unit, (d) adjustment of the slice into the chamber unit, (e) tissue slicer, (f) liver slices, (g) manipulation of liver slice and (h) static bioreactor culture of the liver slices.

This methodology can reproducibly yield tissue specimens which maintain the tissue structural integrity as well as cell populations with grade of differentiation, proliferative activity and phenotypes virtually identical to those in vivo(R. O. N. De Graaf, Have, and Van Dorsselaer 2010). More importantly, it preserves the phenotype (including morphology and marker expression) of the lymphocytes and macrophages infiltrates present in the tissue at the moment of explant, making it an accurate and precise "snapshot" of the organ at the moment of the explant. Since this ex vivo technique does not disrupt the three-dimensional architecture of the organ, it is anticipated that the interactions between the biological components are preserved, factor that makes this model highly desirable in the context of drug testing(Misra et al. 2019)(R. O. N. De Graaf, Have, and Van Dorsselaer 2010). At the least in theory, PCTS preserves also molecular heterogeneity, at both genomic and epigenomic level, eliminating the main cause of divergence between the results of cytotoxicity, efficacy, pharmacodynamic and pharmacokinetic studies. In such a prospective, ex vivo precision-cut tissue slices could provide a significant advantage when testing drug sensitivity of a patient's specimen and would represent a state-of-the-art tool for precision and personalized medicine(Poosti et al. 2015)(Misra et al. 2019).

Despite PCTS and similar patient-derived xenograft models offer, at least in principle, the interesting possibility to develop individualized drug treatment plans, they have important ethical and practical drawbacks that impede their applications or strongly dissuade their adoption into the pharmaceutical industry and in clinical trials(Pompili et al. 2016)(Poosti et al. 2015). First, biopsies sound scary, are generally painful and present risk for the patient(Overman et al. 2013)(Pompili et al. 2016), facts that strongly dissuade volunteers to undergo such procedure, second, human research biopsies are not always obtainable from patients for ethical (it is not correct to harm people to make profit) and healthy reasons (removing pieces of tissue, however small, creates damages to the organ that affect its normal functionality)(Petrini 2012)(Overman et al. 2013).

Therefore, even neglecting the ethical issues associated with PCTS and similar practices, the amount of tissue samples that could be collected from volunteers would be extremely limited for large scale applications(Petrini 2012). In the future, humanized animals could solve the limited supply of organ specimens and bring to the fore this practice, but again it would not completely solve the ethical issues because there will be the need to solve the atrocities committed against animals undergoing explant practice(Nardini 2014)(Petrini 2012). Moreover, processing organ specimens requires highly specialized personnel and is an expensive and time-consuming process. Considering the large number of humanized biopsy samples required for drug testing, PCTS would not be economically sustainable or compatible with any large-scale drug testing, at least, using the current technologies(I. A. M. de Graaf, Groothuis, and Olinga 2007b)(Poosti et al. 2015).

Practical problems also raise from the handling and analysis on these specimens because they represent a very complex microenvironment in which most of the biological elements are unknown(Compton et al. 2019). One critical aspect is the fact that PCTS provides inferior viability compared to primary human tissue cultures. Limited viability for ex vivo samples, in most case limited to only few days after explant, is mostly an unexplored field(I. A. M. de Graaf, Groothuis, and Olinga 2007b). Currently, the synthetic media used in the vary culture systems have been developed to support the viability and differentiation of only one or few cell types belonging to a specific biological niche. Because the specific metabolic requirements (nutrients, hormones and other biological factors) greatly differs between each cell-type belonging to the same organ, media currently available are ineffective in supporting the long-term viability of the complex microenvironment of the organ slices(Kanter et al. 2005)(I. A. M. de Graaf, Groothuis, and Olinga 2007b). At present, the impact of the media adopted in PCTS cultures on cell viability, grade of differentiation, proliferative activity and cell subpopulation selection inside the specimen remains mostly undetermined(Obatomi et al. 1998)(Kanter et al. 2005).

Furthermore, extracted specimens cannot be perfused despite they have vascularization because of the technical challenges and the complexity of connection required to link pre-existing vasculature vessels to a pump system(Schumacher et al. 2007). As consequence, slices are commonly cultured in static condition atop of a fluctuating raft or similar more specialized support (as for instance a well insert) and fed with medium by passive diffusion(Xia Wu et al. 2018)(I. A. M. de Graaf, Groothuis, and Olinga 2007b)(Schumacher et al. 2007). Typically, medium is provided from the bottom of the insert while oxygen is supplied by exposing the top part of the slice directly to air(I. A. M. de Graaf, Groothuis, and Olinga 2007b). Thin slicing is the ploy scientists have come out to maximize oxygenation and transport of nutrients which, as known, are processes diffusion limited (Xia Wu et al. 2018)(Obatomi et al. 1998). Mechanical damage and oxidative stress occurring during sample manipulation and culturing are also

important aspects to take in consideration when using this culturing system because they could affect cellular behavior and potentially their response to stimuli(Ruigrok et al. 2019)(Kanter et al. 2005).

In fact, oxidative stress produced by the direct exposure of the tissues to the oxygen present into the air and the mechanical slicing often trigger local inflammation and the release of pro-inflammatory cytokines inside the cut specimens(Ruigrok et al. 2019). The inflammatory condition promotes the opening of adherens junctions making the entire slice more permeable to the migration of leucocytes across the tissue and induces their activation which further acerbate the inflammatory pleiotropic effects, while oxidative stress can induce cellular dysfunction by oxidation of crucial cellular constituents such as proteins, lipids and DNA as well as the activation of oxidative stress response pathways(Ruigrok et al. 2019). The cumulative outcome of all these actions happening inside the tissue and their effects on the tissue slice response to drug and other compounds are not completely understood. The effects described are also sensitive to the surface to volume ratio making them much more evident in thinner slices(Mittal et al. 2014)(Ruigrok et al. 2019)(I. A. M. de Graaf, Groothuis, and Olinga 2007b).

Slice thickness and tissue local composition can also affect the ability to analyze the tissue slices. For instance, the differential diffusion rate between the tissue parts and the geometrical complexity of the natural tissue complicates the staining of slices, as in the case of antibodies that typically have difficulty to penetrate coriaceous areas of tissues, while differences in local tissue composition influence the direct observation of slices, as in the case of dense areas that typically tend to completely absorb or strongly scatter light, sometimes totally precluding the imaging of the tissue even when using contrast agents (fluorescent conjugated antibodies and other dyes)(Davies et al. 2015)(Obatomi et al. 1998)(Compton et al. 2019). Complications in the qualitative imaging can also affect quantitative analysis such as hybridization or enzyme immunoassays (EIA, qRNA, ISH, etc.) either directly by impeding delivery of the reagent to the area of investigation or indirectly because qualitative analyses lose most of their investigative value when the knowledge on the tissue composition is not available(Khan et al. 2019)(Davies et al. 2015). In fact, the lack of information on the cell-type and their relative ratio make it hard, if not impossible, to normalized values or track the origin of a particular cellular response (i.e. from what cell type a specific factor is released)(Lyons-Cohen et al. 2017)(Khan et al. 2019).

Organotypic culture

Technical advancement in basement membrane (BME) and extracellular matrices (ECM) extraction, and improvements in the understanding of the regenerative potential of these biomaterials led scientists to the development of hydrogels culture models which involves growing epithelial or parenchymal cells atop a stromal equivalent(Mano et al. 2007). It consists of live mesenchymal cells (mostly fibroblasts and smooth muscle cells) within a three-dimensional scaffold lattice made of natural occurring extracellular matrix polymers (as Collagen I) or synthetic man-made biocompatible polymers (as Polylactic acid) assembled into a hierarchical structure reminiscent of native tissues(Tibbitt and Anseth 2009). The third dimension provides a closer to in vivo biomimetic microenvironment allowing for ECM-cell and cell-cell interactions which regulate intracellular signaling and induce cellular behaviors resembling more closely those found in real tissues and organs(Geckil et al. 2010)(Tibbitt and Anseth 2009)(Mano et al. 2007).

Among the vary organotypic cultures, the three-dimensional organotypic culture of keratinocytes was particularly successful because of its ability to differentiate keratinocytes in a fully stratified epidermis

resembling those found in the native skin(Tsunenaga et al. 1994). In this model, keratinocytes are seeded atop a dermal equivalent, which typically consists of a collagen I hydrogel with embedded fibroblasts, proliferate until reaching confluence and differentiate in a multi-stratified epithelium when lifted to the air-liquid interface over approximately a two weeks period(Tsunenaga et al. 1994)(Anacker and Moody 2012). The entire biological system is fed by diffusion through the bottom of the dermal equivalent similar to in vivo (note: human epidermis does not contain nerves or vasculature, but nerve endings, capillaries, and lymphatic vessels are present below it, in the dermis)(Anacker and Moody 2012). It happened that the organotypic tissue culture of keratinocyte authentically recapitulates many aspects of the epidermal differentiation, to the point that was possible to replicate the human papillomavirus (HPV) life cycle and the dysplastic lesions induced in vivo by HPV (Varone et al. 2014). But most importantly, the possibility of differentiating keratinocytes in epidermis and to reproduce the squamous epithelium differentiation-dependent replication cycle of human papillomavirus in vitro was an important milestones for the study of biology and a proof of the principle that providing the right conditions to the cells, they can be induced to behave physiologically outside of the body environment(Levitt et al. 2011)(Kajitani et al. 2012). Such achievements have been interpreted as a demonstration of the validity of in vitro 3D culturing(Varone et al. 2014)(Kajitani et al. 2012).

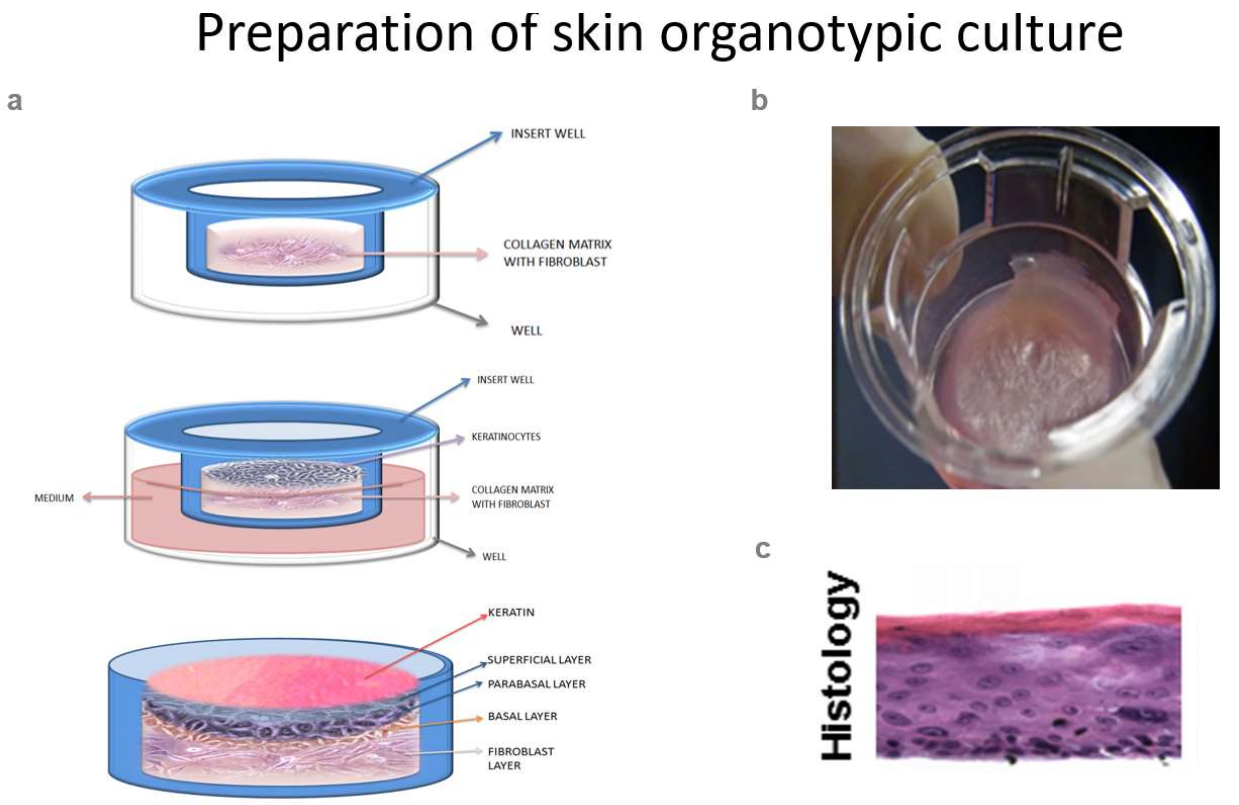

Image courtesy of Varone et al., Cancer research 2014; (DOI: 10.1158/0008-5472.CAN-13-2713).

Figure 1.1: Preparation of skin organotypic culture: (a) Schematic showing the preparation of the dermal layer inside the insert well (top draw), the keratinocyte layer seeded atop the dermal layer (meddle draw) and the full-thickness skin (bottom draw). (b) Picture of the skin differentiated using organotypic culture. (c) Histology of the epithermal layer showing the multi-stratified epithelium.

Nowadays, thanks to manufacturing progresses, technology improvements and commercialization of tools specifically engineered to simplify organotypic epithelial culture such as Transwell® support, organotypic raft epidermal culture has matured into a more general methodology which can be applied to other epithelial and parenchymal cells(Shamir and Ewald 2014). This more general method maintains substantially the original basic setup that involves the growth of cells on collagen plugs with embedded fibroblasts, but provides organ specific regime of medium, air-liquid or liquid-liquid interface. Over the course of several weeks (typically 2 to 4), the cells differentiate in a mature tissue that produces differentiation-specific markers(Salas et al. 2020)(Shamir and Ewald 2014). The recreated tissue can be examined histologically, as well as by standard molecular and biochemical techniques(Shamir and Ewald 2014).

Although organotypic cultures have proven themselves powerful research tools for studying human organs, especially skin, it is important to be aware of their limitations. The biological models engineered using organotypic modelling recapitulate only partially the native organ organization and its functions, because the microanatomy of the organ is simpler than that of native tissue(Rhim and Rustgi 2015)(Shamir and Ewald 2014). In fact, the organotypic models generally contain only a limited variety of the cell types normally present in the native organ niche and lack signaling and feedback mechanism normally coming from a variety of biological systems such as nervous system, immune system, circulatory system, which are typically intimately interconnected in the real organs(Langhans 2018)(Y. Fang and Eglen 2017). For instance, these simplified models cannot replicate the full complexity of the inflammatory response when performing a wound healing assay because they miss the immune system cells. Another limitation of organotypic tissue often restricting the application of this culture method is the requirement for primary cell sources, which is particularly penalizing in model of disease where the donors are scarcely available. Scarce availability of tissue makes these models not a good candidate for drug testing because they do not support large scale application(Rhim and Rustgi 2015)(Langhans 2018)(Shamir and Ewald 2014).

Additionally, culture media used when performing experiment can dramatically affect the behavior of cultured cells and consequently the response of the organotypic system to the stimuli. For instance, not characterized biologically active compounds used in organotypic culture media, such as fetal bovine serum, can interfere with the reproducibility of the experiment outcomes(Zheng et al. 2008). Often cultures undergo special feeding regime before treatment, such as serum starvation, which can acerbate or mitigate the effect of drugs when compared to the control(Cooper and Gonzalez-Hernandez 2009). Defined serum-free culture medium should be always the choice, but unfortunately, they are rarely available for organotypic systems because of the incompatible feeding requirements necessary to support the viability of the different cells used in the system(M. Arora 2013). For instance, fibroblasts and smooth muscle cells, which are often used in the stromal layer, require relatively high concentration of serum (up to 10% V/V with medium) to grow, while many epithelial cells tend to abnormally grow or differentiate when exposed to serum(Cooper and Gonzalez-Hernandez 2009). Cell-medium incompatibility can limit severely the usage of organotypic models, in other cases, it requires the acceptance of compromise between having a better differentiated epithelium than the stroma and the endothelium, or vice versa(Goers, Freemont, and Polizzi 2014). Organotypic cultures have also been criticized for their limited capacity to sustain cell growth and differentiation for long-time before undergoing involution or dead, a clear indication that they don't manage to recapitulate most of the cell turn-over mechanisms, which raise doubts on the real capacity of these systems to recapitulate the normal in vivo physiology(Oh et al. 2013)(Zheng et al. 2008)(Y. Fang and Eglen 2017).

Despite 3D organotypic cultures based on synthetically or naturally-derived polymers have proved to be capable to recreate more physiological relevant micro-environment than 2D cultures, they are still not able to replace them on large scale due to several limitations such as complexity in sample handling (scalability, reproducibility, complex protocol), high cost, and their low compatibility with high-throughput screening instruments(Nam et al. 2015)(Goers, Freemont, and Polizzi 2014). To obviate at some of these limitations, a modern variant of the organotypic culture has recently emerged promising to be more scalable, such technology is known as organoids or spheroids.

Organoids & Spheroids

Organoid 3D cultures are an in vitro model derived from a single embryonic or induced adult stem cell and commonly described as miniaturized or simplified versions of an organ because they display a very accurate microanatomy(Kretzschmar and Clevers 2016). Organoids have been established for many organs from primary biopsy explants, including small and large intestine, lung, liver, stomach, kidney, and retina or generated from induced pluripotent stem cells (iPSCs) that have been reprogrammed into an embryonic-like pluripotent state and then differentiated into a mature organ, such as skin or brain(Kretzschmar and Clevers 2016). These types of cultures exploit the innate ability of cell to self-renew, self-repair and the endogenous capacity of self-organizing themselves in complex structures when supplemented with cocktails of organ-specific growth factors(Kretzschmar and Clevers 2016)(Kretzschmar and Clevers 2016).

The ability to manipulate stem cell niche with growth factors was first achieved in 2009 at Clevers lab, where the intestinal tissue-specific factors for stimulating Wnt 3A, R-spondin, Noggin and gastrin pathways were first identified and classified(Sato et al. 2009). In the same year, it was also demonstrated that using these factors (Wnt 3A, R-spondin, Noggin and gastrin) was possible to stimulate single Lgr5(+) intestinal stem cells to self-organize into crypt-like structures in vitro(Sato et al. 2009)(Kretzschmar and Clevers 2016). This culture method based on stimulating intrinsic tissue-specific pathways using growth and differentiation factor analogs became what is currently described as organoids (note: with time the original organoid protocol became more and more sophisticated and specific for the vary organs to which it was used for, but the principles used to develop other protocols, as well as most of the factors used remained practically the same)(Sato et al. 2009)(Nakamura and Sato 2018).

Organoid systems also rely on extrinsic biochemical signals to control the stem cell fate. Extrinsic elements refer mainly to basement membrane proteins, such as collagens, laminins and heparan sulfate proteoglycans, and to growth factors, such as bFGF and EGF, ALK inhibitor such as A-83-01 or other essential supplements such as vitamins A, E, and linolenic acid(Nakamura and Sato 2018)(Sato et al. 2009). Basement membrane proteins are essential components of the system because they provide physical support for cell attachment and additional signaling via basement membrane ligands for survival and differentiation during the organoid culturing(Murrow, Weber, and Gartner 2017)(Kaushik, Ponnusamy, and Batra 2018). As mentioned, both the intrinsic and extrinsic biochemical cues of the stem cell niche control the self-renewal, differentiation or assist self-organization of stem cells(Sato et al. 2009).

Because stem cells, either embryonic or induced, used in the organoid systems are highly dependent on autonomous cellular self-organization (Lancaster and Knoblich 2014a) and are based on intrinsic mechanisms not fully understood or easily controllable(Lancaster and Knoblich 2014b)(Sato et al. 2009). Often, a heterogeneous mix of progenitor, partially differentiated and terminally differentiated cell types are present in these systems creating substantial problems in data interpretation and experiment reproducibility(K. G. Chen et al. 2014). To obviate to lack of complete terminal differentiation and to limit the problems associated with a biological system containing cells with intermediate phenotypes of unknown origin (either deriving from stem cell differentiating at different time or deriving from transdifferentiating cells expressing mixed markers from different maturation stages), a modified culturing system based on the original "organoid" concept emerged, the spheroids, which are three-dimensional organotypic cultures generated by combining terminally differentiated cells (cell lines, primary cells or fragments of human tissue) deriving from different lineages and stimulating this mixture of cells to self-aggregate into budding sphere-shaped structures (from which the name spheroid)(K. G. Chen et al. 2014). The spheroid aggregates contain layers of cells self-organized into a complex micro-architecture that replicates the tissue-tissue interface interactions, the structural properties and the essential functions of the tissue cells are derived from on a microscopic scale (therefore, are considered a organotypic miniaturized versions of tissues)(Granato et al. 2017)(Maritan, Lian, and Mulligan 2017).

Cellular organization in spheroid culture

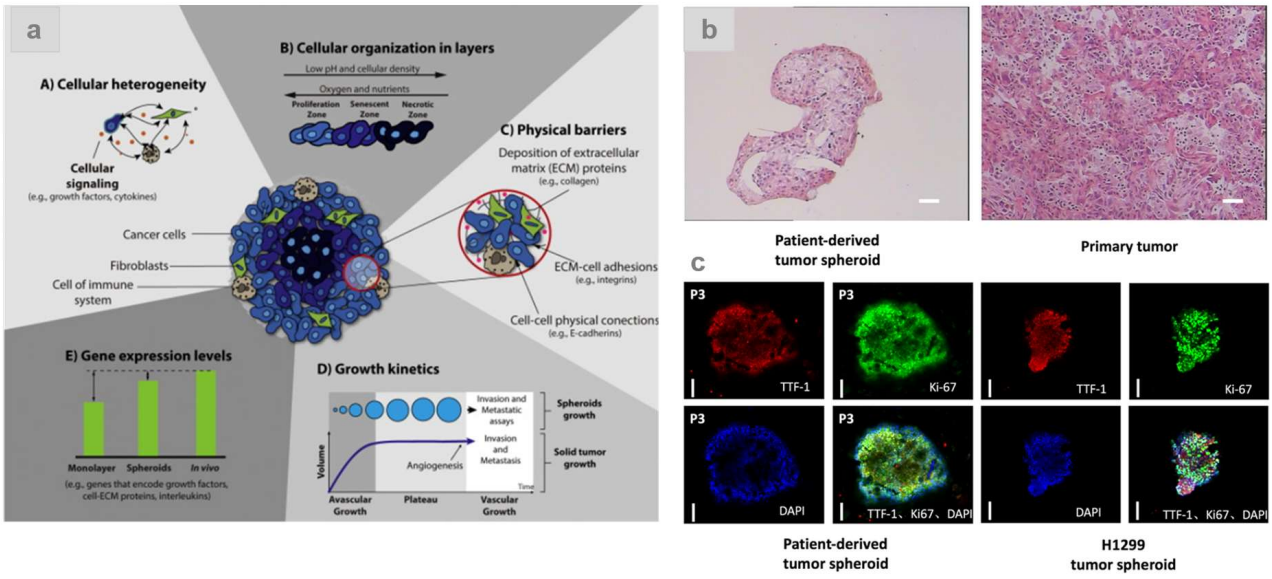

Image courtesy of Elisabete C.Costa et al., Biotechnology Advances 2016; (DOI: 10.1016/j.biotechadv.2016.11.002).
Image courtesy of Zengli Zhanget al., PloS One 2016; (DOI: 10.1371/journal.pone.0194016).

Figure 1.3: Cellular organization in spheroid culture: (a) Schematic showing the spheroid cellular organization, heterogeneity, and culture development, (b) Histology slides comparing morphology of patient-derived tumor spheroid versus primary tumor. (c) Immuno-fluorescence images comparing cellular organization of a patient-derived lung tumor spheroid versus the organization of a tumor-spheroid derived from human non-small cell lung carcinoma cell line.

Typically, tissue biopsies are dissected, and cells isolated from the tissue are engineered to form spherical aggregates (or spheroids) that imitate the architecture of the parental tissue. Spheroid models are cultured in 3D within a matrix or in suspension to properly reproduce stimuli from the local environment, as in vivo(Jeppesen et al. 2017)(Granato et al. 2017). Under the recreated three-dimensional microenvironment, the morphology and polarity of the cells can be maintained or improved as in the case of human bronchial acinar-like spheroids. In this model, which is an imitation of glandular acini of the bronchi, was observed the formation of an hollow lumen in which cells displayed a typical glandular apicobasal polarization with basal markers expressed at the external edge of the spheroid structure, the part that interacts with the ECM, and the apical markers located in the part of epithelium facing the lumen(Xiaofang Wu et al. 2011). The formation of the central lumen is the result of cell apoptosis occurring in the internal section of the spheroids, and the preferential cell proliferation at the edge of the structure. Inside the spherical structures, growth, gene expression, signaling and metabolism of cells strongly depends on the topological location of cells similarity to what is observed in glandular cell growing in vivo(Xiaofang Wu et al. 2011)(Granato et al. 2017)(Jeppesen et al. 2017).

Apart from using spheroids in glandular models, spheroids are often applied in cancer studies. Cancer cells isolated from patient biopsy can be encapsulated into ECM hydrogel (or other scaffolds) to replicate the specific cancer and generate multiple copies of it, which are useful to study carcinogenesis, tumor invasion and metastasis, as well as tumor mass drug resistance or response of the tumor mass to irradiation(Y. Li and Kumacheva 2018). Suspension of spheroids are widely used as a model for cancer because primary tumor and cancer spheroids are relatively easy to establish, simple to maintain and low cost(Kunz-Schughart et al. 2004)(Y. Li and Kumacheva 2018). The method also preserve the original cancer phenotype characterized by natural loss of adherence-junction, overexpression of putative stem cell genes such as Sox2, Oct4 and Nanog, and cancer proteins such as CD133 and ALDH which typically occurs in tumor-initiating cells (TICs), also known as cancer stem cells (CSCs)(A. Liu, Yu, and Liu 2013). Cancer spheroids cultured in medium under non-adhesive conditions also display loss of anchorage-dependent proliferation and a great number of cells escape from anoikis managing to divide and create spheres in a process useful to study metastasis formation and the metastatic process(Al Habyan et al. 2018)(J. L. Chen et al. 2017). Similarly, cancer spheres embedded into Matrigel® have been widely used to study the process of cancer invasion and angiogenesis(Al Habyan et al. 2018). Authors also reported that, under 3D conditions, spheroids can express morphological, physiological and enzymatic characteristics of migrating cancer cells including the presence of invadopodia, and the secretion of high level of metallo-proteinase (MMP1, 2, 3, 7, 9, 13, and 14), fibronectin or collagen I and epithelial-mesenchymal transition with loss of epithelial markers(Al Habyan et al. 2018).

Tumor spheroids are often used in suspension or soft-hydrogel cultures not only to evaluate the role of cancer specific genes in self-renewal and maintenance of tumor stemness, but also because they replicate tumor sensitivity to drugs much more accurately than 2D cultures(Nath and Devi 2016). It has been reported that spheroids have the capacity to replicate drug response comparable to that observed in solid tumor of comparable size. Such characteristic seems to be related to the geometry of the spheroids which limits the contact area to drug compounds (small surface area to volume ratio) and to the physio-pathological differences in cell metabolism generated by the hypoxia in the internal region of the spheroid aggregates(Brüningk et al. 2020)(Nath and Devi 2016). Structure and geometry of spheroids also seems to play a critical role in the response of the cancer spheroids to irradiation(Brüningk et al. 2020). An

increased radiation survival is in part due to the physical 3D architecture of spheroid because external cell layers absorb radiation preserving the inner layers from being destroyed, and in part to the layer epigenetic differences in histone H3 lysine 9 acetylation (H3K9ac) which influences DNA acetylation and heterochromatinization in the different layers of the spheroids. Higher levels of heterochromatin, a structure where the DNA is tightly packed around histone proteins, protect the DNA against radiations(Storch et al. 2010)(Kapałczyńska et al. 2018). Similarly, cell density and cell extracellular matrix interactions, as reported by Hsieh and colleagues, also seems to play a critical role in the tumor behavior by significantly influencing cellular metabolic activity, cell proliferation and, ultimately, changing cell sensitivity to drug(Chia-Hsun Hsieh, 2015)(Kapałczyńska et al. 2018). For instance, Donglai and colleagues have reported that spheroids growth on three-dimensional silk scaffolds mimicking the fiber orientation and dimensions of native tumor become less sensitive to paclitaxel(Donglai et al. 2017).

Organoids and spheroids are becoming very popular in many applications especially disease modeling and regenerative medicine. Their growing relevance in various fields of research has earned the award of "Method of the Year 2017"(Method of the Year 2017: Organoids 2018). Organoids and spheroids are considered an upgrade from the traditional monolayer primary cultures because they offer the opportunity to study complex biology (self-renewal and tissue damage repair mechanisms) in a more physiologically relevant context than 2D models, which are often non effective in reproducing 3D human biology(Yin et al. 2016). Furthermore, they are relatively easy to grow and are scalable, therefore fitting the current drug screening protocols as well as they have produced impressive biological results, at least, in studies involving glandular tissue where they achieved superior morphology and function mimicking(Kapałczyńska et al. 2018)(Yin et al. 2016).

The great biological value of organoid and spheroid systems reflects also in the increased demand of these types of 3D cultures on the market. However, although spheroids and organoids are now widely used, they are still poorly validated models(Kondo and Inoue 2019)(Kapałczyńska et al. 2018). Some of the critical points that are still required to be addressed are the effects that basement membrane proteins and the cocktail of hormones used to feed them have on cellular behavior and development, if and how ECM and hormones support natural cellular differentiation or if they reprograms cellular growth toward pre-determined pathways(Yan et al. 2019). Furthermore, it is poorly understood if cells seeded into these types of cultures get selected or reflect the cellular heterogeneity of the patient they are extracted from(Kondo and Inoue 2019)(Yan et al. 2019).

It is often emphasized that one critical disadvantage of the spheroid and organoid culture resides in the fact that aggregates are not from a single cell type, but rather a cluster of cells of different origin and metabolic activity(Yan et al. 2019)(Kapałczyńska et al. 2018). Since the topographic position of the cells inside the aggregate strongly affect their metabolism and phenotype often single cell analysis is required to extract interpretable information from the aggregates. The processing can require the disaggregation of the cellular components by proteolytic degradation and their separation by sorting, which takes time and costly specialized treatments and equipment. Many extraction methods have low efficiency and low repeatability(Xiao, Dai, and Locasale 2019)(Yan et al. 2019). Since organoids and spheroids are not homogeneous structure and are built from cells of various phenotypes and their morphology and polarity of the cells are strongly influenced by stimuli from the local environment, often each volume of cell contain a gaussian distribution of spheroid of different size, shape and at different metabolic and differentiation stage making them hard to handle or to analyze reproducibly, even considering them as a

full system(N. Arora et al. 2017)(Xiao, Dai, and Locasale 2019). The extreme sensitivity of the organoids and spheroids to culture conditions, which, in turn, influence cell signaling, proliferation rate and resistance to anoikis, makes these models, particularly, problematic to work with and finnicky to optimize in order to obtain reproducible results between experiments(Colella et al. 2018).

Both organoid and spheroid systems are reported to perform poorly in replicating organ with highly organized biological structures such as stratified tissues (i.e. skin) or muscle. Lack of in vivo conformational dynamics generates poor structural and functional in vivo biological equivalence and results in models not suitable for studying complex interactions(Clevers 2016)(Colella et al. 2018). Other concerns in the use of these systems raised from studies involving organoids where was observed the ability of these cells to bypass the anchorage dependence growth mechanisms and to proliferate in suspension, unattached to any matrix, which is considered a characteristic of transformed cells, that correlates with tumorigenic potential in vivo(Eglen and Reisine 2019). Similarly, it has been observed that tumor-derived basement membrane extracts, such as Matrigel®, derived from Engelbreth-Holm-Swarm (EHS) mouse sarcoma, can stimulate anchorage-independent proliferation mechanism and loss of contact inhibition. Such mechanisms are part of the classical definition of cancer and have many implications on the physiological relevance of such systems(Nath and Devi 2016)(Eglen and Reisine 2019).

In addition, organoids and spheroids derived from in vivo solid masses (or biopsies) showed a natural tendency to form hollow spheres, effect speculated to be derived in part from limited capability of medium to diffuse deeply into the organoid mass, partially dictated by the inability of the system to maintain cell polarity in the 3D structures(Hui Zhao et al. 2019). The limitation of recreating the native patient tissue architecture is particularly evident in organoids derived from organs or tissues that have a highly complex structural organization as, for instance, the previously mentioned skin, which raised also doubts on the physiological equivalence of these systems(Clevers 2016)(Eglen and Reisine 2019).

Apart the morphology of the tissue (either of diseased or healthy models) other aspects are relevant and important to carefully consider in organoid-spheroid cultures such as, for instance, the relative ratios of cells and cell heterogeneity of the model under investigation(Hui Zhao et al. 2019). Diseased cultures derived from tissue biopsies, which represent the majority of the organoid-spheroid culture models, generally contain a mix of cell types that are more or less contaminated by neighboring healthy tissues depending on the sampling technique used to isolate the biopsy. Studies on personalized medicine based on organoid and spheroid models indicated that among the 25% to the 95% of tumor derived organoids (across a range of tissues) were normal cells(Tellez-Gabriel et al. 2019)(Hui Zhao et al. 2019). Standard techniques to ensure absence of biological contaminants in these models are quite hard to achieve, but it would be necessary to bring this technology to the next level(Tellez-Gabriel et al. 2019).

Organoid and spheroid culture cell heterogeneity is sometime reported as a positive aspect of this type of culture, but it must be recognized that it has also negative implications especially when studying the mechanism of action of targeted compounds into models derived from tumor cells containing acquired genetic alterations of metabolic pathways, because heterogeneous mix of cells will not generate univocal response to a stimulus(Kapałczyńska et al. 2018)(Hui Zhao et al. 2019). On the other hand, cells in organoid-spheroid culture have also the opposite risk to undergo clonal expansion, which can dramatically affect the original heterogeneity of the cellular mix and shift the cellular ratio in favor of a specific clone that for random reason is more adapted to the culture conditions. This means that as the culture grows

certain clones will dominate while others will die out(Maru and Hippo 2019). The consequences of these selection processes are to continuously modify the cellular composition and the genetic heterogeneity of the systems from one experiment to the next, heavily reducing the experimental reproducibility(Dobbin et al. 2014)(Maru and Hippo 2019).

Genetical instability, clonal selection, limited capacity to reproduce complex architecture and to homogeneously terminally differentiate the entire pool of cells inside the organ models have consequences on the interpretation of experiment results either intended for drug testing or for understanding of the mechanism of action of genetic diseases(Verheijen 2019)(Dobbin et al. 2014). Therefore, despite organoid/spheroid cultures can induce self-organization in many cell-types, their microtissue structure lacks the cell diversity and, even in the cases where self-organization occurs to astonishing level (i.e. glad organoids), they never fully recapitulate the tissue or organ *in vivo* architecture or complexity. Consequently, lack of validation and poor reproducibility make the organoid-spheroid models too mutable and unpredictable to be considered the ultimate alternative to in vitro biology(Montes-Olivas, Marucci, and Homer 2019)(Dobbin et al. 2014)(Kapałczyńska et al. 2018)(Verheijen 2019).

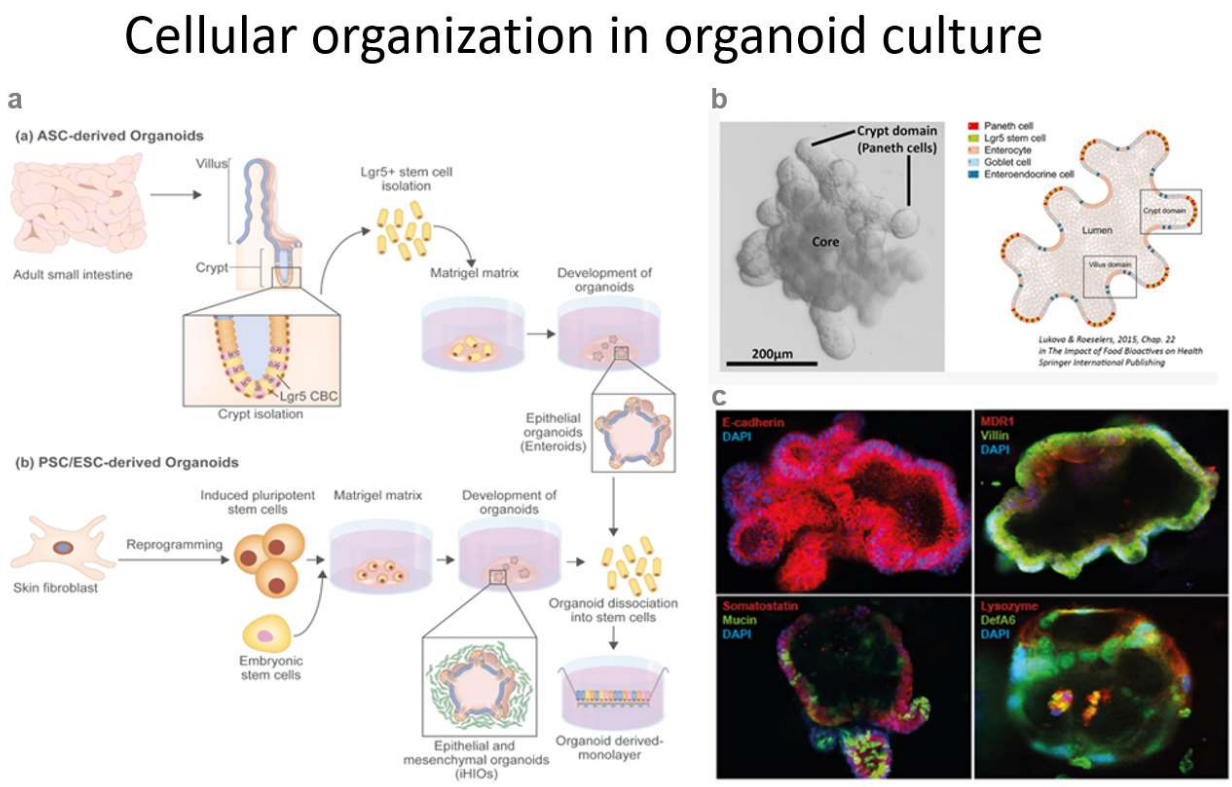

Image courtesy of Sara Rahmani et al., Biomaterials 2019; (DOI: 10.1016/j.biomaterials.2018.12.006. Epub 2018 Dec 10.).
Image courtesy of Lukova & Roeselers, Intestinal Crypt Organoids as Experimental Models 2015; (ISBN 978-3-319-16104-4.).
Image courtesy of https://www.definigen.com/products/intestinal/organoid/.

Figure 1.4: Cellular organization in organoid culture: (a) Schematic showing adult stem cell (ASC), pluripotent/embryonic stem cell (PSC/ESC) organoid culture development, (b) Phase-contrast image and schematic

showing the morphology and cellular organization in intestinal organoid. (c) Immuno-fluorescence images showing canonical intestinal crypt marker spatial distribution within the intestinal organoid.

Biomimetic devices

Despite hydrogel cultures, such as organotypic or organoid cultures, are considered the most likely way to achieve in vivo-like cell culturing, a new tissue-engineering concept is emerging. The concept of combining biology and engineering to recreate artificial environment that resembles more closely the in vivo milieu, which is believed to stimulate cells to act more as in vivo(F. M. Chen and Liu 2016). Scientists are, in fact, re-evaluating the previous idea of just counting on the natural ability of cells to self-organize, self-renew and self-repair to achieve in vivo-like conditions, partially because of the disadvantages associated with the use of such systems, partially because they only minimally achieved the recapitulation of in vivo organ functions and response(Y. Fang and Eglen 2017)(F. M. Chen and Liu 2016).

The different interpretations of this new concept go under three main classes: micro-patterned culture, microfluidic device, and Organ-on-a-Chip.

Micro-Patterned Cultures

Cell micropatterning technology involves the fabrication of biocompatible substrates manufactured to have microscopic features to impose a defined adhesion pattern to the cells and to investigate the cell response to such spatial environmental cues(Khalili and Ahmad 2015). Cells are highly sensitive to geometrical and mechanical constraints of the microenvironment, whose composition dictates specific boundary conditions that, in turn, affects tissue architecture, signal transduction, cell mechanics and cellular functions(Chaw et al. 2007)(Khalili and Ahmad 2015).

The geometry of the microenvironment limits the spreading, spatial arrangement and positioning of cells, similarly to how the orientation, stiffness and biochemical composition of ECM fibers influence the cell spatial distributions in the organ niche(Yang et al. 2017). Physical constrains affect intra-cellular signaling pathways by acting on the assembly and dynamics of cytoskeleton networks and have a critical role in influencing gene expression and cell differentiation(X. Wang et al. 2016). However, despite, evidences strongly suggest that the properties of the microenvironment are crucial for the regulation of cellular functions, often these parameters are neglected and left uncontrolled under classic culture conditions, which are consequently artefactual(Ingber 2003)(Lehnert et al. 2004).

The modern micro-fabrication techniques have provided tools to modify at nano and micrometer scales (micropatterning) the geometrical properties of many biocompatible substrates which can now be used to restrict the regions of the surface where cells can attach(Ermis, Antmen, and Hasirci 2018). Microscale engineered micropatterns have been used to reconstruct in vitro tissue interfaces that resemble those present in native tissues to observe the effect of geometrical in situ constrain on cellular morphogenetic processes and to understand how manipulating micropattern shapes impacts cell migration, growth and differentiation(Nelson 2009).

The microenvironment spatial organization through micropatterning methods is becoming increasingly popular in biomedical research. The most popular method to achieve high-quality micro-patterning has become micro-contact printing (µCP)(Alom Ruiz and Chen 2007)(D'Arcangelo and McGuigan 2015). This method consists in using a polydimethylsiloxane (PDMS) stamp (or mask) with a desired motif to deposit molecules of interest in specific areas of a substrate material (see Kumar & Whitesides, 1994 for more details on the fabrication methods). In biological applications, micro-contact printing is used for patterning ECM proteins on synthetic substrates used to culture cells(Kane et al. 1999)(D'Arcangelo and McGuigan 2015). The ECM proteins have the role to functionalize specific areas of the substrate making it adhesive for cells. Playing on the design of the pattern, it is possible to create quite complex and intricate adhesive and non-adhesive geometries, which are used to align or confine cells on the specific regions of the patterned surface(D'Arcangelo and McGuigan 2015). While the concept of micro-patterning consists essentially in achieving a controlled 2D spatial architecture within a bioengineered system, it has been interpreted differently from different groups, giving raise to patterning at different scales ranging from single cell patterns to tissue level patterns (Fig. 1.5)(Théry et al. 2006)(Paz, Javaherian, and McGuigan 2011).

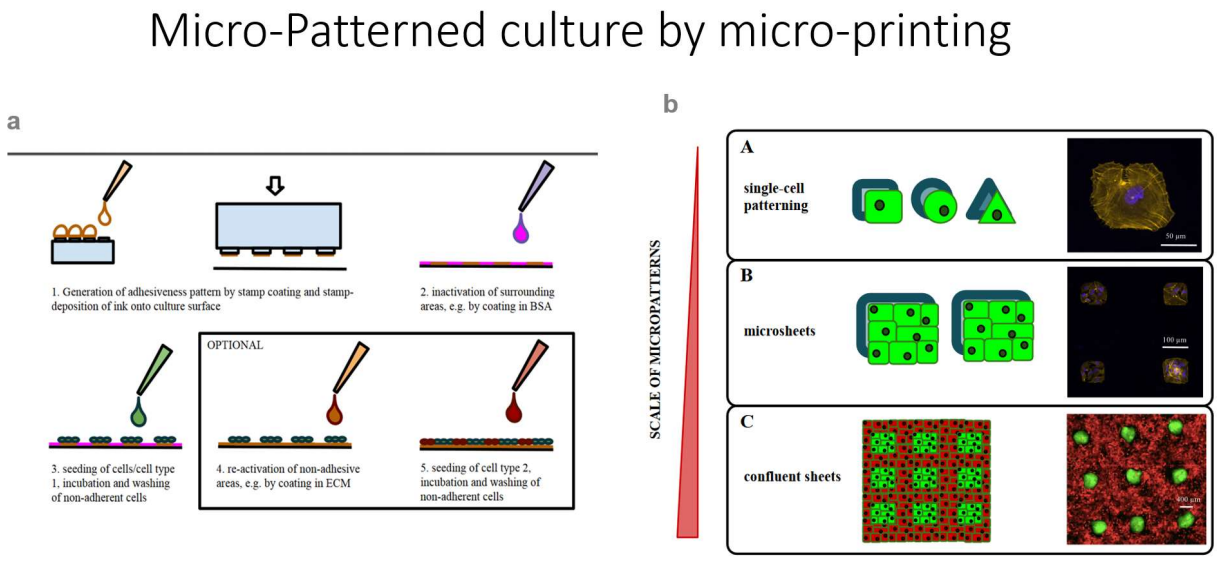

Image courtesy of https://www.future-science.com/doi/full/10.2144/000114245.

Figure 1.5: Micro-Patterned culture by micro-printing: (a) Schematic showing the micro-printing of adhesive pattern on a substrate (b) Schematic showing the different micro-printing scale.

Depending on the scale of the pattern used, it can be distinguished:

Micropatterns at subcellular to single cell resolution (approx. 5-30 µm), with this approach it is possible to confine spreading to a single cell and investigate the effects of geometrical constraints on its behavior, morphology and marker expression(Lehnert et al. 2004). Restriction of the cell attachment area can be achieved either by patterning physical barriers around the cell which limits the cellular spreading area or by printing patterning at subcellular scale on the substrate (called island), which induce a re-arrangement

of the cytoskeleton, and stimulate specific cellular behaviors(Ermis, Antmen, and Hasirci 2018). Typically, an array of multiple single cell chambers micropatterned with sub-cellular sized features is imprinted on a substrate to screen the effect of several micropattern designs on gene expression and cellular morphology(Ermis, Antmen, and Hasirci 2018). Using this approach, it has been demonstrated the importance of the cytoskeletal organization on signal transduction (mechanotrasduction(Martino et al. 2018)(Moujaber and Stochaj 2020)), cellular migration(Welf and Haugh 2011), polarization (McCaffrey and Macara 2012)(Kodama, Lechler, and Fuchs 2004), and its effect on cellular differentiation(Müller et al. 2013) in a variety of cell types(Fletcher and Mullins 2010). Physical separation between single cells has been also used to study the cellular response to signaling molecules (cytokines, hormone) (Barthes et al. 2014) in different pattern surfaces showing that the micro-patterning affects gene expression and cell behavior of osteoblast, macrophage and t-cells(S. Wang et al. 2019).

Micropatterns at multi-cellular scale resolution (approx. 50-200 μm). The goal when using this approach is to confine in close proximity populations of cells within micropatterns(D'Arcangelo and McGuigan 2015). The geometry of the area is specifically controlled, but the shape of the individual cells within the area is not. However, the geometrical constraints of the micropatterned area can induce specific alterations in the shapes of the cells within the surface edges(Lunova et al. 2016)(S. Wang et al. 2019). The dimensions of the micropattern designs are generally such that cells can form a monolayer , which is called microsheet(Paz, Javaherian, and McGuigan 2011)(Lunova et al. 2016). For example, microsheets can be designed to align cells to specific directions or form edges reminiscent of specific organ niches to enable apical-basal polarization when using air-liquid or liquid-liquid interface cultures(Paz et al. 2014). Patterned designs can also be generated on solid substrates or hydrogel to create pattern that enable maximum packing of the cells within specific volumes(Kocgozlu et al. 2016). Similarly, to the sub-cellular sized designs, multi-scale patterning is usually generated in arrays to allow multiple screenings within one experiment to have a quantitative and statistical relevant analysis of the cellular response(Kocgozlu et al. 2016)(Gong and Mills 2018).

This latest approach was successfully applied to recreate simplified interconnected neuronal network to explore neuronal polarization(W. Li et al. 2014) and synapsis formation(Vogt et al. 2004)(Sood et al. 2019). Similarly, micropatterning has been employed to guide the alignment of neurons and myocardial cells(Zhu et al. 2018) on natural or synthetic supports to more accurately reproduce the arrangement of the native biological structure of nerves and heart muscle(Shachar et al. 2011). The same approach has also been adopted to discriminate the effect of paracrine signaling on the proliferation and differentiation of stem cell when culture in colonies(Hsiao and Palecek 2012). It has been observed that stem cell can differentiate in different phenotypes depending on the specific size of the colony they are cultured into(Joshi et al. 2018) as well as to study the collective movement (called mechanotaxis) of defined groups of cells on surfaces with define micropatterned geometries(X. Lin and Helmke 2008)(He et al. 2015).

A variant of the micropatterns at multi-cellular scale resolution recently has become more popular, it involves the use of micropatterning to generate microsheets containing different cell populations directly interacting to form a microtissue(Khalili and Ahmad 2015)(D'Arcangelo and McGuigan 2015). In this specific setup, cells are attached on specific areas of the substrate using a two-step seeding procedure. The first step involves the generation of an adhesive pattern extending from around fifty to hundreds of microns on a non-adhesive substrate either by chemical modification or ECM coating(Khalili and Ahmad 2015). In the second step, the entire surface is functionalized and rendered adhesive for a second

population of cells which attaches in the unoccupied areas(Khalili and Ahmad 2015). The proximity of the two patterns facilitate the direct interaction of the two-dimensional (monolayer) and three-dimensional (well filled with cells) cellular structures forming the biological interface(Basu et al. 2005). The technical capability to selectively functionalize or activate the specific regions of the substrate to make them adhesive is critical to grouping multi-cellular populations and manage to form the microtissues(C. Lin and Khetani 2017).

Micropatterned microsheet co-culture has been successfully applied to homotypic (hepatocyte-epithelial cells) and heterotypic (hepatocyte-fibroblast) microsheet of hepatocytes to study how such interactions modulate hepatocyte functions in vitro(March et al. 2015). This approach represents an improvement of the initial co-culture attempts, which involved the co-seeding of two or more cell types at specific ratio on a support (flask, well or Petri dish)(Aengenheister et al. 2018)(Goers, Freemont, and Polizzi 2014). The limitation on the initial setup consisted in the fact that cells seeded on the support tended to attach and grow at unpredictable rate and to have a random distribution onto the planar surfaces which made impossible to explore the role of each cell in the biological system and to quantify the enhancement of the specific biological functions(March et al. 2015)(Aengenheister et al. 2018).

To avoid some of the limitations associated with conventional co-culture in 2D, Bhatia and colleagues decided to employ a more sophisticated approach based on photolithography. Specifically, they created a mask pattern to selectively adsorb ECM on specific and defined areas (called islands) of a plastic substrate on which they seeded primary hepatocytes(Bhatia et al. 1998). Following the hepatocyte attachment, they coated the substrate with another ECM mixture and seeded a second layer of epithelial (human cholangiocytes) or feeder cells (primary or 3T3 murine embryonic fibroblasts) atop. Both the magnitude of albumin secretion and the longevity of hepatocyte was significantly increased by the direct contact with other cell types(Bhatia et al. 1998)(Hui and Bhatia 2007). The double step micropatterning also allowed to maintain the cell numbers and ratios among the hepatocytes, the cholangiocytes and fibroblasts constant along the entire length of the experiment and between experiments(March et al. 2015)(Bhatia et al. 1998)(Hui and Bhatia 2007). These studies demonstrated that cell-cell interactions play a critical role in modulating hepatocyte functions, but also evidenced that having a reproducible methodology to seed a precise number of cells on a substrate is important to properly quantify results. Using this technique was possible to compare the level of albumin secretion induced by fibroblasts from multiple species (human, rat, mouse) and even from 3T3 sub-clones (i.e. NIH-3T3, Swiss-3T3, L1-3T3), which revealed that the J2 sub-clone of 3T3 induced higher albumin secretion in hepatocytes(C. Lin and Khetani 2017)(Bhatia et al. 1998).

The direct and intimate interaction between the juxtaposed sheets of different cell types generated biological architectures somehow reminiscent of the tissue interface observed in vivo and enabled the investigation of key physiological processes that require direct interaction between cells(Bogdanowicz and Lu 2013). Thank to these two characteristics, this approach has been heavily employed to investigate the signaling mechanism occurring between cells and the invasion mechanisms occurring at the tumor interface(Ziyad and Iruela-Arispe 2011)(Bogdanowicz and Lu 2013). However, the biological relevance of this approach is strongly depended on the characteristics of the cell populations being patterned, their ability to interact to each other, and count strongly on the ability of cells to self-organize themselves within the microsheets(Xavier da Silveira dos Santos and Liberali 2019)(Ziyad and Iruela-Arispe 2011).

Despite micropatterning methodologies to generate microtissues have often been criticized for its limited versatility due to fabrication issues, difficult handling and limited throughput as well as for its limitations in the ability to mimic in vivo tissue architecture due to lack of the third dimension and to their inability to include multiple cell-types when not compatible with the same medium(D. E. J. Anderson and Hinds 2011). The studies conducted using micro-patterned cultures recreated level of tissue functionality unprecedented at the time. But they also evidenced the importance of having control over the organization and the spatial localization of the single elements forming the biological unit to obtain a stable system in which variables, such as cell number, relative ratios, proliferation rate, or the other variable affecting the "cellular stoichiometry" of the system, are stable and not continuously changing(Gautrot et al. 2012)(Shen, Fu, and Chen 2008). Avoiding the presence of confounding variables its necessary when performing mechanistic studies on the processes that regulate cell-cell interactions to extrapolate data useful for pharmaceutical and healthcare applications.(Lundquist and Renftel 2002)(Gautrot et al. 2012)

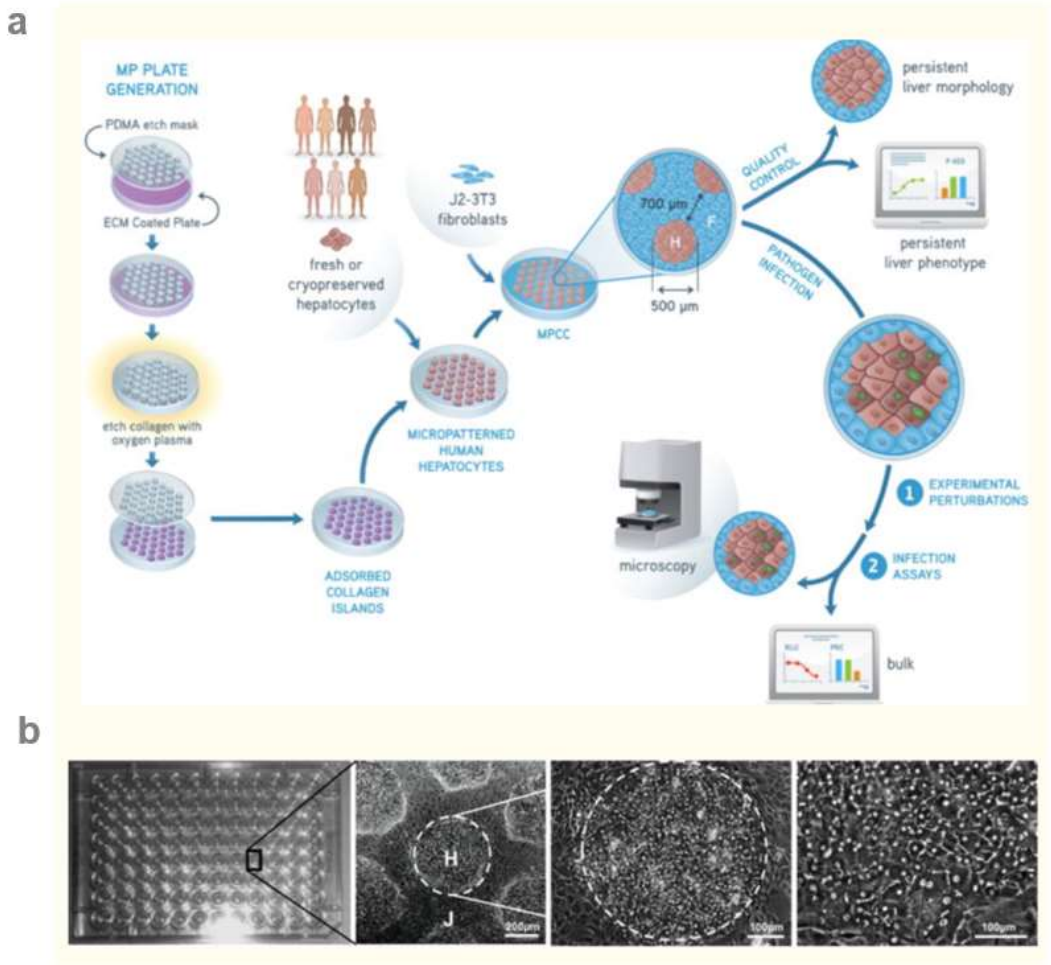

Image courtesy of Sandra March et al., Nature Protocol 2018; (DOI: 10.1038/nprot.2015.128).

Figure 1.6: Micro-Patterned culture by micro-printing: (a) Schematic showing a step-by-step sequence to prepare micropatterned microsheet co-culture of hepatocytes and J2-3T3 fibroblasts. (b) Picture sequence showing a 96 well plate seeded with spherical hepatocyte microsheets surrounded by a confluent layer of fibroblast which make a very defined and constant boarder with the hepatocyte monolayer.

Microfluidic devices

Microfluidics is a science that deals with the technology to manufacture miniaturized perfusable devices containing multiple channels (and/or chambers) and studies the behavior of fluids through them. A microfluidic device typically contains microchannels linked to microchambers, which form micro-environments where cells are cultured under direct flow (or, in more rare cases, where cells are separated from the direct exposure of the fluid shear by micro fabricated baffle)(Yu et al. 2014)(Khabiry and Jalili

2015). Fluids (gasses or liquids) are injected and perfused through the channels and chambers with external active systems (pressure controllers, syringe and peristaltic pumps) or in a passive way (hydrostatic pressure)(Y. J. Kang et al. 2014).

Microfluidic devices are gaining more and more interest in the biomedical fields because of their potential to perform large-scale culture operations at a much smaller scale, which presumably will help reducing sample consumption and costs(Cui and Wang 2019). Another critical advantage of these systems resides in their ability to perform time-lapse effluent collection, which is ideal for time course or real time analysis(Golchin et al. 2012). Time course analyses are critical in situation where analytes change their chemical composition over time or have a limited half-life. Additionally, most microfluidic devices are set for microliter-size volumes which are suitable for situations where cost and amount of biological resources (i.e. cells, proteins, compounds) are limited(Paguirigan and Beebe 2008)(C. Zhao, Ge, and Yang 2017)(Golchin et al. 2012).

Microfluidic applications depend strongly on the chemistry of the device surfaces and the tailoring of its properties. In order to achieve value for biomedical and diagnostic applications, microfluidic devices must match two fundamental requirements(Paguirigan and Beebe 2008): first, the inner surfaces of the channels and/or chambers must eliminate or strongly reduce non-specific adsorption, because, due to the limited dimensions of the microfluidic devices, the inner microchannel surface to fluid volume ratio is low and, consequently, the potential for surface adsorption is high(Roach, Song, and Ismagilov 2005)(Chiu et al. 2017). This is especially true when using biological fluids which are rich in amphiphilic proteins that have high propensity to stick on both hydrophilic and hydrophobic surfaces. Basically, to obtain analytical performance in biological applications, the materials which devices are made of should not absorb biomolecules while still providing a stable, inert, non-toxic and not chemically reactive microenvironment(Poncin-Epaillard et al. 2012)(Chiu et al. 2017).

Second, for cell-based assays, the microfluidic surfaces must have the possibility to be selectively functionalized (either be chemical modification or coating) to allow cell attachment. Surface functionalization is important because it can make a significant difference in cell adhesion(Halldorsson et al. 2015), but it has also a much higher biological relevance than just increasing cell-attachment per se, because the possibility to immobilize biological active molecules on the artificial substrate forming the microfluidic device can be essential for establishing and maintaining the proper tissue organization(Halldorsson et al. 2015), functionality and, generally, it strongly helps cell survival making it a requirement in most microfluidic applications(J. Zhou, Ellis, and Voelcker 2010).

Surface activation to covalently immobilize biocompatible molecules on the internal surfaces of a microfluidic device can be achieved by a myriad of surface treatments, but the specific strategies strongly depend on the properties of the material in first place(Tallawi et al. 2015). For instance, the most popular functionalization technique used to achieve covalent bonding of biological active molecules to a substrate was plasma surface activation(Solouk et al. 2011). It was achieved by exposing the materials to ionized gas to form free radicals on the surface and making them react with biomolecules (i.e. ECM, BSA, etc.) to cross-link them to the surface(Bilek and McKenzie 2010). The strength of this technique resides in the fact that it does not require the presence of specific chemical groups whose availability vary from material to

material but has the weakness to perform optimally only on flat directly exposed surfaces(Punet et al. 2015). In fact, plasma poorly penetrates inside enclosed geometries such as a channel, especially, of microscopic dimensions(Shakeri et al. 2019)(Bilek and McKenzie 2010).

The generation of radical species, which can make the material permanently cytotoxic to cells, and the requirement for specialized equipment lead researchers to opt for different activation methods than plasma(Jastrzebska et al. 2018). For instance, hetero-bifunctional linkers (mono or poly hetero-bifunctional crosslinking) have gained some popularity to activate material surfaces(Posa et al. 2019). This typology of activation is preferred to physical surface treatment as corona discharge and oxygen plasma because much easier to perform, less cytotoxic than plasma and because it offers some flexibility on the specific surface reactive group to which can bond and the functional groups on the biomolecule to which can crosslink. Despite, the use of linkers is limited by the presence of specific chemical groups on the surface to activate, it still offers more versatility compared to physical activation methods because a large variety of linkers that are compatible with functionalization of the substrates commonly used in biological applications have been identified, classified and are commercially available at reasonable price(Alegria-Schaffer 2014)(Posa et al. 2019).

Currently, adsorptive protein coatings have become more broadly used than covalent immobilization by linkers, because of the simplicity of the treatment. In fact, coating only requires low concentration protein solutions to be in direct contact with the surface to functionalize(Krutty et al. 2016). This method, at least in theory, does not involve the use of any artificial chemicals, therefore eliminate the problem of toxicity and solvent biocompatibility. Coating surfaces with ECM proteins takes advantage of the natural tendency of these proteins, often poly-amphiphilic, to stick on both hydrophobic and hydrophilic surfaces(Llopis-Hernández et al. 2011). Furthermore, the fact of using ECM protein solutions (at low concentration and low viscosity) makes the coating procedure more adapt to functionalize the enclosed surfaces of a channel or any other enclose geometry as a chamber(Krutty et al. 2016). Moreover, the fact that the chemistry is not specific to a particular chemical group makes it appliable to a much broader variety of physical substrates(Straley 2009). For specific materials which are particularly inert and naturally low protein binding as for instance PDMS, a combination of physical modification and adsorptive protein coating is often contemplated. Independently from the method used to functionalize the substrate, it is important to carefully consider and evaluate the particular protein or protein mixture to apply on the surface because of the implications they have on cellular behaviors we have discuss previously(Meyers and Grinstaff 2012)(DeFife et al. 1999).

Early **microfluidic devices** were simple single channel configuration micro-fluidics laser-machined into cover slip-sized silica wafers and bonded on a cover glass. An early application of microfluidics for studying biology was a “Y shaped” microfluidic device designed to produce a passive chemoattractant gradient using as loading mechanism the hydrostatic pressure generate by a 200 µl pipette tip inserted into one of the three access ports (Fig. 1.7)(Zhang et al. 2008). Despite their simplicity and the complex manufacturing, microfluidic devices became immediately very popular in biological applications because these miniaturized systems offered new capabilities such as the control over laminar flow to study its effects on cells, the production of chemical gradients that mimic natural stimuli occurring in biological processes and high-throughput parallel processing(Velve-Casquillas et al. 2010). An additional impetus to

the spread of this technology occurred when Whitesides and colleagues in 1998 taking advantage of the improvement in soft-lithography and in replica molding techniques started using poly(dimethylsiloxane) (PDMS) to produce microfluidic device relatively inexpensive and easy to fabricate(Duffy et al. 1998)(J. R. Anderson et al. 2000). This material become the choice of preference in biological applications also thanks to its properties of transparency, biocompatibility, gas permeability and easy manufacturability(Duffy et al. 1998).

One of the early applications of microfluidic devices was the study of cellular chemotaxis because flow provided the unique possibility to generate a controllable gradient of chemoattractant and surface functionalization offered control over the properties of the in vitro environment(W. Zhao et al. 2020)(Kim and Wu 2012). Bio-functionalization of substrates and flow provided an excellent platform to recreate ideal migration conditions to understand the effect of physical regulators(Kim and Wu 2012) (e.g. shear stresses and gradients of nutrients or chemoattractants) and cytoskeleton effectors (e.g. active biomolecule as ECM proteins) on the spatio-temporal activation of cytoskeleton protrusions, which ultimately lead to different migration modes(Kim and Wu 2012)(Friedl and Wolf 2010) (note: surface functionalization as we mentioned previously, was developed for similar biological applications, but in a different ambit and scientific context which was mainly cell attachment, not chemotactic effect). Using this simple “open Y” shaped fluidic channel design, it was unequivocally demonstrated the chemotactic ability of human T cells in response to gradient of chemokine (specifically, CCL19 and CXCL12)(F. Lin and Butcher 2006).

The device apart offering control over the generation of chemoattractant gradients in space and time, allowed the production of integrated multichannel array into a single silica wafer (defined as “chip”) to generate multiple gradients in a single chip and, consequently, to perform high throughput parallel chemotaxis experiments(Wan and Yin 2018)(F. Lin and Butcher 2006). The concept of “chip” generated a lot of interest because miniaturization not only allowed to lower experimental cost, but also parallel processing which greatly increasing the experimental throughput(Sosa-Hernández et al. 2018). Another advantage offered by the chips was the direct visualization of cells inside the channel during chemotaxis experiment which allowed to monitor in live the phenomenon(Zhang et al. 2008). In previous experimental assays performed on three-dimensional thrombin or agarose plugs cell visualization was very limited and highly ineffective because of the scattering of light occurring in these materials(Salam et al. 2018). Most of all, the first studies using microfluidics evidenced the importance of adding physiological cues when studying biological systems, at least, in the contest of lymphocyte migration and chemotaxis in vitro, and evidenced also that having precise control over them is absolutely necessary to recreate in vivo-like physiological response(Tsai and Kuo 2013)(Polacheck et al. 2013).

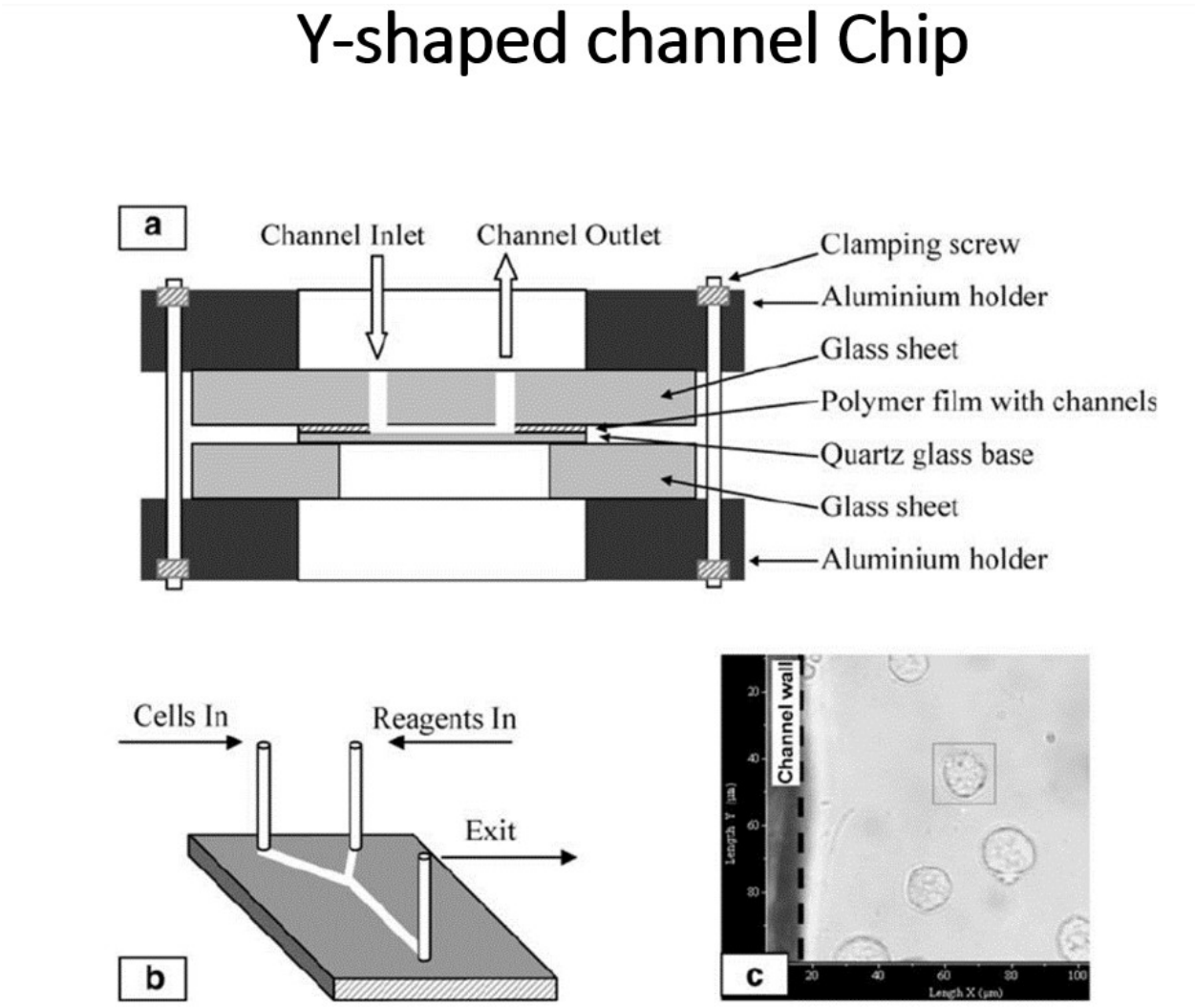

Image courtesy of Xunli Zhang et al., Analytical and Bioanalytical Chemistry 2008; (DOI: 10.1007/s00216-007-1564-9).

Figure 1.7: Y-shaped channel Chip: (a) Schematic showing Y-shaped Chip assembly using manifold clamping methods. (b) Sketch of the Chip fluidic. (c) Phase-contrast image showing perfusion of cell inside the channel.

The concept of microfluidic device with time evolved into the concept of microfluidic chip, but even if many times they have been used interchangeably, they differ for their respective intended application. The first refers to device where cells are temporarily flown or added to be studied under specific regime, while the second refers to microfluidic device where cells are cultured inside (Aziz et al. 2017)(Q. Wu et al. 2020). A great example of functional microfluidic chip is offered by the liver-sinusoid Chip from Philip J. Lee and colleagues (Fig, 1.8), who achieved astonishing restoration of liver functionality in vitro and obtained unprecedented mimicry of the human liver-sinusoidal barrier. The chip model used micro-geometry to physically confine cells and enables morphogenesis of hepatic 3D tissue structures under

continuous perfusion. Since hepatocytes easily lose their functionality and enzymatic activities when exposed to direct flow, it was particularly important to replicate their natural niche to support their viability in vitro(Aziz et al. 2017).

The liver-sinusoid Chip has two parts, a chamber that act as a scaffold and serves to contain the 3D hepatocyte aggregates, and a "U" shaped channel which surrounds the chamber and from which it is separated by a porous baffle that is used to perfuse the culture at a shear rate within the physiological range(Lee, Hung, and Lee 2007). Typically, high levels of oxygen and nutrients are required to support hepatocyte viability and those can only be achieved by providing elevated fluid shear. Unfortunately, hepatocytes are extremely sensitive to the shear stress generated by the flow(Gori et al. 2016)(Lee, Hung, and Lee 2007).

Therefore, to circumvent the cell dead caused by direct exposure of the hepatocytes to the shear stress while still providing adequate level of oxygenation, the geometry of the liver chip was modelled on a structure reminiscent of hepatic acini(Lee, Hung, and Lee 2007)(Gori et al. 2016). The chip contained a chamber used to seed hepatocytes surrounded by a parallel microchannel array structure (a microfabricated porous baffle) lined with liver sinusoidal endothelial cells that isolate hepatocytes from the direct fluidic shear, while allowing the diffusion of nutrients through the porous baffle. The geometry of the chamber promotes the self-organization of the hepatocytes in multiple lines and the formation of functional bile-canaliculi along the hepatic lobule structure(Lee, Hung, and Lee 2007)(Gori et al. 2016).

This model did not only manage to reproduce the complex architecture of the hepatic lobule but also the metabolic, biosynthetic, and bio-transformative properties of LSEC -hepatocyte interface. The model was capable to metabolize carboxydichlorofluorescein diacetate (CDFDA) by hepatic esterase(C.-J. Lin et al. 2016) and its bioproduct, a fluorescent compound called carboxydichlorofluorescein (CDF) accumulated in the bile and was excreted into the bile canaliculi similarly to in vivo(Nakao et al. 2011)(Murray, Han, and Wolkoff 2014). This result is a good example that demonstrates how replicating the bioarchitecture of tissue can restore organ in vivo functions, including metabolic pathways, maintaining cellular phenotype, tissue polarity, bio-synthetic and transportation ability of tissues(F. M. Chen and Liu 2016). Worth mentioning that despite this Chip recreated the essential conditions to culture functional hepatocytes and that the fenestrae-like baffle lined with LSEC prevented the direct exposure of hepatocyte to shear stress which closely mimic the local organization of the LSEC-hepatocyte barrier(Lee, Hung, and Lee 2007)(Gori et al. 2016), the architecture of the hepatocyte-acinus missed completely each non-parenchymal interactions(Godoy et al. 2013).

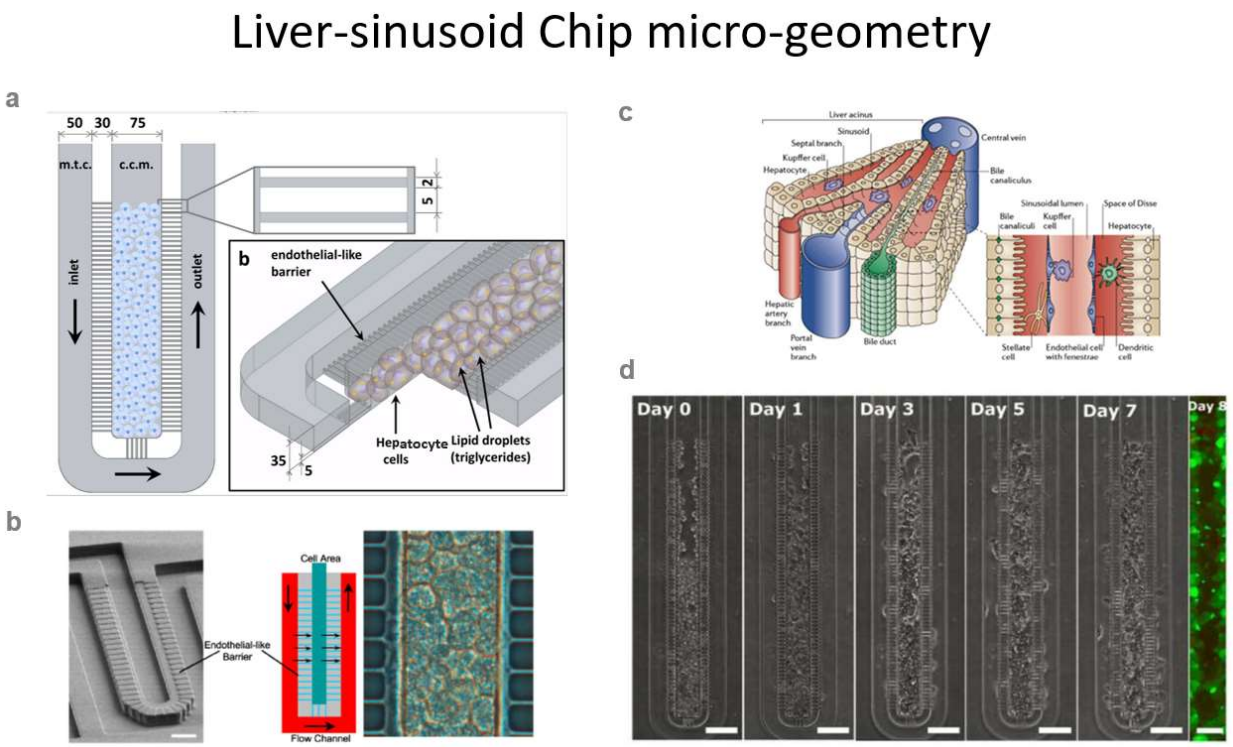

Image courtesy of Manuele Gori et al., Plos One 2017; (DOI: 10.1371/journal.pone.0159729).
Image courtesy of Mores C et al., Annals of Biomedical Engineering 2011; (DOI: 10.1007/s10439-011-0455-6).
Image courtesy of Yu Du et al., Methods in Cell Biology 2018; (DOI: 10.1016/bs.mcb.2018.06.002).
Image courtesy of Philip J. Lee et al., Biotechnology and Bioengineering 2007; (DOI:10.1002/bit.21360).

Figure 1.8: Liver-sinusoid Chip micro-geometry: (a) Schematic of the microfluidic Chip design. (b) Sketch of the Chip fluidic showing perfusion of chip microdevice evidencing the direction of the flow (big arrow) and nutrient transport across the porous baffle (small arrow); scalebar: 20µm. (c) Liver sinusoid boundary schematics. (d) Phase-contrast image showing hepatocyte cell growth between day 0 and day 7 of culture. In vivo, the sinusoid space is bordered by fenestrated endothelial cells, and this highly permeable barrier enables hepatocytes to absorb nutrient from blood plasma, while protected from shear stresses. Fluorescent image showing live/dead assay performed at day 8 of culture (living cells in green, calcein-AM; dead cells in red, Ethidium Homodimer-1; scalebar: 50µm).

Organs-on-a-Chip

An Organ-on-a-Chip (OOC) is a microfluidic cell culture method where a system of channels and interconnected chambers allow the three-dimensional interaction between cells. The peculiar design of these types of devices simulates the cellular microenvironment with the goal of stimulating cells to behave physiologically, or at least, inducing cellular behavior more closely resembling those observed in vivo. The main goal when using this device is to improve preclinical drug toxicity and efficacy screening in vitro offering an alternative to the use of animal models(Ghaemmaghami et al. 2012)(Q. Wu et al. 2020).

The improvement of micro-fabrication techniques and advancement in tissue engineering gave rise to this technology which is now commonly known as Organ-on-a-Chip. The main OOC advocated strength resides mostly in the ability to mimic key aspects of in vivo human physiology which often results indispensable

for replicating tissue and organ functionality in vitro and for understanding their effects on cellular metabolism, on drug pharmacodynamic and pharmacokinetic(Huh et al. 2013). Broadly speaking, Organ-on-a-Chip technology consists of two or more microfluidic channels separated by a semi-permeable porous material. In such devices, different types of cells are grown in juxtaposed microfluidic channels (or chambers) so that the cells lining on the two opposite sides of the porous material can interact directly between each other and recapitulate the native cell-cell interactions between the two cell layers(Huh, Hamilton, and Ingber 2011). These systems are commonly fabricated to resemble tissue-tissue interfaces at micrometer scale, to incorporate physical forces such as shear stress, stretching (cyclic stain), and to sustain air liquid interface with the intent to better recapitulate the milieu from which the cells were isolated and to restore the major functions of the tissue(Huh et al. 2013)(Huh, Hamilton, and Ingber 2011).

The first most convincing proof of principle of the validity of the Organ-on-a-Chip biomimetic approach was showed by Dongeun Huh in 2010 when he developed a microdevice capable to reproduce key structural and functional properties of the human alveolar-capillary interface. The microfluidic device enclosed two closely opposed microchannels separated by a thin (10μm), porous, flexible membrane made of poly(dimethylsiloxane) (PDMS)(Huh et al. 2010). The interposed membrane was coated with extra-cellular matrices: fibronectin on the epithelial side and collagen I on the microvascular endothelial side to improve cellular attachment and differentiation. The idea behind these coatings was substantially to mimic the basal lamina of the native alveolar and endothelial lung tissues respectively, while the cells were cultured on opposite sides of the semi permeable PDMS porous membrane to allow direct contact between each other recreating in this way the fundamental functional unit of the living lung (Fig. 1.9 a, b)(Huh et al. 2012) (Huh et al. 2010).

When epithelial alveolar cells reached confluence, they formed a tight barrier which allowed to introduce air into the epithelial compartment without the leaking of fluid from the endothelial compartment. Under this condition, defined as air-liquid interface, the system achieved a superior and more precise mimicry of the alveolar air space(Huh et al. 2012). The spatial configuration of the microdevice made the two channels independently compartmentalized, but closely interconnected through the porous membrane(Huh et al. 2010). The design of the chip also allowed to achieve control over the fluid shear rate during the culturing phase when the endothelial compartment was perfused continuously with medium to feed both endothelium and epithelium while at air-liquid interface(Huh et al. 2010). The specific geometry offered also a superior spatial confinement which facilitated the optical sectioning of the two cell monolayers(Huh et al. 2010)(Huh, Hamilton, and Ingber 2011)(Huh et al. 2012).

Perhaps, the main achievement of the design proposed by Dr. Huh was the capability to replicate for the first time in a microdevice the dynamic mechanical distortion of the alveolar-capillary interface caused by breathing motions(Huh et al. 2010). In fact, during the normal human breathing, in the phase of inspiration, air is cyclically pulled into lungs which increases the intrapleural pressure into the alveoli which undergo to a cyclic series of expansion which stretch the alveolar epithelium and the adjacent endothelium (Fig. 1.9 c)(OpenStax 2013b).

To mimic the natural pressure-driven lung stretching mechanism, Dr. Huh took advantage of the PDMS mechanical elastic properties by incorporating two lateral microchambers at the two side of the microfluidic channels. When negative pressure was applied to the vacuum chambers, an elastic deformation was produced on the thin membrane that separates the two microchannels which generated

a strain deformation of the two cellular layers adherent to the membrane (Fig. 1A)(Huh et al. 2010). When the vacuum pressure was released PDMS underwent to elastic recoil which caused the membrane and the two cellular layers adherent to the membrane to relax to their original position(Huh et al. 2010)(Huh et al. 2012). A computer vacuum actuator was integrated with the microdevice to produce sinusoidal wave of negative pressure which generated stretching cycle of 10% strain at 0.2 Hz. Applied cyclic strain (or stretching cycle) in the range 4% to 15% at 0.2Hz closely mimic in vivo natural levels of strain observed in alveoli during physiological breathing motion during rest and exercise, respectively. (Birukov et al. 2003)(Huh et al. 2010).

Despite these amazing achievements, Organ-on-a-chip technology is still failing to fully reconstitute the additional dimensionality of the 3D architecture of living tissue and to adequately recapitulate the spatial organization of the cells with its surrounding (especially, the stromal components such as fibroblasts, smooth muscle and ECMs)(Kamm et al. 2018)(Jodat et al. 2019). In fact, Organ-on-a-chip technology more than a real 3D culture system is a 2D culture on a 3D surface, such setup gives some degree of three dimensionality as, for instance, in the case of direct contact between cell seeded on the opposed side of an artificial semi-permeable membrane, but lack completely the radial cell interactions with the stromal cells and the ECM lattice(Duval et al. 2017). It is well known that in the native micro-environment spatial and physical interactions occurring among cells and between cells and ECM affect the transduction of signals from the outside to the inside of cells, influence gene expression and ultimately cellular behavior(Jodat et al. 2019). Therefore, the opportunity of precisely recreating the physical and biochemical cell environments is thought to be essential for inducing cells to behave more physiologically and to generate in vitro system more predictive of in vivo cell response to drug, stress and chemical(Nakayama, Hou, and Huang 2014)(Duval et al. 2017).

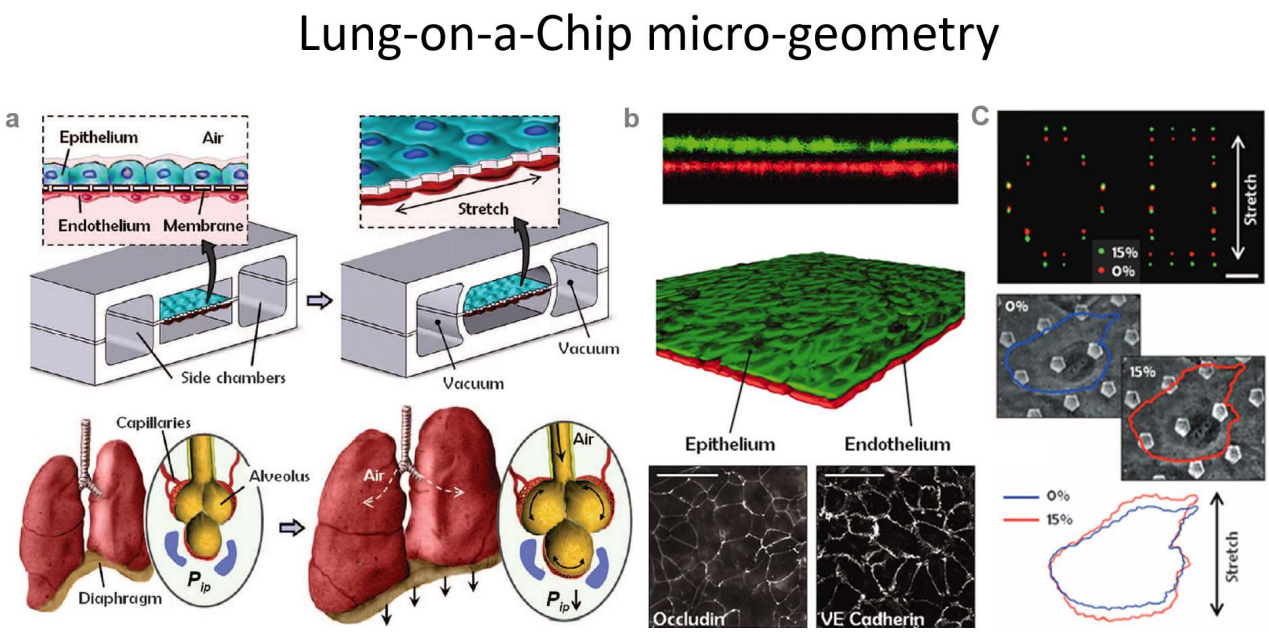

Image courtesy of Dongeun Huh et al., AAAS 2010; (DOI: 10.1126/science.1188302).

Figure 1.9: Lung-on-a-Chip micro-geometry: (a) Schematic of the microfluidic Chip design showing the alveolar-capillary barrier recreated on the thin flexible porous membrane (10μm) lined with endothelium and epithelium. In

the alveoli the contraction of the diaphragm create a decrease in pressure which push air in (inhalation) causing the stretching of the alveolar-capillary barrier (b) Fluorescence image showing the epithelium (green) and endothelium(red) co-cultured into the chip at ALI, the expression of intracellular junction epithelial (occluding) and endothelial(VE-Cadherin) confirm the presence of compact monolayer; scalebar: 50µm. (c) Image showing the physical displacement of the membrane pores when under stretching at 0% and 15%, respectively; scalebar: 100µm).

Open-Top Alveolus-Chip

In this study, we describe a platform that integrates microfabrication techniques, organotypic culture and microfluidics, and that offers fine control over stretching via pneumatic actuation and over the flow (shear rate) via electric pressure-driven pumping. We used a modular assembly concept to design a fully enclosed and tightly sealed bottom microfluidic channel interconnected by a semi-porous membrane with a cavity accessible to deposit gels, to cast the hydrogel surface and to seed cells. It is surmounted by an openable microfluidic lid on top used to keep sterility and to flow medium (or other fluids including air) at controlled rate or to introduce the air-liquid interface. The system supports the viability and differentiation of organotypic epithelial tissues and provides a controllable microenvironment with an easy and direct access to the reconstructed human organ unit. We illustrate how the micro-engineered device, called Open-top Chip, enables the culturing of the alveolus providing a proof of principle of the validity of this type of integrated micro-engineered platform technology. We also show the application of this technology to other organs such as skin, airway, and intestine (examples of stratified, pseudo stratified and simple epithelium, respectively).

Lung alveolar physiology

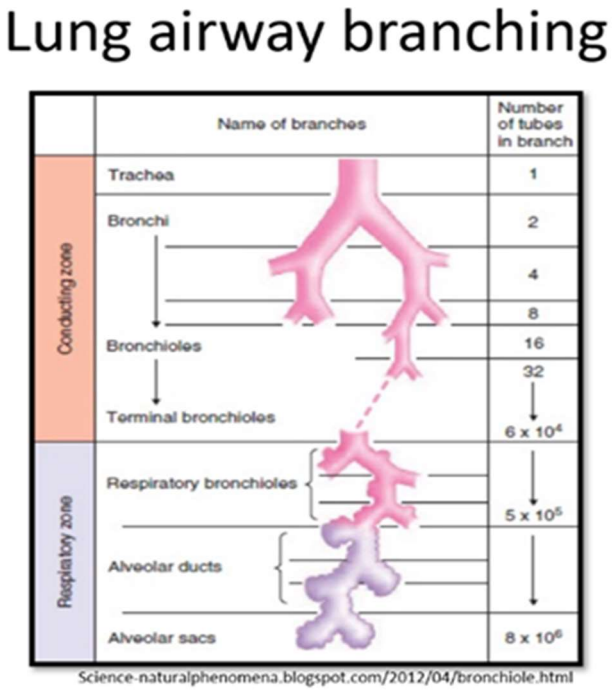

Figure 1.10: Lung airway branching: Schematic of the airway branching from the trachea to the alveolar sacs

The lung consists of 4 major biological distinct components: trachea, bronchi, bronchioles, and alveoli. In the lungs, the trachea, a cartilaginous tube, connects the larynx to the bronchi, which branch off into smaller and smaller passageways called bronchioles and lead to tiny ducts, called alveolar ducts, each containing a collection of tiny air sacs (alveoli) (Fig. 1.10)(OpenStax 2013a).
Inside the alveoli the surface exposed to the gaseous environment is lined by two distinct types of epithelial cells: alveolar type I (ATI) cells, which phenotypically look squamous and cover approximatively 93-97% of human epithelial alveolar surface and alveolar type II (ATII) cells, which are cuboidal epithelial cells specialized in the production of surfactants, and act as progenitor for ATI, according to the current most accepted paradigm(WARD and NICHOLAS 1984). These two cell types form the structural and functional epithelium of the alveolus. The cytoplasm of the type II pneumocytes contains

specialized structures composed of lipids, called lamellar bodies, which store pulmonary surfactants (A,B,C,D), before being secreted by exocytosis into the alveolus(Cerrada et al. 2015). All of the pulmonary surfactants are complex lipoproteins (composed of about 90% lipids and 5%–10% surfactant-specific proteins) synthesized by the alveolar type II cells with surfactant protein C being unique to the ATII (it constitutes a unique marker for alveolar type II cells)(Nkadi, Merritt, and Pillers 2009)(Andreeva, Kutuzov, and Voyno-Yasenetskaya 2007). The main purpose of the surfactant proteins is to reduce the interfacial surface tension and stabilize the alveolar interface to prevent atelectasis during breathing. In fact, without surfactants alveolar epithelial surfaces will sticks together after exhalation, causing the alveolus to collapse(Nkadi, Merritt, and Pillers 2009). Surfactants are also part of the innate immune system. These proteins can bind molecules on the surface of pathogens and opsonize them to facilitate their phagocytosis by resident macrophages or other components of the adaptive immune system(Han and Mallampalli 2015)Surfactant synthesis occurs in various compartments between the endoplasmic reticulum and the Golgi complex, and they self-assemble into the mature surfactant forms inside the lamellar bodies(Brasch et al. 2004)(Ridsdale and Post 2004). The assembly and exocytosis of lamellar bodies are mediated by ATP-binding cassette (ABC) transporters (ABCA3) while the storage of surfactants inside the lamellar bodies is mediated by lysosome-associated membrane glycoprotein 3 (LAMP3, also known as DC-LAMP, Dendritic cell lysosomal associated membrane glycoprotein) which are prevalently localized at the border of the lamellar body membrane inside ATII cells (fig.1.11)(Weaver, Na, and Stahlman 2002)(Cheong et al. 2007).

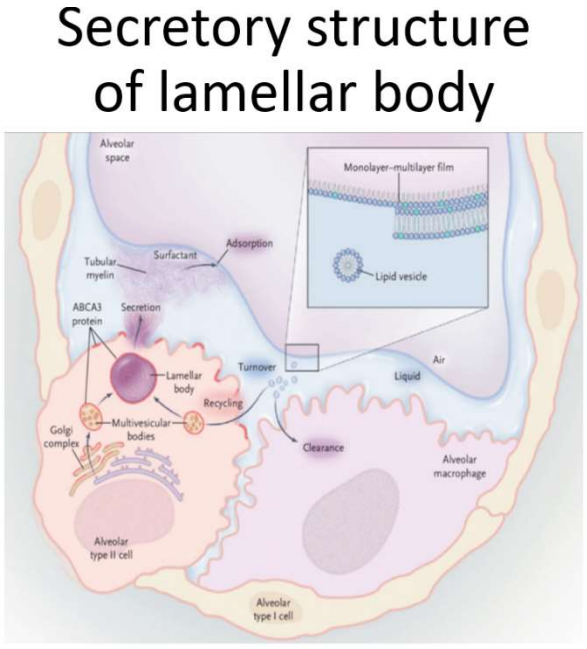

Image courtesy of N.V. Bhagavan, Chung-Eun Ha, Essentials of Medical Biochemistry (Second Edition), 2015; (ISBN 978-0-12-416687-5).

Figure 1.11: Secretory structure of lamellar body: Diagram showing formation and secretion of lamellar bodies from alveolar type II cells mediated by ATP-binding cassette transporter A3 (ABCA3).

The alveolar acinus is surrounded by a dense capillary network which forms the blood-air barrier through which circulating red blood cells get enriched with oxygen(X. J. Chen et al. 2000). In the area where gas exchange occurs, the alveolar epithelial and endothelial membranes are closely juxtaposed and the adherens junctions of the two membranes directly interface forming a tight barrier capable to restrict liquid fluxes between the two compartments, while allowing oxygen diffusion (Fig.12, a)(X. J. Chen et al. 2000). The inability of the alveolar structure to restrict liquid fluxes lead to edema, leakage of fluid into the alveolus, which impedes any gas exchange causing oxygen deficiency. In the area where the capillaries do not interface directly with the epithelium of the alveolar wall, these structure interface directly with the stroma which completely encases them (Fig.1.12, b)(X. J. Chen et al. 2000)(Bagnato and Harari 2015). The lung stroma is populated of highly specialized, but not well characterized mesenchymal cells, which constitute a major proportion of the lung stromal cell population and are essential for maintaining the integrity of the lung epithelial tissue and to sustain their normal homeostasis(Belair and Abbott 2017)(Yuan et al. 2018). Indeed, most of the acquired and hereditary forms of lung diseases, as

well as some drug toxicities, are characterized by fibroblast loss or dysfunction, which results in idiopathic pulmonary fibrosis (IPF), chronic obstructive pulmonary disease (COPD) and other types of lung degenerations(Yuan et al. 2018)(Tanjore et al. 2009)(White 2015).

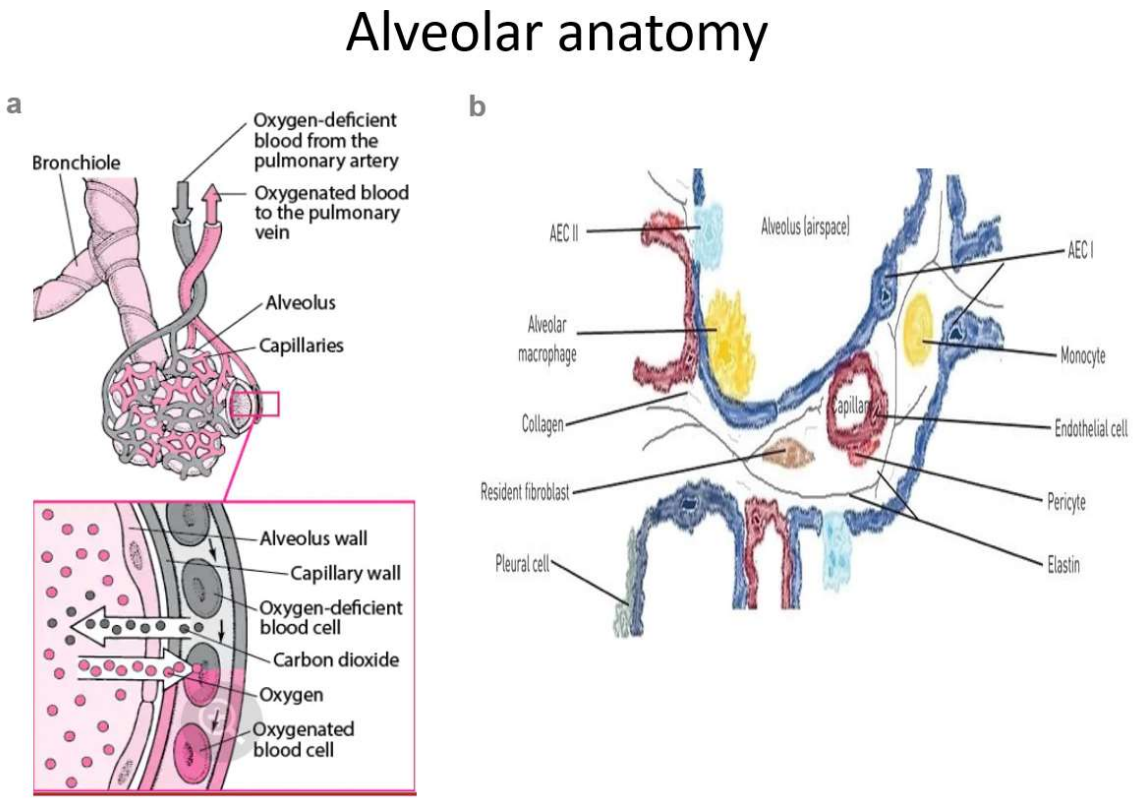

Image courtesy of Gianluca Bagnato & Sergio Harari, European Respiratory Review 2015; (DOI: 10.1183/09059180.00003214).
Image courtesy of https://www.merckmanuals.com/home/lung-and-airway-disorders/biology-of-the-lungs-and-airways/exchanging-oxygen-and-carbon-dioxide.

Figure 1.12: Alveolar anatomy: (a) Schematic of alveolar duct and alveolar sacs (top) and gas exchange occurring at alveolar epithelial-endothelial barrier (bottom). (b) Sketch showing the basic biological element forming the alveolus including the alveolar epithelial cells type I (AECI) and type II (AECII), the resident macrophage and monocyte, the endothelial cells forming the capillary, and the elements of the stroma (collagen, elastin, and resident fibroblast).

State of in vitro models in the contest of the lung

The alveolar epithelium-endothelium barrier represents the main site of oxygen exchange inside the human body and, at the same time, the first barrier against environmental insults(Knudsen and Ochs 2018). As such, defects of the lung structure or diseases affecting the functions of the alveolar tissue can have lethal consequences(Miller and Spence 2017). Animal models have been instrumental to understand the lung physiological processes and to study lung development and disease mechanisms(Conway et al. 2020). However, given the physiological and anatomical differences between animal and human lungs, there is an unmet need for human in vitro lung models that can complement animal studies and improve our knowledge on human lung functioning(Miller and Spence 2017). For example, the lung branching

morphogenesis in mouse follow a completely different pattern compared to human including differences in the periodicity and in the sequence of branching (human undergo additional rounds of splitting within each domain). Rodent lungs also present anatomical differences in the spatial distribution of the alveolar progenitor cells compared to human and their lung alveolarization do not begin until after birth(Metzger et al. 2008). Consequently, it is not surprising that animal models are not capable to recapitulate the full spectrum of human pathophysiology(Shanks, Greek, and Greek 2009)(Metzger et al. 2008), which is further highlighted by the fact that up to 90% of drugs that pass preclinical animal tests in rodents fail to effectively treat human disease during clinical trials(Mak, Evaniew, and Ghert 2014).

Since in vivo animal models for testing new therapeutics has been extremely unsuccessful, apart being extremely expensive and time consuming. The ability to develop in vitro models that recapitulate human lung functions would greatly help to advance our understanding of the mechanisms that underlies alveolus response to stimuli and facilitate the establishment of disease models to guide therapeutic discovery(Jain et al. 2018)(Benam et al. 2016). Unfortunately, there is still no many sources of functional adult pneumocytes available for the development of in vitro models of human alveolus(Jacob et al. 2017)(Ghaedi et al. 2013), despite multiple methods for isolating human alveolar type II cells are published in literature, (since the first report of the isolation of a surfactant-producing epithelial cell from lung of a rodent by Kikkawa and Yoneda in the 1974)(Kikkawa and Yoneda 1974), the lack of alveolar cell sources and the lack of knowledge on which signals within the alveolar microenvironment contributes to the cellular ontogenesis, lineage specification and maturation strongly limited our ability to build in vitro models of the human alveolus that maintain the adult differentiated phenotypes, cellular functions and restore the production of surfactant C. (Mason and Williams 1980)(X. Fang et al. 2006)(Ren, Birch, and Suresh 2016).

Most of the currently available in vitro systems are designed to model the alveolar epithelium or the alveolar-capillary interface but neglect the contribution of stromal components(Knudsen and Ochs 2018). Also, common in vitro platforms do not recapitulate the biomechanical forces that regulate organ-level function including alveolar cell differentiation and surfactant secretion(Nawroth et al. 2019). These systems, frequently utilize cell lines, including the human lung carcinoma cell lines (i.e. A549, H1299, etc.) that by definition do not recapitulate the biology of healthy tissue(Jean-Pierre Gillet, Sudhir Varma 2013). Existing 2D cultures of primary alveolar epithelial cells also bear limitations. Specifically, when grown in vitro, alveolar epithelial cells acquire a squamous phenotype and lose most key markers, including surfactant proteins C and B and various molecular transporters such as the acquporin5 or the epithelial-sodium-channel(Mao et al. 2015). Additionally, cells frequently become insensitive to biological stressors, and certain biochemical pathways associated with tissue inflammation and relevant to drug testing are no longer functional(Beers and Moodley 2017). Recent advancements in the fields of developmental biology and regenerative medicine have elucidated the roles of the pulmonary stroma and biomechanical forces in determining the fate and maturation of pulmonary epithelial cells and the expression of tissue-specific markers, such as surfactant C and aquaporin 5(Y. Zhou et al. 2018)(Beers and Moodley 2017)(Mao et al. 2015).

The role of mechanical forces acting on alveolar cell (epithelial, endothelial and mesenchymal cells) during respiration has been controversially discussed, with no uniquely accepted theory about their biological

and physiological relevance (Waters, Roan, and Navajas 2012b). Much of the uncertainty about physiological role of mechanical forces acting on alveolar cell is due to technical difficulties (such as limited imaging and sampling systems, small size of the alveolar cells and relatively large cell displacement during breathing) in analyzing the phenomenon (Jett 2005)(Soda et al. 1993). Therefore, most of the information about alveolar and lung mechanics has been largely inferred by pulmonary functional tests and static histopathology, which although have improved our understanding of lung functions, are still not specific.

However, the scientific world commonly agrees on the hypothesis that cells respond to external and internal mechanical stimuli by converting them in signals that regulate various cellular processes and functions including gene expression, polarization-depolarization of the cytoskeleton, cell proliferation and differentiation, and secretion of matrix proteins(Kazumasa Ohashi, Sachiko Fujiwara 2017). The researches seem to suggest that mechanical forces play a much larger role than previously believed in regulating cell behavior, and therefore to better understanding alveolar physiology and alveolar based diseases and disfunctions, it would be necessary to integrate mechanical forces in future models(Kazumasa Ohashi, Sachiko Fujiwara 2017). Integration of mechanical forces into in vitro models are seen as a practical way to have direct experience and evidence of the effect of mechanics on alveolar cell behavior(Waters, Roan, and Navajas 2012a)(Vining and Mooney 2017).

Organ-Chip technology and its use to overcome current in vitro model limitations

To overcome some of these limitations, we set out to develop an in vitro three-dimensional model of human alveolus based on Organ-on-Chip technology. Our model, that we named human Open-Top Alveolus-Chip, is a transparent medical grade polydimethylsiloxane (PDMS) microfluidic platform that possesses open-top capability created by utilizing microchip manufacturing methods (Huh 2015). It contains a continuously perfused hollow microchannel lined with living endothelial cells, which interface through a porous transparent elastic membrane with a stretchable chamber where is deposited a lung recreated stroma (3D collagen I hydrogel coated with ECM protein in which are embedded lung fibroblasts). The recreated stroma serves as a scaffold for alveolar cells, which are seeded on the top of the 3D hydrogel in direct contact with fibroblasts. This platform simulates the overall alveolar architectures by mimicking, to the highest degree described so far, the tissue-tissue interfaces, chemical gradients, mechanical cues, and vascular perfusion occurring in the human body and produces levels of tissue and organ functionality not achievable with other conventional 2D or 3D culture systems. Noteworthy, the Open-Top Alveolus-Chip supports dynamic fluid flow, fact that has important implications in testing therapeutics in a pharmacologically relevant context(Huber et al. 2018)(Jain et al. 2018). Using this platform, it is possible to study how pharmacological active compounds and therapeutics actively or passively across the alveolar barrier under flow, which is key information to understand drug pharmacokinetics. In addition, since the Open-top Alveolus-Chip platform offers the possibility to flow human whole blood or circulating immune cells isolated from blood through the endothelium-lined channels, it also allows to investigate immune recruitment, collect cytokines and study pharmacokinetics under more physiological relevant conditions compared to a static culture system.

In particular, in here we show that simultaneous modulation of few signaling pathways that have been implicated in alveolar development enables the rapid and efficient adult primary alveolar cell conversion

into more terminally differentiated cells that exhibit morphological, molecular and functional characteristics of mature adult alveolar pneumocytes. By co-culturing the adult alveolar pneumocytes on a stroma layer in contact with the endothelium in the Open-top Chip, we developed a functional micro-fluidic device that mimics the tissue-tissue interface and some of the mechanical properties of the alveolar epithelium-capillary interface. It also recapitulates some of the stromal interaction happening in the lung which are critical to study the lung induced injury and other disfunctions in vitro. Therefore, Alveolus-Chip could offer a new way to study alveolar functions, toxicity, and mechanisms of alveolar disease in vitro.

2. MATERIALS & METHODS

Materials and Methods

Fabrication and assembling of the Organ-Chip platform

All the constituents of the Open-top Chip as well as the tooling to cast the individual components were designed using SolidWorks. Each part was fabricated by soft lithography/replica molding using polydimethylsiloxane (PDMS) (Dow Corning® Sylgard Elastomer 184 Kit, available from Ellsworth Adhesive), at weight ratio of PDMS base to curing agent 10:1, from mold created with high resolution SLA 3D printing (Protolabs). Specifically, the platform comprises of four parts made of PDMS: a bottom spiral shaped microfluidic channel, a porous membrane, a circular stroma cavity, and a lid that also serves as a microfluidic channel. The bottom spiraled shaped microfluidic channel, the circular stroma cavity and the top fluidic channel were fabricated by replica molding of PDMS from a 3D printed mold (Protolabs). The membrane was fabricated using previously published methods (Novak et al. 2018). Briefly, membranes are made by casting PDMS over a photolithographically prepared master that containing a positive post-array organized in a hexagonal packing with 40µm spacing pattern silane coated. Specifically, 100µl of PDMS were poured onto wafers and then compressed using a polycarbonate backing against the post array. At this point, pressure was applied constantly by an in house built pneumatic control valve actuator consisting of a piston which applies a pressure of 40 PSI (276KPa) to the master during the curing of PDMS to ensure intimate contact and penetration of PDMS through the silane coated master while being cured at 65°C overnight. This process produced 50µm thick PDMS membranes with circular through-holes. The PDMS parts, bottom spiraled shaped microfluidic channel, membrane and circular stromal cavity were manually aligned and then, bonded together by oxygen plasma treatment (30W for 30 seconds at 335mtorr using a Femto Science Covance Oxygen plasma machine). Irreversible bonding was achieved by curing the PDMS parts at 60°C overnight.

Open-Top technical features

The Open-top chip assembly has a 35 mm × 17 mm footprint and comprises of four parts: the bottom spiraled shaped microfluidic channel, the membrane, the circular stromal cavity, and the lid that also serves as microfluidic channel. The bottom spiraled shaped microfluidic channel has a cross-section profile of 400µm × 600µm and communicates through the porous membrane to the circular cavity. This cavity is 4mm tall and 6mm in diameter and is surrounded on either side by two semi-circular shaped hollow vacuum chambers that are 1mm wide and 3.5mm tall (Fig. 3.0 a, b). The surface area of the bottom spiraled microfluidic channel that directly interfaces with the tissue culture area of the cavity is 0.18cm^2. The membrane, a porous flexible PDMS membrane (50µm thick, 7µm diameter pores with 40µm spacing, and 2.5% porosity) (Fig. 3.0 d), interposed between the spiraled microfluidic channel and the circular cavity acts as a support structure for the organotypic culture while allowing diffusive transport of nutrients, metabolites and compounds. The bottom microfluidic channel is connected to an inlet and an outlet port and is used to perfuse organotypic tissue with culture media, blood, or other fluids. When it is lined with endothelial cells during the culturing phase, it forms what we define the **vascular compartment** (Fig. 3.0 c). The circular cavity has a tissue culture area of 0.32cm^2 used for the deposition of hydrogel which is chemically crosslinked to the PDMS wall and membrane to form what we define **stromal compartment** (Fig. 3.0 c). The microfluidic channel of the lid has a cross-sectional profile of 200µm height

× 600µm width leading to circular geometry (6mm in diameter, 200µm height) matching the top section of the circular cavity. The geometry of the cavity is round to equilibrate the tension forces acting on the hydrogel-wall interface and eliminate geometric stress concentration that would occur on the vertices of a rectangular shaped wall, which in prototype designs resulted in delamination of the hydrogel from the PDMS wall.

Fluidic system design (Human Emulation System Bioreactor, Zoe)

The Open-Top Chip is supported by the Human Emulation System, which enables two main functions one is the independent fluid flow in the two culture channels of the Chip and second the mechanical actuation of the tissue in order to emulate stretching (pneumatic deformation of the hydrogel). Fluid flow is achieved via a pressure-driven system; the instrumentation provides positive pressure, which drives fluid through a plastic pre-assembled, four-compartment microfluidic sterile cartridge, termed the "Pod", that holds media in reservoirs and routes media both into the chip and then, subsequently, into sampling reservoirs. The combination of variable pressure from the Human Emulation System instrument, termed the "Zoe", and the fluidic resistance of the Pod set the flow rate. An auxiliary instrument, termed the "Orb", allows for gasses to be mixed, in particular CO_2 is mixed with air, to create the proper carbon dioxide concentration to buffer the pH of sodium bicarbonate buffered media. Additionally, the Orb provides the negative vacuum pressure to the Zoe instrument, which in turn translate to the vacuum chambers of the Chip through the Pod interface. The instrument applies a sinusoidal vacuum/strain wave as a default, with user in control of the magnitude and amplitude of the wave. The Zoe allows for 12 Chips to be run in parallel, with the same flow rates and stretch parameters between Chips. Most standard cell culture incubators can host two Zoes simultaneously, with a typical incubator 2-stack being able to run four Zoes for a total of 48 Chips run in parallel. Each Zoe can be controlled independently, including different flow and stretch conditions, with a single Orb is needed for a four Zoe system when deployed in this manner.

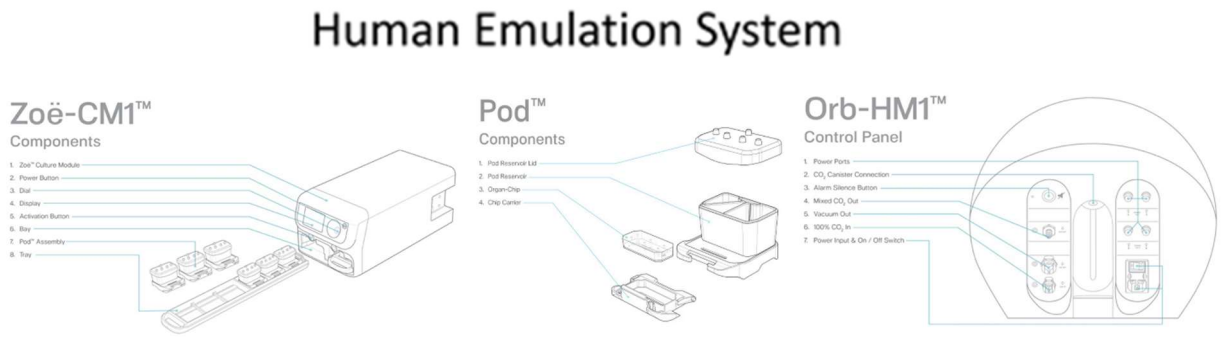

Image courtesy of Emulate, Inc.

Figure 2.0: Component of the human emulation system: the bioreactor, called ZÖE-CM1, the microfluidic cartridge, called Pod™ and the pump a system, called Orb-HM1™.

Pneumatic actuator

Pneumatic actuation of the Open-top microfluidic platform was performed by using a programmable vacuum regulator system built in-house. The system consisted of an electro-pneumatic vacuum regulator (ITV0091-2BL, SMC Corporation of America) controlled electronically by an Arduino Leonardo and MAX517 digital to analogue converter. The electro-pneumatic vacuum regulator generates a sinusoidal vacuum profile with amplitude and frequency tunable by the user. Cyclic strain (up to 15%) was applied to vacuum chamber of the Open-top Alveolus-Chips at an amplitude of -25 or -90kPa and frequency of 0.2 Hz.

Pneumatic stretching

The two semi-circular shaped hollow vacuum chambers surrounding the cavity of the stromal compartment can be subjected to negative vacuum pressure that deforms the cavity walls, and subsequently the hydrogel attached to those walls. This process is termed pneumatic stretching or simply **stretching**. When the negative vacuum pressure is decreased, the PDMS returns back (elastic recoil) to its original shape relaxing the strain on the stromal compartment. Within the circular cavity both recreated stroma and epithelium undergo mechanical stretching. Using this design, it is possible to model the breathing and peristaltic motion (repetitive contraction and relaxation cycle) observed in living organs. The application of negative pressures to the vacuum chambers by an in house built pneumatic actuator in the range 0 to 90KPa generates a dynamic range of strain in the range 0 to 15% (Fig. 3.3 a). Strain in the gel was characterized by embedding fluorescent beads in the gel and by optically measuring the distance between fluorescent beads at a specific height within the gel. For each pressure increment, distance was measured with vacuum applied in steady state. The strain is then calculated by the difference between the measured distances divided by the distance with no vacuum applied. This stretching range was chosen because there is a quasi-linear dependence between the amount of vacuum pressure applied and the magnitude of strain. The pneumatic actuator also modulates the frequency of the vacuum cycle in the range 0.01 to 0.5 Hz, which generates stretching/relaxation cycles ranging from 2 to 100 seconds.

Open-top Chip microfluidics

The spiraled section of the bottom channel interacts directly with the basal side of the recreated stroma by the PDMS semi-permeable porous membrane. When this membrane is populated with endothelial cells, it mimics the stoma-capillary interface where exchange of nutrients and waste products between cells and the circulatory system occurs (Fig. 3.0 c). The PDMS porous membrane has the structural function to physically contain the hydrogel in place and to feed and hydrate the recreated stroma and the epithelium with medium. We opted for a spiraled shaped channel to maximize the area of fluid (medium) in direct contact with the circular section of the stromal compartment and simultaneously to maintain constant laminar flow along the entire length of the channel. The geometry of the vascular compartment allows consistent control over the wall-shear rate along the entire length of the endothelial compartment by changing the flow rate. Constant laminar flow was chosen because it enables to correlate physical parameters with biological effects induced by specific shear rate. Flow rates between 60 and 1000 µl/hr are generated using Zoe or alternatively a peristaltic pump system (Ismatec IPC ISM934C Digital Peristaltic Pump: EW-78001-42).

Stamp for micropatterning

Micro-patterning of extracellular matrix (ECM) proteins is a technique we use to replicate the spatial configuration of tissue interface with intricate microarchitecture to enable the study of cellular response to irregular ECM geometries. The process of micropatterning by stamping was inspired by lithography, a process used to transfer geometric patterns from a wafer stamp to a soft substrate. Similarly, we engineered the surface of a wafer stamp (or simply stamp) made of biocompatible materials to transfer a cell-size geometric pattern to an ECM substrate (Fig.2.1). The micropatterning technique involves four basic steps: first, remove the top lid to deposit the hydrogel into the cavity by pipetting; second, introduce the micropatterned stamp over the hydrogel into the cavity; third, pattern the gel by letting the hydrogel polymerize with the stamp inserted into the cavity; and forth, remove the stamp and aspirate the excess of hydrogel. The micropatterning stamps were designed by SolidWorks software and 3D printed in a non-cytotoxic resin (MicroFine Green, Proto Labs) with 15µm layer resolution. A cylindrical shaped design about 6mm in diameter (slightly undersized at 5.95mm) and variable height was chosen to closely fit the chip cavity without completely sealing it. Undersizing the stamp permits the escape of air during the casting operation and avoids trapping bubbles into the hydrogel. The surface of the stamps can be patterned with positive or negative micro-scale texture such as pillars or holes with different geometrical packing or free style/random pattern. We take advantage of the openable Open-top lid to introduce these specially designed micropatterned cylindrical stamps which mimic the topography of the natural human epithelium-stroma interface to cast hydrogel surface at micrometer scale or to form a flat gel surface which are often convenient over complex geometries because flatness facilitates the spatial confinement of the epithelial layer and makes easier imaging the cells. In this paper, we have tested an array of micropillars of 250 x 500µm (aspect ratios 1:2) to mimic the surface of human intestinal crypts (Fig.4.2).

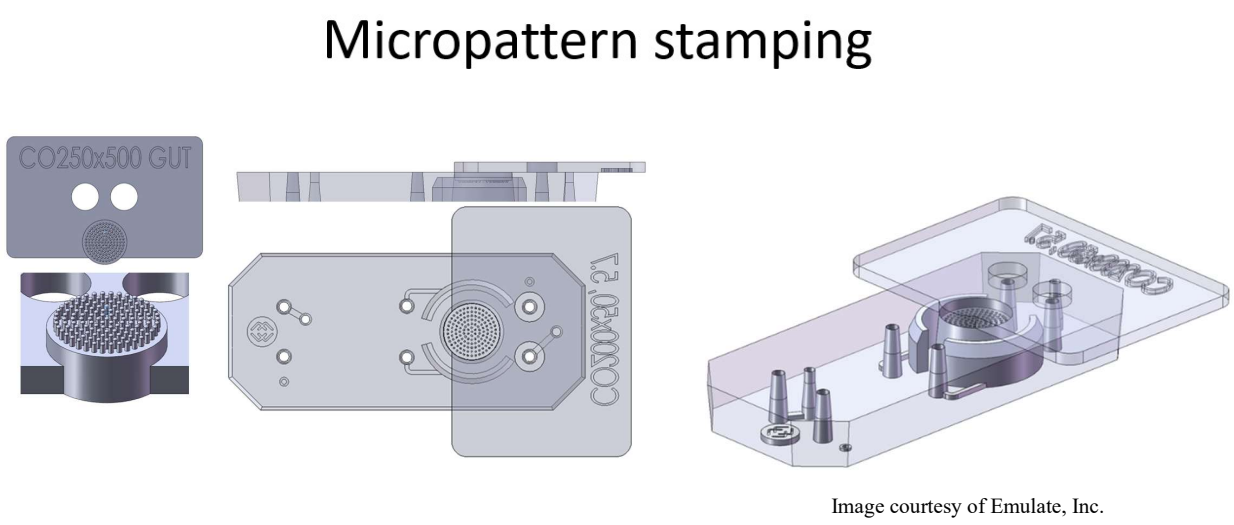

Image courtesy of Emulate, Inc.

Figure 2.1: Micropattern stamping: On the left, a stamp example showing micro-scale texture (500µm in height and 250µm width pillar-array). At center, a lateral and top view of the stamp/Chip assembly showing the fitting of the two elements when used to cast hydrogel. Angled lateral view showing the stamp and Chip interfacing.

2D Cell culture (cell expansion)

Human Primary Alveolar Epithelial Cells (Cell Biologics: H-6053), Lung Fibroblasts (Cell Biologics: H-6013), Normal Human Small Airway Epithelial Cells (Lifeline®: FC-0016), Normal Human Lung Smooth Muscle Cells (Lifeline®: FC-0046), Normal Human Lung Fibroblasts, Primary (Lifeline®: FC-0049) and Human Lung Microvascular Endothelial Cells (Lonza: CC-2527) were grown in T-75 culture flasks in an atmosphere of 5% CO_2 at 37°C according to the instructions provide by the manufacturers. Briefly, Primary Alveolar Epithelial Cells (P1) and Normal Human Small Airway Epithelial Cells (P1) were cultured in SAGM medium (Lonza: CC-4124). Lung Fibroblasts (P1), Normal Human Lung Smooth Muscle Cells, Normal Human Lung Fibroblasts, Primary (P1) were cultured in DMEM/F-12 (GIBCO®: 11320082) supplemented with 10% Heat Inactivated HyClone™ FetalClone™ II Serum (U.S.) (GE Healthcare Life Sciences: SH30066.03) and 1% penicillin-streptomycin (GIBCO®: 15140122) and 1% GlutaMAX (GIBCO®: 35050061). Human Lung Microvascular Endothelial Cells were cultured in EGM™-2MV (Lonza: CC-3202). Primary Epidermal Keratinocytes; Normal, Human, Neonatal Foreskin (HEKn) (ATCC®: PCS-200-010™), Primary Dermal Fibroblast Normal (HDFn) (ATCC®: PCS-201-010™) and Human Microvascular Endothelial Cell (ATCC®: CRL-3243™) were grown in T-75 culture flasks in an atmosphere of 5% CO_2 at 37°C according to the instructions provide by the manufacturers. Normal Human Neonatal Foreskin (P1) were cultured in Keratinocyte-SFM (1X) medium (Thermo: 17005042). Primary Dermal Fibroblast Normal (P1) were cultured in DMEM/F-12, GlutaMAX™ supplement (GIBCO®: 10565018) supplemented with 10% Heat Inactivated HyClone™ FetalClone™ II Serum (U.S.) (GE Healthcare Life Sciences: SH30066.03) and 1% penicillin-streptomycin (GIBCO®: 15140122) and 1% GlutaMAX. Human Microvascular Endothelial Cells were cultured in EGM™-2MV.

Human duodenal enteroids were grown as monolayers and differentiated by the methods developed by the laboratory of Dr. Hans Clevers. Primary Human Intestinal Fibroblast Normal (P1) were cultured in Advanced DMEM F12 (Thermo: 12634010) supplemented with 10% Heat Inactivated HyClone™ FetalClone™ II Serum (U.S.) and 1% penicillin-streptomycin (GIBCO®: 15140122). De-identified biopsies were isolated from healthy adult donors who provided informed consent at Johns Hopkins University in accordance with approved guidelines and regulations. All experimental protocols were approved by the Johns Hopkins University Institutional Review Board (IRB: NA00038329). Briefly, enteroids generated from isolated intestinal crypts were grown embedded in Matrigel® (Corning®: 356231) in 24-well plates in Expansion Medium (EM) consisting of Advanced DMEM F12 (Thermo: 12634010) supplemented with 50% v/v Wnt3A conditioned medium (produced by L-Wnt3A cell line, ATCC®: CRL-2647), 20% v/v R-spondin-1 conditioned medium (produced by HEK293T cell line stably expressing mouse R-spondin1; kindly provided by Dr Calvin Kuo, Stanford University, Stanford, CA), 10% v/v Noggin conditioned medium (produced by HEK293T cell line stably expressing mouse Noggin), 10mM HEPES (Thermo 15630080), 0.2 mM GlutaMAX (Thermo: 35050061), B27 supplement (1X) (Thermo: 17504044), N2 supplement (1X) (Thermo: 17502001), 1mM n-acetylcysteine (Sigma: A9165), 50ng/ml human epithelial growth factor (Thermo: PHG0311), 10nM human [Leu15] -gastrin (Sigma: G9145), 500nM A83-01 (Tocris: 2939), 10µM SB202190 (Tocris: 1264/10), 100µg/ml primocin (InvivoGen: ant-pm-1). EM was replaced every other day and supplemented with 10µM CHIR99201 (Tocris: 4423) and 10µM Y-27632 (Tocris: TB1254-GMP/10) during

the first 2 days after passaging. Organoids were passaged every 7 days and used for chip seeding between passage number 5 and 30.

Detailed protocols

Media preparation

Preparation of ALI-M (199A) Medium (1 liter)

1) Add 800ml of Medium 199, no phenol red to a Corning® Easy-Grip round, plastic, 1 liter storage bottles (Corning®: 430518)
2) Add 1ml EGF solution (10µg/ml)
3) Add 1ml KGF solution (10µg/ml)
4) Add 1ml VEGF-165 solution (2.5µg/ml)
5) Add 1 ml of Hydrocortisone solution (1mg/ml)
6) Add 1ml of Heparin solution (1KU/ml)
7) Add 800µl of 8-Br-cAMP solution (100µM)
8) Add 20µl of Dexamethasone solution (1mM)
9) Add 10ml of GlutaMAX™ Supplement (Thermo: 35050061)
10) Add 10ml of antibiotics penicillin-streptomycin (GIBCO®: 15140122)
11) Mix everything
12) Bring to final volume of 900 liter (remember to put 100ml of Heat Inactivated HyClone™ FetalClone™ II Serum)
13) Filter the 900ml solution using one liter low-protein-binding (0.22µm pore mesh) Filtration System Membrane (Corning®: 25952)

Before use

14) Add 100 ml of Heat Inactivated HyClone™ FetalClone™ II Serum to one-liter bottle

(alternatively Heat-inactivation of HyClone™ FetalClone™ II Serum (FCS) can be performed by heating the FCS for 30min at 56˚C)

Note: ALI-M medium is storable up to 4 weeks at 4˚C (refrigerator)

ALI-M (199A) Medium

Medium 199, no phenol red	**Thermo 11043023**	**Basal Media**
Heat Inactivated HyClone™ FetalClone™ II Serum (U.S.)	GE Healthcare Life Sciences: SH30066.03	10% (V/V)
Epidermal Growth Factor (EGF) human, recombinant in E. coli	PromoCell: C-60170	10ng/mL
Keratinocyte Growth Factor (KGF), also known as Basic	PromoCell: C-63821	10ng/mL

Fibroblast Growth Factor 7 (FGF-7), human, recombinant in HEK		
Vascular Endothelial Growth Factor 165 (VEGF-165) human, recombinant in E. coli	PromoCell: C-64420	0.250ng/mL
Hydrocortisone 21-hemisuccinate sodium salt	Sigma: H4881	1µg/mL
Heparin sodium salt from porcine intestinal mucosa	Sigma: H3149	1Unit/mL (1KU/L)
8-Bromoadenosine 3',5'-cyclic monophosphate sodium salt (8-Br-cAMP)	Sigma: B7880	80µM
GlutaMAX™ Supplement	Thermo: 35050061	1mM
Dexamethasone	Sigma: D4902	20nM
Penicillin Streptomycin	GIBCO®: 15140122	1% (V/V)

Preparation ALI-M (199A) Medium supplements:

EGF (PromoCell: C-60170)

- Reconstitute: 10ug of EGF in 1ml of Medium 199
- Store in -20˚C, replace every 3 months

KGF (also known as FGF7) (PromoCell: C-63821)

- Reconstitute: 10ug of KGF in 1ml of Medium 199
- Store in -20˚C, replace every 3 months

VEGF-165 (PromoCell: C-64420)

- Reconstitute: 10ug of VEGF in 4 ml of Medium 199
- Store in -20˚C, replace every 3 months

Hydrocortisone (Sigma: H4881)

- Reconstitute: 100 mg of Hydrocortisone 21-hemisuccinate sodium salt in 100 ml of Medium 199
- Store in -20˚C, replace every 6 months

Heparin (Sigma: H3149)

- Reconstitute: 50,000 (or 50 Kilo) Unit Heparin sodium salt from porcine intestinal mucosa in 50ml of Medium 199
- Store in -20˚C, replace every 6 months

8-Br-cAMP (Sigma: B7880)

- MW: 430.08
- Reconstitute: 100mg in 2.3251ml culture grade water for 100mM
- Store in -20˚C, replace every 1 year

Dexamethasone (Sigma: D4902)

- MW: 392.46
- Reconstitute: 25mg in 63.7008mL DMSO for 1mM concentration
- Store in -20˚C, replace every 6 months

Preparation of SAGM (complete) Medium

1) Add 500ml of Small Airway Basal Medium (CC-3119) to a Corning® Easy-Grip round, plastic, 500ml storage bottles (Corning®: 430282)
2) Add 2ml Bovine Pitituary Extract (BPE), SAGM™ SingleQuots™ supplements
3) Add 0.5ml Hydrocortisone, SAGM™ SingleQuots™ supplements
4) Add 0.5ml human Epidermal Growth Factor (hEGF), SAGM™ SingleQuots™ supplements
5) Add 0.5ml Epinephrine, SAGM™ SingleQuots™ supplements
6) Add 0.5ml Transferrin, SAGM™ SingleQuots™ supplements
7) Add 0.5ml Insulin, SAGM™ SingleQuots™ supplements
8) Add 0.5ml Retinoic Acid, SAGM™ SingleQuots™ supplements
9) Add 0.5ml Triiodothyronine, SAGM™ SingleQuots™ supplements
10) Add 5ml Bovine Serum Albumin – Fatty Acid Free (BSAFAF), SAGM™ SingleQuots™ supplements
11) Add 10ml of antibiotics penicillin-streptomycin (GIBCO®: 15140122)
12) Mix everything

Preparation of KIAD Culture Boost Medium

1) Make a solution of 10% (V/V) of Heat Inactivated HyClone™ FetalClone™ II Serum (GE Healthcare Life Sciences: SH30066.03) in SAGM (complete) Medium
2) Add 1 µl of 10µg/ml KGF solution for milliliter of SAGM (complete) Medium (10% Heat Inactivated HyClone™ FetalClone™ II Serum) to obtain a final concentration of 10ng/ml
3) Add 1 µl of 100mM IBMX solution for milliliter of SAGM (complete) Medium (10% Heat Inactivated HyClone™ FetalClone™ II Serum) to obtain a final concentration of 100µM

4) Add 1 µl of 100mM 8-Br-cAMP solution for milliliter of SAGM (complete) Medium (10% Heat Inactivated HyClone™ FetalClone™ II Serum) to obtain a final concentration of 100µM
5) Add 0.2µl of 1mM Dexamethasone solution for milliliter of SAGM (complete) Medium (10% Heat Inactivated HyClone™ FetalClone™ II Serum) to obtain a final concentration of 200nM

Note: SAGM (complete) Medium with added KIAD boost must be prepared fresh every time before use

KIAD (Culture Boost) Medium

Small Airway Basal Medium (SABM ™)	Lonza: CC-3119	Basal Media
SAGM™ SingleQuots™ supplements	Lonza: CC-4124	Bovine Pituitary Extract (BPE), 2ml; Hydrocortisone, 0.5ml; human Epidermal Growth Factor (hEGF), 0.5ml; Epinephrine, 0.5ml; Transferrin, 0.5ml; Insulin, 0.5ml; Retinoic Acid, 0.5ml; Triiodothyronine, 0.5ml; Bovine Serum Albumin – Fatty Acid Free (BSAFAF), 5.0ml
Heat Inactivated HyClone™ FetalClone™ II Serum (U.S.)	GE Healthcare Life Sciences: SH30066.03	10% (V/V)
Keratinocyte Growth Factor (KGF), also known as Basic Fibroblast Growth Factor 7 (FGF-7), human, recombinant in HEK	PromoCell C-63821	10ng/mL
Isobutyl methylxanthine (IBMX)	Sigma: I7018	100µM
8-Bromoadenosine 3',5'-cyclic monophosphate sodium salt (8-Br-cAMP	Sigma: B7880	100µM
Dexamethasone	Sigma: D4902	200nM
Penicillin Streptomycin	GIBCO®: 15140122	1%

Preparation KIAD supplements:

KGF (also known as FGF7) (PromoCell: C-63821)

- Reconstitute: 10µg of KGF in 1ml of culture grade water (Corning®: 25055CM)
- Store in -20˚C, replace every 3 months
- Dilution in medium: add 50µL (of 10µg/ml KGF solution) in 50mL of ALI-M for obtaining a final concentration of 10ng/ml

IBMX (3-Isobutyl-1-methylxanthine) (Sigma: I7018)

- MW: 222.24
- Reconstitute: 100mg in 4.4996ml of DMSO for obtaining a stock solution of 100mM
- Store in -20˚C, replace every 6 months
- Dilution in medium: add 50µl (of 100mM IBMX stock solution) in 50ml of SAGM for obtaining a final concentration of 100µM (0.1% DMSO)

8-Br-cAMP (Sigma: B7880)

- MW: 430.08
- Reconstitute: 100mg in 2.3251ml culture grade water for obtaining a stock solution of 100mM
- Store in -20˚C, replace every 1 year
- Dilution in medium: add 50µL (of 100mM 8-Br-cAMP stock solution) in 50ml of SAGM for obtaining a final concentration of 100µM

Dexamethasone (Sigma: D4902)

- MW: 392.46
- Reconstitute: 25mg in 63.7008ml DMSO for obtaining a stock solution of 1mM
- Store in -20˚C, replace every 6 months
- Dilution in medium: add 10µl (of 1mM Dexamethasone stock solution) in 50ml of ALI-M for obtaining a final concentration of 200nM (0.02% DMSO)

Preparation of the Open-Top Chip

Preparation of the Open-Top Chip is a multistep process that includes: preparation of the stroma equivalent, preparation of tissue-specific ECM coating, seeding of primary epithelial cells, seeding of primary endothelial cells, establishment of air-liquid-interface (ALI), and introduction of mechanical stretching. Typically, the best differentiation of epithelial tissues occurred when primary fibroblasts, smooth muscle and epithelial cells have not been subject to multiple expansions in flask (passage 1). Primary fibroblasts, endothelial and epithelial cells were harvested for seeding into the chip while in their active growth phase and were not allowed to reach full confluence on plate. In the first step of chip handling, the lid encased with top fluidic channel was removed to initiate the PDMS **chemical activation** by ER-1/ER-2 treatment.

ER1/ER2 Chemical activation

Chemical activation of the PDMS cavity is a critical step to ensure the covalent cross-linking of the ECM polymer to the PDMS and to guarantee the adhesion of the hydrogel throughout the entire length of the culture. Briefly, ER-1 (Emulate: 10461) and ER-2 (Emulate: 10462) are mixed at a concentration of 1mg/ml and added to the bottom microfluidic channel and to the circular cavity. The platform is then irradiated with high power UV light having peak wavelength of 365nm and intensity of 100µJ/cm^2 for 20min using a UV oven (CL-1000 Ultraviolet Crosslinker AnalytiK-Jena: 95-0228-01). The procedure is repeated twice to maximize the surface chemically activated.

Preparation ER1/ER2 cross-linker

1) Wrap an aluminum foil, approximately 15cm X 15cm, around a 15ml Falcon® tube (Corning®: 352196)
2) Reconstitute 5mg of ER-1 (Emulate: 10461) in 5ml of ER-2 (Emulate: 10462) for obtaining a stock solution of 1mg/ml in a 15ml falcon protected from light
    a. Add 3ml of ER2 to the 15ml Falcon® tube (Corning®: 352196) wrapped previously with aluminum foil
    b. Add 2ml of ER2 directly into the vial (5mg) and gently pipette up and down using a 1000µl pipette until the powder completely dissolves to obtain a stock solution of 2.5mg/ml
    c. Transfer the ER1/ER2 2.5mg/ml solution to the 15ml Falcon® tube (Corning®: 352196) wrapped previously with aluminum foil
    d. Thoroughly mix ER2/ER1 to obtain a homogeneous 1mg/ml solution
3) Add the ER2/ER1 1mg/ml solution directly to the bottom microfluidic channel and to the circular cavity

Image courtesy of Emulate, Inc.

Figure 2.2: Preparation of ER1/ER2 solution: On the left, image showing ER1/ER2 solution after mixing. At center, ER1/ER2 solution being inserted into aluminum cover to protect from light. On the right, ER1/ER2 solution covered with aluminum, important step to avoid that the solution photobleaches.

Chip functionalization by ER1/ER2 cross-linker activation (two-step activation procedure)

First activation cycle

1) Transfer the Open-top Chips loaded with ER1/ER2 solution into a Sterilin™ 100mm Square Petri Dishes (Thermo: 103)
2) Accommodate the Square Petri Dishes containing the Chips into the UV oven (CL-1000 Ultraviolet Crosslinker AnalytiK-Jena: 95-0228-01) leaving them at an approximate distance of 5cm from the UV lamps
3) Chose the "Time Program" on the machine (which correspond to an intensity of 100μJ/cm^2)
4) Select the time to 20 minutes
5) Turn on the UV oven

Second activation cycle

1) Transfer the activate Chips back into the hood (note: ER1/ER2 solution should have changed color from orange to brown)
2) Aspirate the ER1/ER2 solution
3) Wash the chip three time with ER2 to remove cross-linker residues
4) Repeat step 1 to 5

    1) Transfer the Open-top Chips loaded with ER1/ER2 solution into a Sterilin™ 100mm Square Petri Dishes (Thermo: 103)
    2) Accommodate the Square Petri Dishes containing the Chips into the UV oven (CL-1000 Ultraviolet Crosslinker AnalytiK-Jena: 95-0228-01) leaving them at an approximate distance of 5cm from the UV lamps
    3) Chose the "Time Program" on the machine (which correspond to an intensity of 100μJ/cm^2)
    4) Select the time to 20 minutes
    5) Turn on the UV oven on

5) Transfer the activate Chips back into the hood (note: ER1/ER2 solution should have changed color from orange to brown)
6) Aspirate the ER1/ER2 solution
7) Wash the chip three time with ER2 to remove cross-linker residues
8) Aspirate any ER2 solution
9) Completely dry the Chips leaving the Square Petri Dishes containing the Chips opened without the lid inside the hood for 5-10min
10) Chip are ready to be loaded with hydrogel

Open-Top Chip activation

Image courtesy of Emulate, Inc.

Figure 2.3: Open-top Chip activation: On the top, Open-top Chips loaded with ER1/ER2 solution into a Sterilin™ 100mm Square Petri Dishes. Magnified images showing the load of the cavity (left) and bottom channel (right). On the bottom, Sterilin™ 100mm Square Petri Dishes containing Open-top Chip accommodated inside the UV oven when turned off (left) and on (right).

Generation of the recreated stroma (or stroma equivalent)

We typically started the preparation of the stroma during the 20 minutes of the UV treatment. To prepare the stroma equivalent, a solution of bovine type I collagen (Advanced BioMatrix: 5133) was used. Briefly, 8 volumes of collagen I gel solution (10mg/ml) were mixed with 1 volume of 10X EMEM and 1 volume of 10X Reconstruction buffer while kept on ice to obtain a collagen solution at a final concentration of 8.0mg/ml. Typically, 10µl of 1 N NaOH for ml of collagen mixture were added to adjust its pH at around 7.4. Following the addition of NaOH the collagen mixture was thoroughly mixed. The change to the proper pH was visually evaluated by the switch in color from yellow to a brown/light pink of the collagen mixture. At this point, 1 volume of fibroblast (and/or Smooth muscle cells) solution (0.5×10^6 cells/ml) was added to the neutralized collagen solution and fully mixed by pipetting up and down without introducing

bubbles. Once the circular cavity is chemically activated by ER1/ER2 treatment, hydrogel embedded with primary fibroblasts and/or smooth muscle cells was loaded into the cavity and let crosslink with the PDMS, it forms what we define as: **recreated stroma (or stroma equivalent).** Additionally, a cylindrical 3D printed stamp (WaterShed XC11122, DSM Somos resin, ProtoLab) can be used to micromold the hydrogel surface to specific heights and with specific micropatterned geometries.

Preparation of the recreated stroma (or stroma equivalent):

Materials:

FibriCol® Type I Collagen Solution, 10mg/ml (Bovine) (Advanced BioMatrix: 5133)

NaOH (1 N) solution (Sigma: S2770)

Stamp (Emulate, Inc)

Preparation Hydrogel supplements:

10X Reconstruction buffer:

1) Dissolve in 2.2g sodium bicarbonate in 75 ml 0.067 M NaOH
2) add 4.7g HEPES (Sigma: H4034)
3) Adjust the PH to 7.4 using NaOH 1 N solution (Sigma: S2770)
4) Filter the 900 ml solution using 1 liter low-protein-binding (0.22µm pore mesh) Filtration System Membrane (Corning®: 431154)
5) Store working aliquots at –20˚C, up to 6 months.

10X DMEM:

1) Dissolve in 13.37g powdered DMEM (Thermo: 12100046) in 100ml of DI H_2O
2) Store working aliquots at –20˚C, up to 6 months.

Preparation of the recreated stroma (or stroma equivalent):

Calculate the number of stroma equivalent that are needed
based on this number, calculate the final volume of collagen I mixture needed

Following we report an example based on a typical experiment of 12 Open-top chips:

Calculation of the volume of hydrogel needed for 12 Open-top Alveolus-Chip: consider 12 cavity + 3 extras (which are needed to compensate FibriCol® losses due to collagen I that adheres to the surface of pipette)

Total number of fibroblasts needed:

$3.0X10^4$ lung fibroblasts per cavity X number of cavity (12+3) = $4.5X10^5$ fibroblasts

Total volume of collagen I solution needed:

In this contest, collagen I solution refer to a solution made of 8 parts of FibriCol®, 1 part of 10X Reconstruction Buffer and 1 part of 10X DMEM

Note: in order to prepare the collagen I solution, it is important to perform the entire procedure on ice using fridge cold (4˚C) FibriCol®, 10X Reconstruction Buffer and 10X DMEM supplements. This will avoid collagen I unwanted polymerization. **Important:** collagen I undergoes to reverse phase transition at 37˚C, which means that it irreversibly polymerizes when warmed at 37˚C.

150µl per cavity X (12+3) cavity = 2250µl of collagen I solution
10% of 10X DMEM = 225µl
10%of 10X Reconstruction buffer = 225µl.
80% (FibriCol® bovine type I collagen (10mg/ml) = 1800µl.
(Add 10µl of 1 N NaOH for each milliliter of collagen I solution, in this example you would add 2.25ml of collagen I solution x 10µl of 1N NaOH solution = 22.5µl of 1 N NaOH solution
(NaOH makes collagen to coagulate)

Stroma equivalent preparation:

1) Trypsinize the lung fibroblast using standard tissue-culture techniques.
   Note: best results are obtained when lung fibroblasts are collected in the phase of active growth, between 70% and 90% confluence
2) Resuspend the cell pellet in the predetermined amount of 10X DMEM
   Note: in our example you will use 225µl of 10X DMEM
3) Add with an equal amount of 10X Reconstitution buffer
4) **Note:** in our example you will add 225µl, when adding the reconstruction buffer, you will notice a change in color from orange to pink/red
5) Mix well the solution
6) Gently mix the previously calculated volume of FibriCol® without making bubbles
   Note: in our example you will use 1800µl of FibriCol®, you will notice a change in color from pink/red to yellow.
7) Add the previously calculated volume of 1 N NaOH
   Note: in our example you will add 22.5µl of 1N NaOH
8) Thoroughly mix the collagen I with the solution of 10X DMEM, Fibroblasts and 10X reconstruction buffer
   Note: you will notice the FibriCol®, 10X DMEM,10X Reconstruction buffer and NaOH will change in color from yellow to brown/red
9) Fill the Open-top Chip cavity previously activated by ER1/ER2 treatment with the prepared collagen I solution
10) Add a drop of collagen on the Stamp for 200µm tall gel
11) Insert the stamp inside the cavity by drop-to-drop fluidic connection to avoid trapping bubbles inside the hydrogel while casing it
12) Put the chip back into a Sterilin™ 100mm Square Petri Dishes (Thermo: 103)
13) Repeat the sequence of action 11 through 14 for all the 12 Open-top Chips

14) Put the Petri dishes containing the chips into the incubator at 37˚C
15) Let the collagen I solution polymerize for 2-4 hours

Preparation of Basal Lamina

Basal lamina has an important role in stimulating the expression of epithelial and endothelial specific markers. The procedure for recreating the basal lamina consist of coating the surface of the collagen I hydrogel (stroma) and the bottom channel surface with component of the extra cellular matrix (ECM) to enhance cellular adhesion, proliferation and differentiation.

Preparation ECM protein

Collagen IV from human placenta (Sigma: C5533-5MG)

Note: in order to reconstitute collagen IV powder, it is important to perform the entire procedure on ice using fridge cold (4˚C) culture grade water (Corning®: 25055CM). This will avoid any collagen IV polymerization during the aliquoting.

Collagen IV solubilization

1) Open the collagen IV vial being careful to keep the sealing cap clean and sterile
2) Add 5ml of fridge cold (4˚C) culture grade water (Corning®: 25055CM) directly into the collagen IV vial (5mg)
3) Close the collagen IV vial with the sealing cap you kept
4) Bring the collagen IV vial into the fridge (4˚C)
5) Let the powder slowly rehydrate overnight

Collagen IV aliquoting

1) Transfer the collagen IV vial into the hood vial on ice
2) Open the collagen IV sealing cap
3) Gently pipette up and down using a 1000µl pipette until the dense solution completely homogenize for obtaining a stock solution of 1mg/ml
4) Transfer the 1mg/ml collagen IV solution to microcentrifuge tube (Eppendorf: 0030121589) making aliquots of 1200µl and 200µl.
5) Store in -20˚C, replace every 3 months

Fibronectin, Human, Natural, (Corning®: 47743-654)

Note: in order to reconstitute fibronectin powder, it is important to perform the entire procedure on ice using fridge cold (4˚C) culture grade water (Corning®: 25055CM). This will avoid any fibronectin polymerization during the aliquoting.

Fibronectin solubilization

1) Open the fibronectin vial being careful to keep the sealing cap clean and sterile
2) Add 5ml of fridge cold (4˚C) culture grade water (Corning®: 25055CM) directly into the fibronectin vial (5mg)
3) Close the fibronectin vial with the sealing cap you kept
4) Bring the fibronectin vial into the fridge (4˚C)
5) Let the powder slowly rehydrate overnight

Fibronectin aliquoting

1) Transfer the fibronectin vial into the hood vial on ice
2) Open the fibronectin sealing cap
3) Gently pipette up and down using a 1000µl pipette until the dense solution completely homogenize for obtaining a stock solution of 1mg/ml
4) Transfer the 1mg/ml fibronectin solution to microcentrifuge tube (Eppendorf: 0030121589) making aliquots of 300µl.
5) Store in -20˚C, replace every 3 months

Laminin, 521 CTG (CT521), human recombinant laminin 521 (Biolamina: CT521-0501)

Note: in order to aliquot laminin, it is important to perform the entire procedure on ice. This will avoid any laminin polymerization during the aliquoting.

Laminin solubilization

1) Thaw the laminin vial into the fridge (4˚C) overnight

Laminin aliquoting

1) Transfer the laminin vial into the hood on ice
2) Open the laminin vial being careful to keep the vial clean and sterile
3) Gently pipette up and down using a 200µl pipette until the dense solution completely homogenize (do not discard the tip, but use this tip to aliquot the solution to avoid loss of material along the pipette tip)
4) Transfer laminin to microcentrifuge tube (Eppendorf: 0030121589) making aliquots of 30µl
5) Store in -20˚C, replace every 3 months

Alveolar epithelium basal lamina coating

Note: in order to prepare the alveolar epithelium basal lamina coating, it is important to perform the entire procedure on ice. This will avoid any protein polymerization during the aliquoting.

Collagen IV-Fibronectin-Laminin coating

1) Slowly thaw the collagen IV (containing 1200µl of 1mg/ml collagen IV solution), fibronectin (containing 300µl of 1mg/ml fibronectin solution) and laminin (containing 30µl of laminin) microcentrifuge tube into the fridge (4˚C) overnight
2) Move the collagen IV, fibronectin and laminin microcentrifuge tube into the hood on ice
3) Transfer the content of the fibronectin microcentrifuge tube (300µl of 1mg/ml fibronectin solution) into the collagen IV microcentrifuge tube (containing 1200µl of 1mg/ml collagen IV solution), being careful to keep them clean and sterile
4) Transfer the content of the laminin microcentrifuge tube (containing 30µl of laminin) into the collagen IV/fibronectin microcentrifuge tube (containing 1200µl of 1mg/ml collagen IV solution + 300µl of 1mg/ml fibronectin solution), being careful to keep them clean and sterile
5) Gently pipette up and down using a 1000µl pipette until the dense solution completely homogenize
6) Transfer 50µl of Collagen IV-Fibronectin-Laminin solution directly on the hydrogel surface

7) Let polymerize for 2-4 hours inside the incubator at 37 °C, 5% CO_2

Alveolar endothelium basal lamina coating

Note: in order to prepare the alveolar endothelium basal lamina coating, it is important to perform the entire procedure on ice. This will avoid any protein polymerization during the aliquoting.

Collagen IV- FibriCol® coating

1) Slowly thaw the collagen IV (containing 200µl of 1mg/ml collagen IV solution) microcentrifuge tube into the fridge (4˚C) overnight
2) Move the collagen IV microcentrifuge tube and FibriCol® into the hood on ice
3) Prepare 10ml fridge cold (4˚C) culture grade water (Corning®: 25055CM) in a 15ml Falcon® tube (Corning®: 352196) on ice
4) Transfer 200µl of FibriCol® (10mg/ml collagen I solution) into 10ml of fridge cold (4˚C) culture grade water (Corning®: 25055CM), which give a 200µg/ml Collagen I solution
5) Transfer the 800µl FibriCol® solution (200µg/ml Collagen I) to the collagen IV microcentrifuge tube (containing 200µl of 1mg/ml collagen IV solution), being careful to keep the microcentrifuge tube clean and sterile
6) Gently pipette up and down using a 1000µl pipette until the dense solution completely homogenize
7) Transfer 20µl of Collagen IV- FibriCol® coating solution directly into the spiraled bottom channel of the Chips
8) Let polymerize for 2-4 hours in the incubator at 37°C, 5% CO_2

Generation of the epithelium compartment

The epithelial cells are typically seeded on the top of the recreated stroma and cultured in a submerged state until the cells form a compact monolayer. The monolayer lining the top of the stomal equivalent together with the top microfluidic channel forms what we define: **epithelium compartment** (Fig S 1). The top microfluidic channel is connected to an inlet and an outlet port that can be used to perfuse the epithelial tissue with culturing medium, airflow or to expose it to static air. This feature is particularly important because it enables the establishment of an **air-liquid interface (ALI)**. The top microfluidic channel can also be opened or removed to allow direct access to the stromal compartment (**open-top capability**).

Preparation of the epithelium compartment:

Materials
Human Primary **Alveolar Epithelial** Cells (Cell Biologics Cat. #: H-6053)
Recombinant Human **Epidermal Growth Factor** (E. coli-derived) (PromoCell C-60170)
SAGM™ Small Airway Epithelial Cell Growth Medium BulletKit™ (Lonza CC-3118)
Materials
Trypan blue counting solution
Hemocytometer

15 mL conical tubes
Serological pipettes
Pipettes and filtered tips
Aspirator and sterile tips
Ice bucket and ice

Preparation of SAGM (seeding) Medium

1) Add 500ml of Small Airway Basal Medium (CC-3119) to a Corning® Easy-Grip round, plastic, 500ml storage bottle (Corning®: 430282)
2) Add 2ml Bovine Pititуary Extract (BPE), SAGM™ SingleQuots™ supplements
3) Add 0.5ml Hydrocortisone, SAGM™ SingleQuots™ supplements
4) Add 0.5ml human Epidermal Growth Factor (hEGF), SAGM™ SingleQuots™ supplements
5) Add 0.5ml Epinephrine, SAGM™ SingleQuots™ supplements
6) Add 0.5ml Transferrin, SAGM™ SingleQuots™ supplements
7) Add 0.5ml Insulin, SAGM™ SingleQuots™ supplements
8) Add 0.5ml Retinoic Acid, SAGM™ SingleQuots™ supplements
9) Add 0.5ml Triiodothyronine, SAGM™ SingleQuots™ supplements
10) Add 5ml Bovine Serum Albumin – Fatty Acid Free (BSAFAF), SAGM™ SingleQuots™ supplements
11) Add 10ml of antibiotics penicillin-streptomycin (GIBCO®: 15140122)
12) Mix everything
13) Add 50ml of Heat Inactivated HyClone™ FetalClone™ II Serum (GE Healthcare Life Sciences: SH30066.03) to 500ml storage bottle

Before use

14) Add 1 µl of 10µg/ml EGF solution for milliliter of SAGM (seeding) Medium to obtain 10ng/ml final concentration

SAGM (seeding) Medium

Small Airway Basal Medium (SABM ™)	Lonza: CC-3119	Basal Media
SAGM™ SingleQuots™ supplements	Lonza: CC-4124	Bovine Pititуary Extract (BPE), 2ml; Hydrocortisone, 0.5ml; human Epidermal Growth Factor (hEGF), 0.5ml; Epinephrine, 0.5ml; Transferrin, 0.5ml; Insulin, 0.5ml; Retinoic Acid, 0.5ml; Triiodothyronine, 0.5ml;

		Bovine Serum Albumin – Fatty Acid Free (BSAFAF),5.0 ml
Heat Inactivated HyClone™ FetalClone™ II Serum (U.S.)	GE Healthcare Life Sciences: SH30066.03	10% (V/V)
Recombinant Human Epidermal Growth Factor (E. coli-derived) recombinant EGF	Invitrogen: PHG0313	10ng/mL
Penicillin Streptomycin	GIBCO®: 15140122	1% (V/V)

EGF (Invitrogen: PHG0313)

- Reconstitute: 10µg of EGF in 1ml of SAGM full medium
- Store in -20˚C, replace every 3 months
- Dilution in medium: add 10µl (of 10µg/ml EGF solution) in 10mL of SAGM (seeding) Medium for obtaining a final concentration of 10ng/ml

Preparation of the alveolar epithelium

Calculate of the number of alveolar epithelia that are needed
based on this number, calculate the final volume of alveolar cells needed:

Following we report an example based on a typical experiment of 12 Open-top chips:

Total number of alveolar cells needed:

$1X10^5$ Alveolar Epithelial Cells per cavity X number of cavity (12) = $1.2X10^6$ alveolar cells

Alveolar cells preparation:

1) Pre-warm DPBS and SAGM complete medium by placing them at 37°C.
2) Bring the culture flask (e.g., T-75) containing Human Primary Alveolar Epithelial Cells (Cell Biologics: H-6053) from the incubator into the biological safety cabinet (BSC)
3) Aspirate culture medium and add 10ml of warm 1X DPBS to the sides of the flask away from the cells. Wash the culture surface by rocking the flask. Aspirate the DPBS wash from the side of the flask
4) Add 4 ml of TrypLE™ Express Enzyme (1X), no phenol red (Thermo: 12604013) to the flask Incubate for 5 minutes maximum at 37°C
5) Tap the side of the flask gently and inspect the culture under the microscope once per minute until complete detachment of cells from the culture surface is achieved

6) Add 8 ml of warm SAGM complete medium to the flask and pipette gently collect all cells from the culture surface
7) Transfer the contents of the flask (12 ml) into a sterile 15 m conical tube

Alveolar cell counting

8) Pipette gently to create a homogeneous mixture and transfer 20µl of the cell suspension to the 20µl trypan blue cell counting solution (Sigma: 93595). This will make a 1:1 dilution
9) Transfer 10µl to the two cell counting chambers of the hemocytometer
10) Gently mix the counting suspension and count cells using a manual hemocytometer

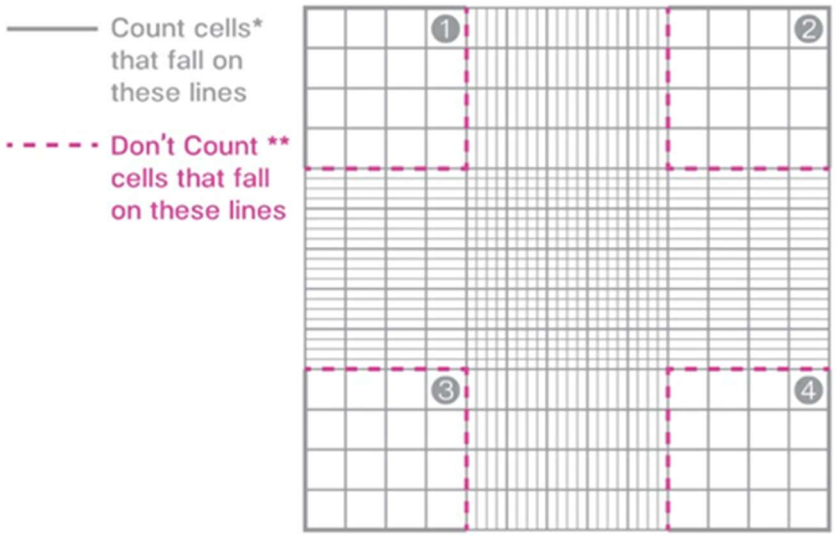

Manual hemocytometer

11) Count both viable and non-viable cells in each quadrant of the hemocytometer. Live Cell Count; Dead Cell Count; Total Cell Count
12) Calculate percent viability of the cell solution.
Note: (Live Cells) ÷ (Total Cells) x 100 = % Viability
13) Calculate viable cell concentration.
Note: The dilution factor is 2 when using a 1:1 mix with trypan blue solution as described above. The total volume with cells is 12 ml.
(Live Cell Count x dilution factor x total volume x 10^4) ÷ 4 = Viable Cell Concentration (cells / ml)
14) Calculate viable cell yield.
Note: (Viable Cell Concentration) x (Cell Suspension Volume) = Viable Cell Yield (cells)
15) Pellet alveolar cells by centrifugation at 1200 r.p.m. for 5 min in a 15ml conical tube
16) Aspirate the supernatant solution
17) Re-suspend the cell pellet in SAGM (seeding) Medium at a concentration of $2x10^6$ cell/ml
18) Add 50µl of the $2x10^6$ alveolar cell solution + EGF to each of the recreated stroma
19) Leave alveolar cells attach for 1 hours into incubator

After **2 hours:**

1. Aspirate the supernatant SAGM (seeding) medium being careful to not touch the epithelium surface
2. Add 200µl of fresh SAGM complete medium
3. Change SAGM complete medium every day (every about 18-24 hours)

Generation of the endothelial lumen (double cell seeding procedure)

Primary human endothelial cells are cultured on all surfaces of the bottom microfluidic channel. The full channel coverage is achieved by chemically activating the PDMS surface of the microfluidic channel wall and by coating it with ECM to improve endothelial cell adhesion and coverage. Following the ECM coating a double seeding technique is used to form a complete endothelial lumen that can be perfused with medium, blood or other fluids (serum, medium with PBMC, blood surrogate). The double seeding procedure is a two-part process, the first part involves the loading of the chip bottom microfluidic channel with an endothelial cell suspension of 3×10^6cells/ml. The chip is then flipped upside down to let endothelial cells attach to the membrane side of the microfluidic channel during a one-hour incubation. The second part involves flushing the bottom microfluidic channel with medium to remove cellular debris and a second loading of the microfluidic channel with an endothelial cell suspension of 3×10^6cells/ml. During this second seeding the chip is not flipped and set flat to let endothelial cells attach to the bottom wall of the microfluidic channel during a one-hour incubation, which is once again flushed to remove cellular debris. After flushing, the chips are kept into the incubator in static condition for a few hours to overnight to let endothelial cells proliferate and form a complete lumen before connecting to the pump.

Preparation of the endothelium compartment:

Materials

Human **Lung Microvascular** Endothelial Cells – HMVEC-L (Lonza: CC-2527)
EGM™ -2MV Microvascular Endothelial Cell Growth Medium-2 (Lonza: 3202)
Trypan blue counting solution
Hemocytometer
15 ml conical tubes
Serological pipettes
Pipettes and filtered tips
Aspirator and sterile tips
Ice bucket and ice

Preparation of EGM-2 MV (complete) Medium

1) Add 500ml of EBM™-2 Basal Medium (CC-3156) to a Corning® Easy-Grip round, plastic, 500ml storage bottles (Corning®: 430282)
2) Add Bottle FBS, 25.0mL, EGM™-2 MV SingleQuots™ supplements
3) Add 0.2ml Hydrocortisone, EGM™-2 MV SingleQuots™ supplements
4) Add 0.5mL VEGF, EGM™-2 MV SingleQuots™ supplements
5) Add 0.5mL R3-IGF-1, EGM™-2 MV SingleQuots™ supplements
6) Add 0.5ml Ascorbic Acid, EGM™-2 MV SingleQuots™ supplements
7) Add 0.5ml hEGF, EGM™-2 MV SingleQuots™ supplements
8) Add 10ml of antibiotics penicillin-streptomycin (GIBCO®: 15140122)
9) Mix everything

EGM™-2MV (complete) Medium

EGM™ -2 MV Microvascular Endothelial Cell Growth Medium-2 BulletKit™	Lonza: CC-3202	EBM™-2 Basal Medium (CC-3156)
EGM™-2 MV Microvascular Endothelial Cell Growth Medium SingleQuots™ supplements	Lonza: CC-4147	Bottle FBS, 25.0mL Hydrocortisone, 0.20mL hFGF-B, 2.0mL VEGF, 0.50mL R3-IGF-1, 0.50mL Ascorbic Acid, 0.50mL hEGF, 0.50mL
Penicillin Streptomycin	GIBCO®: 15140122	1% (V/V)

Preparation of the endothelium compartment:

Calculate of the number of HMVEC-L endothelial cells that are needed
Note: This is a double seeding so the number of cells must be multiplied by 2
based on this number, calculate the final volume of HMVEC-L endothelial cells needed:

Following, we report an example based on a typical experiment of 12 Open-top chips:

HMVEC-L endothelial cells preparation:

1) Pre-warm DPBS and EGM-2MV complete medium by placing them at 37°C.
2) Bring the culture flask (e.g., T-75) containing HMVEC-L – Human Lung Microvascular Endothelial Cells (Lonza: CC-2527) from the incubator into the biological safety cabinet (BSC).
3) Aspirate culture medium and add 10ml of warm 1X DPBS to the sides of the flask away from the cells. Wash the culture surface by rocking the flask. Aspirate the DPBS wash from the side of the flask.
4) Add 4 ml of TrypLE™ Express Enzyme (1X), no phenol red (Thermo: 12604013) to the flask. Incubate for 5 minutes maximum at 37°C

5) Tap the side of the flask gently and inspect the culture under the microscope once per minute until complete detachment of cells from the culture surface is achieved.
6) Add 8 ml of warm EGM-2MV complete medium to the flask and pipette gently collect all cells from the culture surface
7) Transfer the contents of the flask (12ml) into a sterile 15ml conical tube
8) Pipette gently to create a homogeneous mixture and transfer 20 µl of the cell suspension to the 20 µl trypan blue cell counting solution (Sigma: 93595). This will make a 1:1 dilution
9) Transfer 10µl to the two cell counting chambers of the hemocytometer
10) Gently mix the counting suspension and count cells using a manual hemocytometer
    a.

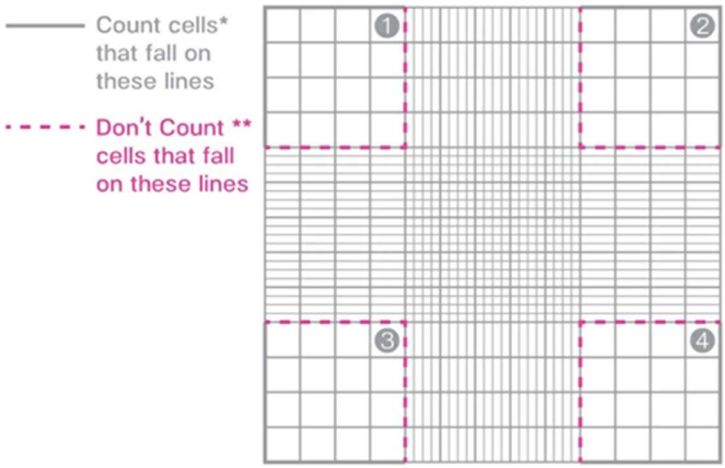

Manual hemocytometer

11) Count both viable and non-viable cells in each quadrant of the hemocytometer.
    Note: Live Cell Count; Dead Cell Count; Total Cell Count
12) Calculate percent viability of the cell solution.
    Note: (Live Cells) ÷ (Total Cells) x 100 = % Viability
13) Calculate viable cell concentration.
    Note: The dilution factor is 2 when using a 1:1 mix with trypan blue solution as described above. The total volume with cells is 12 ml.
    (Live Cell Count x dilution factor x total volume x 10^4) ÷ 4 = Viable Cell Concentration (cells/ml)
14) Calculate viable cell yield.
    Note: (Viable Cell Concentration) x (Cell Suspension Volume) = Viable Cell Yield (cells)
15) Pellet HMVEC-L endothelial cells by centrifugation at 1200 r.p.m. for 5 min in a 15ml conical tube
16) Aspirate the supernatant solution
17) Re-suspend the cell pellet in EGM-2MV complete medium at a concentration of 3x10^6cell/ml

Seeding of HMVEC-Ls to Bottom Channel (double seeding procedure)

Note: work with one chip at a time. After seeding the first chip, invert the chip and seed the next one.

1) Seed 25µl of the HMVEC-L suspension into the bottom channel
2) After seeding, invert each chip and rest the edge of the chip carrier on the chip cradle. **Note:** Each chip cradle can support up to 6 chips inside a 150mm cell culture dish (see figure below).

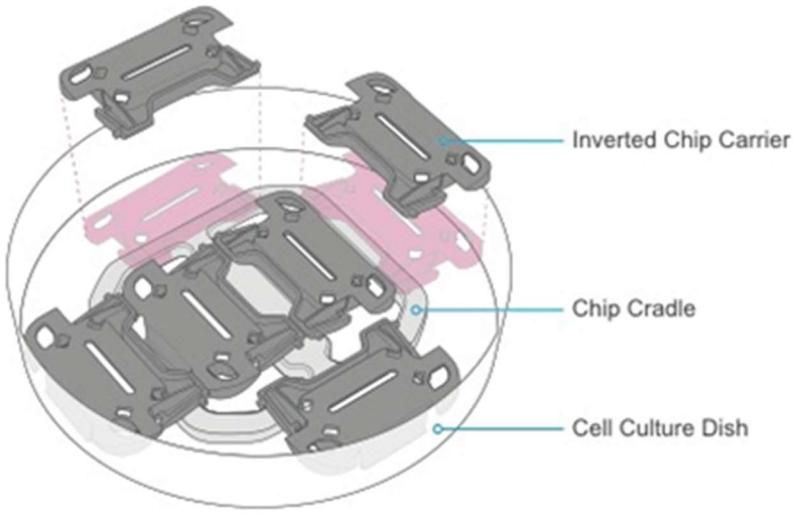

Cradle Inverting chips during endothelial attachment

3) Place the small reservoir (15 ml conical tube cap containing sterile DI H_2O) inside the 150mm Petri dish to provide humidity for the cells
4) Replace dish lid on top
5) Place the dishes with Chips in the incubator at 37°C for approximately 1 hours, or until cells in the bottom channel have attached

After **1 hours:**

6) Bring the chip cradle contained inside a 150mm cell culture dish back to the BSC
7) Repeat HMVEC-L endothelial cells procedure (step 1 to 15)
8) Seed 25µl of the HMVEC-L suspension into the bottom channel
9) Place the small reservoir (15ml conical tube cap containing sterile DPBS) inside the 150 mm dish to provide humidity for the cells. Replace dish lid.
10) Place the chips still in the dish in the 37°C incubator for approximately 1 hours, or until cells in the bottom channel have attached
11) Wash the bottom channel with fresh EGM-2MV complete medium to remove non-attached cells and cell debris.
12) Keep the chip in static, overnight.

Open-Top Chip (sequence of action)

Following the UV activation of the Open-Top Chip, collagen I hydrogel with embedded fibroblasts and/or smooth muscle cells is pipetted in the stromal cavity of the Open-top Chip, compressed using a special cylindrical stamp to 2mm (skin, airway and enteroid) or 200µm (Alveolus) tall gels and let polymerize at 37 °C, 5% CO_2 for 60min. After polymerization, the stamp is removed and the hydrogel surface and bottom spiraled channel is coated with a solution of collagen IV for skin, airway and enteroid and collagen IV,

fibronectin and laminin (1200µl of 1mg/ml solution + 300µl of 1mg/ml solution + 30µl of 1mg/ml) for alveolus. These coatings mimic the basal lamina of the respective epithelia and improve epithelial cell adhesion. ECM coating solutions are left to polymerize for 2-4 hours at 37 °C, 5% CO_2 to ensure that the spiraled channel and the epithelial surface of the stroma equivalents are properly coated. After coating, the recreated stroma is maintained in a static condition. Both top and bottom channels are filled with medium, DMEM/F12 GlutaMax supplemented with 10% serum (Heat Inactivated HyClone™ FetalClone™ II Serum (U.S.) GE Healthcare Life Sciences: SH30066.03) and kept in this submerged status for 24/48 hours to let fibroblasts and/or smooth muscle cells recover from the embedding procedure.

Two days after the generation of the stromal equivalent human primary epithelial cells (airway, alveolar pneumocytes and keratinocytes) are detached from the T75 flask using TrypLe (GIBCO®: A1285901), or in the case of enteroids, extracted from Matrigel® (Corning®: 356231) by enzymatic digestion with cell recovery solution (Corning®: 354243), and collected in 15ml conical containing medium supplemented with 10% serum, centrifuged at 1200 r.p.m. for 5min, and re-suspended in SAGM complete medium (alveolar and airway cells), Keratinocyte-SFM (keratinocytes) and Expansion Medium (enteroids) at a concentration of 2×10^6cells/ml. Cells are then cultured in static conditions until they formed a confluent monolayer (typically in 24-48 hour). Following the formation of a confluent epithelium monolayer, human endothelial cells were added to the bottom spiraled shaped microfluidic channel for skin, airway and alveolus models. Two sequential seedings were performed, a first seeding in which chips were flipped upside down to allow endothelial cells to attach to the membrane side and a second seeding in which chips were seeded to allow endothelial cells to attach to the bottom of the spiraled shaped microfluidic channel. Endothelial cells were let attach for 1 hour and fed in static condition for 8 hours (overnight) using EGM-2MV complete medium, while epithelial cells were kept submerged in their respective epithelial medium. Following the endothelial seeding procedure, we proceed to connect chip to the pump system. In this first stage, medium is continuously perfused for 24 hours in both the lower spiral shaped and the upper channel to provide cells with nutrients and to remove metabolic wastes. Depending on the tissue type, cells can be maintained in this regime (defined as submerged) indefinitely for the entire length of the experiment (typically 14 to 21 days) or brought at air-liquid interface (ALI), which means that the medium was removed from the upper channel to expose the epithelial cells to direct contact with air. In the bottom spiraled microfluidic channel, the flow rate is maintained at 60µl/hr (0.008 dyne/cm^2) to supply nutrients to the epithelium, which occurs by diffusion through the membrane and the stroma equivalent. Depending on the organ, negative vacuum pressure can be applied to the vacuum chambers to stretch the recreated stroma along with the epithelium. In this study, we tested 5% stretching at a frequency of 0.2Hz, value comparable with that observed in living human organ (as reported by Kostantin and colleagues). Chips are stretched starting on day 9 using this condition until they were sacrificed for analysis (generally at day 12days).

List of Materials & Equipment

Equipment	Description	Supplier	Catalog Number
Zoë-CM1™ Culture Module	1 per 12 chips	Emulate	-

Orb-HM1® Hub Module	1 per 4 Zoës	Emulate	-
OT-Chip™ Stretchable Chip	12 per Zoë	Emulate	-
Pod™ Portable Modules	1 per Chip-S1	Emulate	-
UV Light Box	1 per Zoë	Emulate	-
Chip Cradle	Autoclaved, 1 per 6 chips	Emulate	-
150 mm cell culture dish	Sterile, 1 per 6 chips	Corning® / Falcon®	353025
Handheld vacuum aspirator	-	Corning®	4930
Aspirating pipettes	2 mL, polystyrene, individually wrapped	Corning® / Falcon®	357558
Aspirating tips	Sterile (autoclaved)	-	-
Serological pipettes	2 mL, 5 mL, 10 mL, and 25 mL low endotoxin, sterile	-	-
Pipette	P20, P200, and P1000	-	-
Pipette tips	P20, P200, and P1000 sterile, low-adhesion	-	-
Conical tubes	15 mL and 50 mL polypropylene, sterile	-	-
Microcentrifuge tube	1.5 mL, sterile	-	-
Aluminum foil	-	-	-
Microscope (with camera)	For bright-field imaging	-	-
Hemocytometer	-	-	-
Manual counter	-	-	-
Water bath (or beads)	Set to 37°C	-	-
Vacuum set-up	Minimum pressure: -70 kPa	-	-
T25 flasks	-	-	-
T75 flasks	-	-	-
Ice bucket	-	-	-
70% ethanol and wipes	For surface sterilization	-	-

List of Reagents & Supplements

Reagent	Description	Supplier	Catalog Number
ER-1™ surface activation reagent	5 mg powder	Emulate	-
ER-2™ surface activation reagent	25 mL bottle	Emulate	-

Dulbecco's PBS (DPBS-/-) (without Ca^{2+}, Mg^{2+})	1X	Corning®	21-031-CV
Trypan blue	0.4% solution	Sigma	93595
TrypEE solution	Cell detaching solution	Sigma	12604013
Fibronectin, Human, Natural,	human plasma fibronectin	Corning®	47743-654
Laminin, 521 CTG (CT521)	human recombinant laminin 521	Biolamina	CT521-0501
Collagen-I solution	FibriCol® 10 mg/mL	Advanced BioMatrix	5133-20ML
Collagen-IV solution	Collagen from human placenta, 5 mg powder, reconstitute to 1 mg/mL	Sigma	C5533-5MG
Penicillin-streptomycin	10,000 U/mL; 10 mg/mL	Sigma	P4333
Hydrocortisone	Medium supplement	PromoCell	C-64420
Heparin solution	Medium supplement	Sigma	H3149
HyClone™ FetalClone™ II Serum (U.S.)	Sterile FBS heat-inactivated	GE Healthcare	SH30066.02HI
SAGM™ Small Airway Epithelial Cell Growth medium BulletKit™	Medium supplements	Lonza	CC-4124
EGF	Medium supplement	PromoCell	C-60170
KGF (also known as FGF7)	Medium supplement	PromoCell	C-63821
VEGF-165	Medium supplement	PromoCell	C-64420
8-Br-cAMP	Medium supplement	Sigma	B7880
Dexamethasone	Medium supplement	Sigma	D4902
DMEM/F-12, GlutaMAX™	Basal medium for ALI medium	GIBCO®	10565-018

Media

Medium	
SAGM (complete) Medium	See page 66, paragraph: **"Preparation of the epithelium compartment"**

EGM—2MV (complete) Medium	See page 70 paragraph: **"Preparation of the endothelium compartment"**
KIAD boost*	See page 56 paragraph: **"KIAD (Culture Boost) Medium"**
ALI-M (199A) Medium**	See page 53 paragraph: **"ALI-M (199A) Medium"**

Note: cell culture media need to be freshly prepared before starting any new experiment as some of the factors are not stable for more than two weeks

*Starting from day 2, the SAGM (complete) medium can be supplemented with KIAD supplements to enhance surfactant production and barrier function

**Starting from day 6 the ALI can be implemented in the system to enhance surfactant production and barrier function

Open-Top Alveolus-Chip experimental timetable

The experimental timetable below describes the medium and stretching conditions for the vary phases of Open-Top Alveolar-Chip culture.

Note: The medium and stretching regime changes over the course of Alveolus-Chip culture to drive the maturation of the alveolar and endothelial cell populations.

Time	Top Channel medium & flow rate (µl/hr)	Bottom Channel medium & flow rate (µl/hr)	Stretching (%strain)
Day 1	SAGM (complete) Medium + 10% FetalClone™ II Serum (static)	SAGM (complete) Medium + 10% FetalClone™ II Serum (static)	0%
Day 2	SAGM (complete) Medium + 10% FetalClone™ II Serum (static)	SAGM (complete) Medium + 10% FetalClone™ II Serum (static)	0%
Day 3	KIAD boost (static)	SAGM (complete) Medium + 10% FetalClone™ II Serum (static)	0%
Day 4	KIAD boost (static)	EGM-2MV (complete) Medium (static)	0%
Day 5	ALI	ALI-M (199A) Medium	0%
Day 6	ALI	ALI-M (199A) Medium	0%
Day 7	ALI	ALI-M (199A) Medium	0%

Day 8	ALI	ALI-M (199A) Medium	0%
Day 9	ALI	ALI-M (199A) Medium	4%
Day 10	ALI	ALI-M (199A) Medium	4%
Day 11	ALI	ALI-M (199A) Medium	4%
Day 12	ALI	ALI-M (199A) Medium	4%

Day -7 to -1

2D Cell Expansion

Day 0

ER1/ER2 Chemical activation

As protocol

Preparation of the recreated stroma (or stroma equivalent)

As protocol

Preparation of Basal Lamina

As protocol

Preparation of the alveolar epithelium

As protocol

Seeding Human Alveolar Epithelial Cells (HAECs)

1) Gently wash HAECs on flask with PBS
2) Add TrypLE Express to flask and incubate at 37ºC for at least 5 minutes
3) Count cells
4) Collect cells and centrifuge at 1200 r.p.m. for 5 minutes at RT
5) Re-suspend HAECs in appropriate volume to obtain 2 x 10^6 cells/ml
6) Take chips from incubator and aspirate the basal lamina coating solution on the surface of the chip cavity
7) Seed cavity with 50µl of HAEC cell suspension
8) Incubate for at least 2 hours
9) Gently wash the top cavity with SAGM complete medium twice
10) Incubate chips at 37ºC

Day 1

Chip Maintenance

1) Gently wash top cavity with SAGM complete medium twice
2) Refresh media in the top cavity with fresh SAGM complete medium
3) Refresh media in the bottom channel with fresh SAGM complete medium
4) Maintain the culture in static condition

Day 2

Chip Maintenance

1) Gently wash top cavity with SAGM complete medium twice
2) Refresh medium in the top cavity with fresh SAGM complete medium
3) Refresh medium in the bottom channel with fresh SAGM complete medium
4) Maintain the culture in static condition

Day 3

Chip Maintenance

1) Gently wash top cavity with SAGM complete medium twice
2) Refresh medium in top cavity with fresh KIAD boost medium
3) Refresh medium in bottom channel with fresh SAGM complete medium
4) Maintain the culture in static condition

Day 4

Chip Maintenance

1) Gently wash top cavity with SAGM complete medium twice
2) Refresh medium in top cavity with fresh KIAD boost medium
3) Refresh medium in bottom channel with fresh SAGM complete medium
4) Maintain the culture in static condition

Day 4

Double Seeding Human Microvascular Endothelial Cells (HMVEC-Ls)

1) Gently wash HMVEC-Ls on flask with PBS
2) Add TrypLE to flask and incubate at RT for 5 minutes
3) Add media to flask, collect cells, and centrifuge at 1200 r.p.m. for 5 minutes at RT
4) Count the cells
5) Re-suspend HMVEC-Ls in appropriate volume to attain 3 x 10^6 cells/ml
6) Take chips from incubator, wash the vascular channel with EGM-2 MV, and aspirate any media that has accumulated on the surface of the chip
7) Seed bottom channel with 25µl of HMVEC-L cell suspension
8) Flip chips upon seeding
9) Incubate for one hour
10) After one hour, take chips from incubator and flip chips right side up and gently wash bottom channel with EGM-2MV
11) Seed bottom channel with 25µl of HMVEC-L cell suspension
12) Incubate for one hour
13) After one hour, take chips from incubator and gently wash bottom channel with EGM-2MV
14) Gently wash top cavity with fresh SAGM complete medium twice
15) Refresh KIAD boost medium in top cavity
16) Incubate chips at 37ºC
17) Maintain the culture in static condition

Day 5

Chip Maintenance

1) Gently wash top cavity with SAGM complete medium twice
2) Refresh medium in top cavity with fresh KIAD boost medium
3) Refresh medium in bottom channel with fresh ALI-M (199A) medium
4) Maintain the culture in static condition

Day 6

Introduction of Air-Liquid Interface (ALI)

1) Take chips from incubator into the biosafety cabinet (BSC)
2) Refresh ALI-M(199A) medium in the vascular channel
3) Aspirate medium out of the top cavity exposing epithelium at ALI
4) Mount chip top fluidic and connect chips to the pump system
5) Set top channel flow rates to 0µl/hr
6) Set bottom channel flow rates to 60µl/hr

Day 8

Chip Maintenance Under Air-Liquid Interface (ALI)

1) Stop the flow
2) Aspire old leftover ALI-M(199A) medium
3) Add fresh ALI-M(199A) medium to the reservoir of connected to bottom channel
4) Re-start the flow in bottom channel maintaining the previous setup of 60ul/hr

Day 9

Introduction of Stretch (5%)

1) Maintain ALI-M(199A) medium flowing at 60µl/hr in bottom channel
2) Turn-on the pneumatic actuator and set the stretching to 5%

Day 11

Chip Maintenance Under ALI and Stretch (5%)

1) Stop the flow and the pneumatic actuator
2) Aspire old leftover ALI-M(199A) medium
3) Add fresh ALI-M(199A) medium to the reservoir of connected to bottom channel
4) Re-start the flow in bottom channel maintaining the previous setup of 60ul/hr
5) Re-start the pneumatic actuator (previously set to 5% stretch)

Day 11

Finish Experiment

1) Process chips for analysis

Immunohistochemistry

Open-top Organ-Chip were fixed in 10% neutral buffered formalin. Endothelial and epithelial cells were stained directly inside the chip by performing the immunofluorescence staining steps directly inside the respective microfluidic channel. Alternatively, the epithelium equivalents (recreated stroma with epithelium) were extracted from the chip, fixed in 10% neutral buffered formalin for at least 24 hours, dehydrated by a series of alcohol washes of increasing concentrations (70%, 80%, two of 95%, three of 100% ethanol), cleared by two washes in xylene and infiltrated by paraffin using a tissue processor (Leica TP1020) before being embedded into paraffin wax (Leica HistoCore Arcadia H & C) and cut in sections (typically between 8-12 micrometers thick) with a microtome (Leica RM2235). Sections were placed on Poly-L-Lysine coated microscope glass slides (Sigma: P0425) according to standard immunohistochemistry procedure and processed for immunohistochemistry analysis. For H&E staining, paraffin was removed by two changes in xylene of 5 minutes, the slides were rehydrated by sequential ethanol washes (two of 100% ethanol, and one wash each of 95% and 70% ethanol) and a final rinse in ddH_2O for 2 minutes. Slices were then stained by in Gill 2 hematoxylin solution (VWR: 10143-146) for 10 min, washed sequentially with deionized water for one-minute, acetic alcohol for 20 second, bluing agent (VWR: CA95057-852) 10 dip, and 70% ethanol for one minute before being counterstained with eosin Y alcoholic (VWR 10143-132) for 2 minutes. Followed by a series of ethanol washes (two of 95% ethanol, three of 100% ethanol) and finally cleared by two washes in xylene for 5 minutes. Slides were then mounted with Permount (EMS:

17986-05) and glass coverslips. For formalin-fixed paraffin-embedded tissues, antigen-retrieval was performed by boiling the tissue in epitope retrival solution (IHC-Tek: IW-1100) using a pressure cooker (IHC-Tek: 1102).

Immunofluorescence

Cells were permeabilized using 0.1% Triton X-100 (Sigma: T8787) solution in Dulbecco's phosphate-buffered saline for 20 min, followed by blocking of non-specific binding with blocking solution containing 1% bovine serum albumin (Thermo: 37525), and 5% normal donkey serum (Millipore: S30-100ML) in Dulbecco's phosphate-buffered saline. After blocking, epithelium equivalents were incubated with primary antibodies (1:100) at 4°C overnight, followed by washing steps and sandwich labeling with appropriate secondary antibodies (1:200) at 4°C overnight, counterstained with DAPI (Thermo: D1306) and imaged. The primary antibodies used included MUC5AC (Thermo: PA5-34612), beta IV Tubulin (Abcam: ab11315), Isoforms TA p63-α, -β, -γ (Biolengend: 618902), CC16, Human, mAb AY1E6 (HyCultBiotech: HM2178), ABCA3 (Abcam: ab24751), LAMP3 (Abcam: ab111090), Surfactant B (Abcam: ab40876), Connexin 43 (Abcam: ab11370), ENaC (Abcam: ab115272), HTI (Terrace Biotech: TB-29AHT1-56), HTII (Terrace Biotech: TB-27AHT2-280), E-Cadherin (Abcam: ab1416 and ab40772), ZO-1 (ZO1-1A12) conjugated Alexa Fluor 647 (Invitrogen: 33-9100-A647), Podoplanin (AT-1α) (Abcam: ab128994), Aquaporin5 (Abcam: ab215225 and ab92320), Cytokeratin 14 (Abcam: ab7800), Cytokeratin 10 (DE-K10) (ThermoFisher: MA5-13705), Involucrin (SY5) (ThermoFisher: MA5-11803), Filaggrin (FLG01) (Thermo: PA5-79267), VE-cadherin (Abcam: ab33168), PCNA (Thermo: PA5-32541), PECAM-1 (Abcam: ab9498), VWF (Abcam: ab8822) and Surfactant C (Seven Hill: WRAB-9337). Donkey Anti-Mouse IgG H&L (Alexa Fluor® 488) (Abcam: ab150105), Donkey Anti-Mouse IgG H&L (Alexa Fluor® 568) (Abcam: ab175472), Donkey Anti-Mouse IgG H&L (Alexa Fluor® 647) (Abcam: ab150107), Donkey Anti-Rabbit IgG H&L (Alexa Fluor® 488) (Abcam: ab150073), Donkey Anti-Rabbit IgG H&L (Alexa Fluor® 568) (Abcam: ab175470), Donkey Anti-Rabbit IgG H&L (Alexa Fluor® 647) (Abcam: ab150075) and Goat anti-Mouse IgG1 Alexa Fluor 568 (Thermo: A-21124) and anti-Mouse IgM Alexa Fluor 488 (Thermo: A-21042) were used as secondary antibodies. Blood was labelled with CD41 Monoclonal Antibody (VIPL3), PE (ThermoFisher: MHCD4104) by direct addition of the antibody (1:100) into the blood and incubated for 15min at room temperature.

Microscopy and image analysis

All bright field videos were acquired using a Zeiss Observer.Z1 inverted microscope equipped with ORCA-Flash 4.0 digital camera (Hamamatsu, C11440) using Objective LD Plan-Neofluar 40x/0.6 Corr Ph2 M27and ZEN software. Immunostaining was captured with fluorescence microscope Olympus U-LH100-3 microscope equipped with ORCA-Flash 4.0 digital camera (Hamamatsu, C11440) using with a LUC PL FLN 40X/0.6 objective and CellSense software. Confocal images, videos and co-localization measurements were performed using ImageJ software.

Vasculature functionality assay

Experiments to confirm the functionality of the vasculature compartment and its ability to respond to stimuli were conducted by exposing the epithelial compartment of the Open-top Alveolus-Chip to Lipopolysaccharides (LPS) from Escherichia coli O111:B4 (Sigma L4391) at 10ug/ml for 8 hours. After the

treatment, the vascular compartment was perfused with CD41 labelled platelet whole blood at a flow rate of 60µl/min, which yields a wall shear stress ranging approximately from 2.2dyn/cm^2, up to 6.3dyn/cm^2 depending on the viscosity of the blood used(Papaioannou and Stefanadis 2005), a values comparable with that found in veins under physiological conditions. The lumen was perfused for 15min while being imaged in real time.

Preparation LPS supplement:

LPS (Lipopolysaccharides from Escherichia coli O111:B4) (Sigma: L4391)

- Reconstitute 1mg of LPS in 1ml of ALI-M (199A) Medium directly into the vial (1 mg) by gently swirling until the powder completely dissolves for obtaining a stock solution of 1mg/ml
- Store in -20 °C, replace every 6 months
- Dilution in medium: add 500µl (of 1mg/ml LPS stock solution) in 50mL of ALI-M (199A) Medium for obtaining a final concentration of 10µg/ml

Barrier Function assay (Barrier integrity assay)

Experiments to confirm the integrity of the endothelial/epithelial barrier and its ability to maintain air-liquid interface was performed by adding 0.1mg/ml Dextran, Fluorescein (FITC), 3000 MW, Anionic, Lysine Fixable (ThermoFisher: D3306) to the culturing medium. A phenol red free MEM (GIBCO®: 51200-038) was flown on the epithelial compartment to test the leakage of the fluorescent probe from the lumen of the spiraled channel to the epithelial compartment. Media from the epithelial and endothelial side were collected from the outlet reservoirs after the indicated hours of perfusion. The fluorescence intensity was measured with a 96-well fluorimeter (**Synergy™ Neo2** Multi-Mode Microplate Reader BioTek: 14112414) at excitation/emission as indicated by the manufacturer instructions.

Barrier Function: A cell layer forms cell-to-cell junctions that can inhibit molecules from passing between cells. This barrier can be an important measure of the functionality and integrity of the alveolar-capillary interface. To measure the “tightness” of the barrier, a fluid-phase dye such as Dextran-FITC (3000Da) is suspended in medium and perfused through the vascular compartment of the Organ-Chip. The rate of diffusion of the fluorescent dye through the two cell layers depends on the tightness of the adherens junctions of the endothelial and epithelial layers; hence, as tighter are the junctions as higher the barrier function resulting in less fluorescent dye passing into the epithelial compartment at any given time. The amount of fluorescent dye can be measure via a plate reader and can be correlated to the concentration of dye in the media, therefore providing information about the barrier function of the Organ-Chip.

Equipment & supplies

Black 96-well plates (VWR: 29444-018)

Synergy™ Neo2 Multi-Mode Microplate Reader (BioTek: 14112414)

Reagents

Fluid phase dye: Dextran, Fluorescein (FITC), 3000 MW, Anionic, Lysine Fixable (Thermo: D3306)

Cell culture media: ALI-M (199A) Medium, MEM (thermo: 51200038).

Preparation fluid-phase dye supplement:

Fluid-phase dye preparation:

Dextran, Fluorescein (FITC), 3000 MW, Anionic, Lysine Fixable (Thermo: D3306)

- Reconstitute 10mg of Dextran, Fluorescein (FITC), 3000 MW, Anionic, Lysine Fixable in 1mL of tissue culture medium (MEM containing Penicillin Streptomycin GIBCO®: 15140122) directly into the vial (10mg) by gently swirling until the powder completely dissolves for obtaining a stock solution of 10mg/ml
- Filter through 0.22µm syringe (Corning®: 431219) or Steriflip® filter (MilliporeSigma™ SCGP00525)
- Aliquot into 0.5ml volumes
- Store in -20 °C in a box protected from light, replace every 6 months
- Dilution in medium: add 500µl (of 10mg/ml Dextran stock solution) in 50mL of ALI-M (199A) Medium for obtaining a final concentration of 100µg/ml

Permeability Assay Procedure

1) Stop flow
2) Aspirate media from the vascular reservoir
3) Fill vascular reservoir with desired volume of medium with added the fluid-phase dye (Dextran-FITC)
4) Fill the epithelial reservoir with minimal essential medium (MEM containing Penicillin Streptomycin GIBCO®: 15140122)
5) Prime the epithelial compartment of the chip by pipetting 200µl of MEM directly into the top fluidic of the chip paying attention to not trap bubbles (remember the Alveolar-Chip is at Air-Liquid Interface)
6) Prime the system by flowing at 1000µl/hr for 5 minutes top epithelial and bottom endothelial channels
7) Aspirate and discard chip effluents from both epithelial and endothelial chip outlet reservoirs
8) Start flow at the appropriate rate for the experiment (60µl/hr for 24hr, 48hr or 72hr) for both channels

Collecting Effluent

1) Pre-label 96-well sample plate
2) Collect at least 500µl of epithelial and endothelial medium from inlet reservoirs
3) Collect at least 500µl of epithelial and endothelial medium from outlet reservoirs at predetermined timepoint(s) into prelabeled tubes/or collection plate
4) Load 100µl of each sample into the prelabeled 96-well plate called the read plate
5) Samples can be read directly or stored at -80°C in a box protected from light

Barrier Function - Reading Sample

1) Ensure that at least 100µL have been loaded from each sample in the read plate in triplicates
2) Set up the plate reader, to perform read with the following specifications: Ex494 Em521 for Dextran-FITC
3) Record the tabulated results for analysis
   Note: ensure that the file has been saved in the appropriate format (i.e. excel)

Data Analysis

1) Confirm that readings are within linear range of the instrument
2) Always include data from negative control chip
3) For the **Standard** fluorescence curve proceed with 1:10 serial dilution going up to $1:10^6$
4) Use the ALI-M (199A) Medium without any fluorescent dye as Blanc
5) Medium from the outflow reservoir of the epithelial channel should be loaded in triplicates (technical triplicates)
6) Medium from the outflow reservoir of the endothelial channel should be loaded in triplicates (technical triplicates)

Quantitative real-time PCR

RNA was purified using a RNeasy mini kit (Qiagen, Valencia, California, USA). qPCR was performed with the TaqMan Fast Advanced Master Mix (Thermo: 4444964, Thermo Fisher Scientific) and SuperScriptTM IV first-strand synthesis system (Thermo: 18091050, 50 reactions) using a QuantStudio 3 Real-Time PCR system. Endogenous Control Genes for cDNA content (Human GAPDH: FAM/MGB probe, non-primer limited, 4333764T; Eukaryotic 18S rRNA: FAM/MGB probe, non-primer limited, 4333760T). TaqMan™Gene Expression Assay (FAM) Primers used for qPCR are listed following: GAPDH Catalog #: 4453320 Assay ID: Hs02758991_g1; HPRT1 Catalog #: 4453320 Assay ID: Hs99999909_m1; RPL32 Catalog #: 4453320 Assay ID: Hs00851655_g1; TP63 Catalog #: 4453320 Assay ID: Hs00978343_m1; KRT5 Catalog #: 4453320 Assay ID: Hs00361185_m1; FOXJ1 Catalog #: 4453320 Assay ID: Hs00230964_m1; Scgb1a1, Bpifb1 Catalog #: 4453320 Assay ID: Mm00442046_m1; SCGB1A1 Catalog #: 4453320 Assay ID: Hs00171092_m1; TUBA1ACatalog #: 4453320Assay ID: Hs00362387_m1; MUC5ACCatalog #: 4331182Assay ID: Hs00873651_mH;PDPNCatalog #:4331182Assay ID:Hs00366766_m1; SFTPCCatalog #: 4351372Assay ID: Hs00953663_g1;
SFTPCCatalog #: 4331182Assay ID: Hs00951326_g1; HMOX1Catalog #: 4331182Assay ID: Hs01110250_m1; AQP5Catalog #: 4331182Assay ID: Hs00387048_m1; SFTPCCatalog #: 4331182Assay ID: Hs00161628_m1; GABPACatalog #: 4331182Assay ID: Hs01022023_m1; TGIF1Catalog #: 4331182Assay ID: Hs00820148_g1; LAMP3Catalog #: 4331182Assay ID: Hs00180880_m1; HOPXCatalog #: 4331182Assay ID: Hs04188695_m1; NKX2-1-AS1Catalog #: 4331182Assay ID: Hs04408121_m1; SOD1Catalog #: 4331182Assay ID: Hs00533490_m1; ABCA3Catalog #: 4331182Assay ID: Hs00184543_m1; NFE2L2Catalog #: 4331182Assay ID: Hs00975961_g1; SFTPBCatalog #: 4331182Assay ID: Hs00167036_m1; NQO1Catalog #: 4331182Assay ID: Hs01045993_g1; SRXN1Catalog #: 4331182Assay ID: Hs00607800_m1; 18SCatalog #:

4331182Assay ID: Hs03003631_g1; ICAM1Catalog #: 4331182Assay ID: Hs00164932_m1; CDH5Catalog #: 4331182Assay ID: Hs00174344_m1; GPX2Catalog #: 4331182Assay ID: Hs01591589_m1; CDH1Catalog #: 4331182Assay ID: Hs01023895_m1.

ELISA immunoassay

Surfactant B and C was collected from the Chip epithelial cell surface by PBS washing and measured by Human SFTPB / Surfactant Protein B ELISA Kit (Sandwich ELISA) - LS-F4439 and Human SFTPC / Surfactant Protein C ELISA Kit (Sandwich ELISA) - LS-F12438 (LifeSpanBioScience) following the manufacturer's protocol. Samples were stored at -80 °C until analysis. Similarly, the presence of cytokines (IL-6, IL-8 and MPC) was detected from medium samples by Human TLR-induced Cytokines II: Microbial-induced Multi-Analyte ELISArray Kit (MEH-008A) (Qiogen) following the manufacturer's protocol. The color reactions were measured with Synergy NEO HTS Multi-Mode microplate reader (BioTek). Samples were stored at -80°C until analysis.

Cell-viability assay

Cell viability was examined by measuring the released of lactate dehydrogenase (LDH) into microfluidic device medium outflow, cell lysate from Chip (positive control) or fresh cell-culture medium (negative control) by using the CytoTox 96® Non-Radioactive Cytotoxicity Assay kit (Promega®: G1780) performed according to the manufacturer's protocol. Absorbance was measured with a Synergy NEO HTS Multi-Mode microplate reader (BioTek).

1) Thaw the LDH kit (CytoTox 96 Reagent) at room temperature
    a. This usually takes 1-2 hours
    b. Or you can thaw the assay buffer at 37°C water bath
    c. After taking out appropriate volume of assay buffer, store at -20°C in the dark
2) Prepare working CytoTox96 Reagent by adding 12ml of assay buffer into a CytoTox96 Reagent bottle and mix gently
3) Prepare media and blank samples. Keep these at room temperature
    a. Do not freeze the media
    b. LDH is stable at room temperature for several hours
4) To measure100% release of LDH, lysis the cells by adding 10ul of 10x lysis solution into 100ul of cells and incubate for 45 min
5) Centrifuge the sample and 100% lysate at 10,000 r.p.m. for 5 min
    a. Save the supernatant for following assay
6) Add 50ul of samples, blank and 100% lysate to 96 well plate
7) Add 50ul of working solution of CytoTox 96 Reagent into the 96 well plate
8) Incubate 30 min at room temperature in the dark
9) Add 50ul of stop solution to each well 10.
10) Read at 490nm immediately

Note: % Cytotoxicity = 100x Sample LDH release/Maximum LDH release

CellROX™ Green Reagent, for oxidative stress detection

Reactive oxygen species production, considered a direct measure of the oxidative stress in alveolar epithelium, was evaluated by measurement of the average intensity per field of view of alveolar epithelium stretched treated with CellROX reagent, epithelium treated with CellROX reagent after being exposed to H_2O_2 (10mM) per 30min (positive control) or epithelium no stretched treated with CellROX reagent (negative control) by using the CellROX™ Green Reagent (Thermo: C10444) according to the manufacturer's protocol. Fluorescence intensity was measured with a Synergy NEO HTS Multi-Mode microplate reader (BioTek).

1) Thaw the CellROX™ Green Reagent vial at room temperature (stock solution 2.5mM)
    a. This usually takes 5-10 minutes
2) Prepare 5µM working concentration of CellROX™ Green Reagent in medium by adding the 1µM of CellROX® Reagent stock solution for each 500µl (0.5ml) of medium (dilution factor 1:500)
3) Incubate Chips treated with 5µM working concentration of CellROX™ Green Reagent in medium for 30 minutes at 37°C in the dark
4) Remove medium and wash cells three times with PBS per 2 minutes
5) Image Chip with absorption/emission maxima of 485/520 nm, immediately

Scanning electron microscopy

Cells were differentiated into the Open-Top Chip (Emulate, Inc) by following protocols described above. Cells were fixed with 2.5% glutaraldehyde in 0.1 M sodium cacodylate buffer (Electron Microscopy Sciences) for 1hr followed by 1% osmium tetroxide in 0.1 M sodium cacodylate (Electron Microscopy Sciences) for 1hr and then dehydrated in ascending grades (30%, 50%, 70%, 80%, 90%, 95% and 100%) of ethanol. Samples were then chemically dried with hexamethydisilazane (Electron Microscopy Sciences) in a desiccator overnight or critical point dried. Before imaging, samples were mounted and sputter-coated with a thin layer of 5nm layer of platinum–palladium and imaged using a Jeol 5600LV Scanning Electron Microscope.

Statistical analyses

To assess statistical significance of differences between group, we used t-Test, ANOVA, and the Turkey honestly significant different (HSD) test using correlation analysis in the GraphPad Prism software program (San Diego, CA). The significance of the correlations between measurements was determined based on the null hypothesis that R=0. Significance was defined as $\alpha<0.1$. Measurements are reported as means ± SEM, unless otherwise specified.

3. RESULTS

Results

Engineering a tridimensional breathing human Open-Top Alveolus-Chip

The tridimensional human Open-top Alveolus-Chip is a multifunctional microfluidic platform that recapitulates the structural, functional, and mechanical properties of the human alveolus tissue. The platform is composed of 4 layers made of a flexible and transparent elastomeric material (PDMS) which include an elastic and porous membrane interfacing with the vascular bottom channels (Fig.3.0, a, b, c; in magenta) and the stromal compartment (Fig. 3.0, a, b, c, d; in grey). The top microfluidic layer (Fig. 3.0, a, b, c; in blue) can seal the alveolar compartment, allowing the perfusion of alveolar cells with culture medium during the epithelial maturation stage, and is also removable (Fig 3.0, b; top layer). This unique feature allows direct access to the air space of the Open-top Alveolus-Chip, which is particularly important during the introduction and maintenance of an air-liquid interface (ALI), delivery of drugs or other compounds into the epithelial space, and sampling of the alveolar surface.

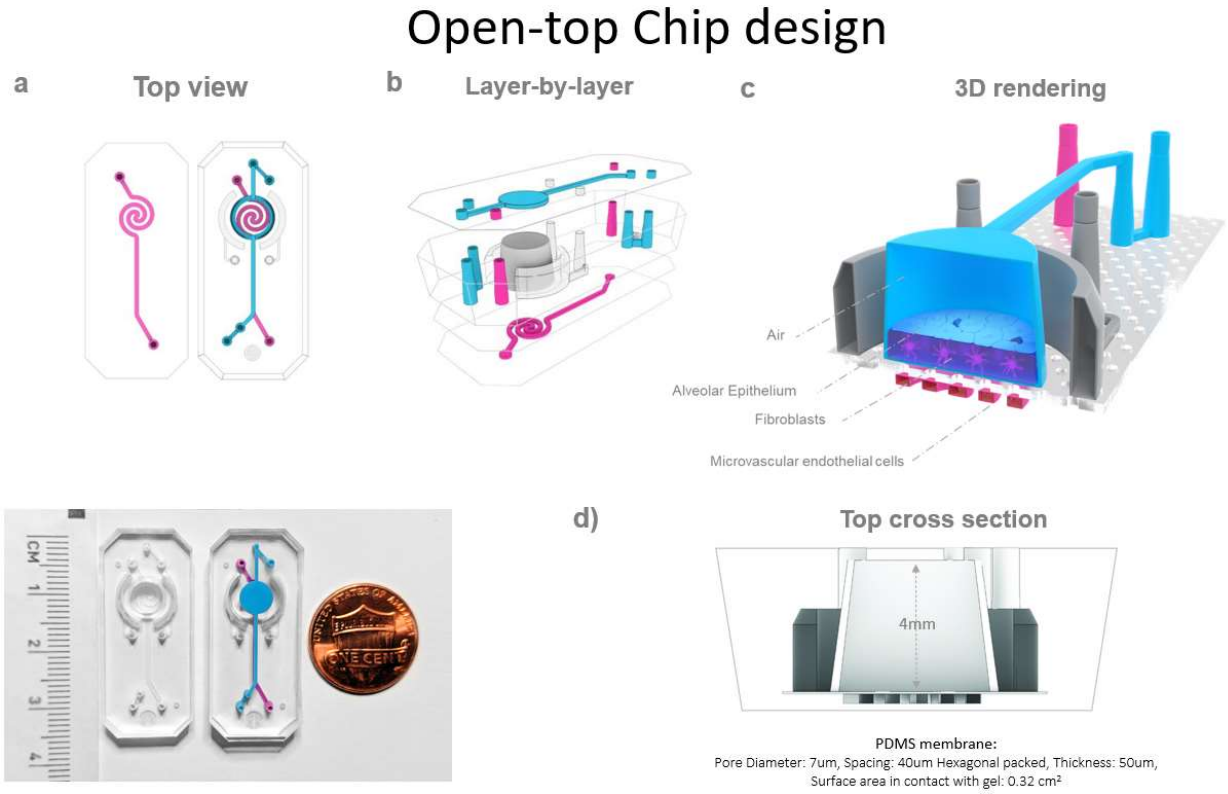

Figure 3.0: Open-top Chip design: (a) Top view schematic and picture of the Open-top platform showing in blue the top microfluidic channel, in gray the stromal chamber equipped with two semi-vacuum lunar hollow chambers alongside its perimeter and in cyan the bottom spiraled channel. (b) Exploded layer-by-layer view showing the intended assembly of mechanical parts forming the Open-top chip design. (c) Cartoon 3D rendering illustrating the Open-top Alveolar-Chip concept and intended application. (d) Top cross section of the Open-top Chip showing the

cavity with effective height of 4mm separated by the bottom microfluidic channel by the porous membrane. On the side of the cavity the two vacuum chambers to which is applied negative pressure to cause mechanical stretching.

While the top chamber has been designed to reconstitute the ALI conditions typical of the pulmonary epithelium (airway and alveolus), the stromal compartment of the Open-top Chip was conceived to provide structural support to the epithelium and to recreate the biological function of connective tissue. The tridimensional inter-alveolar space of the Alveolus-Chip consists of a collagen I-rich hydrogel containing primary human pulmonary fibroblasts (stromal-equivalent) (Fig. 3.15). The composition of the hydrogel has been optimized to match the stiffness of the lung (0.9 – 2.5 kPa)(Azeloglu, Bhattacharya, and Costa 2008)(Rico et al. 2005), and the apical surface of the stromal equivalent was coated with a combination of human collagen IV, fibronectin, and laminin before seeding primary human pneumocytes to match the composition of the basal lamina of the alveolus.

The choice of alveolar coating components was based on a study performed using a stromal equivalent coated with different combinations of ECM proteins typically found in the alveolar tissue basal lamina(Azeloglu, Bhattacharya, and Costa 2008). The results from this study evidenced that no significant changes in type I gene expression are detectable when gelatin is used as coating. Stromal equivalents treated with elastin, fibronectin, laminin, and collagen type I and type IV alone all generate similar upregulation of the epithelial marker for type I and type II. Interestingly, ABCA3 gene seems to not respond to any of the coating tested. In line with previous publications(Olsen et al. 2005)(Azeloglu, Bhattacharya, and Costa 2008) , we found that epithelial cells seeded on an ECM mixture of collagen type I and IV, elastin, laminin and fibronectin (Fig.3.1) expressed highest level of markers of both type I and type II alveolar pneumocytes, including podoplanin (PDPN), Homeobox Only Protein X (HOPX) and aquaporin 5 (AQP5) for type I and ABCA3 and Surfactant B for type II. A significant higher upregulation for both type I and type II markers was observed only for the coating condition collagen type IV, laminin, fibronectin which become the coating of choice for the model.

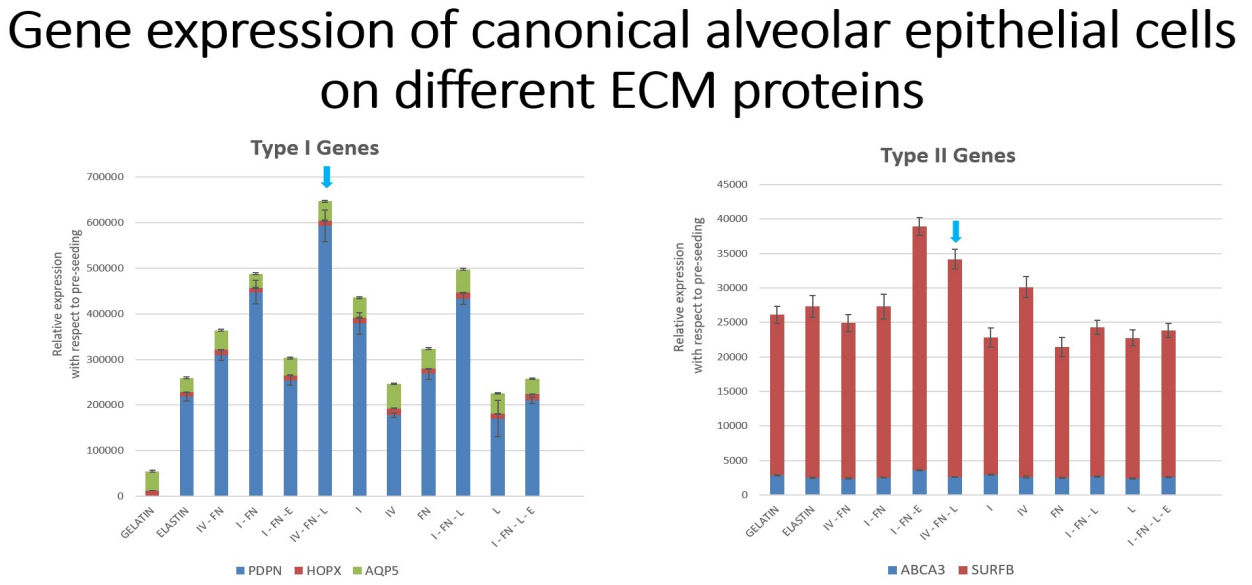

Figure 3.1: Gene expression of canonical alveolar epithelial cells on different ECM proteins: the two table report the relative gene expression of alveolar type I and type II marker when seeded on different composition of ECM. The two arrows (in light blue) evidence the condition we have selected as lamina basal coating for Alveolus-Chip. (n=3 per condition)

Among the various proteins associated with type I and type II pneumocytes, the plasma membrane HTII-280(Gonzalez et al. 2010) and HTI-56(Dobbs et al. 1999)(Newman et al. 2000) proteins are specific to human alveolar cells, making them a more robust indicators of type I and type II phenotype and, consequently, more useful for the identification of the two alveolar types in the epithelium (differently than other lung markers used in the genetic analysis such as podoplanin, surfactant B and aquaporin which are more ubiquitous in the human lung). The marker specificity dictated our choice to use them in the following experiments. Results obtained via confocal imaging of the epithelial monolayer also confirmed the presence of type I (HTI-56 positive) and type II (HTII-280 positive) pneumocytes, as well as cells with an intermediate phenotype that co-expressed marker of both type I and type II pneumocytes. Staining for HTII-280 and HTI-56 markers revealed differential expression and signal segregation for the two markers on the different coatings. In accordance with the gene expression, we observed maximum signal segregation and higher type I marker expression with the collagen type IV, laminin, fibronectin coating (Fig.3.2).

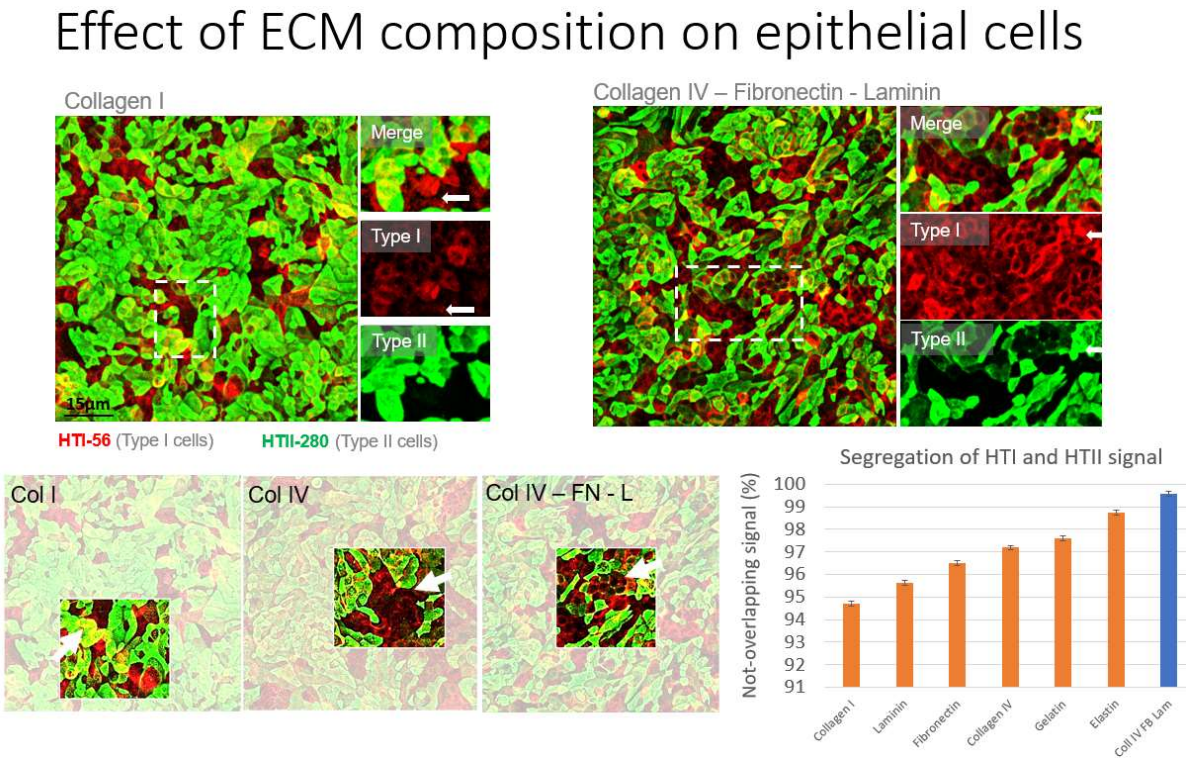

Figure 3.2: Effect of ECM composition on epithelial cells: Immunofluorescent images for HTI-56 and HTII-280 staining showing the difference in signal segregation for the two markers induced on alveolar type I and type II cells by different coating (scale bar 15µm). The white arrows evidence alveolar cells expressing the two markers

simultaneously, indication that a part of the pneumocytes do not fully differentiate if not provided with an appropriate coating. The graph quantified the relative not-signal overlapping allowing to compare different conditions. (n=3 per condition)

Given the relevance of mechanical cues in lung development and modulation of several biological functions, we decided to investigate the relationship between applied vacuum and percent of strain (or stretching) in the Alveolus-Chip, which has been designed to recapitulate the native biomechanical environment of the human alveolus. The entire stromal compartment, including the inter-alveolar space and the epithelial monolayer, is surrounded by two vacuum chambers that can be used to mimic breathing motions similar to previously published systems (Birukov et al. 2003)(Huh et al. 2010)(Huh et al. 2012). When negative pressure in the range of 0 to 90 KPa are applied, the system generates physical strain in the range of 0 to 17% (Fig. 3.3, a). Difference in percent of strain (stretching intensity) were observed between the central and peripheral area of the cavity. Specifically, we detected an anisotropic stretching intensity profile that changes as function of the cavity radius, with maximum percent of strain detected at the external edge of the cavity and minimum percent of strain detected at center of the cavity. Dramatic variation in stretching intensity resulted only between the two inner central sections, which occupy less than 20% of the entire chip surface (Fig. 3.3, b).

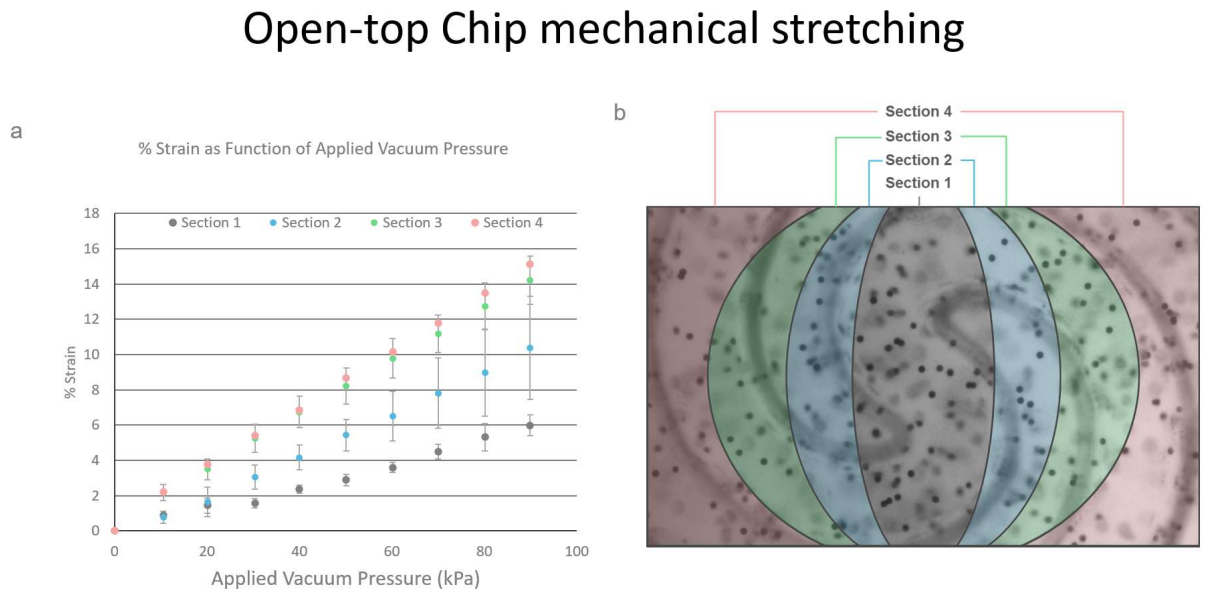

Figure 3.3: Open-top Chip mechanical stretching: (a) Graph showing the correlation between applied vacuum and percent of strain (or stretching) generated on the apical surface of the collagen gel. (b) Color-coded map showing gel areas undergoing similar degree of stretching calculated optically as bead displacement. The graph evidences that gel has an anisotropic displacement (strain) profile that change as function of the radius.

The vascular compartment is designed to recreate laminar flow and to minimize turbulence within the entire channel during perfusion of cell culture medium. Preservation of laminar flow and minimization of turbulence is especially important to recreate a physiological relevant flow. The fluidic modelling generated using the program COMSOL Multiphysics confirmed the maintenance of constant laminar flow

and shear rate along the entire length of the spiraled fluidic bottom channel (Fig. 3.4). The geometry of the top fluidic also preserve the laminar flow along the entire length of the top fluidic, however a drastic decreasing in shear rate is observed when the channel across the cavity area due to the enlarging in cross-section area of the channel. The top channel geometry was selected among others to minimize the fluidic shear stress on the epithelium. Cross view of the laminar flow inside the channels also evidences a shear rate gradient as function of the distance from the channel wall with maximum shear rate (80µm/sec) at the center of the channel and minimum shear rate at the wall (0-5µm/sec).

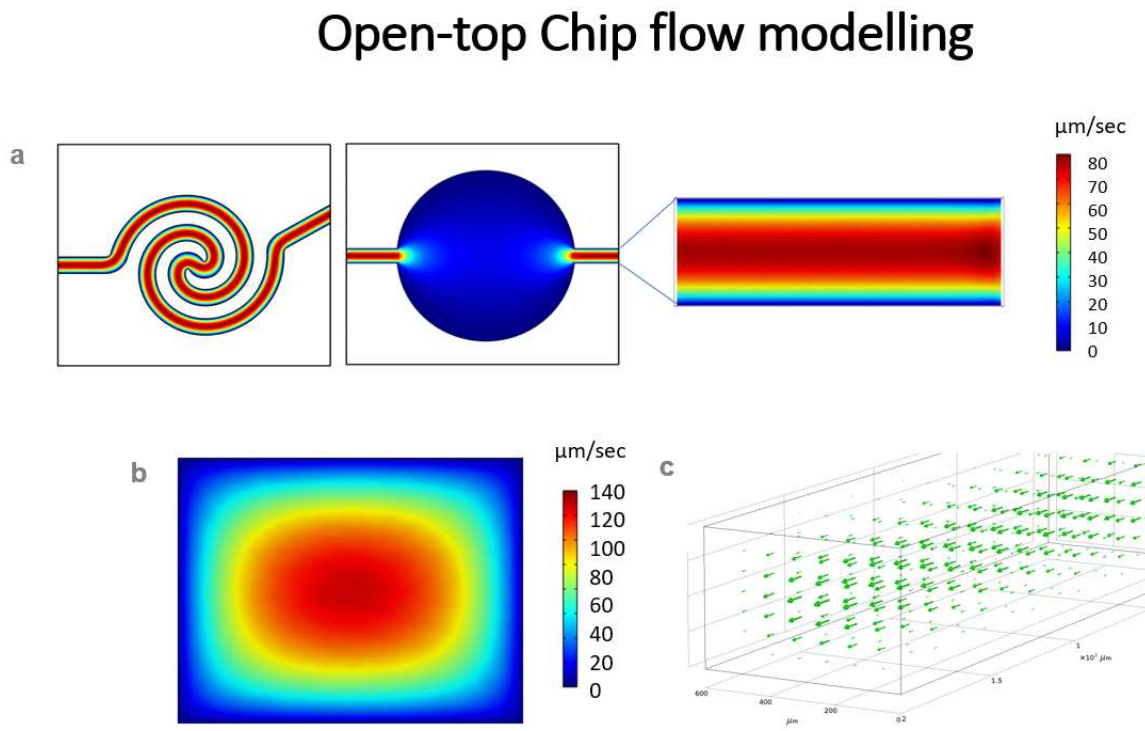

Figure 3.4: Open-top Chip flow modelling: (a) Top view of laminar flow inside the Open-top Chip top and bottom channel. (b) Cross view of laminar flow inside the Open-top Chip top channel. (c) Top view of laminar flow inside Open-Top Chip bottom channel. All fluidic models represented were generated using the program COMSOL Multiphysics.

The choice of a spiraled geometry for the vascular channel was due to the necessity to maximize the area of medium exchange at the stroma-vascular interface since all the three compartments are fed through the vascular channel when the Chip is exposed to air-liquid interface. To the best of our knowledge, this is the first description of an *in vitro* model that has been designed to incorporate the fundamental biological and biomechanical cues that support and regulate alveolar homeostasis in vivo.

Reconstitution of air-liquid interface: its significance and physiological relevance

The alveolar space represents the main site of gas exchange between the external atmosphere and the pulmonary-vascular system of the human body. With the aim of engineering a functional air-liquid interface on the Alveolus-Chip, we introduced sterile atmospheric air into the epithelial channel five days post cell seeding. During the ALI phase, the vascular compartment was continually perfused with cell culture medium at 60ul/hr (a detailed description of the various steps can be found in Fig. 3.5 and 3.6).

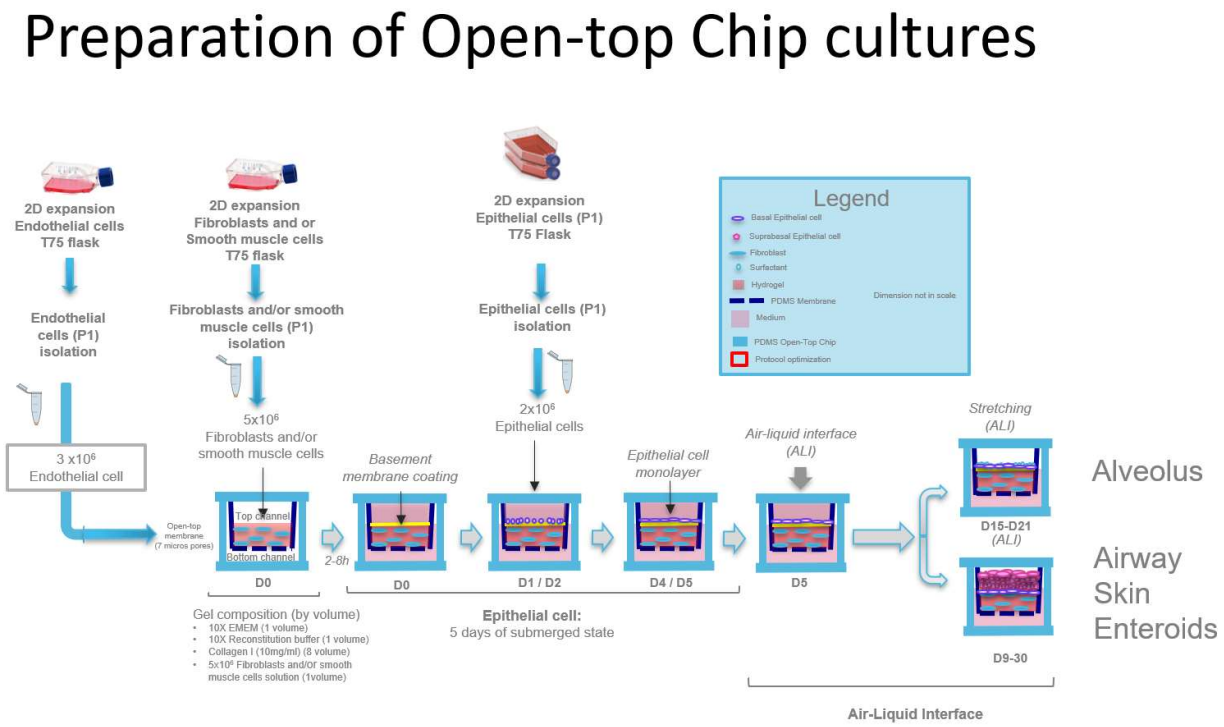

Figure 3.5: Open-top Chip protocol description: Schematic showing the sequence of action for the Open-Top chip preparation and providing some details on how the biological elements forming the Open-top Chip integrates together. In the initial phase of the chip preparation, epithelial, endothelial and mesenchymal cells (fibroblast and/or smooth muscle cells) are expanded in flask. When ready, fibroblasts and/or smooth muscle are embedded into the gel to form the stromal layer which is coated for 2-4 hour and seeded with epithelial cells. Once the epithelial cells form a compact monolayer, endothelial cells are used for seeding the bottom spiraled channel, let attach in static for 8 hours and flown together with epithelial cells with their respective medium for 24 hours. At this point, epithelial cells are exposed to air (ALI). In the case of airway, skin or enteroids, the biological system is kept under this regime until being sacrificed for analysis. In the case of alveolus there is a variation of the protocol which includes the application of stretching at day 9. Stretching is kept until day 15 when the tissue is sacrificed for analysis.

Although a number of studies have highlighted the role of ALI in inducing alveolar cell maturation and the expression of specific markers, the previous models have not included a co-culture of three primary human-derived cell types. The lack of a commercially available medium compatible with the feeding requirements for pneumocytes, fibroblasts and endothelial cells and the geometrical constraints of the

Open-top Chip design which does not allow to feed each biological layer independently, forced us to investigate media compatible with the nutritional needs of the three cell types. In order to determine the effect of different medium compositions on cell viability and maturation, we performed immunohistochemistry on chips that were exposed to air for 7 days (5 days submerged and 7 days ALI, total of 12 days, see Fig.3.6 for more details about the stages).

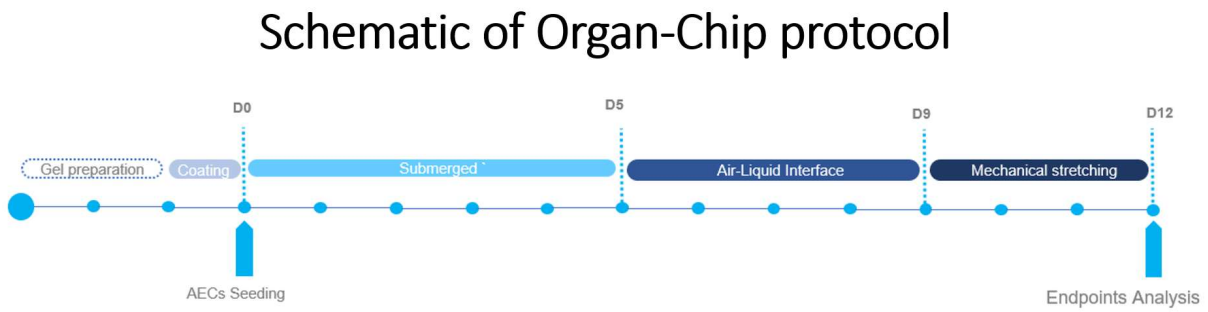

Figure 3.6: Schematic of Open-top Chip protocol: The timeline provides the critical steps and the sequence of action performed during the Open-Top chip preparation and culturing.

Because the small airway growth medium has been previously shown to be compatible with primary alveolar epithelial cells exposed to ALI (Huh et al. 2012), we initially used this medium to feed the Alveolus-Chip. In line with other publications, alveolar cells cultured at ALI with SAGM complete medium showed regular cell morphology and expression of alveolar type I (HTI-56) and type II (HTII-280) cell markers (Fig. 3.7, g). However, the endothelium lining the vascular compartment of the chip showed signs of VE-cadherin discontinuity (Fig. 3.7, h), suggesting that endothelial cells do not tolerate SAGM complete medium. Also, fibroblasts encapsulated within the stromal equivalent shown evident increase in apoptosis levels compared to the control (SAGM 5 day submerged), around 7 days after introduction of ALI, as detected via Caspases 3/9 staining (Fig. 3.7, m). Therefore, the use of SAGM complete medium in the Alveolus-Chip was precluded by its incompatibility with the long-term survival of endothelial cells and fibroblasts. Similarly, EGM-2MV complete medium, which is optimized for culturing of microvascular endothelial cells, caused loss of epithelial cell morphology and occasionally loss of both HTI-56 and HTII-280 markers (Fig. 3.7, d). Seven days after introduction of ALI, the fibroblasts encapsulated within the stromal equivalent showed an aberrant morphology (Fig. 3.7, f) but not statistically significant increase in apoptosis levels compared to the control (SAGM 5 day submerged), as detected via Caspases 3/9 staining (Fig. 3.7, m). Given the lack of any commercially available media formulated to sustain cell viability and function for all the three cell types, we used a proprietary formulation named ALI-M(199A) medium that includes key grow factors (for more details about the medium check in materials and methods) known to promote alveolar cell maturation and endothelial cell viability. Chips perfused with ALI-M(199A) medium expressed both HTI-56 and HTII-280 markers and showed regular morphology (Fig. 3.7, a). Similarly, the endothelium lining the vascular compartment of the chip showed an intact of monolayer (Fig. 3.7, b), suggesting that endothelial cells tolerate ALI-M(199A) medium. Seven days after introduction of ALI, the fibroblasts encapsulated within the stromal compartment shown regular morphology and a not

statistically significant increase in apoptosis levels compared to the control (SAGM 5 day submerged), as detected via Caspases 3/9 staining (Fig. 3.7, m). Interestingly, alveolar epithelial cells shown increase in apoptotic levels when exposed to ALI independently from the medium used to feed them, suggesting that they suffered from the exposure to the air (3.7, l). The difference in percentage of apoptotic epithelial cells suggested that ALI-M(199A) medium performs better than SAGM and EGM-2MV complete medium in supporting the viability of the alveolar epithelium at ALI, since it does show statistically different from the control.

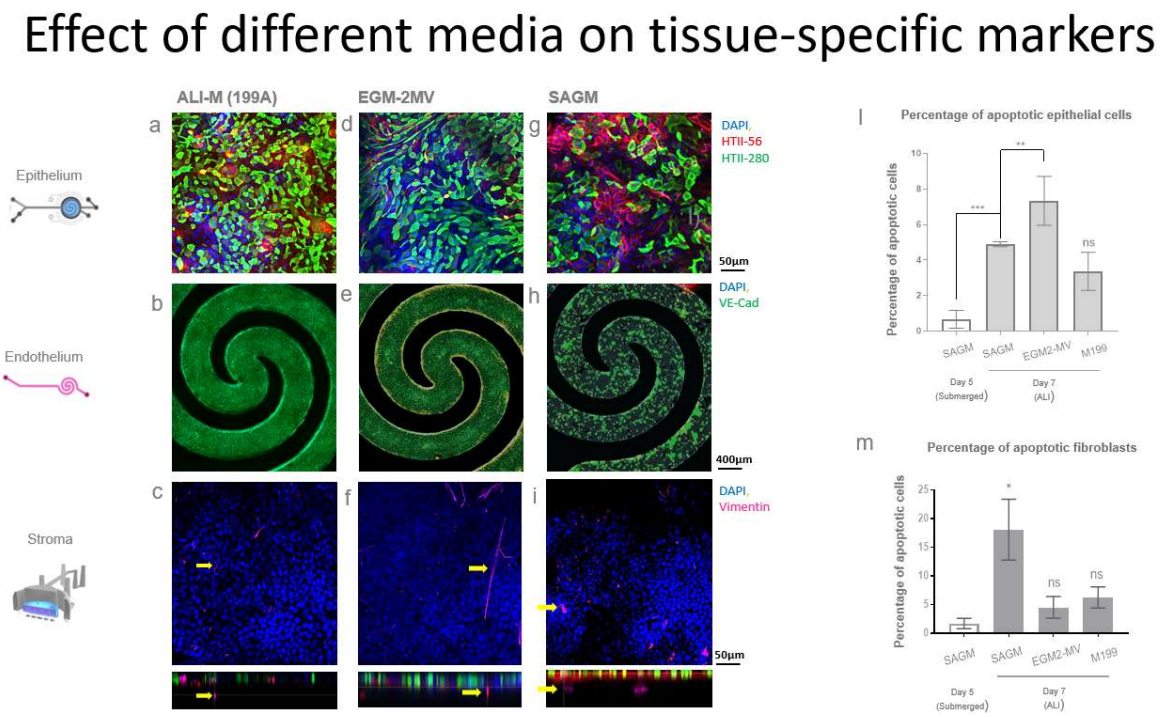

Figure 3.7: Effect of different media on tissue-specific markers: The table show immune fluorescence images of the Open-top Alveolus-Chip cultured using three different media (ALI-M (199A) medium, EGM-2MV and SAGM complete medium). (a, d, g) Comparison of the epithelium growth with the three media. Alveolar cells grown in ALI-M (199A) and SAGM medium showed regular morphology, while cells growth in EGM-2MV evidenced an abnormal phenotype (scale bar 50µm). (b, e, h) Comparison of the endothelium growth with the three media (scale bar 400µm). Endothelial cells grown in ALI-M (199A) and EGM-2MV medium showed regular morphology, while cells grown in SAGM died leaving hole in the monolayer. (c, f, i) Effect on fibroblast morphology of the three media (scale bar 50µm). EGM-2MV seems to stress fibroblasts underneath the epithelial monolayer inducing an elongated phenotype (l, m) Graph quantifying apoptotic cell per field of view induced by the different media. (ANOVA, Turkey's multiple comparison test, n=3 per condition, p*<0.1; p**<0.01; p***<0.001, ns=non statistically significant)

Alveolar cells cultured at ALI with ALI-M (199A) medium showed regular cell morphology and expression of alveolar type I (HTI-56) and type II (HTII-280) cell markers. HTII-280 has been reported as specific to the apical surface of human type II cells, while HTI-56, is a novel apical plasma membrane protein specific to the human type I cells. We took advantage from the markers apical localization to determine if the type I

and type II cells show morphological difference compatible with the respective phenotypes. Confocal 3D stack images confirmed that the spatial distribution of type II (HTII-280) marker signal is localized to the apical region of the epithelium (top of Z-Stack) while the type I (HTI-56) marker signal is shifted below to the basal region of the epithelium close to the stroma (bottom of Z-Stack) (Fig.3.8). The average heights of the intensity signals are shifted few microns apart (the pick of the two curves is about 2.5µm apart), supporting the hypothesis that type I cells are on average flatter (squamous) than type II cells. The finding is compatible with the morphological difference one would expect from the two alveolar phenotypes.

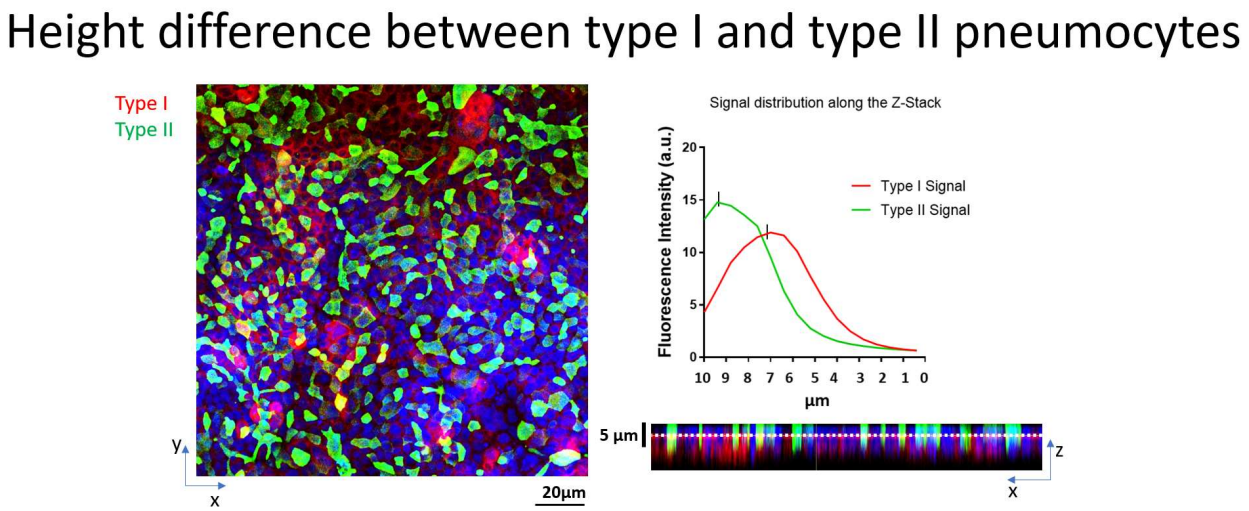

Figure 3.8: Height difference between type I and type II pneumocytes: The image on the right shows a staining for HTI-56 (type I) and HTII-280 (type II) spatial distribution (scale bar 20µm). On the right, the graph quantifies signal distribution of the type I and type II signal along the Z-axis (the pick of the two curves is ≈2.5um apart) while the optical cross-section shows the relative height of type I and type II cells. It is possible to notice that the type II signal is localized in the apical region of the Z-Stack, while the type I signal is shifted few microns below and close to the stroma, supporting the hypothesis that type II cells are "taller" than type I cells.

Once we confirmed that the ALI-M (199A) medium sustains epithelial expression of both type I and type II pneumocytes, we characterized the microvascular compartment of the model. Primary human microvascular endothelial cells were cultured for 12 days under flow (60µl/hr) using ALI-M (199A) medium following the Open-top Alveolus-Chip protocol. Then, fixed and stained for Von Willebrand Factor (VWF), PECAM-1 (DC31) and VE-cadherin. Perinuclear localization of VWF and homogeneous expression of the adherens junction molecules, VE-Cad and PECAM-1, at the cell-periphery (Fig.3.9) indicate that endothelial cells form a compact monolayer and express markers of mature vasculature. Taken all together these results provide confidence in the use of the ALI-M (199A) medium for sustaining the Open-top Alveolus-Chip during ALI.

Endothelial cell viability and maintenance of tissue specific markers

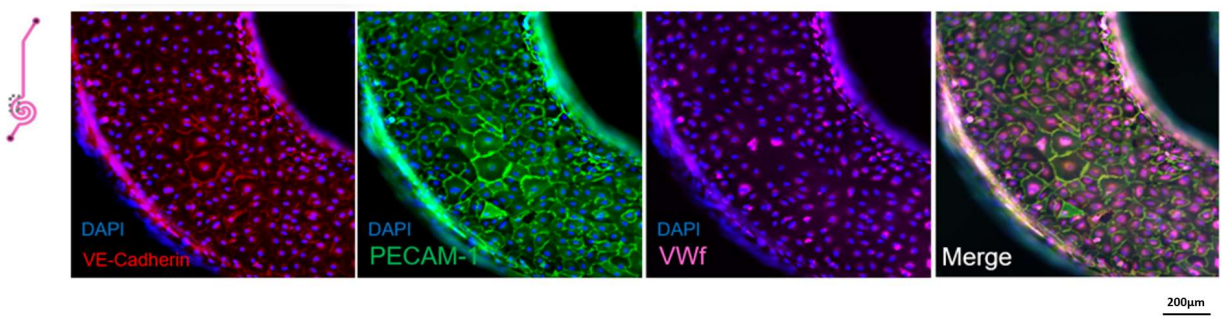

Figure 3.9: Endothelial cell viability and maintenance of tissue-specific markers: Staining for PECAM-1, VWF, VE-Cadherin of the endothelium compartment of the Open-top Alveolus-Chip shows marker expression and spatial localization of endothelium tissue-specific markers. The vascular compartment is lined with a tight monolayer of microvascular endothelial cells expressing endothelial specific markers PECAM-1 (green), VE-Cadherin (Red) and VWF (magenta); (scale bar 200µm).

A number of studies performed using alveolar cell-line A549 have highlighted the potential role of stretching in promoting alveolar type II cell maturation and the expression of specific markers of the type II phenotype(J. Wu et al. 2018)(J. Wu et al. 2018). In order to investigate the role of stretching in the Open-top Alveolus-Chip, we applied strain to the alveolar epithelium at a precise magnitude and frequency. Alveolar cells were stretched cyclically at 0.2Hz for about 3 days at 4% and 15% strain corresponding approximatively physiological (4-5%) or pathological (18%) strain as reported by Konstantin G. Birukov and colleagues. Alveolar cells cultured at ALI with ALI-M (199A) medium undergoing 4% stretching for about 3 days showed regular cell morphology and expression of alveolar type I (HTI-56) and type II (HTII-280) cell markers. We also observed a relative increase in alveolar type II (HTII-280 positive) versus type I (HTI-56 positive) phenotype compared to not stretched conditions and a better segregation between the type II and type I signals, which suggests better maturation of alveolar type II cells. Our findings seem in line with outcomes from publications based on the alveolar cell-line A549. In order to quantify the extent to which stretching contribute to the oxidative stress in Alveolus-Chip, we treated the alveolar epithelium with the reactive oxygen species activated (ROS) fluorogenic probe (CellROX® Green) and quantified the average intensity of the signal in live cells. We observed a slight increase in the production of ROS of the physiological (4%) and pathological (15%) stretching conditions compared to the control condition (no stretching), however not statistically significant. We concluded that the alveolar epithelium is sensitive to stretching, even if oxygen species activated (ROS) fluorogenic probes are assays not sensitive enough to quantify ROS production and to provide a definitive quantitative answer on the contribute of stretching to oxidative stress.

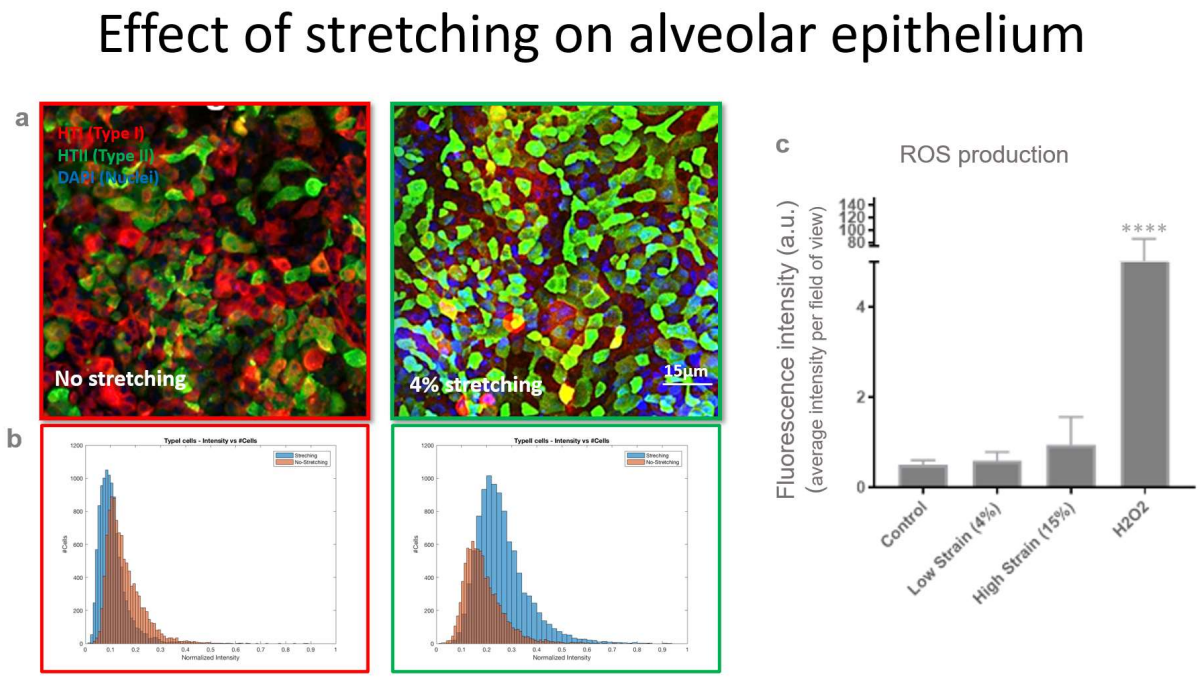

Figure 3.10: Effect of stretching on alveolar epithelium: (a) Image showing spatial distribution of type I (HTI-56) and type II (HTII-280) marker as effect of stretching (scale bar 15µm). (b) Type I (HTI-56) and type II (HTII-280) signal segregation as effect of stretching. Stretching induces better segregation of type I and type II signal which suggests better maturation of alveolar type II cells. (c) Graph showing radical oxygen species production as effect of stretching. Stretching comparable to level of strain observed in the normal breathing show no statistical difference with the control in the level of ROS produced. (ANOVA, Turkey's multiple comparison test, n=4 per condition, p****<0.001)

It is well recognized from many in vivo and in vitro studies that transforming growth factor-beta1 (TGF-β1) plays a key role in pulmonary fibrogenesis(Borthwick, Wynn, and Fisher 2013)(Sgalla et al. 2018) by promoting the transformation of alveolar epithelial cell into mesenchymal cells with a myofibroblast-like phenotype(Saito, Horie, and Nagase 2018)(Wei et al. 2019), a process, called epithelial-mesenchymal transition (EMT)(Kasai et al. 2005). Alveolar epithelial cells undergoing epithelial-mesenchymal transition as effect of exposure to TGF-β1 are reported to display loss cell polarity, epithelial tightness due to the dissociation of membrane-associated adherens junctions (i.e. E-cadherin and ZO-1) and re-arrangement of the cytoskeleton followed by an increase at mRNA level and protein level of in intermediate filament proteins (α-SMA) which ultimately facilitates the cell adopting a mesenchymal phenotype. To understand if and to what extent the alveolar epithelial and endothelial cells maintains the sensitivity to TGF-β1 when cultured in the Open-top Alveolus-Chip, we examined whether increasing concentrations of TGF-β1 create a dose-dependent increase α-SMA expression. Specifically, after maturated the Alveolus-Chips for 12 days (5 days submerged, 7 days ALI, 3 days 4 % stretching) under flow (60µl/hr) using ALI-M (199A) medium, the alveolar epithelium was exposed to 0.1, 1 or 10 ng/ml of TGF-β1 for 24h or 72h. At this point, alveolar epithelial and endothelial cells were examined at mRNA level for evidence of the epithelial-mesenchymal transition marker. We observed that the long exposure (72hr) to low dose (0.1ng/ml) of TGF-β1 was

accompanied by statistically significant increase in gene expression of α-SMA (Fig. 3.11, b) in both epithelial and endothelial cells compared to control while both short (24hr) and long (72hr) exposure at middle (1.0ng/ml) dose of TGF-β1 induced statistically significant variations in gene expression only in endothelial cells. Surprisingly, we observed no statistically significant variation in α-SMA expression for short (24hr) exposure at low (0.1ng/ml), middle (1.0ng/ml) and high (10ng/ml) dose and for long (72hr) exposure at middle (1.0ng/ml) and high (10ng/ml) dose, in the epithelium. Similarly, we observed no statistically significant variation in α-SMA expression for short (24hr) exposure at low (0.1ng/ml) and high (10ng/ml) dose and for long (72hr) exposure at high (10ng/ml) dose, in the endothelium. These results indicate that both epithelial and endothelial cells, which line two opposite surfaces of the Open-top Alveolus-Chip, are directly or indirectly sensitive to the TGF-β1 treatment confirming that the biological system respond to TGF-β1 induction. Since the results were unexpected and contradict our prediction, we decide to select the condition that induced significant upregulation of α-SMA in both alveolar epithelium and endothelium, low dose (0.1ng/ml) long exposure (72hr) and investigate the effect of the TGF-β1 treatment a protein level.

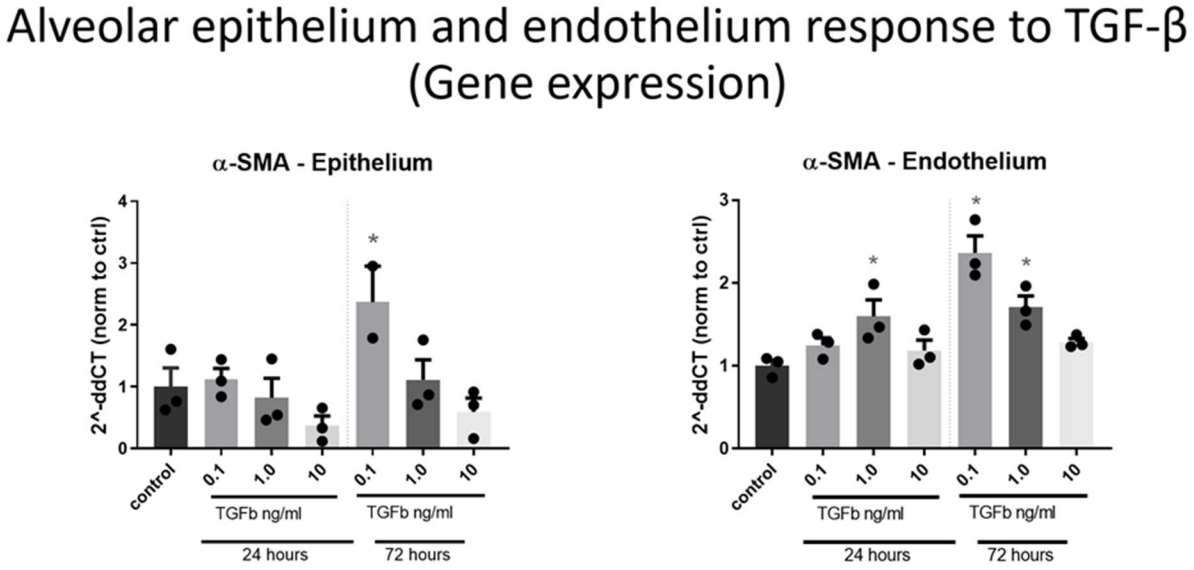

Figure 3.11: Open-top Alveolus-Chip response to TGF-β: Graphs showing α-SMA Gene expression of the Open-top Alveolus-Chip epithelium and the endothelium treated with TGF-β at different concentration (0.1,1.0 and 10ng/ml) for 24 or 72 hours. Notably, endothelial cells lining the vascular compartment of the Alveolus-Chip shown sensitivity to the TGF-β treatment. (ANOVA, Turkey's multiple comparison test, n=3 per condition, p*<0.1).

Specifically, after maturated the Alveolus-Chips for 12 days (5 days submerged, 7 days ALI, 3 days 4 % stretching) under flow (60µl/hr) using ALI-M (199A) medium, the alveolar epithelium was exposed to 0.1ng/ml of TGF-β1 for 72h. At this point, alveolar epithelial cells were stained for E-cadherin and α-SMA and evaluated for EMT. We observed that alveolar epithelial cells exposed at TGF-β1 for 72h showed an

altered arrangement of membrane-associated adherens junctions, E-cadherin, evidencing an elongated epithelial cell morphology indicative of loss of cell polarity and epithelial tightness. We also detected a statistically significant increase in α-SMA positive cells into the epithelium indicative of induced epithelial-mesenchymal transition, and a statistically significant increase in the number of nuclei compare to the control indicative of active proliferation and loss of contact inhibition(confocal imaging, Fig. 3.11, a). We conclude that the results (including upregulation and expression at protein level of α-SMA gene, morphological changes due to rearrangement of E-cadherin and proliferation bypassing contact inhibition) are compatible with the hypothesis that low dose TGF-β1 treatment induces EMT into alveolar epithelium and, consequently, that the Alveolus-Chip is sensitive to TGF-β1, at least at low dose.

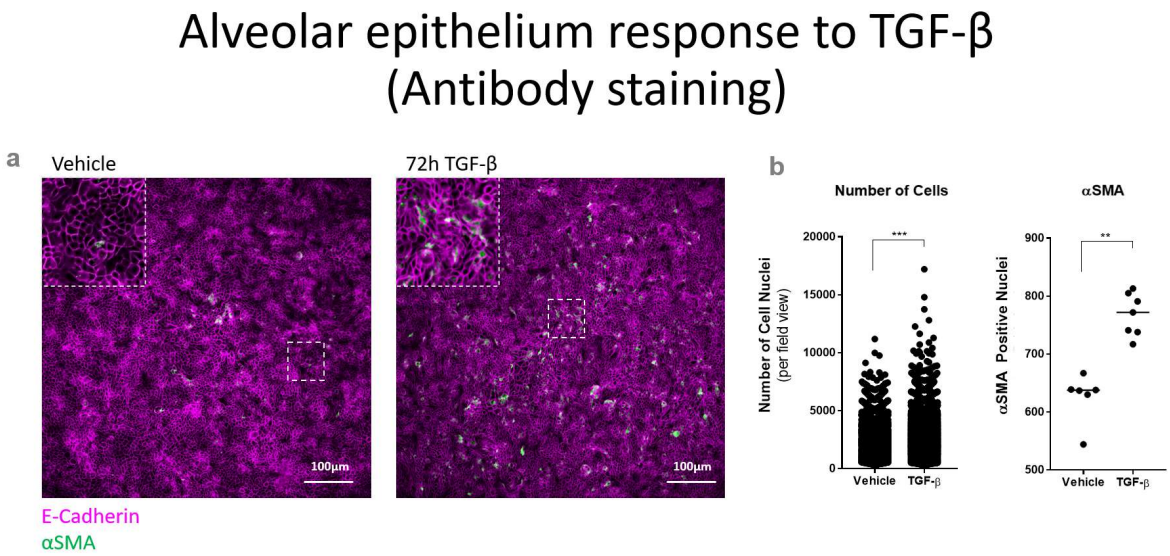

Figure 3.12: Open-top Alveolus-Chip response to TGF-β: Staining for E-cadherin and α-SMA of the epithelium compartment of the Open-top Alveolus-Chip shows marker expression and spatial localization of epithelium (E-cadherin) and epithelial-mesenchymal transition (α-SMA) specific markers. The graphs quantify the α-SMA positive cells per field of view evidencing that TGF-β treated chip express a significant higher level of EMT compared to control. (t-test, n=6 chip per condition, 10 Field-of-view per chip, p**<0.01; p***<0.001).

In order to further investigate a possible epithelial-vascular interaction, we exposed the alveolar epithelium to LPS, a bacterial toxin known to cause acute epithelial inflammation(Nova, Skovierova, and Calkovska 2019) and upregulation of upregulation of ICAM-1(Beck-Schimmer et al. 2002), IL-6(Nova, Skovierova, and Calkovska 2019) and IL-8(Standiford et al. 1990). Following LPS treatment of the Open-top Alveolus-Chip, we observed a net upregulation of inflammatory surface marker ICAM-1 detected on endothelial cells (Fig. 3.13), as well as upregulation of various soluble inflammatory mediators including IL-6 and IL-8 which were detected in the vascular channel of the chip by mass-spectrometry (Fig. 3.13). Notably, chips prepared only with endothelial cells or endothelial cells and fibroblasts, but without epithelial cells released significantly lower level of soluble IL6 and IL8 cytokines and displayed comparably low expression of ICAM-1, suggesting that epithelial-vascular crosstalk modulated most of the LPS-

mediated inflammation of the Open-top Alveolus-Chip. We conclude that the Alveolus-Chip exposed to ALI sustains viability of all three cell types and reconstitutes a physiologically relevant air-liquid interface.

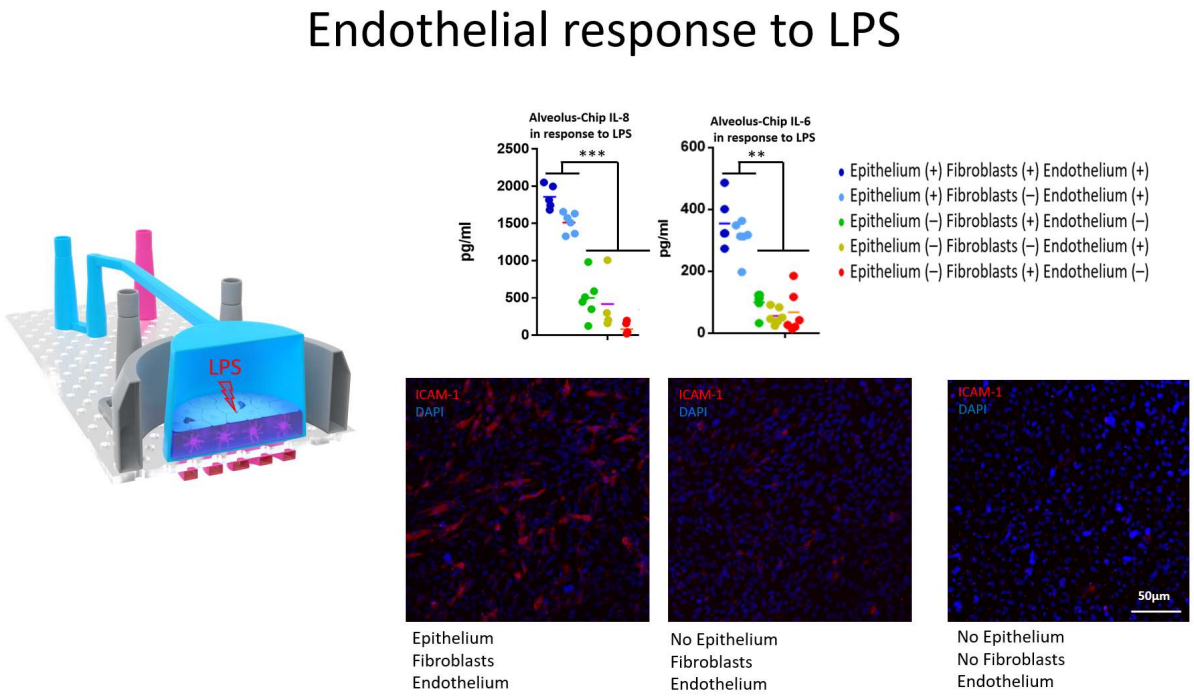

Figure 3.13: Endothelial response to LPS: Image showing ICAM-1 spatial distribution and graphs showing IL6 and IL8 inflammatory cytokine release as stimulation of the epithelial compartment with LPS (scale bar 50µm). The graphs also evidence that induction of inflammation requires the presence of epithelium to stimulate the expression of ICAM-1 which is also sign of the intimate interconnection between the three biological layers inside the chip. Oppositely the presence of fibroblasts has a minimal effect on the ICAM-1 and IL6 and IL8 release. (ANOVA, Turkey's multiple comparison test, n=4 per condition, p**<0.01; p***<0.001)

Next, we conducted a set of experiments aimed to validate the functionality of the endothelial compartment. Following the LPS treatment of the alveolar epithelium, blood labelled with CD41 was perfused in the bottom channel at physiologically relevant shear (60µl/min or 3.6ml/hr). Consistently with the previous observation based on ICAM-1 staining, LPS treatment of the alveolar epithelium induces platelet activation, aggregation, and adhesion to the inflamed endothelial lumen. Notably, the platelet distribution pattern matches the line of flow (Fig. 3.14). We conclude that the vascular compartment of the Alveolus-Chip acts as a semi-selective barrier between the vessel lumen and recreated alveolar tissue, controlling the passage of nutrients and the transit of cytokines into and out of the bloodstream as well as recapitulating the hemodynamic of platelet agglutination.

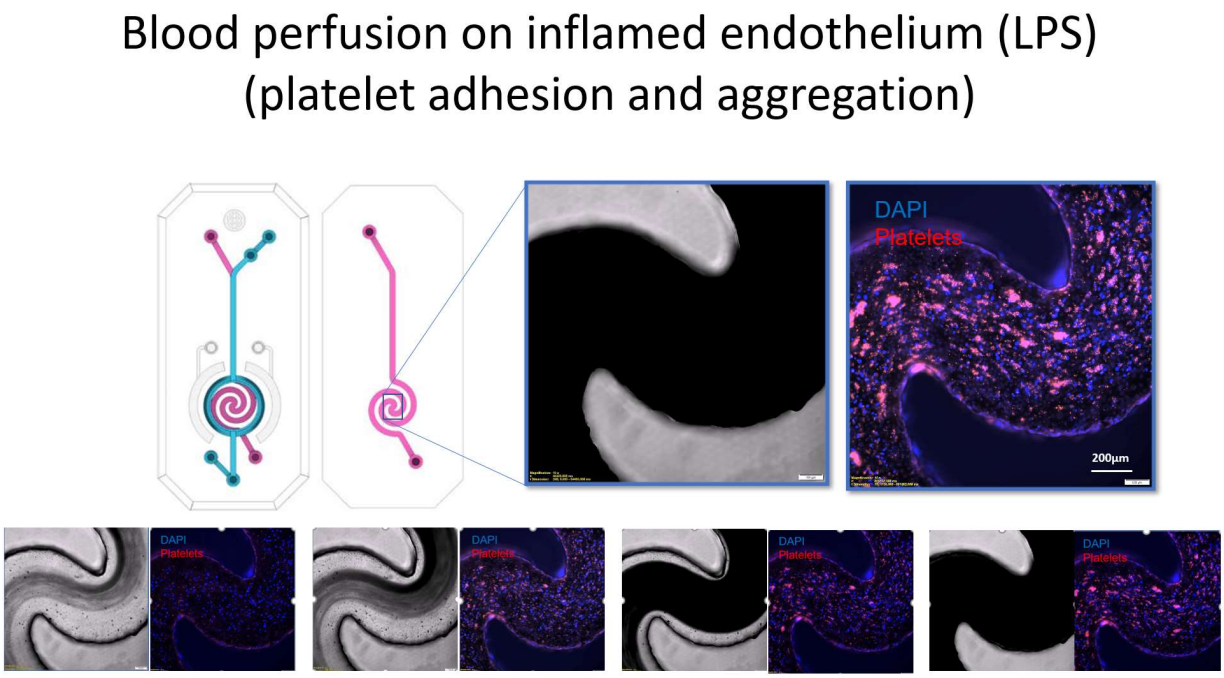

Figure 3.14: Blood perfusion on inflamed endothelium (LPS): Phase contrast and fluorescence footage of blood perfusion inside the vascular compartment showing the spatial distribution and localization of the platelet adhesion and aggregation.

Epithelial-stromal interaction regulates epithelial maturation

Several pieces of evidence indicate that specific topological positions and biomechanical cues are critical for the maintenance of alveolar markers in vivo. Studies conducted on rat cells have shown that epithelial proximity to the pulmonary fibroblasts can improve the surfactant production(Mason et al. 2002)(Shannon et al. 2001) and epithelial cell survival(Sucre et al. 2018). At the same time, mechanical strain experienced by alveolar cells, as a consequence of breathing motion, seems to also support the maturation of functional alveolar cells and secretion of surfactants(Mason et al. 2002). Given our ability to reconstitute a tridimensional breathing Alveolus-Chip, we sought to determine whether the system exhibits critical functions that will enable studies of stromal-epithelial interaction and crosstalk. Results obtained via confocal imaging (Fig. 3.15, a) indicate that fibroblasts tend to form protrusion directed toward the alveolar epithelium within 12 days of cell culture on-Chip. Interestingly, the histological cross-section of the epithelium equivalent (Stroma equivalent lined by the alveolar epithelium) shows the spatial distribution of the fibroblast in the stromal layer evidencing the fibroblast tendency to grow preferentially toward the epithelium (Fig. 3.15, b) probably indicating the release of chemoattractant by the epithelium. This fibroblast growth is in contradiction with our expectations, since we would have expected a preferential growth toward the bottom channel imagining that fibroblasts would have

followed the gradient of nutrients. Maximum intensity projection of the Z-Stack of the live-dead staining evidencing the relatively high (over 90%) viability of fibroblast after 12 days in culture (Fig. 3.15, c).

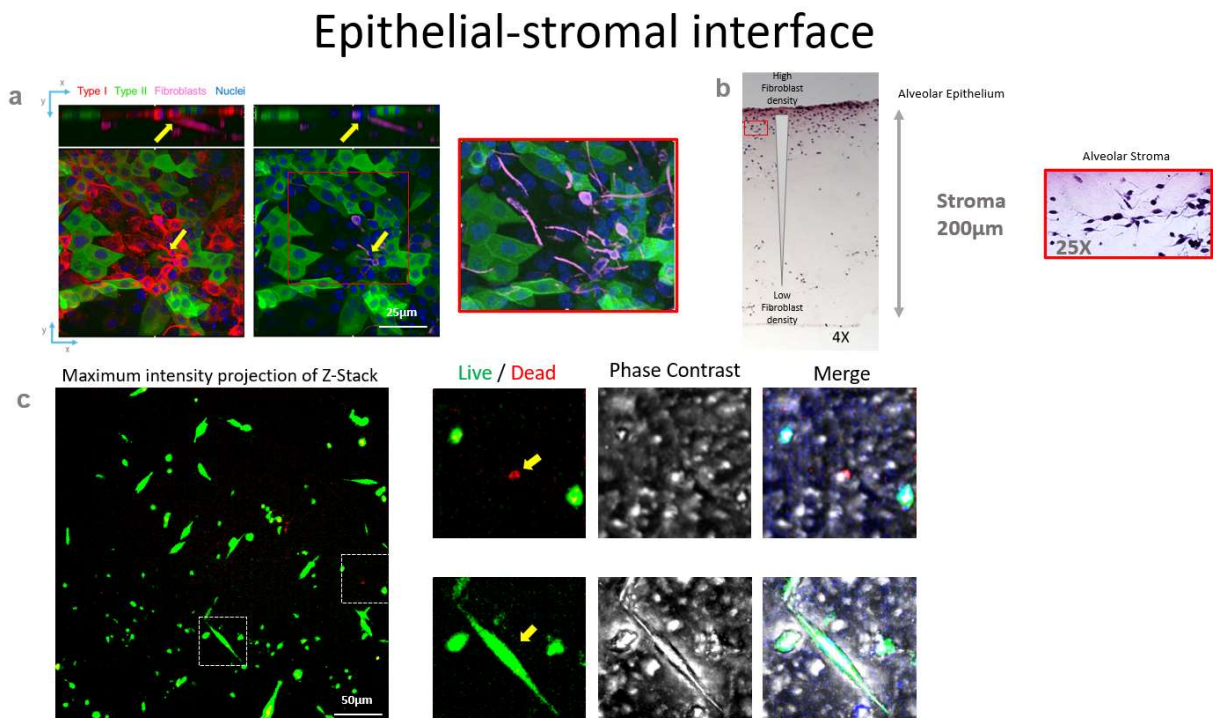

Figure 3.15: Epithelial-stromal interface: (a) Z-stack cross-section and top view image showing spatial distribution and localization of the fibroblast inside the stroma underneath the alveolar cell monolayer. Fluorescent images evidence that at fibroblasts interact with epithelium through direct contact (scale bar 25µm). (b) Histological image of the epithelium equivalent showing the spatial distribution and local density of fibroblast inside the stromal layer. (c) Maximum intensity projection, fluorescence and phase contrast images showing viability of fibroblast inside the stromal layer (living cells in green, calcein-AM; dead cells in red, Ethidium Homodimer-1; scale bar 50µm).

To further investigate the role that fibroblasts and mechanical stretching may have on maintenance of surfactant in the bioengineered Alveolus-Chip, we grew the Alveolus-Chip for 12 days (5 days submerged, 7 days ALI, 3 days 4 % stretching) with or without fibroblasts and with or without mechanical stretching. In line with other publications, we observed that alveolar cells do not express detectable levels of surfactant C when cultured in static conditions without fibroblasts at air-liquid interface (Fig. 3.19, c). However, the presence of fibroblasts in the stromal compartment and application of mechanical stretching enhanced epithelial expression of both surfactant B (Fig. 3.16, a) and surfactant C (Fig. 3.19, c) in soluble form. Image analysis (Fig. 3.16, a) indicates that the presence of fibroblasts has a preponderant role in stimulating surfactant production on-Chip. Importantly, we could confirm that surfactant C and B are both present at protein level, as confirmed via ELISA (surfactant C) and antibody staining (surfactant B). Gene expression (Fig. 3.16, b) also confirmed that the presence of fibroblasts has an important role in stimulating the synthesis of surfactant B and C and in maintaining the expression of podoplanin. The trend

of the graphs also evidence that the fibroblast stimulation is synergetic with that of the medium. In fact, upregulation of both type II (SURFB, SURFC, ABCA3) and type I (HOPX, PDPN, AQP5) markers seems to be amplified by the presence of fibroblasts in all three medium conditions and seems to indicate that fibroblasts might have a fundamental role in the maintenance of the alveolar phenotype inside the chips. Our results demonstrate for the first time that human alveolar epithelial cells, grown on a reconstituted stromal compartment and experiencing mechanical strain, maintain expression of tissue-specific makers and release of soluble surfactant.

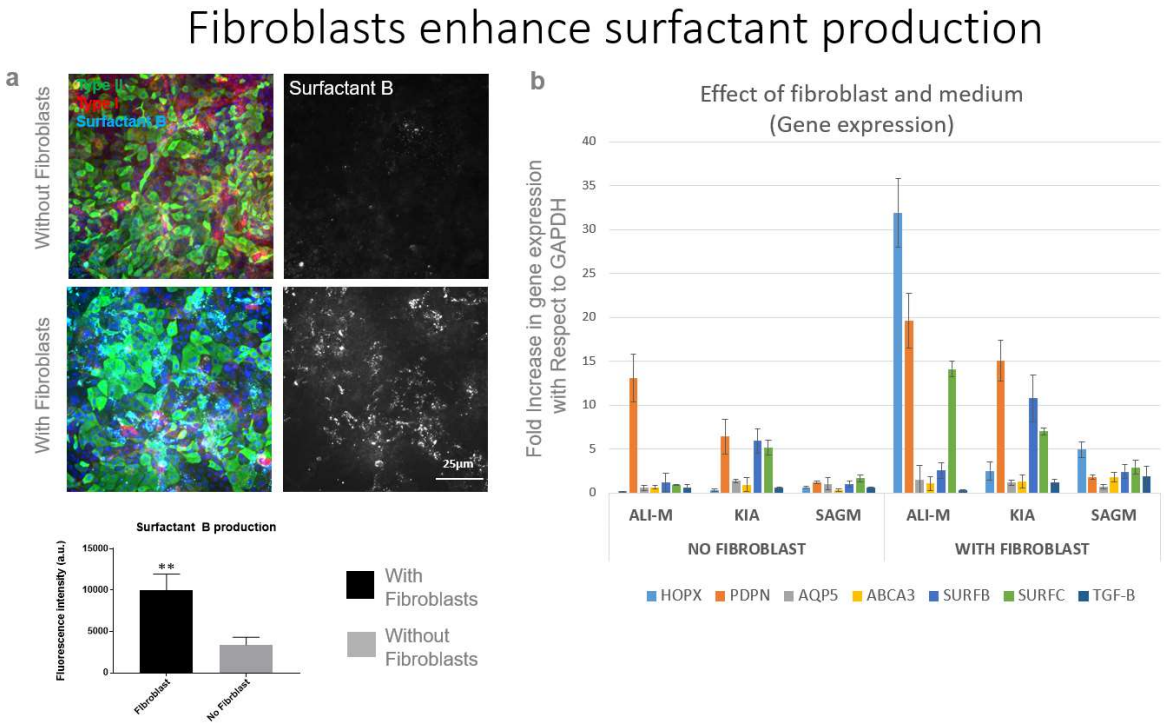

Figure 3.16: Fibroblasts enhance surfactant production: (a) HTI, HTII and surfactant B staining images showing spatial distribution and localization of type I, type II and surfactant B. Graph quantifying surfactant B fluorescence intensity (t-test, n=4 per condition, p**<0.01; scale bar 25µm). (b) Gene expression of canonical alveolar type I and type II markers showing the effect on the gene expression induced by the different media in presence and absence of fibroblasts (n=3 per condition).

The primary human Alveolus-Chip exhibits markers of mature tissue

Next, we characterized the epithelial monolayer of the Alveolus-Chip. Histological sections of the Alveolus-Chip confirm that the epithelium contains two phenotypically distinct cell types: type I pneumocytes with thin, squamous cell bodies and a flattened nucleus and type II pneumocytes with large, cuboidal cell bodies (Fig. 3.19, H&E). Immunofluorescence and image analysis of chips stained for HTI-56 and HTII-280 further confirm that both type I and type II alveolar cells are present in the Alveolus-Chip with different morphological phenotypes (Fig. 3.8). Expression of mature pneumocytes was also confirmed via

immunostaining of pro-surfactant protein C, surfactant protein B, podoplanin (AT-1α) and the epithelial Na^+ channel (ENaC) (Fig. 3.17). The alveolar epithelium was lined with intercellular junctions including adherens, tight junctions and gap junction (detected via immunostaining of E-cadherin, ZO-1 and connexin 43 (Fig. 3.17), respectively.

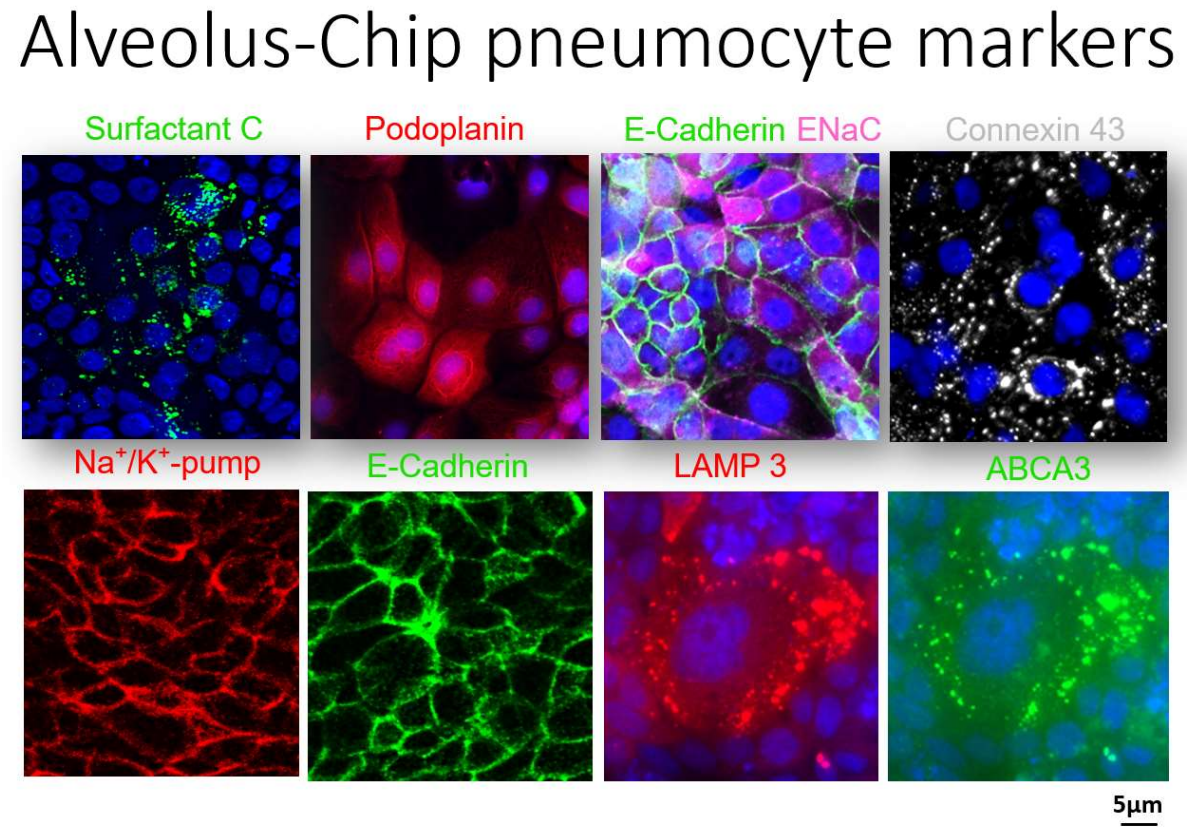

Figure 3.17: Alveolus-Chip pneumocyte markers: Immunofluorescence staining images showing the presence of tight junction E-cadherin and alveolar marker of the type I and type II cells phenotypes (scale bar 5µm).

Additionally, the 3D stack of cells stained for pro-surfactant protein C and the intercellular junction marker E-cadherin demonstrated that a large fraction of pro-surfactant protein C resides within the intracellular space (Fig. 3.18). Surfactant protein B was also localized within the intracellular space.

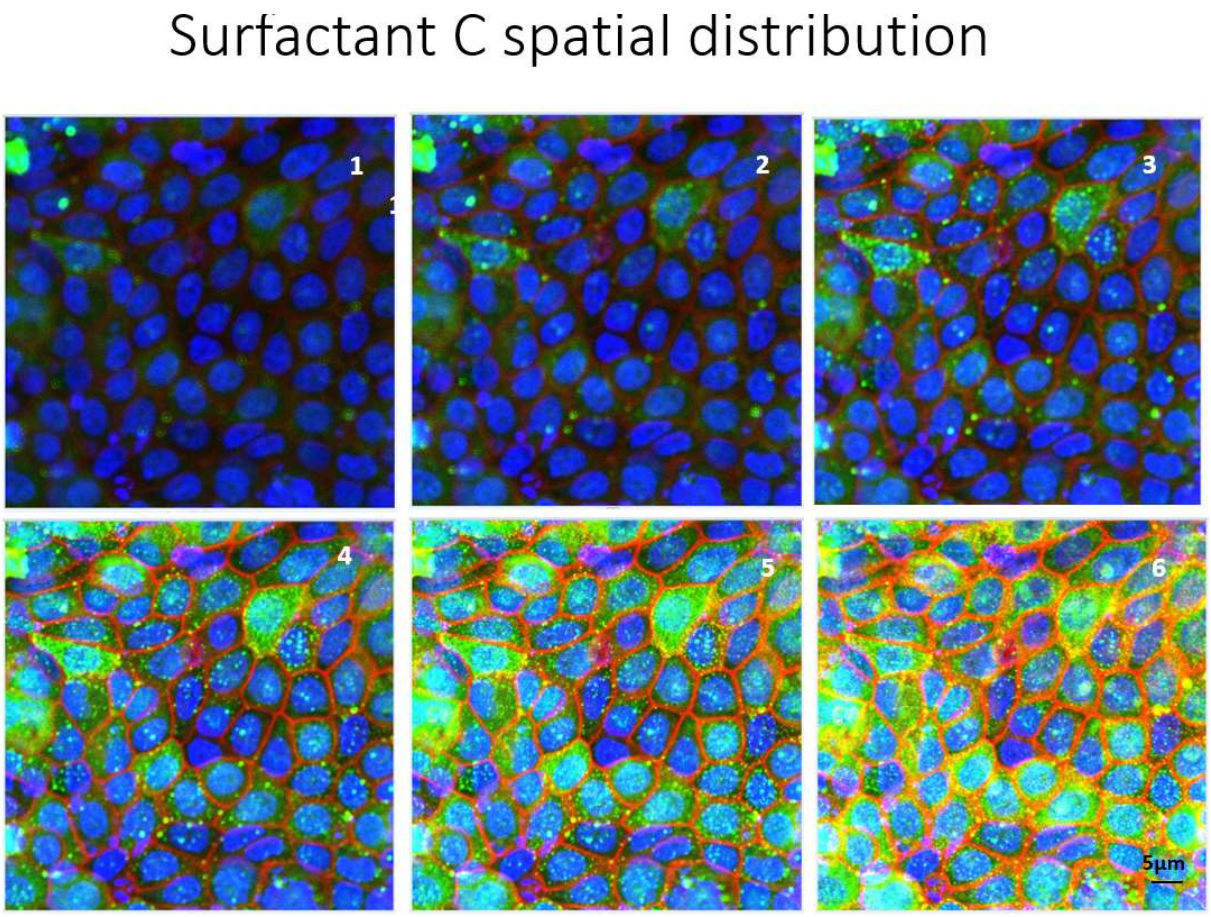

Figure 3.18: Surfactant C intracellular spatial distribution: 3D stack images at different depths, 1 corresponding to the cellular basal side and 6 corresponding to the cellular top side, each step corresponding to 2µm increment. The images represent immunofluorescence staining for nuclei (blue), E-cad (red) and surfactant C (green) images showing the presence of surfactant C vesicles inside the type II cells (scale bar 5µm).

We also detected ATP-binding cassette A3 (ABCA3) and lysosomal associated membrane protein LAMP-3 (also known as DC-LAMP) proteins (Fig. 3.19, a) Those proteins are involved in lipid homeostasis and lamellar body biogenesis and suggest the presence of an active surfactant metabolism. TEM images confirmed the presence of lamellar body inside the alveolar cytoplasm (Fig. 3.19, a). Consistent with the hypothesis that exposure to air promotes epithelial cell maturation, we observed the presence of recognizable alveolar surface microvilli (Fig. 3.19, a). Our results demonstrate that introduction of ALI does not affect cell viability, which remained constant for up to 15 days (Fig. 3.19, c), and promotes secretion of surfactant C proteins (Fig. 3.19, a, c). We conclude that primary alveolar epithelial cells cultured in the Alveolus-Chip for up to 15 days and exposed to air express tissue-specific markers, including secretion of soluble surfactant proteins consistent with mature alveolar phenotypes.

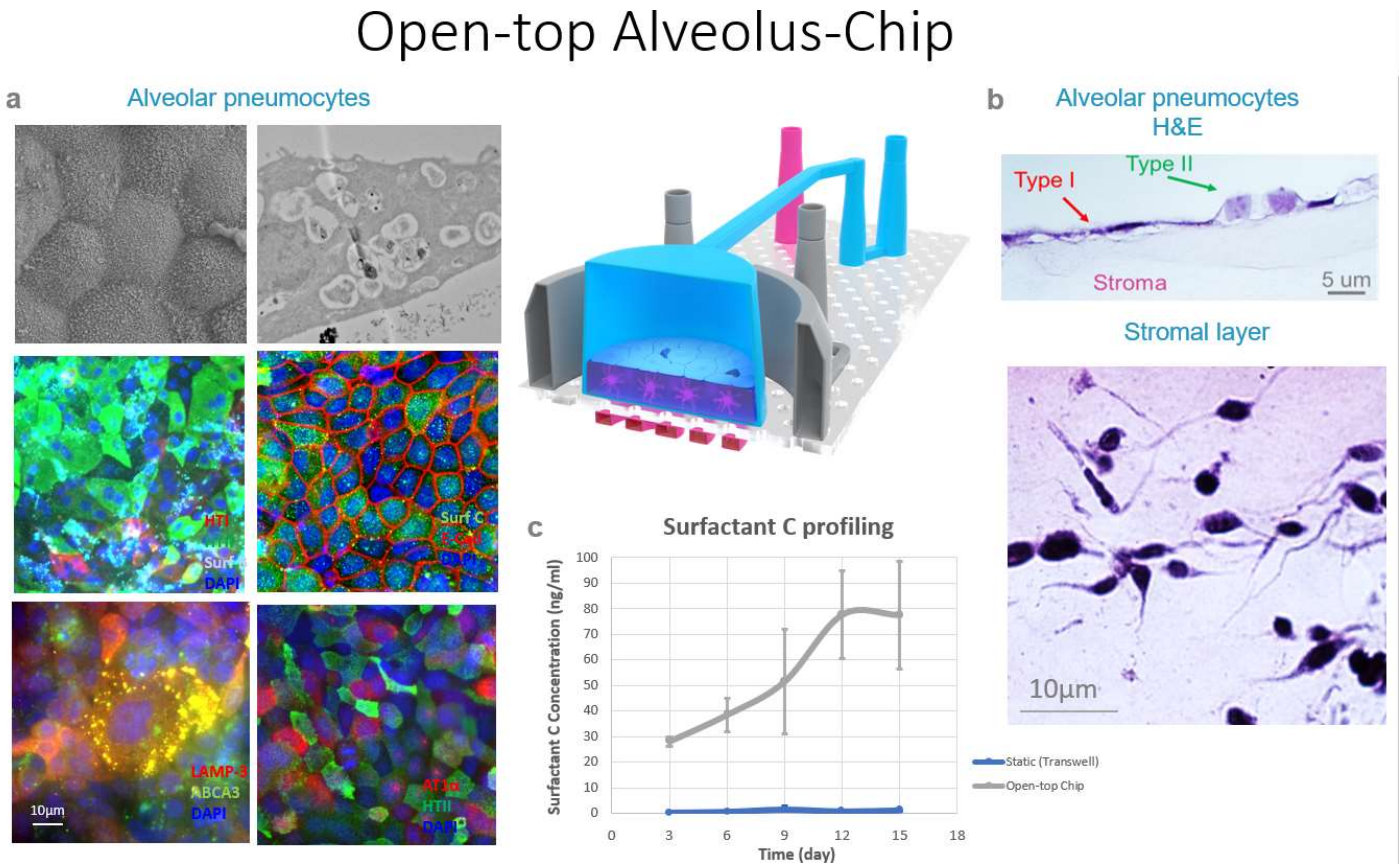

Figure 3.19: Open-top Alveolus-Chip: Alveolus H&E cross section and Immuno-fluorescence images: (a) SEM, TEM and immunofluorescence staining showing Alveolus epithelial marker distribution HTI (alveolar type I cell-specific antigen, red) and HTII (alveolar type II cell-specific antigen), E-cadherin (tight junction epithelial marker, green), Surfactant C (alveolar type II cell-specific secretion marker, red), Lysosomal Associated Membrane Protein 3 (Lamp3) (alveolar type II cell-specific membrane marker, red), ATP binding cassette, class A3 (ABCA3) (alveolar type II cell-specific intracellular marker, green) a lipid transporter involved in the metabolism of surfactants B (lung specific marker, red) and DAPI (nuclei) (scale bar 10µm). (b) Hematoxylin/Eosin-stained cross sections showing stromal layer and alveolar monolayer (scale bar 10 and 5µm, respectively). (c) Surfactant C profiling showing surfactant C release time course value are shown as mean +/- st.error.

Pharmacological modulation of oxidative stress

Injury to the alveolar region is a hallmark of respiratory distress syndrome caused by external insults and acute cell stress. Alveolar injury is associated with the loss of selective barrier function, production of radical oxygen species (ROS), and regulation of specific intracellular pathways, including activation of anti-oxidative genes, such as Sulfiredoxin (SRXN1) and NAD(P)H:quinone oxidoreductase (NQ-1)(L. Li et al. 2014), by Nrf2 and attenuation of oxidative-stress-mediated cell damage(Hailin Zhao et al. 2017)(Q. Liu, Gao, and Ci 2019)(Cho, Reddy, and Kleeberger 2006). Given our ability to engineer a multicellular human Alveolus-Chip, capable of maintaining air-liquid interface, sustaining long term cell culture of epithelial cells, and expressing tissue-specific markers, we sought to explore if canonical intracellular pathways

involved in cell injury and inflammation were conserved and functional in our model because these pathways may reveal key targets for drug discovery to repair the lung following injury. First, we challenged the barrier function of the Alveolus-Chip using a generic noxious stimulus. We exposed the epithelial surface, which was grown for 12 days (5 days submerged, 7 days ALI, 3 days 4 % stretching), to hydroperoxide (H_2O_2, 10mM)(Rao 2008)(E. K. Kang and Kim 2017)(Rahman and Adcock 2006)(Wijeratne, Cuppett, and Schlegel 2005). After 24h of continuous exposure, the chips were fixed and stained for E-cadherin, F-actin and nuclei (Fig. 3.20). H_2O_2 treatment of the alveolar epithelium induced a rearrangement of the actin cytoskeleton and rupture of the intercellular junctions, identified by gaps (arrows) in the cell monolayer.

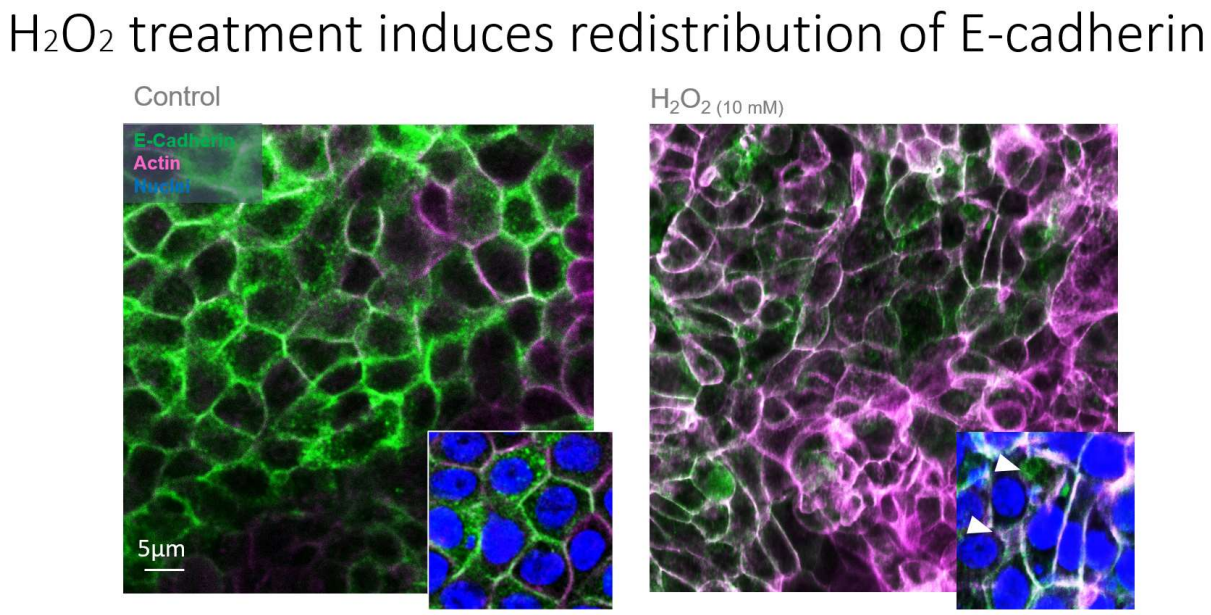

Figure 3.20: H_2O_2 treatment induces redistribution of E-cadherin: Immunofluorescence staining showing the redistribution of E-cadherin within the alveolar epithelium induced by the H_2O_2 treatment (scale bar 5µm).

Disruption of epithelial integrity was accompanied by a significant increase in LDH (Fig. 3.22) detected in the epithelial effluent of the Alveolar-Chip and loss of barrier function (Fig. 3.21), measured from the vascular-to-epithelial diffusion of fluorescent Dextran-FITC (3000Da). The results seem indicate that loss of barrier function is a progressive event which occurs in the course of several hours.

H_2O_2 treatment induces barrier disruption

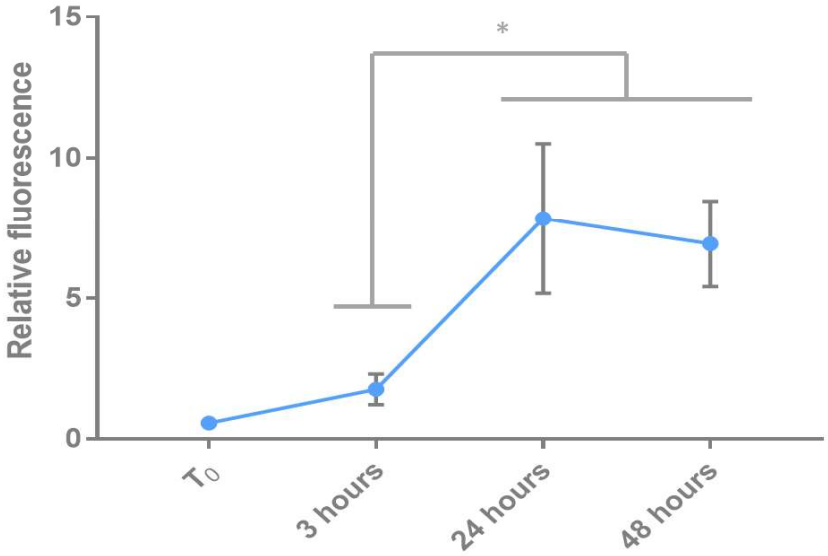

Figure 3.21: H_2O_2 treatment induces barrier disruption: Graph showing the leakage of Dextran-FITC (3000Da) from the endothelial to the epithelial compartment at 3, 24 and 48 hours after treatment with H_2O_2. Dextran leakage is a measure of the barrier-function disruption, induced by the H_2O_2 treatment. (ANOVA, Turkey's multiple comparison test, n=6 per condition, p*<0.1)

In addition, H_2O_2 treatment upregulated ICAM-1 (a well-known marker of tissue inflammation(Beck-Schimmer, Schimmer, and Pasch 2004)), SRXN1 and NQ-1, as detected by real time PCR (Fig. 5, b), demonstrating that the alveolar epithelial cells in the Alveolar-Chip were capable of orchestrating a complex, injury-induced biochemical response that reached the endothelial layer. Since SRXN1 and NQ-1 are both anti-oxidative genes regulated by the Nrf2 pathway(Bischoff et al. 2019), we challenged the system using a pharmacological compound (GSK-1) known to upregulate the Nrf2 pathway and recently reported to protect the airway from noxious treatment in vivo(Xing et al. 2015)(X. Li et al. 2017).The vascular compartment of the Open-top Alveolus-Chip was perfused overnight with increasing concentrations of GSK-1 compound and then exposed to hydroperoxide (epithelial side) for 24h. Following the hydroperoxide treatment, we observed that chips pre-treated with 0.1uM and 1uM of GSK-1 (Fig. 3.22) maintained a barrier function, assessed as vascular-to-epithelial leakage of dextran, close to untreated, control chips. A rather significant loss of barrier function was observed for chips pre-treated with a lower dosage (0.01uM) of GSK-1 and in treated, vehicle chips. Notably, the protective effect of GSK-1 was accompanied by a net transcriptional upregulation of Nrf2 effectors SRXN1 and NQ-1 and a relative decrease in the inflammatory marker ICAM-1, which is in line with the hypothesis that activation of the Nrf2 pathway can protect the tissue from the detrimental effects of hydroperoxide-induced injury.

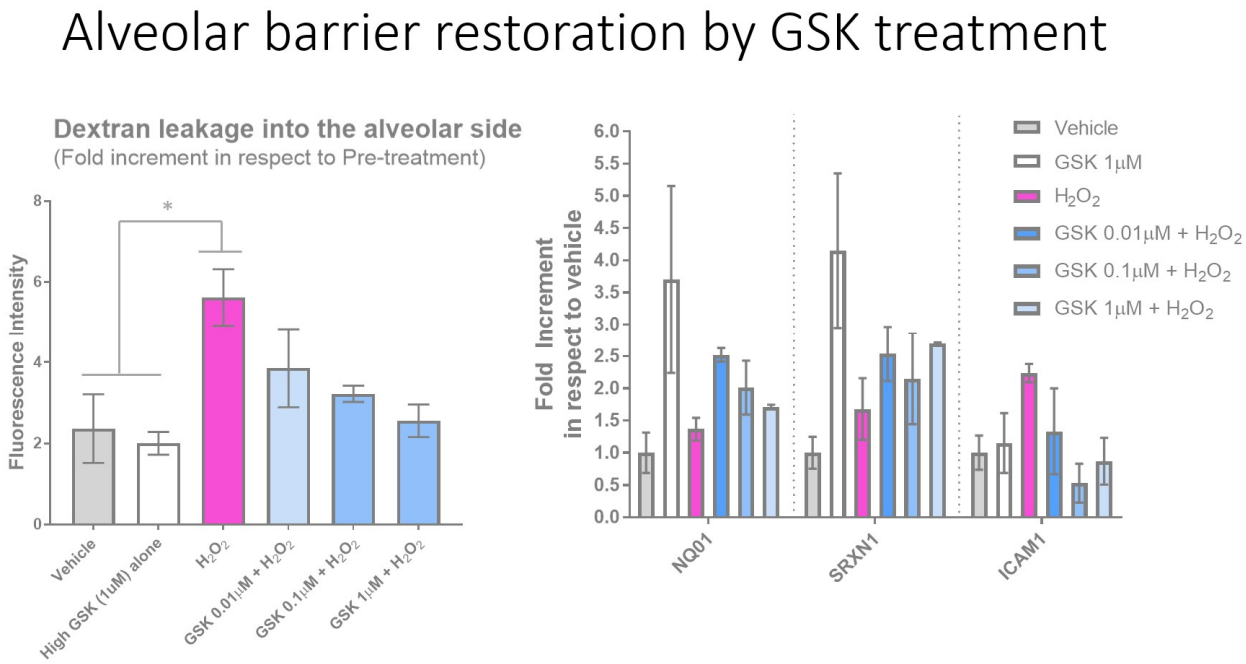

Figure 3.22: Alveolar barrier restoration by GSK treatment: Graph showing dose-dependent barrier function restoration induce by GSK treatments. Gene expression graph showing upregulation of epithelial Nfr2 pathway genes (NQ01, SRXN1) and endothelial inflammatory gene (ICAM-1) induce by GSK treatments. (ANOVA, Turkey's multiple comparison test, n=6 per condition, p*<0.1)

Vascular administration of two small molecule compounds (GSK and JQ1) known to act as Nrf2 stimulants also protected the alveolar tissue from H_2O_2-induced loss of barrier function (Fig. 3.22)(X. Li et al. 2017), demonstrating that the current model of the human alveolus is sensitive to a vast class of compounds designed to target the Nrf2 pathway. Additionally, we found that epithelial exposure to Budesonide, a corticosteroid molecule of well-known anti-inflammatory properties(Adenuga et al. 2010)(Staurengo-Ferrari et al. 2019), also resulted in protection of the epithelial tissue from oxidative stress (Fig. 3.22). These results provide confidence in continued future development of this model as a testing platform for anti-inflammatory molecules that combat oxidative stress.

Open-top Alveolus-Chip pharmacology response

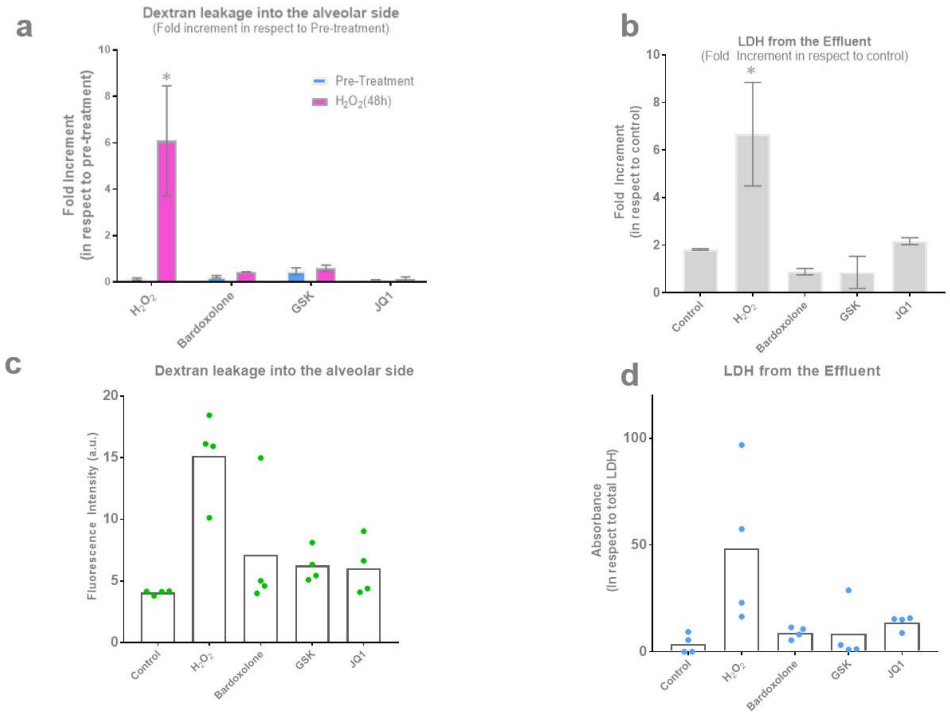

Figure 3.22: Open-top Alveolus-Chip pharmacology response: (a, c) Graphs showing effect of anti-inflammatory drug Bardoxolone, GSK and JQ1 in restoring the barrier function. (b, d) LDH graphs showing dead cell in respect to the control. Notably the two LDH graph profiles correlate with respective barrier function treatment profile graphs. (ANOVA, Turkey's multiple comparison test, n=4 per condition, p*<0.1)

The Open-top multilayered micro-channeled design can be applied virtually to all organs that contains vasculature, stroma and epithelium or parenchyma as well as other cell populations strictly interfacing in close proximity (e.g., cartilage, bone, etc.). We give a proof of the versatility of our biomimetic platform by showing three other organs cultured and differentiated using the Open-top Chip following:

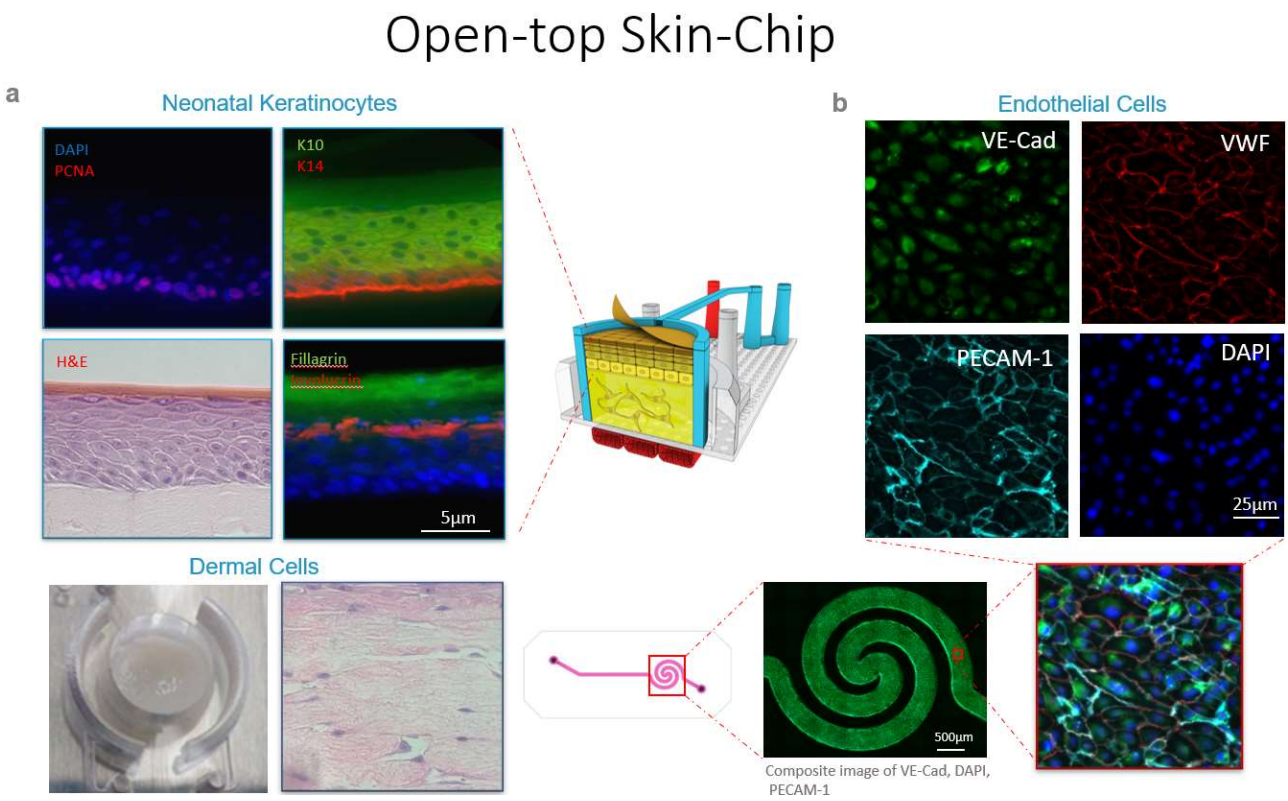

Figure 3.23: Open-top Skin-Chip: (a) Hematoxylin/Eosin-stained full-thickness epidermis sections and immunofluorescence staining of full-thickness epidermis showing proliferative cell (PCNA), keratin 14 (basal layer, red), Keratin 10 (spinous layer, green), Involucrin (red) and Filaggrin (cornified layer, green) distribution and DAPI (nuclei)(scale bar 5µm). (b) Dermal microvascular endothelial cells expressing endothelial specific markers PECAM-1 (VWF), VE-Cadherin (Red) and PECAM-1 (magenta) (scale bar 25µm). (c) Top view of the dermal/epidermal layer and H&E showing fibroblasts embedded inside the dermal layer (scale bar 500µm).

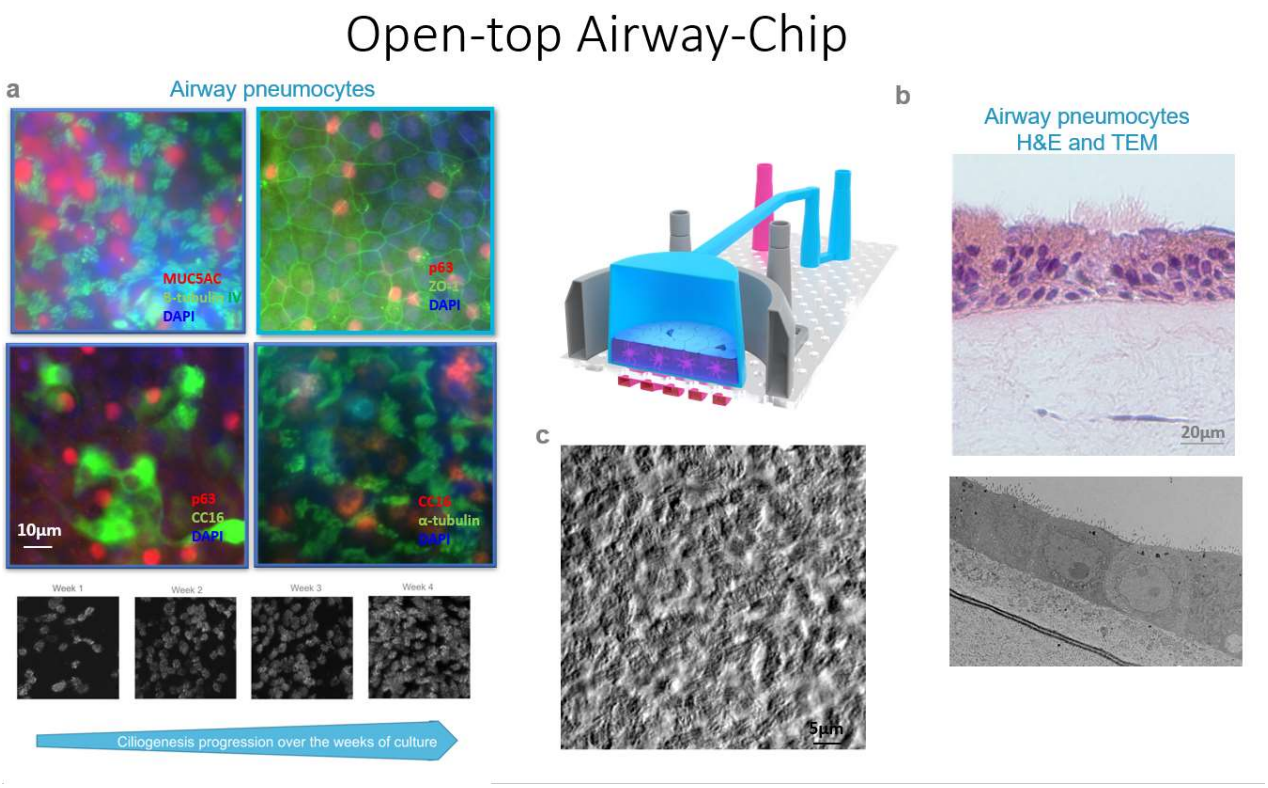

Figure 3.24: Open-top Airway-Chip: (a) SEM, TEM and immunofluorescence staining showing airway epithelial marker distribution Mucin5AC (Goblet cell, red) and β-Tubulin (Ciliated cell, green), ZO-1 (tight junction, green), p63 (basal cell, red), Uteroglobin, also known as secretoglobin family 1A member 1 (CC16) (Clara cell, red), α-tubulin (Cilia, green) and DAPI (nuclei))(scale bar 10µm). Standard deviation video showing increase in ciliation as function of time. (b) Hematoxylin/Eosin-stained cross sections showing airway stromal layer and epithelial monolayer (scale bar 20µm) and TEM image of airway cells. (c) Image showing phase contrast image of the cilia (scale bar 5µm).

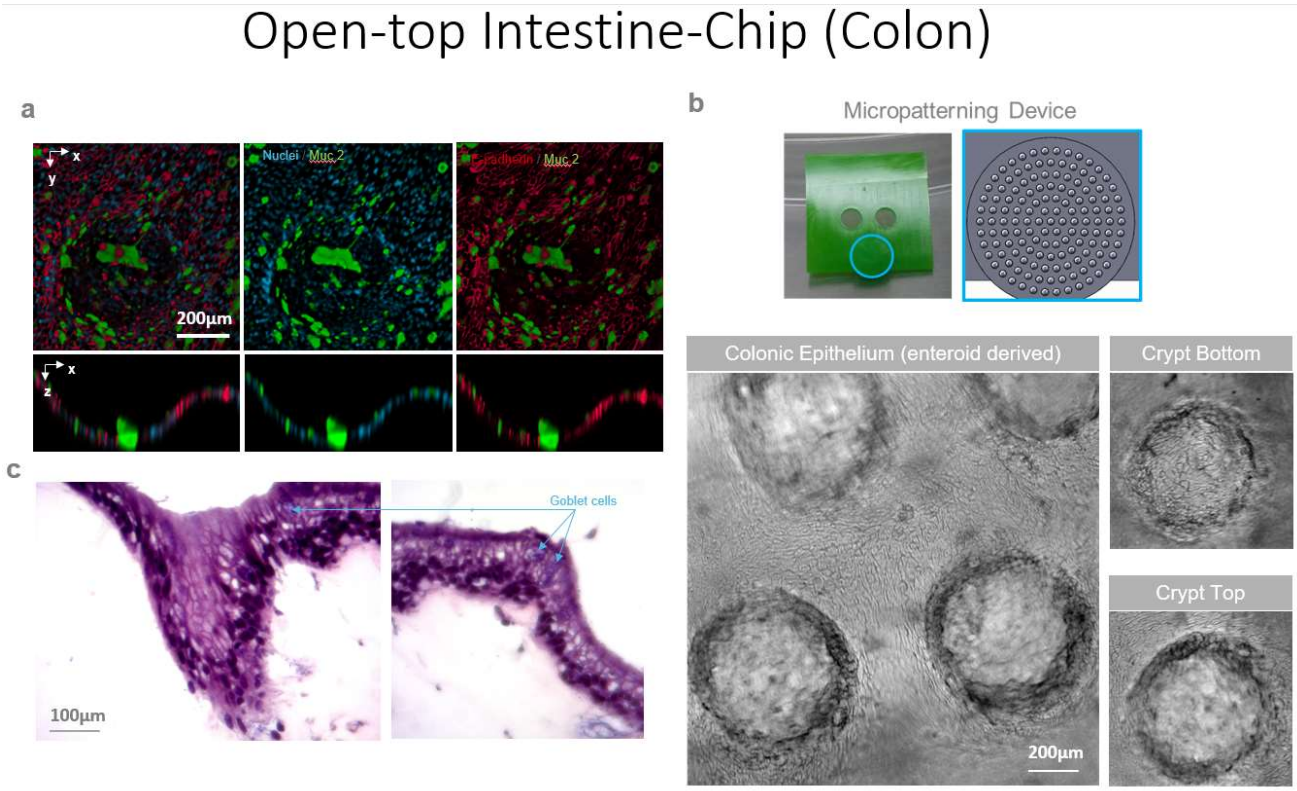

Figure 3.25: Open-top Intestine-Chip (Colon): (a) epithelial marker of Skin and fibroblast distribution across the tridimensional stromal-compartment of the skin Open-Top-Chip (scale bar 200µm). (b) Histological image of the Intestinal organoid (enteroid) layer and intestinal fibroblast distribution across the tridimensional stromal compartment (scale bar 100µm). (c) Phase contrast image of intestinal organoid (enteroid) monolayer lining the micropatterning surface (scale bar 200µm).

4. DISCUSSION

Discussion

Brief Overview

Recapitulating healthy or diseased alveolar physiology in vitro is highly complex because it involves mimicking the chemical and physical interactions and functions of alveolar epithelium, stroma, and endothelium which behaviors are highly sensitive to multiple factors of the local microenvironment. Those include three-dimensionality, chemically defined and spatially organized network of extracellular matrix components, cell-cell interactions (for example, between the pneumocytes, fibroblasts and microvascular endothelial cells), cell-ECM interactions, and local cell-type composition as well as mechanical forces and shear stress. The effects of the microenvironment have been started to be investigated and understood only recently and there is poor knowledge on their relevance at biological level. Consequently, traditional in vitro 2D and 3D alveolar culture methods fail to fully reproduce the structural and functional physiognomies of native alveolar tissue representing an oversimplified model of the human lung, where most of the essential elements of the natural milieu are absent. Stimuli from the microenvironment are generally known to orchestrate many processes in vivo including differentiation, proliferation, and regulation of lung functions, nevertheless the details about their mechanisms of action are still object of scientific investigation or controversial debate. Similarly, animal models showed many limitations in recapitulating human physiological responses, due to the intrinsic biological differences existing within species and among species at several genetic and anatomical levels.

The development and validation of new and more reliable in vitro models that could be a valid alternative to conventional in vivo animal studies has been a long-recognized as a priority in the fields of pharmacology. Organoid and Organotypic 3D culture studies demonstrated how a fine control over the micro-environment, which includes mimicking of cell-cell and cell-ECM interactions; recreation of the complex structures of organs at micrometer scale such as three-dimensional tissue geometry and tissue-tissue interface between the epithelium and stroma or epithelium and endothelium; stimulation of the cells with mechanical forces such as shear stress or cyclic mechanical deformations (peristaltic motion) is essential to recapitulate or restore the basic organ functions and to generate more physiological relevant models to study human biology and human diseases. Three-dimensional cell cultures that achieve such complexity could represent tools to bridge the gap between animal and human in preclinical studies.

In our study, we engineered an alveolar in vitro model comprising the three biological elements of the human lung capillary wall, which includes epithelium, stroma and endothelium, and we used this model, a model that use mechanical stimuli resembling those occurring in the living alveolar interface (stretching, shear wall stress, etc.), to promote differentiation of human pneumocytes in mature type I and type II alveolar cells. we examined whether pneumocytes that had been matured using the methods described above could be used as a tool to test sensitivity of alveolar cells to microenvironmental signals and drugs in vitro. To the best of our knowledge, microfluidic devices that recapitulates multiple functions of the human living lung has not been reported in literature.

Open-Top Stretchable Chip technical considerations

We designed a multifunctional microfluidic platform, the Open-top Chip, to better recapitulate some of the fundamental structural, functional, and mechanical properties of a three-dimensional cross-section of the alveolar-stroma-capillary wall of the human lung. Specifically, we recreate the basic alveolar microenvironment structures which includes the tissue-tissue interface between alveolar microvascular endothelium, stroma and alveolar epithelium, shear stress along the capillary wall and cyclic mechanical deformations on the alveolar epithelium similar to those observed in the breathing lung (breathing motion). To our knowledge a microfluidic human alveolus model that recapitulates multiple functions of the living organ has not been possible due to lack of functional culture method suitable to support the viability and the marker expression of primary adult differentiated human alveolar epithelial cells under in vitro conditions as well as lack of microfabrication techniques compatible with manufacturing devices that efficiently integrate natural biomaterials and replicates at micrometer scale the tissue geometry of the alveolar interface(Mao et al. 2015).

The Open-top chip is composed of a flexible poly(dimethylsiloxane) (PDMS) elastomer. This material was selected because it is the only biocompatible materials currently known that offers gas permeability, which is fundamental to stimulate alveolar cells maturation; elasticity, which is the property that we exploit to mechanically deform the enclosed microenvironment and to study mechanobiology and tensegrity (defined as “the architectural basis of cellular mechanotransduction") of the biological system; full transparency which makes this chip particularly suitable for visualizing and monitoring cells once enclosed inside it; and ultimately, material compatibility with surface modification methods that does not leave toxic residues, which makes this material biocompatible and suitable for biological applications.

In the Open-top Chip, PDMS has primarily the structural function to physically contains the hydrogel in place. This function is achieved through the chemical activation of the PDMS surface by ER1/ER2 treatment which covalently cross-links the collagen fibers with the PDMS surface of the circular cavity wall and the membrane underneath. The crosslinked hydrogel acts as a plug and impedes medium (or other fluid) to leak through the bottom channel and the cavity, while still allowing medium diffusion through the hydrogel fibers to feed the mesenchymal cells embedded into the hydrogel and the epithelium on the top. Moreover, the geometry of the cavity was decided to be circular to equilibrate the tension acting on the hydrogel-PDMS wall interface and eliminate the concentration of mechanical stresses occurring at the vertices of a rectangular shaped wall. Rectangular and oval prototypes tested all resulted in delamination of the hydrogel from the PDMS wall.

We also opted for a spiraled shaped vascular compartment of the Open-Top Chip for two main reasons: primarily, the spiraled shape maximizes the area of PDMS porous membrane, and consequently medium, in direct contact with the recreated stroma allowing its full hydration and secondarily, to maintain constant the laminar flow along the entire length of the bottom channel, a parameter required to perfuse blood or blood surrogates (as for instance, medium with added white blood cells (such as PBMC)) under physiological relevant and not activating conditions. The spiral-geometry of the vascular chamber also allowed fine control of the wall-shear rate along the entire endothelial compartment differently from other geometries.

Yet, PDMS has a secondary "active" function which is that to convert negative pressure (vacuum) in mechanical deformation and generate breathing-like motion. The physical crosslinking between the PDMS cavity wall and the hydrogel is used to convey the deformation generated by the negative pressure applied on the vacuum chambers to both the stroma and epithelium which undergo mechanical stretching (e.g. breathing motion). The geometry of the vacuum chambers was specifically designed to generate a deformation linearly proportional to the intensity of the applied suction in the physiological range such as reported in literature (see for more details Konstantin G. Birukov in "Magnitude-dependent regulation of pulmonary endothelial cell barrier function by cyclic stretch").

Specifically, to model the cyclic mechanical strain observed in living alveoli (the repetitive cycle of stretching and relation to which alveolar cells undergo during breathing) we created an actuation system which allows to define the magnitude and period of the mechanical motion. The integration of three elements including the crosslinking of the PDMS wall surface with the hydrogel, the special vacuum chamber geometry and the modulable pneumatic actuator in a fully integrated system makes the chip particularly suitable to stretch a relatively thick hydrogel (the recreated stroma) throughout its entire height, a feature of the chip that all the other microdevices to our knowledge failed to achieve.

Another important feature of the stromal cavity wall was its drafted angle of 3 degrees. We engineered a drafted wall surface to generate an anisotropic axial displacement of the hydrogel to maximize stretching at the level of the epithelium and minimize mechanical strain at level of the membrane because differently from other reports(Huh et al. 2010)(Huang et al. 2012)(Sumpio et al. 1990), we noticed that human lung microvascular endothelial cells undergoing prolonged stretching/relaxation cycle faded over time. The angled wall resulted particularly effective in mitigating endothelial stress and eliminated the issue.

Open-top Chip is built with a multilayered microchannel architecture which keeps physically separated the culture cavity from the top and bottom microfluidic channels, but chemically interconnected the epithelium and endothelium through exchange of cytokines, hormones, and other chemical signals. The physical separation between the cavity and the microchannels permits independent sampling of cellular fluids and byproducts from the epithelial and endothelial compartment or independent dosing through the top and bottom channel. Physical separation of the bottom and top channel fluidics makes the chip particularly suitable for time lapse collection of effluents (medium or sample washes). This operation has a particular significance in dynamic analysis where top and bottom channel effluents can be examined at predefined time intervals to study directional molecular transport, molecular cell uptake and metabolism of compounds or to extrapolate important pharmacodynamic and pharmacokinetic parameters on metabolites, drugs and other chemical compounds.

The peculiar architecture of the Open-top Chip allows to keep the three biological elements constituting the alveolar organ unit (endothelium, stroma and epithelium) spatially confined in a define portion of the Chip (compartmentalization) and simplifies their localization by optical visualization. Compartmentalization also helps tracking the specific biological element that contribute to cellular response by helping to identify where (or in what compartment) a stimulus is generated and how it propagates in the biological system. For instance, we modelled gram negative bacterial inflammation by stimulating the alveolar epithelium with lipopolysaccharides and observed the effects that it generated

on the endothelium. In this specific application, we took full advantage of the compartmentalization and full transparency of the chip to monitor solely and exclusively the effects occurring on the endothelium.

The modular building block design also offers the possibility to operate on (by adding or removing) the single components of the organ units to investigate the role of the specific biological elements on the response to stimuli. Specifically, by adding or removing biological complexity, it is possible to precisely identify or rule out if a particular stimulus is responsible for specific cellular behaviors or if it is the synergic effect of multiple stimuli to determine a specific cellular and tissue behavior. The possibility to add or remove elements of complexity is important because permits to investigate the contribution of each element of the organ unit to biological process. At the same time, it makes possible to test how the perturbation of single elements of the organ unit affects the organ system integrity, which, in turn, makes it a powerful tool for testing drugs, chemicals and to study the pathway of a drug at biomolecular level.

We performed experiments to test the role of the epithelium and fibroblasts into the inflammatory process where the epithelium compartment was exposed to LPS and the recreated stroma was generated with and without fibroblasts to investigate their effect on inflammation response. We experienced that LPS does not induce cytokine release and only minimally induce ICAM-1 expression in the absence of epithelium even if fibroblasts are present in the recreated stroma (Fig.3.13). Moreover, combining the compartmentalization of the chip with the removal-additional of complexity approach, we were able to decouple the contribution of the stroma in ICAM-1 expression and expression of the IL6 and IL8 cytokine release. That presented is just a simple example, but similarly someone could add or remove other degree of complexity such as endothelial cells, epithelial cells, the gel itself, change the coating, change the micro-patterning of gel surface, the type of hydrogel, and add or remove physical stimuli such as flow or stretching.

The dimensions of the Open-top Chip are specifically optimized for visualizing the biological elements enclosed inside the Chip at high resolution using microscopy (phase and fluorescence), while keeping the organ unit sterile. As previously mentioned, a clearly defined spatial confinement (compartmentalization) of each element of the organ unit is critical to optically isolate cells or tissue layers (endothelium, stroma, or epithelium) while examining their morphology or marker expression. Specifically, to validate the optical compatibility with high-resolution real-time imaging, we acquired videos of ciliated airway cells. Cilia are microscopic filamentous structures present over the airway cell surface long approximately 5-7µm and 1µm in diameter, which beat at a variable frequency from 7 to 16 Hz, depending on the stage of airway maturation. We used cilia coverage as metric to decide when the airway model was mature and ready to be sacrificed for analysis (Fig 3.24, a, c). The possibility to visualize microscopic morphological features of the airway organ unit without the need to sacrifice its sterility during the culture phase allowed to non-invasively monitor cilia beating process in real-time. The optical properties and the dimensions are also compatible with common immunofluorescence staining, which, can be performed directly inside the Open-top Chip after fixation of the organ unit (Fig. 2.23 a, b; 2.24 a; 2.24, a). Alternatively, taking advantage of the Open-top capability the organ unit can be physically extracted from the cavity and stained by traditional immunohistochemistry staining (H&E) (Fig. 2.23 a; 2.24 b; 2.25, c) which has precluded in almost the totality of PDMS microfluidic devices reported.

It is possible to further expand the applications of the system by performing recruitment assays. Such assays permit to model immune responses to chemicals, micro-organisms (bacteria, virus) and pro-inflammatory cytokines. The proposed assays essentially consist in the quantification of the increased adhesion of circulating white blood cells (neutrophils, macrophage and leucocytes) to the endothelium in response to its exposure to pro-inflammatory chemicals, micro-organisms and cytokines (such as TNF-α, Interferon γ). Furthermore, using micro-patterning, it is possible to recreate the complex architecture of epithelium interfaces, to model more closely the effects of cell-cell interaction and tissue-tissue interface and investigate how such architecture influences the molecular metabolism and mass transport across the re-created organ unit (Fig. 3.25, a, b, c). Specific tissue-tissue interfaces and geometries can be acerbated or extremized to mimic pathological conditions, which could be used to develop disease and injury models of specific organs.

Since our biomimetic platform has demonstrated successful in supporting viability and differentiation of many epithelial models, conceptually the next natural step would be to fluidically interconnect multiple organ models into a single instrument to recapitulate multi-organ interactions and emulate a real body response. However, whole-body physiology is currently precluded by the lack of a universal medium capable of supporting long term viability and differentiation of the different models. Nevertheless, it remains an interesting concept to explore which we will try to push forward in the future when advancement in medium production will support the project. We hope that multi-organ interactions lead us one step closer to human-on-chip and to build in the long run a valid alternative to the animal models.

Differentiation of pneumocytes into adult alveolar cells consideration

Although it remains problematic to restore alveolar adult mature phenotype in a robust manner in vitro, there is increasing evidence that multiple factors within the tissue microenvironment, including cell-cell interactions, timing of exposure to soluble growth factors, exposure to air and physicochemical properties of the extracellular matrix (i.e. Young's modulus) can affect alveolar cell fate. Therefore, we decided to explore whether chemically defined soluble factors, the signals induced by the ECM and the bio-mechanical stimuli (stretching and shear stress) can promote the differentiation of adult alveolar pneumocytes into more mature terminally differentiated alveolar cells in Open-top Alveolus-Chip. In all our experiment we cared to use fibroblasts and alveolar pneumocytes from the same patient. This choice was idealistic and based on the assumption that same patient cells could help recreating more physiological relevant alveolar interface and reduce unwanted and unknown donor cross-reaction. However, we want to mention that we have not found any paper supporting or opposing our vision.

We focused our attention in recreating the basement membrane interface of the human alveolar epithelium with the stroma by seeding alveolar cells in direct contact with the recreated stroma (collagen I gel with embedded primary lung fibroblasts) coated with alveolar basal laminal ECM (collagen IV, fibronectin and laminin 521)(Olsen et al. 2005)(Sucre et al. 2018). Inherent heterogeneity associated with adult alveolar cell differentiation(Beers and Moodley 2017)(Jacob et al. 2017) and considerations on practical integration of the cells into the microfluidic Open-top Chip convinced us that coating with basal lamina ECM proteins could facilitate alveolar cell adhesion by serving as anchorage matrices and stimulate the differentiation into mature alveolar epithelial cells. We experienced that to guarantee the correct

differentiation of alveolar pneumocytes, the coating is a critical step and it has maximum impact when performed sequentially right after the gel polymerization. We believe that the reason for such dynamic is because adding the ECM protein-solution right after the gel polymerization maximize the area coated by ECM. We speculated that exposing the hydrogel surface to medium, before the ECM coating, limits the ECM attachment because proteins contained in the medium, especially bovine serum albumin and γ-globulin, compete for attachment on the hydrogel surface limiting the ECM coating coverage. In our experience, the coating performed under this condition strongly enhanced pneumocyte attachment to the recreated stroma by reducing the time for attachment from hours to minutes. The decrease in the time of attachment to the substrate seem to be indicative that pneumocytes express high levels of β integrin that have high affinity for collagen IV, laminin and fibronectin which are abundant in the basal lamina, however it does not seem to be an absolute requirement for cellular attachment.

The information that ECM coating enhances cell-hydrogel binding efficiency improving cell attachment persuaded us to implement this practice into all subsequent experiments. Our studies revealed that collagen IV, fibronectin, and laminin fragments were all effective in increasing alveolar cell attachment to type I collagen hydrogel. Laminins, collagens, and fibronectins are widely expressed in the alveolar basement membrane during development and maturation of the lung, and integrin signaling has a notable role in the maintenance of alveolar structure and functions(Balestrini and Niklason 2015)(White 2015)(Sekiguchi and Yamada 2018). Based on this information, we decided to examine if the coating with commercially available laminin, collagen IV and fibronectin proteins could functionalize the apical surface of the recreated stroma and support better differentiation of primary human alveolar cells. qRNA of alveolar pneumocytes growth and differentiated on several ECM coatings revealed that among the combination of ECM tested, the mixture of collagen IV, laminin and fibronectin enhances more than others, the transcription of type I (PDPN, HOPX and AQP5) and type II (such as type I ABCA3, LAMP3 and SURFB) alveolar markers. Our results indicated that the efficiency in stimulating differentiation varies quite dramatically between coatings highlighting the need for serious considerations when selecting the type and composition of matrices for coating. Independently from the fact that the marker expression relied greatly on the coating, we were able to show that human primary alveolar cells can be induced to re-express the adult alveolar type I and type II markers after the initial loss due to the isolation from the lung.

Following this developmental discovery, we started culturing alveolar pneumocytes on recreated stroma coated with laminin, collagen IV, and fibronectin in submerged state. The initial choice of using a submerged state over air-liquid interface was determined by the low rate of success in culturing alveolar cells at air-liquid interface reported in literature(Mao et al. 2015)(Fuchs et al. 2003). These reports also highlight that under submerged condition, pneumocytes do not properly mature or express all the markers of the adult alveolar phenotype(Fuchs et al. 2003). We also experienced that alveolar cells cultured under submerged state for prolonged time (12 days) in Alveolus-Chip have the tendency to overgrow forming three dimensional clusters or aggregates indicating probably loss of contact inhibition. The tendency of alveolar cells to form aggregate and the inability to express the mature phenotype might indicate presence of alveolar progenitor cells, multipotent alveolar stem cell that retain the capacity to divide indefinitely and differentiate in multiple lineages. Stemness of these cells would also explain their

tendency to lose contact inhibition and form aggregate. Independently from the reason, the results suggested that we would need to improve the culture condition to induce or maintain the adult human alveolar phenotypes.

Based on literature articles reporting that soluble factors such as glucocorticoids and xanthine analogs can enhance expression of alveolar markers and induce alveolar cell differentiation in vitro(J. Wang et al. 2007a)(Fuchs et al. 2003)(Mao et al. 2015), we decided to test the capacity of these soluble factors to promote differentiation in the Open-top Alveolus-Chip. According to the protocol from Jieru Wang and colleagues described in "Differentiated human alveolar epithelial cells and reversibility of their phenotype in vitro(J. Wang et al. 2007a)", pneumocytes cultured in SAGM medium supplemented with epithelial maturation cocktail containing keratinocyte growth factor (KGF), IBMX (3-isobutyl-1-methylxanthine), Cyclic adenosine monophosphate (cAMP) and dexamethasone display distinct markers of the mature alveolar phenotypes. Specifically, it is reported in literature that keratinocyte growth factor (KGF), also known as fibroblast growth factor 7 (FGF7), causes alveolar cell proliferation and spreading helping the formation of a complete monolayer. KGF has also been reported to stimulate the production of surfactant A(Ulich et al. 1994); IBMX (3-isobutyl-1-methylxanthine), like other methylated xanthine derivatives increases membrane lipid synthesis, especially of phosphatidylcholine which is the major constituent of cell membranes and pulmonary surfactants. IBMX has also been reported to stimulate alveolar progenitor maturation; the abundant production of lamellar bodies and to increase the production of surfactant B and C(Gonzales et al. 2002); Cyclic adenosine monophosphate (cAMP), is a second messenger involved in signal transduction of many different pathways and upregulation of many genes. Both IBMX and cAMP stimulates production and release of surfactant and lamellar body synthesis(Gonzales et al. 2002). Dexamethasone, a glucocorticoid which upregulated many hormone-induced genes and transcription factors which has a critical role in lipid metabolism and surfactant protein genes expression (as for instance, Nkx2.1 (thyroid transcription factor-1). Dexamethasone has been reported to stimulate the production of surfactant B and pro-surfactant C, to promote alveolar maturation and is considered as necessary for precocious induction of functional alveolar type II cells in vitro(Gonzales et al. 2002)(J. Wang et al. 2007b). According to literature reports, our findings confirmed that dexamethasone, cAMP analog and IBMX co-regulate in a synergistic manner maturation of alveolar type I and type II cells. Specifically, pneumocytes cultured with KIAD supplements in SAGM exhibited expression of HTI-56 and HTII-280 marker, tight junction (E-Cad and ZO-1), surfactant B and C proteins and showed the presence of lamellar bodies, which were completely absent when not stimulated by KIAD supplements (called KIAD from the initials of the factor names).

Our study also indicates that relative expression of the specific markers varies with the specific culture condition. For instance, we experienced that the exposure of the alveolar epithelium to soluble KIAD factors for the entire length of the experiment (12 days) resulted in an over-proliferation of alveolar type II cells and in the complete takeover of the type I cell population. This indication suggested that the soluble factors KGF, IBMX, cAMP and dexamethasone modulate preferentially key signaling pathways involved the differentiation of pneumocytes into mature alveolar type II.

In order to overcome the limitation associated with the reversibility of the type I phenotype in vitro, we researched in literature the time-dependency between the exposure of pneumocyte to KIAD supplements

and the alveolar cell maturation to select the length of the treatment that best stimulates pneumocytes to form a compact epithelium and that induces alveolar cells to express markers characteristic of both mature phenotypes. Studies on transdifferentiation of alveolar type II to type I cells from Zhao and colleagues showed that pneumocytes exhibit morphogenetic features distinctive of the mature type I phenotype such as HTI-56, caveolin-1 (CAV1), T1-α/podoplanin (PDPN), and the Receptor for Advanced Glycation End-products (RAGE) almost exclusively at day 4 and 5 of culture when supplemented with KIAD(L. Zhao, Yee, and O'Reilly 2013), similar findings were also supported by Wang and colleagues studies(J. Wang et al. 2007a)(J. Wang et al. 2009) and confirmed by Sylveyra and colleagues (Silveyra et al. 2014)(Dominguez et al. 2013). According to literature type I markers tended to rapidly fade after 5 days of culture in favor of the expression of markers characteristic of the type II phenotype such as ABCA3 and surfactant B and C. Literature also reported that expression in marker was significantly higher when cell were exposed at ALI condition. The culture conditions when implemented provided similar results (Fig. 3.16) proving the validity of the protocol on Open-top Alveolus-Chip. The results also highlighted the plasticity of the alveolar pneumocyte and the susceptibility of the phenotype to the microenvironment in our model.

Our understanding was that the pneumocytes we used in this model were alveolar progenitors which had the potential to differentiate in type I and type II cells. KIAD supplements induce the simultaneous differentiation of both cell types, which occurs rapidly for type II cells (2 to 3 days from the exposure) and relatively slowly for type I cells (4 or 5 days from the exposure). The type II phenotype was also more stable compared to the type I, which tended to vanish from the culture over time. The reason for relative type I to type II ratio variability is not clear at this time; however the most plausible explanations are the following: type I cells perish over the course of the culture leaving type II alveolar cells free to take over the space left available from the dying cells. Based on this modality of variation, we speculate that only a subset of the pneumocytes provided by the seller have the genetic potential to differentiate in type I cells using our protocol. It is still unclear if the type II cells differentiated ex novo by KIAD have no capacity to differentiate in type I in vitro as the progenitors freshly isolated from the lung or if the microenvironment does not support the differentiation ex novo of type I phenotype.

Oppositely, another plausible guess might be that the plasticity of the phenotype as reported by several authors (Wang, Dahlin) that the type I cell phenotype is probably not terminally differentiated in vitro(Dahlin et al. 2004)(Demling et al. 2006). The type I-like cell have probably an intermediate phenotype which can transdifferentiate back to type II cells(J. Wang et al. 2007a)(L. Zhao, Yee, and O'Reilly 2013). The presence of alveolar marker co-expressing both HTI-56 and HTII-280 suggest that at least a part of the alveolar cells have an intermediate phenotype.

Once identified the optimal exposure time to form full differentiated epithelium, we decided to test the ability of the system to maintain air-liquid interface and its effect on alveolar type I and type II marker expression. Knowing the precarious stability of the type I progenitor cells, we hypothesized that exposure to air could have been extremely detrimental for this cell phenotype (even if the report from Wang(J. Wang et al. 2009) and Dominguez(Dominguez et al. 2013) suggested the opposite), however both cell types resulted extremely tolerant to air exposure and, surprisingly, ALI helped preserving the mature type I phenotype markers slowing their fading. Immunostaining analysis confirmed that pneumocytes

expressed HTI, AT-1α, HTII, LAMP3, ABCA3, surfactant B and release alveolar specific protein such as mature surfactant C. Notably, this method for pneumocyte induction was highly efficient as most of the alveolar-cell expressed HTII-280 or HTI-56, which is an order of magnitude more efficient than most methods that have been used to differentiate specialized cell types from alveolar stem cells.

Exposure of alveolar epithelium to air for several days during culture stimulated pneumocytes to excrete surfactant C, and TEM images showed incontrovertibly that lamellar bodies shuttle from the cytoplasm and across the plasma membrane releasing their content outside the cell (fig. 3.19 a). Immunofluorescence microscopy analysis confirmed that pro-surfactant C was more localized in the cytoplasm and on the plasma membrane of the alveolar cells. These results evidenced that we developed culture condition appropriate to stimulate and/or preserve differentiation of adult human alveolar type I and type II phenotype. Our induction method for culturing pneumocyte produces alveolar cells displaying morphological and molecular markers that are consistent with mature alveolar type I (squamous cells, expressing, tight junction ZO-1, E-cadherin, podoplanin (AT-1α) and integral membrane protein HTI-56) and mature alveolar type II (cuboidal cells, expressing, tight junction ZO-1, E-cadherin, ABCA3 , LAMP3, surfactant B and C and the integral membrane protein HTI-280) phenotypes.

Co-culture

We have developed a human triple-culture model of the alveolar-stroma-capillary barrier on basement membrane in which stable and confluent monolayers of human primary alveolar epithelium and primary microvascular endothelial cells were co-cultured for 12-15 days on the upper and lower surface of a stroma equivalent establishing a functional barrier in the Open-top Chip. The multilayered interface replicates the lung alveolar-blood barrier allowing cell-cell interaction and direct communication between the cell layers, which in turn influences the cellular morphology, differentiation, and polarization of both the epithelium and endothelium.

The aim of our study was to mimicry the physiological function of the alveolus and to restore functionality of the alveolar barrier in vitro. The recreated functional unit of the alveolus was engineered to comprise the 3 main components of the alveolar barrier, the alveolar epithelium, the stroma, and the capillary which integrate to form a selective barrier mimicking the in vivo alveolar structure. The barrier function is involved in normal alveolar physiology, while destruction of this barrier is a central part in many pathological lung events, therefore barrier function is a metric of alveolar functionality. Both alveolar epithelium and endothelium play a critical role in lung function and selectively response to insult causing lung damage(Dohle et al. 2018). Therefore, we focused our efforts on reproducing the essential properties of the biological elements forming the alveolus-blood barrier. Specifically, to establish the coculture and make sure to replicate the organotypic physiognomy of the human alveolus as accurately as possible, we decided to use only primary cells (alveolar pneumocyte, lung fibroblast and pulmonary microvascular endothelial cells) at low passage.

The choice of relying on primary cells to build the system resulted particularly challenging to implement because the nutrient and hormonal requirements for culturing primary cells are particularly restrictive and media available on market are specifically optimized only for the survival of a specific cell type. In our initial attempt to differentiate the epithelium at ALI, we focused almost exclusively on the nutrient and

hormonal requirements to differentiate pneumocytes in mature alveolar cells, but such thinking resulted short-sighted because we did not consider its interactions and possible incompatibility with the other cells of the alveolus system. For instance, SAGM complete medium, considered the gold standard medium to culture alveolar cells, did not support the viability of endothelial cells or the long-term survival of lung fibroblasts. Similarly, EGM-2MV complete medium which is considered the gold standard for culturing microvascular endothelial cells has detrimental effects on the fibroblast morphology and marker expression of the alveolar epithelial cells even after being differentiated by KIAD treatment. Furthermore, the need for establishing an air-liquid interface combined with the geometry of the system, forced us to use a single medium to feed all three cell types. This situation highlighted a major weakness of the Open-top Chip design which we hope to overcome in the future. Currently, the microfabrication technique used to build the chip does not allow the addiction of more complexity without the sacrifice of some of the Open-top Chip features or functions. Perhaps, improvement in manufacturing will allow to insert a baffle or microchannel to feed the stroma independently from the endothelium compartment.

We investigated if media commercially available could serve the purpose of feeding the entire organ unit. Unfortunately, we found that none of the tested media support the full biological system. Our explanation for such result was that companies optimize the supplements for the survival and full differentiation of a specific cell type, not caring to their compatibility with others. All the commercially available medium surrogates of SAGM and EGM-2MV complete medium resulted in similar effects as the parental medium either dead of endothelium or abnormal phenotype of the epithelium.

Left with no other option, we investigated the possibility to develop a medium compatible with our biological system. Our rationale was as follows: we selected shared supplements between the two gold standard media, SAGM™ and EGM™-2MV, finding glutamine, fetal calf serum, human recombinant epidermal growth factor (EGF) and hydrocortisone as common and complemented those with KGF, cAMP, Dexamethasone based on published genetic and immunological studies that showed how such factors are indispensable for the differentiation and maintaining of both pneumocytes and microvascular endothelial cells in vitro(Zemans and Matthay 2004). Finally, we added human recombinant vascular endothelial growth factor 165 (VEGF-165) and heparin, which regulates vascular endothelial growth factor165-dependent mitogenic activity, because as reported in literature and as verified in-house these two factors are essential for the survival of the endothelial cells in culture(Teran and Nugent 2015b). Based on literature search, we discovered that KGF induces the expression of the alveolar-specific markers such as surfactants and is a potent activator of canonical MAPK signaling, which induces endothelial proliferation and protects endothelial barrier function(Gillis et al. 1999); we learned that cAMP potentiates vascular endothelial cadherin-mediated cell-cell contacts enhancing endothelial barrier function and stimulates alveolar type II cells to produce surfactant C and lamellar bodies and that dexamethasone induces differentiation of both alveolar and endothelial monolayers upregulating the tight junctional protein, ZO-1 and the adherens junction proteins, E-cadherin and VE-cadherin when they are cocultured(Fukuhara et al. 2005)(Hermanns et al. 2004). Our assumptions that these factors could eventually help maintaining the markers and the functions of the primary alveolar type I and type II cells when exposed to air, improve the viability and marker expression of the fibroblasts and support the viability and functionality of the endothelium resulted mostly correct. However, a deep investigation of the role of each supplement in the

system could not be performed because it was not the goal of the project (and due to limitation of resources and time).

During our investigation, we learned that VEGF-165 and heparin were key supplements to support viability of endothelial cells. In fact, under the conditions where these two factors were removed, endothelial cells performed poorly either by not forming a monolayer or by dying. The pro-trophic effect of heparin and VEGF165, and their synergic interaction has also been reported in literature as due to the ability of heparin to augment the interaction of VEGF165 with VEGF-receptors (it binds to VEGFR1, VEGFR2, Nrp1, and Nrp20) which enhances endothelial viability, proliferation and differentiation(Teran and Nugent 2015a). Our findings seem in accordance with the heparin-VEGF165 co-adjuvant hypothesis reported in literature. It is noteworthy to mention that we experienced an adverse cytotoxic effect induced by retinoic acid on the endothelial monolayer. Specifically, all the media containing retinoic acid induced dose dependent endothelial cell death, at least in the range tested which spanned from 0.1ng/ml to 3µg/ml. Unfortunately, we did not have the possibility to investigate mechanism of the cytotoxic effect of the retinoic acid or its specificity toward other lung endothelial cells. Complementary to our finding, we found studies reporting that organ-specific endothelial cells have different sensitivity to retinoic acid(Bonney and Siegenthaler 2017)(Tezel et al. 2006)(Komi et al. 2010).

Immunofluorescent staining of the alveolar epithelium for the E-cadherin and ZO-1, which are junctions strongly involved in the formation of the epithelial barrier, confirmed the properties of the alveolar epithelium to sustain the barrier function. Similarly, immunofluorescence staining for VE-cadherin and PECAM-1 also confirmed the capacity of the endothelium to form a tight barrier. To confirm the functionality of the three-culture system we performed a barrier function assay where we tested the permeability of the system to Dextran-FITC and its capability to selectively regulate the passage of molecules. The system revealed capable to selectively block the flux of dextran-FITC between the endothelium and epithelium compartment of the Alveolus-Chip, proving the functionality of the alveolar barrier in the chip, while permitting the selective transport of nutrients. The capability to feed the system through the pores of the thin PDMS membrane allows to keep separate and compartmentalized the endothelial cell layer from the stroma but maintained sufficient permeability to liquid factors and the direct contact between the fibroblasts and the endothelial cells located on the opposite site of the membrane. Pores also ensured the transfer of growth factors and signals through the entire biological system, while preventing the invasion of fibroblasts or endothelial cells in the other compartments.

Contribution of fibroblasts

The mimicry of the alveolar barrier was further enhanced by the addition of important mesenchymal cells, which are normally found in the respiratory system, specifically lung fibroblasts. The contribution of lung fibroblasts was assessed at optical, gene expression and protein level. A three-dimensional optical reconstruction of the stroma-epithelium interface evidenced how fibroblasts embedded in the hydrogel of the recreated stroma tended to protrude toward the epithelium and to physically touch the epithelial cells (Fig 3.15, a, b). We also noticed that fibroblasts have a preferential growth or migration in the region right underneath the epithelium (Fig. 3.7, b). Our data seem to indicate that the epithelium release factors which stimulate a preferential growth of fibroblasts toward the epithelium. Although we have not had the

possibility to study or identify the factors at bio-molecular level, we speculated that they must have a potent effect on fibroblast behavior since they manage to induce growth toward the epithelium which is at air-liquid interface, overcoming the natural tendency of fibroblasts to follow the gradient of nutrient toward the bottom channel.

Quantitative RNA analysis also evidenced that the presence of fibroblasts in the recreated lung stroma (collagen I gel with embedded fibroblasts coated with ColIV-Fib-Lam) increases the expression of canonical alveolar type I (HOPX, PDPN, AQP5) and type II (ABCA3, SURFB, SURFC) genes such as HOPX, PDPN, AQP5, ABCA3, SURFB, SURFC (Fig 3.16, b) as well as the protein level of surfactant B and C, which we detected by immunofluorescence staining and ELISA (Fig. 3.16, a, b; 3.19, c). In accordance with other reports(Griffin et al. 1993)(Sucre et al. 2018)(Hegab et al. 2015), our data showed that alveolar epithelial cells benefit from the co-culture with fibroblasts and seem to indicate that the close proximity to the stromal cells induce pneumocytes to undergo to a better differentiation. To better understanding the optimal number of fibroblasts to add to the system, we co-cultured a fixed number of alveolar epithelial cells with increasing number of fibroblasts, noticing that there is a sort of direct dependency between the number of fibroblasts and the enhancement of marker expression at RNA level. The highest level of marker expression was obtained at concentration of 500,000 fibroblast per ml of hydrogel. Higher concentration could not be tested, because fibroblasts at higher concentration contract the hydrogel so strongly that it delaminates from the PDMS wall. Hydrogel delamination from the PDMS wall disrupts air-liquid interface making impossible to culture the system under flow for the full length of the experiment. Despite we haven't had the chance to investigate at biomolecular level the specific factor influencing lung differentiative potential, based on literature search and on capacity of KGF (FGF-7) to stimulate alveolar differentiation, we speculate that fibroblast growth factors (FGF2, FGF9, FGF10) might have a critical role in pneumocyte differentiation. We hope that in the future, there will be an opportunity to further investigate the role of factors released by lung fibroblasts and to challenge our biological model with synthetic analogs of them for obtaining a better understanding of the factors that manipulate alveolar progenitor behaviors in the alveolar niche.

Stretching

Normal alveoli are stable and do not have marked changes in volume with each tidal breath (4 – 6% change with each cycle which has an approximate frequency of 0.2 Hz (Hegab et al. 2015)(Namati et al. 2008)(Nieman et al. 2017). To model the natural range of breathing motions observed in living alveoli of the human lung, we applied negative pressure of -25kPa at a frequency of 0.2 Hz which generated a cyclic stretching-relaxation cycles at 4% strain in our system. Specifically, we investigated the effect of three days of stretching-relaxation cycles at 4% strain at a frequency of 0.2Hz on the adherent epithelial cell monolayer lining on the recreated stroma. The stretching, as previously defined, resulted in an increased number of HTII positive cells (calculated as HTII fluorescence signal intensity) per unit surface, which is indicative of an increased presence of alveolar type II phenotype compared to not stretched chips (Fig 3.10, a, b). We observed that stretching helped in the retention or induced de novo transcription of the canonical alveolar markers such as LAMP3, ABCA3, ZO-1, ENaC, E-Cad, Na^+/K^+ pump, AT1-α (Also known as Podoplanin) surfactant B and surfactant C, which were detectable also at protein level by antibody staining (Fig. 3.17). The surfactant C gene expression and release profile also confirmed that stretching

increases surfactant C production in primary alveolar cells (Fig. 3.19, c) as detected by the ELISA time course. Our data indicate that the epithelium is sensitive to the mechanical stimuli, and that stretching increase the release of surfactant C. The reason for this variation is still not completely clear because cell cultured under stretching condition start displaying a distinct type II phenotype, cuboidal shape and lamellar inclusions, which let us suspect that the addition of the stretching affects the plasticity of the alveolar cells. We speculate that the shifting of the biological system towards a type II phenotype is indicative either that alveolar type I cells inside our system gradually die under stretching condition leaving the space to type II cells to take over or that alveolar type I cell are state not terminally differentiated. In the future, we plan to study how stretching regimes enhances surfactant secretion and marker expression in alveolar cells in our system.

Barrier function assessment

We studied interaction between different chip compartments by perturbating the system with biological and chemical stressors such as LPS, and H_2O_2 which are known to induce a reversible disruption of the cellular monolayer after acute administration both in vivo and in vitro(E. K. Kang and Kim 2017). Studies in static insert demonstrated a dose dependent loss of barrier function as doses up to 100ng/ml for LPS(Jain et al. 2018)(E. K. Kang and Kim 2017)(Crestani et al. 1994)(Nighot et al. 2017) and 10mM for H_2O_2(E. K. Kang and Kim 2017)(Wijeratne, Cuppett, and Schlegel 2005)(Katsube, Tsuji, and Onoda 2007). To assess changes in the barrier function following the exposure to these insults, we added a fluorescent dye (Dextran-FITC, 3000Da) to the endothelial compartment which under control condition confirmed that the endothelium and epithelium form a tight barrier to the dyes. The presence of a strong barrier is also indirectly confirmed by the presence of continuous pattern of E-cadherin and VE-cadherin in the monolayer of alveolar epithelial and endothelial monolayers, respectively. As previously reported in literature, we found that treatment with LPS (10ng/ml)(Nighot et al. 2017)(Stephens and von der Weid 2019) and/or H_2O_2 (10mM)(Katsube, Tsuji, and Onoda 2007)(Chapman, Waters, and Miller 2002) causes barrier breakdown and disruption of intracellular junction which results in an influx of medium from the endothelial compartment to the epithelial compartment. Analysis of the medium effluents after 24 hours of exposure to LPS show increase of lung specific cytokines such as IL-6, and IL-8 (Fig. 3.13) while no apparent correlation between releasing of IL-6, IL-8 and exposure to H_2O_2 has been observed. We also decoupled the effect of single biological component to the inflammatory response by selectively removing them from the system in an integrated matrix. We cross-tested several cell combinations: full system including fibroblasts, endothelial and epithelial cells, system formed of endothelial and epithelial cells, system formed of fibroblasts and endothelial cells, system formed of fibroblasts and epithelial cells and fibroblasts alone which evidenced that each component of the biological model responds to the insult differently and we identified epithelial cells as the main releaser of IL-6 and IL-8, while fibroblasts and endothelial cells seems to give little to no contribution to IL-6 and IL-8 release. The data also evidenced that epithelial, endothelial, and stromal compartment contribute to the inflammatory response and that the cytokine cross talk between epithelial and endothelial cells amplifies the response. In fact, the recorded values for IL6 and IL-8 are not the algebraic sum of the concentration of the factors released by the single cellular components. Endothelial cell lining the vascular surface of the chip stained for ICAM-1 at 24 hours post LPS treatment making in evidence that LPS induces ICAM-1 expression only in presence

of epithelial cells and, to a much lesser extent, fibroblasts confirming some degree of interconnectivity between the endothelial and epithelial compartment, or at least, that soluble factors released by epithelial cells can reach the endothelium through the recreated stroma. These results also suggest that some peculiar aspects of the inflammatory response cannot be modulated without the presence of multiple cell types.

In vitro modelling of pneumocyte toxicity, acute and chronic inflammation

The epithelium lining the pulmonary airway acts as a protective barrier against external insults, including inhaled toxins and inflammatory agents in vivo. In fact, epithelial cells direct diverse and synchronized defense mechanisms to counteract cellular stress and the intracellular buildup of noxious radical oxygen species (ROS)(Nieman et al. 2017)(Nita and Grzybowski 2016). Genetic or environmental perturbations of these pathways have been associated with the progression of different respiratory disease states, including adult acute distress syndrome (ARDS), fibrosis and cancer. The Nuclear factor erythroid2-related factor2 (Nrf2) is a master regulator of redox homoeostasis and a key transcription factor regulating a wide array of genes for antioxidant and detoxification enzymes, which protect the epithelial tissue from various kinds of toxic insults including acute injury(Kumar and Goswami 2009)(Nita and Grzybowski 2016).

Given our ability to mimic a living portion of the human alveolus into the Open-top Chip, we explored whether the alveolar barrier responds to acute and chronic oxidative stresses. Acute oxidative damage was recreated by direct exposure of the alveolar epithelium to hydrogen peroxide (H_2O_2). Similarly, the chronic pathological damage was recreated by long term exposure of the alveolar epithelium to transforming growth factor beta 1 (TGF-β1), which is a cytokine known to modulate pathogenesis of several chronic pulmonary disease in vivo, particularly pulmonary fibrosis, chronic obstructive pulmonary disease (COPD), and pulmonary vascular disease.

We investigated whether insults generated by H_2O_2 and TGF-β1 would disrupt the integrity of the alveolar epithelial barrier. As expected, both conditions altered the alveolar-capillary barrier which was measured as change in the resistance to the permeability of exogenous molecules (specifically, dextran-FITC, 3000Da). We found that the alveolar air-liquid interface barrier was severely altered after 24 hours of acute exposure to H_2O_2 or 72hours of exposure to TGF-β1. Immuno-fluorescence images of the epithelium stained for E-cadherin and phalloidin confirmed pronounced loss and re-distribution of the E-cadherin into the epithelial monolayer exposed to acute injury (Fig. 6b, c), which correlates with the decrease in alveolar-capillary barrier as determined by the barrier function. Our data suggested that exposure to H_2O_2 increases permeability by direct damage on the alveolar epithelium which results in the depletion of adherens junction, while TGF-β1 directly increased alveolar epithelial permeability by a mechanism that involved reorganization of intraepithelial junction and induction of the EMT phenotype. Increased expression of α-SMA marker was detected at both RNA and protein level. High level of the mesenchymal marker α-SMA is indicative of epithelial-mesenchymal transition (EMT). Our observation is in agreement with previous studies where is demonstrated that TGF-β1 induces EMT in alveolar epithelial cells both in vitro and in vivo(Kumar and Goswami 2009). Co-localization of epithelial (E-cadherin) and mesenchymal marker (α-SMA) are commonly observed in hyperplastic alveolar type II cells in lung tissue from patients

with idiopathic pulmonary fibrosis (IPF), suggesting that alveolar epithelial cells may exhibit extreme plasticity and serve as a source of fibroblasts and/or myofibroblasts in lung fibrosis.

After proving that Alveolus-Chip model responds to both acute and chronic oxidative stresses, we examined whether our alveolar model retains the Nrf2/ARE redox-sensitive signaling pathway which plays a central role in modulating the protection mechanisms of the alveolar cells against oxidative stress. Based on pharmaceutical studies we identify three anti-inflammatory drugs, known to inhibit inflammation and reduce oxidative-induced damage in vivo through the Nrf2 pathway. Specifically, Bardoxolone, a triterpenoid molecule (or glucocorticoid) in trial to treat idiopathic pulmonary fibrosis (IPF) (ClinicalTrials.gov Identifier: NCT02036970); JQ1 (K. Chen et al. 2016), a thienotriazolodiazepine, a potent inhibitor of the bromodomain proteins (BRD2, BRD3, BRD4), known to alleviate TGFβ-induced intracellular oxidative stress and suggested to treat cystic fibrosis lung inflammation and GSK(Yonchuk et al. 2017), a small molecule in clinical trial as non-steroidal anti-inflammatory drugs (NSAIDs) and suggested for the treatment of COPD, sarcoidosis, connective tissue disorder and cancer patients. We evaluated the effectiveness of three anti-inflammatory drugs in preventing the leakage of the alveolar epithelial barrier.

We also investigate the sensitivity of the Alveolus-Chip to the anti-inflammatory compounds. Specifically, we detected a positive dose dependent correlation between the administration of a fixed concentration of H_2O_2 (10mM) and different doses of GSK (1μM, 0.1μM and 0.01μM). Consistent with the previous observation, our biological system exhibited significant loss of barrier function when treated with H_2O_2 (10mM), while it showed concentration-dependent restoration of barrier function and depletion of oxidant-induced inflammatory marker such as intercellular adhesion molecule-1 (ICAM-1). Our data suggest that GSK compound expression of phase II antioxidant genes such as NQO1 and SRXN1 via Nrf2 translocation into the nucleus and the subsequent transcription in a Nrf2-dependent manner and seems to confirm some of the finding reported in literature about the critical role of Nfr2 pathway in regulating cell homeostasis and tissue response to oxidative stresses. I would like to highlight that the sensitivity of our alveolus models to multiple classes of drug compounds and the capacity of the model to preserve the functionality of the Nfr2 pathway in vitro is extremely important especially now that the aberrant functionality for Nerf2 has been also linked to cancer and fibrosis, and that Nrf2 has become one of the main targets of interest for development of novel therapeutics.

Currently, Nrf2 activators are in clinical trials for the treatment of diseases such as cancer , IBD and COPD associated with oxidative stress(Rojo et al. 2014)(AL et al. 2016)(Gardi et al. 2015) therefore our alveolus model which showed capable to recapitulate unprecedented aspect of the alveolar microenvironment might represent a valid model to better understanding of the mechanisms that control Nrf2 functions in a more appropriate context and contribute to development of effective therapeutic strategies based on Nrf2 modulation by allowing to make quantitative predictions about alveolar barrier specificity and sensitivity to drugs and to create dose-response curve to extrapolate pharmacokinetic parameters.

Open-top biology recapitulation

To form a layer of differentiated pneumocytes, we seeded the epithelial cells on the top of the stroma (collagen I hydrogel with embedded fibroblasts) and differentiated them in situ using the pneumocyte differentiation medium produced in house in the presence of fluid flow. Generating a combination of fluid

flow and cyclic mechanical strain to mimic physiological conditions present in the alveolar milieu. Notably, cells that were differentiated under fluid flow in combination with mechanical strain, expressed to a greater degree (or showed higher levels in the expression of) alveolar protein compared to cells not exposed to cyclic stretching (control cultures) suggesting that mechanical forces can influence pneumocyte differentiation by enhancing expression of alveolar specific markers at both genetic and protein level (Fig. 3.16, a, b; 3.19, c). Application of flow also significantly increased the viability and the retention (or ex novo expression) of PECAM-1, VWF and VE-Cadherin markers of the differentiated endothelial cells whether cultured in monoculture or in co-culture with alveolar cells and lung fibroblast (Fig. 3.9). These cells remained viable during culture in the microfluidic devices for at least 7 days of culture. These results demonstrate the possibility to maintain viable and functional human primary alveolar epithelial, stromal, and endothelial cells for extended times in vitro. In the future, the application of the Alveolus-Chip, at least in theory, could help generating patient-specific biological models (model generated from cells isolated by patient tissue biopsies) to examine drug tolerance and efficacy and help selecting therapeutic and treatment specific for patients.

We found that pneumocytes differentiated in presence of fluidic shear rate (60µl/hr) corresponding to shear stress (0.07 dyn/cm^2) in the bottom channels and exposed to cyclic strain (4%) exhibited a significant increase of cytoplasmic surfactant B (evaluated by staining intensity for surfactant B) (Fig. 3.16, a, b) and release of surfactant C (Fig. 3.19, c) (evaluated by Elisa for surfactant C) compared to pneumocytes differentiated under fluid flow alone or in static. This is a clear indication that mechanical stimuli can induce higher level of pneumocyte maturation and restore biological functions.

Remarkably, confocal immunofluorescence microscopy analysis revealed that while pneumocytes and microvascular endothelial cells remained confined to their respective compartment, fibroblasts formed a direct contacts with the basal abluminal surface of the epithelium (Fig. 3.15, a, b), presumably similarly to those observed in alveolar interstitium in vivo. The exact reason for the fibroblast behavior was not object of investigation of this study, therefore it has not been deeply investigated, but we speculated that alveolar epithelial cells release chemo-attractant factors which induce such behavior, because, otherwise, we would have expected fibroblasts to grow preferentially toward the bottom channel following the gradient of nutrients.

The recreated tissue-tissue interface combined with flow and stretching generated a significant increase in the number of pneumocytes that expressed canonical alveolar epithelial markers, which is an important breakthrough for modern lung in vitro modelling. In fact, to our best knowledge, there are no reported biological alveolar in vitro model capable to restore or stimuli ex novo the expression of canonical alveolar markers when using primary human adult alveolar cells. It should also be highlighted that this is the first reported systems where primary human alveolar cells where growth at air-liquid interface on a recreated stroma for an extended period of time under flow and to which was applied stretching. However, there is also to mention that the alveolar marker expression even though present was not always homogeneous across the epithelium. In fact, on the epithelium was possible to find areas where the level of marker expression varied significantly. The lack of a homogeneity in the expression is probably a sign that further optimization steps must be performed in order to obtain less variability in the distribution of cell maturation.

Taken together, these results indicate that co-culture of human primary pneumocytes, lung fibroblasts and human lung microvascular endothelial cells cultured under flow and undergoing prolonged cyclic mechanical stretching at ALI enable the partial restoration of canonical markers normally present at alveolar epithelium-stroma-endothelial capillary interface in vivo. Level of resemblance not achievable using conventional primary human alveolar culture models.

Given our ability to mimic a living portion of the human alveolus, we explored whether this microfluidic device could also reconstitute the alveolar functions such as alveolar barrier function and releasing of surfactant C. To investigate the barrier function of the recreated biological unit, we exposed the Alveolus-Chip to specific chemical insults such as H_2O_2, LPS (involved in acute pathological events) and TGF-β1 (involved in chronic pathological events), which are known to alter the permeability of the alveolar barrier in vivo. Because cyclic mechanical deformation of the alveolus occurs in vivo while breathing, we performed the barrier function studies applying cyclic strain considered in the physiological range when at rest (4% at 0.2Hz). We found that the alveolus barrier permeability to exogenous molecules (dextran (3000Da)) in the Open-top Chip was severely altered after 24 hours of exposure to H_2O_2 (acute injury) or 72 hours of exposure to TGF-β (chronic injury), whereas acute and chronic injury treated with anti-inflammatory compounds restored the barrier functionality and its capability to stop leakage of large and small molecules.

Conclusion

Because the existing models of the alveolus based on immortalized alveolar cell lines and primary alveolar cultures poorly recapitulate alveolar functions, and animal studies often fail to predict the human in vivo physiological response, we contributed to develop a new technology which can enable a better mimicry of alveolus as well as other organ units. Our results support the potential of Open-top Alveolus-Chip to provide a better in vitro system for predicting alveolar compound toxicity, drug efficacy and new therapeutic discovery and development. The Open-top Alveolus-Chip might be particularly suitable for personalized medicine applications, in studies on chronic obstructive pulmonary disease (COPD), asthma, and idiopathic pulmonary fibrosis (IPF) or other rarer hereditary forms of pulmonary syndromes (Alpha-1 antitrypsin (AAT) deficiency, interstitial lung diseases (ILDs)) which often lead to severe or fatal events and for which do not exist robust models. It is imaginable that Open-top technology, and specifically the human Alveolus-Chip described here, could facilitate investigations to illuminate on the etiology and pathophysiology of both genetic and acquired forms alveolar diseases as well as provide a low-cost alternative to animal models for the development of preventative and therapeutic medications for of human lung diseases. It would also be of interest to explore whether Open-top technology might be useful for tissue engineering of implantable organ units or for cell-based therapies in regenerative medicine in the future.

Future direction:

Since further development and characterization of this model are needed to consolidate cell-culture protocols and to ensure higher level of experimental reproducibility, we will keep optimizing the model to obtain a better mimicry of the alveolar physiology. We also envision to progressively engineer new chip designs or integrate new features that will allow to mimic even more closely organ level functions. Our

study also evidenced the need to work on creating media with broader cellular compatibility, which appears fundamental for the success of the Open-top Chip technology.

5. REFERENCES

Adenuga, David et al. 2010. "Nrf2 Deficiency Influences Susceptibility to Steroid Resistance via HDAC2 Reduction." *Biochemical and Biophysical Research Communications* 403(3–4): 452–56.

Aengenheister, Leonie et al. 2018. "An Advanced Human in Vitro Co-Culture Model for Translocation Studies across the Placental Barrier." *Scientific Reports* 8(1): 1–12.

AL, Furfaro et al. 2016. "The Nrf2/HO-1 Axis in Cancer Cell Growth and Chemoresistance." *Oxidative medicine and cellular longevity* 2016.

Alegria-Schaffer, Alice. 2014. "General Protein-Protein Cross-Linking." In *Methods in Enzymology*, Academic Press Inc., 81–87.

Alom Ruiz, Sami, and Christopher S. Chen. 2007. "Microcontact Printing: A Tool to Pattern." *Soft Matter* 3(2): 168–77.

Anacker, Daniel, and Cary Moody. 2012. "Generation of Organotypic Raft Cultures from Primary Human Keratinocytes." *Journal of Visualized Experiments* (60).

Anderson, Deirdre E.J., and Monica T. Hinds. 2011. "Endothelial Cell Micropatterning: Methods, Effects, and Applications." *Annals of Biomedical Engineering* 39(9): 2329–45.

Anderson, Janelle R. et al. 2000. "Fabrication of Topologically Complex Three-Dimensional Microfluidic Systems in PDMS by Rapid Prototyping." *Analytical Chemistry* 72(14): 3158–64.

Andreeva, Alexandra V., Mikhail A. Kutuzov, and Tatyana A. Voyno-Yasenetskaya. 2007. "Regulation of Surfactant Secretion in Alveolar Type II Cells." *American Journal of Physiology - Lung Cellular and Molecular Physiology* 293(2).

Anton, Delphine, Hélène Burckel, Elodie Josset, and Georges Noel. 2015. "Three-Dimensional Cell Culture: A Breakthrough in Vivo." *International Journal of Molecular Sciences* 16(3): 5517–27.

Arora, Meenakshi. 2013. "Cell Culture Media: A Review." *Materials and Methods* 3.

Arora, Natasha et al. 2017. "A Process Engineering Approach to Increase Organoid Yield." *Development (Cambridge)* 144(6): 1128–36.

Atkinson, Arthur J. et al. 2007. Principles of Clinical Pharmacology *Principles of Clinical Pharmacology*. Second Edi. ed. S. P. Atkinson, A. J., Abernethy, D. R., Daniels, C. E., Dedrick, R. L., & Markey. Elsevier Inc.

Azeloglu, Evren U., Jahar Bhattacharya, and Kevin D. Costa. 2008. "Atomic Force Microscope Elastography Reveals Phenotypic Differences in Alveolar Cell Stiffness." *Journal of Applied Physiology* 105(2): 652–61.

Aziz, Aziz Ur Rehman et al. 2017. "The Role of Microfluidics for Organ on Chip Simulations." *Bioengineering* 4(2).

Bagnato, Gianluca, and Sergio Harari. 2015. "Cellular Interactions in the Pathogenesis of Interstitial Lung Diseases." *European Respiratory Review* 24(135): 102–14.

Bairoch, Amos. 2018. "The Cellosaurus, a Cell-Line Knowledge Resource." *Journal of Biomolecular Techniques* 29(2): 25–38.

Balestrini, Jenna L., and Laura E. Niklason. 2015. "Extracellular Matrix as a Driver for Lung

Regeneration." *Annals of Biomedical Engineering* 43(3): 568–76.

Barthes, Julien et al. 2014. "Cell Microenvironment Engineering and Monitoring for Tissue Engineering and Regenerative Medicine: The Recent Advances." *BioMed Research International* 2014.

Basu, Subhayu et al. 2005. "A Synthetic Multicellular System for Programmed Pattern Formation." *Nature* 434(7037): 1130–34.

Beck-Schimmer, B. et al. 2002. "Role of Alveolar Epithelial ICAM-1 in Lipopolysaccharide-Induced Lung Inflammation." *European Respiratory Journal* 19(6): 1142–50.

Beck-Schimmer, B., R.C. Schimmer, and T. Pasch. 2004. "The Airway Compartment: Chambers of Secrets." *Physiology* 19(3): 129–32. https://www.physiology.org/doi/10.1152/nips.01508.2003 (May 14, 2020).

Beers, Michael F., and Yuben Moodley. 2017. "When Is an Alveolar Type 2 Cell an Alveolar Type 2 Cell?: A Conundrum for Lung Stem Cell Biology and Regenerative Medicine." *American Journal of Respiratory Cell and Molecular Biology* 57(1): 18–27.

Belair, David G., and Barbara D. Abbott. 2017. "Engineering Epithelial-Stromal Interactions in Vitro for Toxicology Assessment." *Toxicology* 382: 93–107.

Benam, Kambez H. et al. 2016. "Small Airway-on-a-Chip Enables Analysis of Human Lung Inflammation and Drug Responses in Vitro." *Nature Methods* 13(2): 151–57.

Bhatia, S. N., U. J. Balis, M. L. Yarmush, and M. Toner. 1998. "Microfabrication of Hepatocyte/Fibroblast Co-Cultures: Role of Homotypic Cell Interactions." *Biotechnology Progress* 14(3): 378–87.

Bilek, Marcela M., and David R. McKenzie. 2010. "Plasma Modified Surfaces for Covalent Immobilization of Functional Biomolecules in the Absence of Chemical Linkers: Towards Better Biosensors and a New Generation of Medical Implants." *Biophysical Reviews* 2(2): 55–65. http://link.springer.com/10.1007/s12551-010-0028-1 (May 13, 2020).

Birukov, Konstantin G. et al. 2003. "Magnitude-Dependent Regulation of Pulmonary Endothelial Cell Barrier Function by Cyclic Stretch." *American Journal of Physiology - Lung Cellular and Molecular Physiology* 285(4 29-4).

Bischoff, Luc J.M. et al. 2019. "A Systematic Analysis of Nrf2 Pathway Activation Dynamics during Repeated Xenobiotic Exposure." *Archives of Toxicology* 93(2): 435–51.

Bogdanowicz, Danielle R., and Helen H. Lu. 2013. "Multifunction Co-Culture Model for Evaluating Cell–Cell Interactions." In *Methods in Molecular Biology (Clifton, N.J.)*, NIH Public Access, 29–36.

Bonney, Stephanie, and Julie A. Siegenthaler. 2017. "Differential Effects of Retinoic Acid Concentrations in Regulating Blood–Brain Barrier Properties." *eNeuro* 4(3).

Borthwick, Lee A., Thomas A. Wynn, and Andrew J. Fisher. 2013. "Cytokine Mediated Tissue Fibrosis." *Biochimica et Biophysica Acta - Molecular Basis of Disease* 1832(7): 1049–60.

Brasch, Frank et al. 2004. "Surfactant Protein B in Type II Pneumocytes and Intra-Alveolar Surfactant Forms of Human Lungs." *American Journal of Respiratory Cell and Molecular Biology* 30(4): 449–58.

Brüningk, Sarah C. et al. 2020. "3D Tumour Spheroids for the Prediction of the Effects of Radiation and Hyperthermia Treatments." *Scientific Reports* 10(1): 1–13.

Bulck, Michiel Van et al. 2019. "Novel Approaches for the Treatment of Alzheimer's and Parkinson's Disease." *International Journal of Molecular Sciences* 20(3).

Cerrada, Alejandro, Thomas Haller, Antonio Cruz, and Jesús Pérez-Gil. 2015. "Pneumocytes Assemble Lung Surfactant as Highly Packed/Dehydrated States with Optimal Surface Activity." *Biophysical Journal* 109(11): 2295–2306.

Chaicharoenaudomrung, Nipha, Phongsakorn Kunhorm, and Parinya Noisa. 2019. "Three-Dimensional Cell Culture Systems as an in Vitro Platform for Cancer and Stem Cell Modeling." *World Journal of Stem Cells* 11(12): 1065–83.

Chapman, Kenneth E., Christopher M. Waters, and William M. Miller. 2002. "Continuous Exposure of Airway Epithelial Cells to Hydrogen Peroxide: Protection by KGF." *Journal of Cellular Physiology* 192(1): 71–80. http://doi.wiley.com/10.1002/jcp.10115 (May 15, 2020).

Chaw, K. C., M. Manimaran, E. H. Tay, and S. Swaminathan. 2007. "Multi-Step Microfluidic Device for Studying Cancer Metastasis." *Lab on a Chip* 7(8): 1041–47.

Chen, Fa Ming, and Xiaohua Liu. 2016. "Advancing Biomaterials of Human Origin for Tissue Engineering." *Progress in Polymer Science* 53: 86–168.

Chen, James L. et al. 2017. "Autophagy Induction Results in Enhanced Anoikis Resistance in Models of Peritoneal Disease." *Molecular Cancer Research* 15(1): 26–34.

Chen, Kevin G., Barbara S. Mallon, Ronald D.G. McKay, and Pamela G. Robey. 2014. "Human Pluripotent Stem Cell Culture: Considerations for Maintenance, Expansion, and Therapeutics." *Cell Stem Cell* 14(1): 13–26.

Chen, Kong et al. 2016. "Antiinflammatory Effects of Bromodomain and Extraterminal Domain Inhibition in Cystic Fibrosis Lung Inflammation." *JCI Insight* 1(11).

Chen, X. Josette et al. 2000. "Detection of Emphysema in Rat Lungs by Using Magnetic Resonance Measurements of 3He Diffusion." *Proceedings of the National Academy of Sciences of the United States of America* 97(21): 11478–81.

Cheong, Naeun et al. 2007. "ABCA3 Is Critical for Lamellar Body Biogenesis in Vivo." *Journal of Biological Chemistry* 282(33): 23811–17.

Chia-Hsun Hsieh, Yi-Dao Chen, Shiang-Fu Huang, Hung-Ming Wang, Min-Hsien Wu. 2015. "The Effect of Primary Cancer Cell Culture Models on the Results of Drug Chemosensitivity Assays: The Application of Perfusion Microbioreactor Syste... - PubMed - NCBI." : 2015: 470283. https://www.ncbi.nlm.nih.gov/pubmed/25654105 (May 12, 2020).

Chiu, Daniel T. et al. 2017. "Small but Perfectly Formed? Successes, Challenges, and Opportunities for Microfluidics in the Chemical and Biological Sciences." *Chem* 2(2): 201–23.

Cho, Hye Youn, Sekhar P. Reddy, and Steven R. Kleeberger. 2006. "Nrf2 Defends the Lung from Oxidative Stress." *Antioxidants and Redox Signaling* 8(1–2): 76–87.

Clevers, Hans. 2016. "Modeling Development and Disease with Organoids." *Cell* 165(7): 1586–97.

Colella, Gianluca et al. 2018. "Sarcoma Spheroids and Organoids— Promising Tools in the Era of Personalized Medicine." *International Journal of Molecular Sciences* 19(2).

Compton, Carolyn C. et al. 2019. "Preanalytics and Precision Pathology: Pathology Practices to Ensure Molecular Integrity of Cancer Patient Biospecimens for Precision Medicine." *Archives of Pathology and Laboratory Medicine* 143(11): 1346–63.

Conway, Renee F., Tristan Frum, Ansley S. Conchola, and Jason R. Spence. 2020. "Understanding Human Lung Development through In Vitro Model Systems." *BioEssays*: 2000006. https://onlinelibrary.wiley.com/doi/abs/10.1002/bies.202000006 (May 14, 2020).

Cooper, Stephen, and Mariam Gonzalez-Hernandez. 2009. "Experimental Reconsideration of the Utility of Serum Starvation as a Method for Synchronizing Mammalian Cells." *Cell Biology International* 33(1): 71–77.

Crestani, Bruno et al. 1994. "Alveolar Type II Epithelial Cells Produce Interleukin-6 in Vitro and in Vivo: Regulation by Alveolar Macrophage Secretory Products." *Journal of Clinical Investigation* 94(2): 731–40.

Cui, Ping, and S. Wang. 2019. "Application of Microfluidic Chip Technology in Pharmaceutical Analysis: A Review." *Journal of Pharmaceutical Analysis* 9(4): 238–47.

Curtis, A. S.G., J. V. Forrester, C. McInnes, and F. Lawrie. 1983. "Adhesion of Cells to Polystyrene Surfaces." *Journal of Cell Biology* 97(5 I): 1500–1506. http://www.ncbi.nlm.nih.gov/pubmed/6355120 (May 11, 2020).

D'Arcangelo, Elisa, and Alison P McGuigan. 2015. "Micropatterning Strategies to Engineer Controlled Cell and Tissue Architecture in Vitro." *BioTechniques* 58(1): 13–23. https://www.future-science.com/doi/10.2144/000114245 (May 12, 2020).

Dahlin, Katherine et al. 2004. "Identification of Genes Differentially Expressed in Rat Alveolar Type I Cells." *American Journal of Respiratory Cell and Molecular Biology* 31(3): 309–16.

Davies, Emma J. et al. 2015. "Capturing Complex Tumour Biology in Vitro: Histological and Molecular Characterisation of Precision Cut Slices." *Scientific Reports* 5(1): 1–17.

DeFife, Kristin M. et al. 1999. "Effects of Photochemically Immobilized Polymer Coatings on Protein Adsorption, Cell Adhesion, and the Foreign Body Reaction to Silicone Rubber." *Journal of Biomedical Materials Research* 44(3): 298–307.

Demling, Nina et al. 2006. "Promotion of Cell Adherence and Spreading: A Novel Function of RAGE, the Highly Selective Differentiation Marker of Human Alveolar Epithelial Type I Cells." *Cell and Tissue Research* 323(3): 475–88.

Dobbin, Zachary C. et al. 2014. "Using Heterogeneity of the Patient-Derived Xenograft Model to Identify the Chemoresistant Population in Ovarian Cancer." *Oncotarget* 5(18): 8750–64.

Dobbs, Leland G., Robert F. Gonzalez, Lennell Allen, and Deborah K. Froh. 1999. "HTl56, an Integral Membrane Protein Specific to Human Alveolar Type I Cells." *Journal of Histochemistry and Cytochemistry* 47(2): 129–37.

Dohle, Eva et al. 2018. "Human Co- and Triple-Culture Model of the Alveolar-Capillary Barrier on a Basement Membrane Mimic." *Tissue Engineering Part C: Methods* 24(9): 495–503.

https://www.liebertpub.com/doi/10.1089/ten.tec.2018.0087 (May 16, 2020).

Dominguez, Samuel R., Emily A. Travanty, Zhaohui Qian, and Robert J. Mason. 2013. "Human Coronavirus HKU1 Infection of Primary Human Type II Alveolar Epithelial Cells: Cytopathic Effects and Innate Immune Response." *PLoS ONE* 8(7).

Donglai et al. 2017. "Three-Dimensional Cell Culture: A Powerful Tool in Tumor Research and Drug Discovery." *Oncology Letters* 14(6): 6999–7010.

Duffy, David C., J. Cooper McDonald, Olivier J.A. Schueller, and George M. Whitesides. 1998. "Rapid Prototyping of Microfluidic Systems in Poly(Dimethylsiloxane)." *Analytical Chemistry* 70(23): 4974–84.

Durães, Fernando, Madalena Pinto, and Emília Sousa. 2018. "Old Drugs as New Treatments for Neurodegenerative Diseases." *Pharmaceuticals* 11(2).

Duval, Kayla et al. 2017. "Modeling Physiological Events in 2D vs. 3D Cell Culture." *Physiology* 32(4): 266–77.

Edmondson, Rasheena, Jessica Jenkins Broglie, Audrey F. Adcock, and Liju Yang. 2014. "Three-Dimensional Cell Culture Systems and Their Applications in Drug Discovery and Cell-Based Biosensors." *Assay and Drug Development Technologies* 12(4): 207–18.

Eglen, Richard M., and Terry Reisine. 2019. "Human IPS Cell-Derived Patient Tissues and 3D Cell Culture Part 2: Spheroids, Organoids, and Disease Modeling." *SLAS TECHNOLOGY: Translating Life Sciences Innovation* 24(1): 18–27. http://journals.sagepub.com/doi/10.1177/2472630318803275 (May 12, 2020).

Ermis, Menekse, Ezgi Antmen, and Vasif Hasirci. 2018. "Micro and Nanofabrication Methods to Control Cell-Substrate Interactions and Cell Behavior: A Review from the Tissue Engineering Perspective." *Bioactive Materials* 3(3): 355–69.

Fang, Xiaohui et al. 2006. "Contribution of CFTR to Apical-Basolateral Fluid Transport in Cultured Human Alveolar Epithelial Type II Cells." *American Journal of Physiology - Lung Cellular and Molecular Physiology* 290(2).

Fang, Ye, and Richard M. Eglen. 2017. "Three-Dimensional Cell Cultures in Drug Discovery and Development." *SLAS Discovery* 22(5): 456–72.

Fletcher, Daniel A., and R. Dyche Mullins. 2010. "Cell Mechanics and the Cytoskeleton." *Nature* 463(7280): 485–92.

Friedl, Peter, and Katarina Wolf. 2010. "Plasticity of Cell Migration: A Multiscale Tuning Model." *Journal of Cell Biology* 188(1): 11–19.

Fuchs, Sabine et al. 2003. "Differentiation of Human Alveolar Epithelial Cells in Primary Culture: Morphological Characterization and Synthesis of Caveolin-1 and Surfactant Protein-C." *Cell and Tissue Research* 311(1): 31–45.

Fukuhara, Shigetomo et al. 2005. "Cyclic AMP Potentiates Vascular Endothelial Cadherin-Mediated Cell-Cell Contact To Enhance Endothelial Barrier Function through an Epac-Rap1 Signaling Pathway." *Molecular and Cellular Biology* 25(1): 136–46.

Gardi, C. et al. 2015. "Quercetin Reduced Inflammation and Increased Antioxidant Defense in Rat Adjuvant Arthritis." *Archives of Biochemistry and Biophysics* 583: 150–57.

Gautrot, Julien E. et al. 2012. "Mimicking Normal Tissue Architecture and Perturbation in Cancer with Engineered Micro-Epidermis." *Biomaterials* 33(21): 5221–29.

Geckil, Hikmet et al. 2010. "Engineering Hydrogels as Extracellular Matrix Mimics." *Nanomedicine* 5(3): 469–84. http://www.ncbi.nlm.nih.gov/pubmed/20394538%0Ahttp://www.pubmedcentral.nih.gov/articlerender.fcgi?artid=PMC2892416 (May 12, 2020).

Ghaedi, Mahboobe et al. 2013. "Human IPS Cell-Derived Alveolar Epithelium Repopulates Lung Extracellular Matrix." *Journal of Clinical Investigation* 123(11): 4950–62.

Ghaemmaghami, Amir M. et al. 2012. "Biomimetic Tissues on a Chip for Drug Discovery." *Drug Discovery Today* 17(3–4): 173–81.

Gillis, Paul et al. 1999. "Keratinocyte Growth Factor Induces Angiogenesis and Protects Endothelial Barrier Function." *Journal of Cell Science* 112(12): 2049–57.

Godoy, Patricio et al. 2013. "Recent Advances in 2D and 3D in Vitro Systems Using Primary Hepatocytes, Alternative Hepatocyte Sources and Non-Parenchymal Liver Cells and Their Use in Investigating Mechanisms of Hepatotoxicity, Cell Signaling and ADME." *Archives of Toxicology* 87(8): 1315–1530. http://link.springer.com/10.1007/s00204-013-1078-5 (May 14, 2020).

Goers, Lisa, Paul Freemont, and Karen M. Polizzi. 2014. "Co-Culture Systems and Technologies: Taking Synthetic Biology to the next Level." *Journal of the Royal Society Interface* 11(96).

Golchin, Solmaz A., James Stratford, Richard J. Curry, and Johnjoe McFadden. 2012. "A Microfluidic System for Long-Term Time-Lapse Microscopy Studies of Mycobacteria." *Tuberculosis* 92(6): 489–96.

Gong, Xiangyu, and Kristen L. Mills. 2018. "Large-Scale Patterning of Single Cells and Cell Clusters in Hydrogels." *Scientific Reports* 8(1).

Gonzales, Linda W. et al. 2002. "Differentiation of Human Pulmonary Type II Cells in Vitro by Glucocorticoid plus CAMP." *American Journal of Physiology - Lung Cellular and Molecular Physiology* 283(5 27-5).

Gonzalez, Robert F. et al. 2010. "HTII-280, a Biomarker Specific to the Apical Plasma Membrane of Human Lung Alveolar Type II Cells." *Journal of Histochemistry and Cytochemistry* 58(10): 891–901.

Gori, Manuele et al. 2016. "Investigating Nonalcoholic Fatty Liver Disease in a Liver-on-a-Chip Microfluidic Device" ed. Jordi Gracia-Sancho. *PLOS ONE* 11(7): e0159729. https://dx.plos.org/10.1371/journal.pone.0159729 (May 14, 2020).

de Graaf, Inge A.M., Geny M.M. Groothuis, and Peter Olinga. 2007a. "Precision-Cut Tissue Slices as a Tool to Predict Metabolism of Novel Drugs." *Expert Opinion on Drug Metabolism and Toxicology* 3(6): 879–98.

———. 2007b. "Precision-Cut Tissue Slices as a Tool to Predict Metabolism of Novel Drugs." *Expert Opinion on Drug Metabolism and Toxicology* 3(6): 879–98.

De Graaf, R. O.N., Margreet Ten Have, and Saskia Van Dorsselaer. 2010. "The Netherlands Mental Health Survey and Incidence Study-2 (NEMESIS-2): Design and Methods." *International Journal of Methods in Psychiatric Research* 19(3): 125–41. http://www.ncbi.nlm.nih.gov/pubmed/20641046 (May 11, 2020).

Granato, Giuseppina et al. 2017. "Generation and Analysis of Spheroids from Human Primary Skin Myofibroblasts: An Experimental System to Study Myofibroblasts Deactivation." *Cell Death Discovery* 3(1): 1–10.

Griffin, M. et al. 1993. "Alveolar Type II Cell-Fibroblast Interactions, Synthesis and Secretion of Surfactant and Type I Collagen." *Journal of Cell Science* 105(2): 423–32.

Al Habyan, Sara, Christina Kalos, Joseph Szymborski, and Luke McCaffrey. 2018. "Multicellular Detachment Generates Metastatic Spheroids during Intra-Abdominal Dissemination in Epithelial Ovarian Cancer." *Oncogene* 37(37): 5127–35.

Halldorsson, Skarphedinn, Edinson Lucumi, Rafael Gómez-Sjöberg, and Ronan M.T. Fleming. 2015. "Advantages and Challenges of Microfluidic Cell Culture in Polydimethylsiloxane Devices." *Biosensors and Bioelectronics* 63: 218–31.

Han, Seung Hye, and Rama K. Mallampalli. 2015. "The Role of Surfactant in Lung Disease and Host Defense against Pulmonary Infections." *Annals of the American Thoracic Society* 12(5): 765–74.

He, Shijie et al. 2015. "Dissecting Collective Cell Behavior in Polarization and Alignment on Micropatterned Substrates." *Biophysical Journal* 109(3): 489–500.

Hegab, Ahmed E. et al. 2015. "Mimicking the Niche of Lung Epithelial Stem Cells and Characterization of Several Effectors of Their in Vitro Behavior." *Stem Cell Research* 15(1): 109–21.

Hermanns, Maria Iris et al. 2004. "Lung Epithelial Cell Lines in Coculture with Human Pulmonary Microvascular Endothelial Cells: Development of an Alveolo-Capillary Barrier in Vitro." *Laboratory Investigation* 84(6): 736–52.

Hsiao, Cheston, and Sean P. Palecek. 2012. "Microwell Regulation of Pluripotent Stem Cell Self-Renewal and Differentiation." *BioNanoScience* 2(4): 266–76.

Huang, Wenjing, Naoya Sakamoto, Ryotaro Miyazawa, and Masaaki Sato. 2012. "Role of Paxillin in the Early Phase of Orientation of the Vascular Endothelial Cells Exposed to Cyclic Stretching." *Biochemical and Biophysical Research Communications* 418(4): 708–13.

Huber, Deborah et al. 2018. "Hydrodynamics in Cell Studies." *Chemical Reviews* 118(4): 2042–79.

Hughes, J. P., S. S. Rees, S. B. Kalindjian, and K. L. Philpott. 2011. "Principles of Early Drug Discovery." *British Journal of Pharmacology* 162(6): 1239–49.

Huh, Dongeun et al. 2010. "Reconstituting Organ-Level Lung Functions on a Chip." *Science* 328(5986): 1662–68.

———. 2012. "Microengineered Physiological Biomimicry: Organs-on-Chips." *Lab on a Chip* 12(12): 2156–64.

———. 2013. "Microfabrication of Human Organs-on-Chips." *Nature Protocols* 8(11): 2135–57.

———. 2015. “A Human Breathing Lung-on-a-Chip.” In *Annals of the American Thoracic Society*, American Thoracic Society, S42–44.

Huh, Dongeun, Geraldine A. Hamilton, and Donald E. Ingber. 2011. “From 3D Cell Culture to Organs-on-Chips.” *Trends in Cell Biology* 21(12): 745–54.

Hui, Elliot E., and Sangeeta N. Bhatia. 2007. “Microscale Control of Cell Contact and Spacing via Three-Component Surface Patterning.” *Langmuir* 23(8): 4103–7.

Ingber, Donald E. 2003. “Tensegrity II. How Structural Networks Influence Cellular Information Processing Networks.” *Journal of Cell Science* 116(8): 1397–1408.

Jacob, Anjali et al. 2017. “Differentiation of Human Pluripotent Stem Cells into Functional Lung Alveolar Epithelial Cells.” *Cell Stem Cell* 21(4): 472-488.e10.

Jain, A. et al. 2018. “Primary Human Lung Alveolus-on-a-Chip Model of Intravascular Thrombosis for Assessment of Therapeutics.” *Clinical Pharmacology and Therapeutics* 103(2): 332–40.

Jastrzebska, Elzbieta et al. 2018. “Biological Characterization of the Modified Poly(Dimethylsiloxane) Surfaces Based on Cell Attachment and Toxicity Assays.” *Biomicrofluidics* 12(4).

Jean-Pierre Gillet, Sudhir Varma, and Michael M. Gottesmancorresponding author. 2013. “The Clinical Relevance of Cancer Cell Lines.” *Journal of National Cancer Institute*: 105(7): 452–458. https://www.ncbi.nlm.nih.gov/pmc/articles/PMC3691946/ (May 14, 2020).

Jedrzejczak-Silicka, Magdalena. 2017. “History of Cell Culture.” In *New Insights into Cell Culture Technology*, InTech.

Jeppesen, Maria et al. 2017. “Short-Term Spheroid Culture of Primary Colorectal Cancer Cells as an in Vitro Model for Personalizing Cancer Medicine” ed. Min-Hsien Wu. *PLOS ONE* 12(9): e0183074. https://dx.plos.org/10.1371/journal.pone.0183074 (May 12, 2020).

Jett, J. R. 2005. “Limitations of Screening for Lung Cancer with Low-Dose Spiral Computed Tomography.” *Clinical Cancer Research* 11(13): 4988s-4992s. http://www.ncbi.nlm.nih.gov/pubmed/16000601 (February 2, 2019).

Jodat, Yasamin A. et al. 2019. “Human-Derived Organ-on-a-Chip for Personalized Drug Development.” *Current Pharmaceutical Design* 24(45): 5471–86. http://www.eurekaselect.com/170582/article (May 14, 2020).

Joshi, Ramila, Brendan Fuller, Jun Li, and Hossein Tavana. 2018. “Statistical Analysis of Multi-Dimensional, Temporal Gene Expression of Stem Cells to Elucidate Colony Size-Dependent Neural Differentiation.” *Molecular Omics* 14(2): 109–20.

Kajitani, Naoko, Ayano Satsuka, Akifumi Kawate, and Hiroyuki Sakai. 2012. “Productive Lifecycle of Human Papillomaviruses That Depends upon Squamous Epithelial Differentiation.” *Frontiers in Microbiology* 3(APR).

Kamm, Roger D. et al. 2018. “Perspective: The Promise of Multi-Cellular Engineered Living Systems.” *APL Bioengineering* 2(4): 040901.

Kane, Ravi S. et al. 1999. “Patterning Proteins and Cells Using Soft Lithography.” In *The Biomaterials: Silver Jubilee Compendium*, Elsevier Ltd, 161–74.

Kang, Eun Kyeong, and Han Suk Kim. 2017. "The Effects of Hydrogen Peroxide and Lipopolysaccharide on Rat Alveolar L2 Cells." *Experimental Lung Research* 43(8): 293–300.

Kang, Yang Jun, Eunseop Yeom, Eunseok Seo, and Sang Joon Lee. 2014. "Bubble-Free and Pulse-Free Fluid Delivery into Microfluidic Devices." *Biomicrofluidics* 8(1).

Kanter, R., M. Monshouwer, D. Meijer, and G. Groothuis. 2005. "Precision-Cut Organ Slices as a Tool to Study Toxicity and Metabolism of Xenobiotics with Special Reference to Non-Hepatic Tissues." *Current Drug Metabolism* 3(1): 39–59. http://www.ncbi.nlm.nih.gov/pubmed/11878310 (May 11, 2020).

Kapałczyńska, Marta et al. 2018. "2D and 3D Cell Cultures – a Comparison of Different Types of Cancer Cell Cultures." *Archives of Medical Science* 14(4): 910–19.

Kasai, Hidenori et al. 2005. "TGF-B1 Induces Human Alveolar Epithelial to Mesenchymal Cell Transition (EMT)." *Respiratory Research* 6(1): 56.

Katsube, Takanori, Hideo Tsuji, and Makoto Onoda. 2007. "Nitric Oxide Attenuates Hydrogen Peroxide-Induced Barrier Disruption and Protein Tyrosine Phosphorylation in Monolayers of Intestinal Epithelial Cell." *Biochimica et Biophysica Acta - Molecular Cell Research* 1773(6): 794–803.

Kaushik, Garima, Moorthy P. Ponnusamy, and Surinder K. Batra. 2018. "Concise Review: Current Status of Three-Dimensional Organoids as Preclinical Models." *Stem Cells* 36(9): 1329–40.

Kazumasa Ohashi, Sachiko Fujiwara, Kensaku Mizuno. 2017. 161 The Journal of Biochemistry *Mechanisms of Mechanical Signaling in Development and Disease*. Company of Biologists.

Khabiry, Masoud, and Nader Jalili. 2015. "A Microfluidic Platform Containing Sidewall Microgrooves for Cell Positioning and Trapping." *Nanobiomedicine* 2.

Khalili, Amelia Ahmad, and Mohd Ridzuan Ahmad. 2015. "A Review of Cell Adhesion Studies for Biomedical and Biological Applications." *International Journal of Molecular Sciences* 16(8): 18149–84.

Khan, Muzamil Majid et al. 2019. "Multiomic and Quantitative Label-Free Microscopy-Based Analysis of Ex Vivo Culture and TGFbeta1 Stimulation of Human Precision-Cut Lung Slices." *bioRxiv*: 2019.12.13.875963. http://biorxiv.org/content/early/2019/12/13/2019.12.13.875963.abstract (May 12, 2020).

Kikkawa, Y., and K. Yoneda. 1974. "The Type II Epithelial Cell of the Lung. I. Method of Isolation." *Laboratory Investigation* 30(1): 76–84.

Kim, Beum Jun, and Mingming Wu. 2012. "Microfluidics for Mammalian Cell Chemotaxis." *Annals of Biomedical Engineering* 40(6): 1316–27.

Knudsen, Lars, and Matthias Ochs. 2018. "The Micromechanics of Lung Alveoli: Structure and Function of Surfactant and Tissue Components." *Histochemistry and Cell Biology* 150(6): 661–76.

Kocgozlu, Leyla et al. 2016. "Epithelial Cell Packing Induces Distinct Modes of Cell Extrusions." *Current Biology* 26(21): 2942–50.

Kodama, Atsuko, Terry Lechler, and Elaine Fuchs. 2004. "Coordinating Cytoskeletal Tracks to Polarize Cellular Movements." *Journal of Cell Biology* 167(2): 203–7.

Komi, Yusuke et al. 2010. "Acyclic Retinoid Inhibits Angiogenesis by Suppressing the MAPK Pathway." *Laboratory Investigation* 90(1): 52–60.

Kondo, Jumpei, and Masahiro Inoue. 2019. "Application of Cancer Organoid Model for Drug Screening and Personalized Therapy." *Cells* 8(5): 470.

Kretzschmar, Kai, and Hans Clevers. 2016. "Organoids: Modeling Development and the Stem Cell Niche in a Dish." *Developmental Cell* 38(6): 590–600.

Krutty, John D., Samantha K. Schmitt, Padma Gopalan, and William L. Murphy. 2016. "Surface Functionalization and Dynamics of Polymeric Cell Culture Substrates." *Current Opinion in Biotechnology* 40: 164–69.

Kumar, Adepu Kiran, and Pranab Goswami. 2009. "Imported from Https://Www.Ncbi.Nlm.Nih.Gov/m/Pubmed/25862810/?I=47&from=src%20kinase%20tumor&filters=Review." *The Journal of Biochemistry* 145(2): 259–65.

Kunz-Schughart, Leoni A., James P. Freyer, Ferdinand Hofstaedter, and Reinhard Ebner. 2004. "The Use of 3-D Cultures for High-Throughput Screening: The Multicellular Spheroid Model." *Journal of Biomolecular Screening* 9(4): 273–85.

Lancaster, Madeline A., and Juergen A. Knoblich. 2014a. "Generation of Cerebral Organoids from Human Pluripotent Stem Cells." *Nature Protocols* 9(10): 2329–40.

———. 2014b. "Organogenesisin a Dish: Modeling Development and Disease Using Organoid Technologies." *Science* 345(6194).

Langhans, Sigrid A. 2018. "Three-Dimensional in Vitro Cell Culture Models in Drug Discovery and Drug Repositioning." *Frontiers in Pharmacology* 9(JAN).

Lee, Philip J., Paul J. Hung, and Luke P. Lee. 2007. "An Artificial Liver Sinusoid with a Microfluidic Endothelial-like Barrier for Primary Hepatocyte Culture." *Biotechnology and Bioengineering* 97(5): 1340–46. http://doi.wiley.com/10.1002/bit.21360 (May 14, 2020).

Lehnert, Dirk et al. 2004. "Cell Behaviour on Micropatterned Substrata: Limits of Extracellular Matrix Geometry for Spreading and Adhesion." *Journal of Cell Science* 117(1): 41–52.

Levitt, Jonathan M., Margaret E. McLaughlin-Drubin, Karl Münger, and Irene Georgakoudi. 2011. "Automated Biochemical, Morphological, and Organizational Assessment of Precancerous Changes from Endogenous Two-Photon Fluorescence Images." *PLoS ONE* 6(9).

Li, Lingrui et al. 2014. "Nrf2/ARE Pathway Activation, HO-1 and NQO1 Induction by Polychlorinated Biphenyl Quinone Is Associated with Reactive Oxygen Species and PI3K/AKT Signaling." *Chemico-Biological Interactions* 209(1): 56–67.

Li, Wei et al. 2014. "NeuroArray: A Universal Interface for Patterning and Interrogating Neural Circuitry with Single Cell Resolution." *Scientific Reports* 4.

Li, Xiuying et al. 2017. "Oxidative Stress Destabilizes Protein Arginine Methyltransferase 4 via Glycogen Synthase Kinase 3β to Impede Lung Epithelial Cell Migration." *American Journal of Physiology - Cell Physiology* 313(3): C285–94.

Li, Yunfeng, and Eugenia Kumacheva. 2018. "Hydrogel Microenvironments for Cancer Spheroid Growth

and Drug Screening." *Science Advances* 4(4).

Lin, Chih-Ju et al. 2016. "Direct Visualization of Functional Heterogeneity in Hepatobiliary Metabolism Using 6-CFDA as Model Compound." *Biomedical Optics Express* 7(9): 3574.

Lin, Christine, and Salman R. Khetani. 2017. "Micropatterned Co-Cultures of Human Hepatocytes and Stromal Cells for the Assessment of Drug Clearance and Drug-Drug Interactions." *Current Protocols in Toxicology* 2017: 1–23.

Lin, Francis, and Eugene C. Butcher. 2006. "T Cell Chemotaxis in a Simple Microfluidic Device." *Lab on a Chip* 6(11): 1462–69.

Lin, Xiefan, and Brian P. Helmke. 2008. "Micropatterned Structural Control Suppresses Mechanotaxis of Endothelial Cells." *Biophysical Journal* 95(6): 3066–78.

Liu, Anfei, Xiya Yu, and Shanrong Liu. 2013. "Pluripotency Transcription Factors and Cancer Stem Cells: Small Genes Make a Big Difference." *Chinese Journal of Cancer* 32(9): 483–87.

Liu, Qinmei, Yun Gao, and Xinxin Ci. 2019. "Role of Nrf2 and Its Activators in Respiratory Diseases." *Oxidative Medicine and Cellular Longevity* 2019.

Liu, Ye, Elisabeth Gill, and Yan Yan Shery Huang. 2017. "Microfluidic On-Chip Biomimicry for 3D Cell Culture: A Fit-for-Purpose Investigation from the End User Standpoint." *Future Science OA* 3(2).

Llopis-Hernández, Virginia et al. 2011. "Role of Surface Chemistry in Protein Remodeling at the Cell-Material Interface" ed. Wei-Chun Chin. *PLoS ONE* 6(5): e19610. https://dx.plos.org/10.1371/journal.pone.0019610 (May 13, 2020).

Lundquist, Stefan, and Mila Renftel. 2002. "The Use of in Vitro Cell Culture Models for Mechanistic Studies and as Permeability Screens for the Blood-Brain Barrier in the Pharmaceutical Industry - Background and Current Status in the Drug Discovery Process." *Vascular Pharmacology* 38(6): 355–64.

Lunova, Mariia et al. 2016. "Modulation of Collective Cell Behaviour by Geometrical Constraints." *Integrative Biology (United Kingdom)* 8(11): 1099–1110.

Lyons-Cohen, Miranda R., Seddon Y. Thomas, Donald N. Cook, and Hideki Nakano. 2017. "Precision-Cut Mouse Lung Slices to Visualize Live Pulmonary Dendritic Cells." *Journal of Visualized Experiments* 2017(122).

Mak, Isabella W.Y., Nathan Evaniew, and Michelle Ghert. 2014. "Lost in Translation: Animal Models and Clinical Trials in Cancer Treatment." *American Journal of Translational Research* 6(2): 114–18.

Mano, J. F. et al. 2007. "Natural Origin Biodegradable Systems in Tissue Engineering and Regenerative Medicine: Present Status and Some Moving Trends." *Journal of the Royal Society Interface* 4(17): 999–1030. http://www.ncbi.nlm.nih.gov/pubmed/17412675 (May 12, 2020).

Mao, Pu et al. 2015. "Human Alveolar Epithelial Type II Cells in Primary Culture." *Physiological Reports* 3(2).

March, Sandra et al. 2015. "Micropatterned Coculture of Primary Human Hepatocytes and Supportive Cells for the Study of Hepatotropic Pathogens." *Nature Protocols* 10(12): 2027–53.

Maritan, Sarah M., Eric Y. Lian, and Lois M. Mulligan. 2017. "An Efficient and Flexible Cell Aggregation Method for 3d Spheroid Production." *Journal of Visualized Experiments* 2017(121).

Martino, Fabiana et al. 2018. "Cellular Mechanotransduction: From Tension to Function." *Frontiers in Physiology* 9(JUL).

Maru, Yoshiaki, and Yoshitaka Hippo. 2019. "Current Status of Patient-Derived Ovarian Cancer Models." *Cells* 8(5): 505.

Mason, Robert J. et al. 2002. "Maintenance of Surfactant Protein A and D Secretion by Rat Alveolar Type II Cells in Vitro." *American Journal of Physiology - Lung Cellular and Molecular Physiology* 282(2 26-2).

Mason, Robert J., and Mary C. Williams. 1980. "Phospholipid Composition and Ultrastructure of A549 Cells and Other Cultured Pulmonary Epithelial Cells of Presumed Type II Cell Origin." *Biochimica et Biophysica Acta (BBA)/Lipids and Lipid Metabolism* 617(1): 36–50.

McCaffrey, Luke Martin, and Ian G. Macara. 2012. "Signaling Pathways in Cell Polarity." *Cold Spring Harbor Perspectives in Biology* 4(6): 1–15.

"Method of the Year 2017: Organoids." 2018. *Nature Methods* 15(1): 1.

Metzger, Ross J., Ophir D. Klein, Gail R. Martin, and Mark A. Krasnow. 2008. "The Branching Programme of Mouse Lung Development." *Nature* 453(7196): 745–50.

Meyers, Steven R., and Mark W. Grinstaff. 2012. "Biocompatible and Bioactive Surface Modifications for Prolonged in Vivo Efficacy." *Chemical Reviews* 112(3): 1615–32.

Miller, Alyssa J., and Jason R. Spence. 2017. "In Vitro Models to Study Human Lung Development, Disease and Homeostasis." *Physiology* 32(3): 246–60.

Misra, Sougat et al. 2019. "Ex Vivo Organotypic Culture System of Precision-Cut Slices of Human Pancreatic Ductal Adenocarcinoma." *Scientific Reports* 9(1): 2133–2133.

Mittal, Manish et al. 2014. "Reactive Oxygen Species in Inflammation and Tissue Injury." *Antioxidants and Redox Signaling* 20(7): 1126–67.

Mohs, Richard C., and Nigel H. Greig. 2017. "Drug Discovery and Development: Role of Basic Biological Research." *Alzheimer's and Dementia: Translational Research and Clinical Interventions* 3(4): 651–57.

Montes-Olivas, Sandra, Lucia Marucci, and Martin Homer. 2019. "Mathematical Models of Organoid Cultures." *Frontiers in Genetics* 10.

Moujaber, Ossama, and Ursula Stochaj. 2020. "The Cytoskeleton as Regulator of Cell Signaling Pathways." *Trends in Biochemical Sciences* 45(2): 96–107.

Müller, Petra, Anne Langenbach, Alexander Kaminski, and Joachim Rychly. 2013. "Modulating the Actin Cytoskeleton Affects Mechanically Induced Signal Transduction and Differentiation in Mesenchymal Stem Cells." *PLoS ONE* 8(7).

Murray, John W., Dennis Han, and Allan W. Wolkoff. 2014. "Hepatocytes Maintain Greater Fluorescent Bile Acid Accumulation and Greater Sensitivity to Drug-Induced Cell Death in Three-Dimensional

Matrix Culture." *Physiological Reports* 2(12).

Murrow, Lyndsay M., Robert J. Weber, and Zev J. Gartner. 2017. "Dissecting the Stem Cell Niche with Organoid Models: An Engineering-Based Approach." *Development (Cambridge)* 144(6): 998–1007.

Nakamura, Tetsuya, and Toshiro Sato. 2018. "Advancing Intestinal Organoid Technology Toward Regenerative Medicine." *CMGH* 5(1): 51–60.

Nakao, Yosuke, Hiroshi Kimura, Yasuyuki Sakai, and Teruo Fujii. 2011. "Bile Canaliculi Formation by Aligning Rat Primary Hepatocytes in a Microfluidic Device." *Biomicrofluidics* 5(2).

Nakayama, Karina H., Luqia Hou, and Ngan F. Huang. 2014. "Role of Extracellular Matrix Signaling Cues in Modulating Cell Fate Commitment for Cardiovascular Tissue Engineering." *Advanced Healthcare Materials* 3(5): 628–41.

Nam, Ki Hwan et al. 2015. "Biomimetic 3D Tissue Models for Advanced High-Throughput Drug Screening." *Journal of Laboratory Automation* 20(3): 201–15.

Namati, Eman, Jacqueline Thiesse, Jessica De Ryk, and Geoffrey McLennan. 2008. "Alveolar Dynamics during Respiration: Are the Pores of Kohn a Pathway to Recruitment?" *American Journal of Respiratory Cell and Molecular Biology* 38(5): 572–78.

Nardini, Cecilia. 2014. "The Ethics of Clinical Trials." *ecancermedicalscience* 8(1).

Nath, Sritama, and Gayathri R. Devi. 2016. "Three-Dimensional Culture Systems in Cancer Research: Focus on Tumor Spheroid Model." *Pharmacology and Therapeutics* 163: 94–108.

Nawroth, Janna C. et al. 2019. "Stem Cell-Based Lung-on-Chips: The Best of Both Worlds?" *Advanced Drug Delivery Reviews* 140: 12–32.

Nelson, Celeste M. 2009. "Geometric Control of Tissue Morphogenesis." *Biochimica et Biophysica Acta - Molecular Cell Research* 1793(5): 903–10.

Newman, Valerie, Robert F. Gonzalez, Michael A. Matthay, and Leland G. Dobbs. 2000. "A Novel Alveolar Type I Cell-Specific Biochemical Marker of Human Acute Lung Injury." *American Journal of Respiratory and Critical Care Medicine* 161(3 I): 990–95.

Nieman, Gary F. et al. 2017. "Physiology in Medicine: Understanding Dynamic Alveolar Physiology to Minimize Ventilator-Induced Lung Injury." *Journal of applied physiology (Bethesda, Md. : 1985)* 122(6): 1516–22.

Nighot, Meghali et al. 2017. "Lipopolysaccharide-Induced Increase in Intestinal Epithelial Tight Permeability Is Mediated by Toll-Like Receptor 4/Myeloid Differentiation Primary Response 88 (MyD88) Activation of Myosin Light Chain Kinase Expression." *American Journal of Pathology* 187(12): 2698–2710.

Nita, Małgorzata, and Andrzej Grzybowski. 2016. "The Role of the Reactive Oxygen Species and Oxidative Stress in the Pathomechanism of the Age-Related Ocular Diseases and Other Pathologies of the Anterior and Posterior Eye Segments in Adults." *Oxidative Medicine and Cellular Longevity* 2016.

Nkadi, Paul O., T. Allen Merritt, and De Ann M. Pillers. 2009. "An Overview of Pulmonary Surfactant in the Neonate: Genetics, Metabolism, and the Role of Surfactant in Health and Disease." *Molecular*

Genetics and Metabolism 97(2): 95–101.

Nova, Zuzana, Henrieta Skovierova, and Andrea Calkovska. 2019. "Alveolar-Capillary Membrane-Related Pulmonary Cells as a Target in Endotoxin-Induced Acute Lung Injury." *International Journal of Molecular Sciences* 20(4).

Novak, Richard et al. 2018. "Scalable Fabrication of Stretchable, Dual Channel, Microfluidic Organ Chips." *Journal of visualized experiments : JoVE* (140): e58151.

Obatomi, D K et al. 1998. "Optimizing Preincubation Conditions for Precision-Cut Rat Kidney and Liver Tissue Slices: Effect of Culture Media and Antioxidants." *Toxicology in vitro : an international journal published in association with BIBRA* 12(6): 725–37. http://www.ncbi.nlm.nih.gov/pubmed/20654462 (May 12, 2020).

Oh, Ji Won et al. 2013. "Organotypic Skin Culture." *Journal of Investigative Dermatology* 133(11): 1–4. http://www.ncbi.nlm.nih.gov/pubmed/24129782 (May 12, 2020).

Olsen, Colin E. et al. 2005. "Extracellular Matrix-Driven Alveolar Epithelial Cell Differentiation in Vitro." *Experimental Lung Research* 31(5): 461–82.

OpenStax. 2013a. "22.1 Organs and Structures of the Respiratory System."

———. 2013b. "22.3 The Process of Breathing."

Overman, Michael J. et al. 2013. "Use of Research Biopsies in Clinical Trials: Are Risks and Benefits Adequately Discussed?" *Journal of Clinical Oncology* 31(1): 17–22.

Paguirigan, Amy L., and David J. Beebe. 2008. "Microfluidics Meet Cell Biology: Bridging the Gap by Validation and Application of Microscale Techniques for Cell Biological Assays." *BioEssays* 30(9): 811–21.

Papaioannou, Theodoros G., and Christodoulos Stefanadis. 2005. "Vascular Wall Shear Stress: Basic Principles and Methods." *Hellenic Journal of Cardiology* 46(1): 9–15.

Paz, Ana C. et al. 2014. "Challenges and Opportunities for Tissue-Engineering Polarized Epithelium." *Tissue Engineering Part B: Reviews* 20(1): 56–72. https://www.liebertpub.com/doi/10.1089/ten.teb.2013.0144 (May 13, 2020).

Paz, Ana C., Sahar Javaherian, and Alison P. McGuigan. 2011. "Tools for Micropatterning Epithelial Cells into Microcolonies on Transwell Filter Substrates." *Lab on a Chip* 11(20): 3440–48.

Petrini, Carlo. 2012. "Ethical and Legal Considerations Regarding the Ownership and Commercial Use of Human Biological Materials and Their Derivatives." *Journal of Blood Medicine* 3: 87.

Polacheck, William J., Ran Li, Sebastien G.M. Uzel, and Roger D. Kamm. 2013. "Microfluidic Platforms for Mechanobiology." *Lab on a Chip* 13(12): 2252–67.

Pompili, Luca et al. 2016. "Patient-Derived Xenografts: A Relevant Preclinical Model for Drug Development." *Journal of Experimental and Clinical Cancer Research* 35(1).

Poncin-Epaillard, Fabienne et al. 2012. "Surface Treatment of Polymeric Materials Controlling the Adhesion of Biomolecules." *Journal of Functional Biomaterials* 3(3): 528–43.

Poosti, Fariba et al. 2015. "Precision-Cut Kidney Slices (PCKS) to Study Development of Renal Fibrosis

and Efficacy of Drug Targeting Ex Vivo." *DMM Disease Models and Mechanisms* 8(10): 1227–36.

Posa, Francesca et al. 2019. "Copresentation of BMP-6 and RGD Ligands Enhances Cell Adhesion and BMP-Mediated Signaling." *Cells* 8(12): 1646.

Punet, Xavier et al. 2015. "Biomolecular Functionalization for Enhanced Cell–Material Interactions of Poly(Methyl Methacrylate) Surfaces." *Regenerative Biomaterials* 2(3): 167.

Raey, W. S., W. Hertl, E. D. Nowlan, and N. J. Binkowski. 1984. "Surface Treatments and Cell Attachment." *In Vitro: Journal of the Tissue Culture Association* 20(10): 802–8. http://www.ncbi.nlm.nih.gov/pubmed/6519665 (May 11, 2020).

Rahman, Irfan, and I. M. Adcock. 2006. "Oxidative Stress and Redox Regulation of Lung Inflammation in COPD." *European Respiratory Journal* 28(1): 219–42.

Rao, Radhakrishna. 2008. "Oxidative Stress-Induced Disruption of Epithelial and Endothelial Tight Junctions." *Frontiers in Bioscience* 13(18): 7210–26.

"Regulatory Framework for Drugs for Rare Diseases - Rare Diseases and Orphan Products - NCBI Bookshelf." https://www.ncbi.nlm.nih.gov/books/NBK56185/ (May 10, 2020).

Reid, L M, and M Rojkind. 1979. "New Techniques for Culturing Differentiated Cells: Reconstituted Basement Membrane Rafts." *Methods in enzymology* 58: 263–78. http://www.ncbi.nlm.nih.gov/pubmed/423766 (May 11, 2020).

Ren, Hui, Nigel P. Birch, and Vinod Suresh. 2016. "An Optimised Human Cell Culture Model for Alveolar Epithelial Transport." *PLoS ONE* 11(10).

Resh, Vincent H., and Ring T. Cardé. 2009. *Encyclopedia of Insects*. Elsevier/Academic Press.

Rheinwatd, James G., and Howard Green. 1975. "Seria Cultivation of Strains of Human Epidemal Keratinocytes: The Formation Keratinizin Colonies from Single Cell Is." *Cell* 6(3): 331–43.

Rhim, Andrew D., and Anil K. Rustgi. 2015. "Three-Dimensional Organotypic Culture of Stratified Epithelia." *Cold Spring Harbor Protocols* 2015(4): 349–53.

Rico, Félix et al. 2005. "Probing Mechanical Properties of Living Cells by Atomic Force Microscopy with Blunted Pyramidal Cantilever Tips." *Physical Review E - Statistical, Nonlinear, and Soft Matter Physics* 72(2).

Ridsdale, Ross, and Martin Post. 2004. "Surfactant Lipid Synthesis and Lamellar Body Formation in Glycogen-Laden Type II Cells." *American Journal of Physiology - Lung Cellular and Molecular Physiology* 287(4 31-4).

Rijal, Girdhari, and Weimin Li. 2018. "Native-Mimicking in Vitro Microenvironment: An Elusive and Seductive Future for Tumor Modeling and Tissue Engineering." *Journal of Biological Engineering* 12(1): 1–22.

Roach, L. Spencer, Helen Song, and Rustem F. Ismagilov. 2005. "Controlling Nonspecific Protein Adsorption in a Plug-Based Microfluidic System by Controlling Interfacial Chemistry Using Fluorous-Phase Surfactants." *Analytical Chemistry* 77(3): 785–96.

Rojo, Ana I. et al. 2014. "The PTEN/NRF2 Axis Promotes Human Carcinogenesis." *Antioxidants and*

Redox Signaling 21(18): 2498–2514.

Rooke, Jenny. 2013. "Synthetic Biology as a Source of Global Health Innovation." *Systems and Synthetic Biology* 7(3): 67–72.

Ruigrok, Mitchel J.R. et al. 2019. "The Effects of Oxygen Concentration on Cell Death, Anti-Oxidant Transcription, Acute Inflammation, and Cell Proliferation in Precision-Cut Lung Slices." *Scientific Reports* 9(1): 1–13.

Rutty, C. J. 1996. "The Middle-Class Plague: Epidemic Polio and the Canadian State, 1936-37." *Canadian bulletin of medical history = Bulletin canadien d'histoire de la médecine* 13(2): 277–314.

Saito, Akira, Masafumi Horie, and Takahide Nagase. 2018. "TGF-β Signaling in Lung Health and Disease." *International Journal of Molecular Sciences* 19(8).

Salam, Nasseem et al. 2018. "Assessment of Migration of Human Mscs through Fibrin Hydrogels as a Tool for Formulation Optimisation." *Materials* 11(9).

Salas, Ana et al. 2020. "Organotypic Culture as a Research and Preclinical Model to Study Uterine Leiomyomas." *Scientific Reports* 10(1): 1–12.

Sato, Toshiro et al. 2009. "Single Lgr5 Stem Cells Build Crypt-Villus Structures in Vitro without a Mesenchymal Niche." *Nature* 459(7244): 262–65.

Satyada, Tim Sandle and Ravikrishna. 2016. "Determination of the Cleaning Efficiency for Glassware in the Pharmaceutical Microbiology Laboratory." *European Journal of Parenteral and Pharmaceutical Sciences*: 21(1):16-22. https://www.researchgate.net/publication/301626790_Determination_of_the_cleaning_efficiency_for_glassware_in_the_pharmaceutical_microbiology_laboratory (May 11, 2020).

Schlaepfer, David D., Christof R. Hauck, and David J. Sieg. 1999. "Signaling through Focal Adhesion Kinase." *Progress in Biophysics and Molecular Biology* 71(3–4): 435–78.

Schumacher, Karl et al. 2007. "Perfusion Culture Improves the Maintenance of Cultured Liver Tissue Slices." In *Tissue Engineering*, , 197–205. http://www.liebertonline.com/doi/abs/10.1089/ten.2006.0046 (May 12, 2020).

Sekiguchi, Rei, and Kenneth M. Yamada. 2018. "Basement Membranes in Development and Disease." In *Current Topics in Developmental Biology*, Academic Press Inc., 143–91.

Seyhan, Attila A. 2019. "Lost in Translation: The Valley of Death across Preclinical and Clinical Divide – Identification of Problems and Overcoming Obstacles." *Translational Medicine Communications* 4(1): 1–19.

Sgalla, Giacomo et al. 2018. "Idiopathic Pulmonary Fibrosis: Pathogenesis and Management." *Respiratory Research* 19(1).

Shachar, Michal et al. 2011. "The Effect of Immobilized RGD Peptide in Alginate Scaffolds on Cardiac Tissue Engineering." *Acta Biomaterialia* 7(1): 152–62.

Shakeri, Amid et al. 2019. "Plasma-Induced Covalent Immobilization and Patterning of Bioactive Species in Microfluidic Devices." *Lab on a Chip* 19(18): 3104–15.

Shamir, Eliah R., and Andrew J. Ewald. 2014. "Three-Dimensional Organotypic Culture: Experimental Models of Mammalian Biology and Disease." *Nature Reviews Molecular Cell Biology* 15(10): 647–64.

Shanks, Niall, Ray Greek, and Jean Greek. 2009. "Are Animal Models Predictive for Humans?" *Philosophy, Ethics, and Humanities in Medicine* 4(1): 2.

Shannon, J. M. et al. 2001. "Lung Fibroblasts Improve Differentiation of Rat Type II Cells in Primary Culture." *American Journal of Respiratory Cell and Molecular Biology* 24(3): 235–44.

Shen, Colette J., Jianping Fu, and Christopher S. Chen. 2008. "Patterning Cell and Tissue Function." *Cellular and Molecular Bioengineering* 1(1): 15–23.

Silveyra, Patricia et al. 2014. "Knockdown of Drosha in Human Alveolar Type II Cells Alters Expression of SP-A in Culture: A Pilot Study." *Experimental Lung Research* 40(7): 354–66. http://www.tandfonline.com/doi/full/10.3109/01902148.2014.929757 (May 16, 2020).

Singh, Vijay Pal et al. 2016. "Critical Evaluation of Challenges and Future Use of Animals in Experimentation for Biomedical Research." *International Journal of Immunopathology and Pharmacology* 29(4): 551–61.

Soda, H, H Tomita, S Kohno, and M Oka. 1993. "Limitation of Annual Screening Chest Radiography for the Diagnosis of Lung Cancer. A Retrospective Study." *Cancer* 72(8): 2341–46. http://www.ncbi.nlm.nih.gov/pubmed/8402447 (February 2, 2019).

Solouk, Atefeh, Brian G. Cousins, Hamid Mirzadeh, and Alexander M. Seifalian. 2011. "Application of Plasma Surface Modification Techniques to Improve Hemocompatibility of Vascular Grafts: A Review." *Biotechnology and Applied Biochemistry* 58(5): 311–27. http://doi.wiley.com/10.1002/bab.50 (May 13, 2020).

Sood, Disha et al. 2019. "3D Extracellular Matrix Microenvironment in Bioengineered Tissue Models of Primary Pediatric and Adult Brain Tumors." *Nature Communications* 10(1).

Sosa-Hernández, Juan Eduardo et al. 2018. "Organs-on-a-Chip Module: A Review from the Development and Applications Perspective." *Micromachines* 9(10).

Standiford, Theodore J. et al. 1990. "Interleukin-8 Gene Expression by a Pulmonary Epithelial Cell Line: A Model for Cytokine Networks in the Lung." *Journal of Clinical Investigation* 86(6): 1945–53.

Staurengo-Ferrari, Larissa et al. 2019. "Contribution of Nrf2 Modulation to the Mechanism of Action of Analgesic and Anti-Inflammatory Drugs in Pre-Clinical and Clinical Stages." *Frontiers in Pharmacology* 9(JAN).

Stephens, Matthew, and Pierre Yves von der Weid. 2019. "Lipopolysaccharides Modulate Intestinal Epithelial Permeability and Inflammation in a Species-Specific Manner." *Gut Microbes*.

Storch, Katja et al. 2010. "Three-Dimensional Cell Growth Confers Radioresistance by Chromatin Density Modification." *Cancer Research* 70(10): 3925–34. http://www.ncbi.nlm.nih.gov/pubmed/20442295 (May 12, 2020).

Straley, Karin. 2009. "Design and Adsorption of Modular Engineered Proteins to Prepare Customized, Neuron-Compatible Coatings." *Frontiers in Neuroengineering* 2(JUN): 9. http://journal.frontiersin.org/article/10.3389/neuro.16.009.2009/abstract (May 13, 2020).

Sucre, Jennifer M.S. et al. 2018. "Successful Establishment of Primary Type II Alveolar Epithelium with 3D Organotypic Coculture." *American Journal of Respiratory Cell and Molecular Biology* 59(2): 158–66.

Sumpio, Bauer E., Albert J. Banes, G. William Link, and Toshiaki Iba. 1990. "Modulation of Endothelial Cell Phenotype by Cyclic Stretch: Inhibition of Collagen Production." *Journal of Surgical Research* 48(5): 415–20.

Tallawi, Marwa et al. 2015. "Strategies for the Chemical and Biological Functionalization of Scaffolds for Cardiac Tissue Engineering: A Review." *Journal of the Royal Society Interface* 12(108).

Tanjore, Harikrishna et al. 2009. "Contribution of Epithelial-Derived Fibroblasts to Bleomycin-Induced Lung Fibrosis." *American Journal of Respiratory and Critical Care Medicine* 180(7): 657–65.

Tellez-Gabriel, Marta et al. 2019. "Circulating Tumor Cell-Derived Pre-Clinical Models for Personalized Medicine." *Cancers* 11(1).

Teran, Madelane, and Matthew A. Nugent. 2015a. "Synergistic Binding of Vascular Endothelial Growth Factor-a and Its Receptors to Heparin Selectively Modulates Complex Affinity." *Journal of Biological Chemistry* 290(26): 16451–62.

———. 2015b. "Synergistic Binding of Vascular Endothelial Growth Factor-A and Its Receptors to Heparin Selectively Modulates Complex Affinity." *Journal of Biological Chemistry* 290(26): 16451–62. http://www.jbc.org/lookup/doi/10.1074/jbc.M114.627372 (May 17, 2020).

Tezel, Tongalp H., Lijun Geng, Henry J. Kaplan, and Lucian V. Del Priore. 2006. "Retinal Pigment Epithelium Rescues Vascular Endothelium from Retinoic Acid-Induced Apoptosis." *Investigative Ophthalmology and Visual Science* 47(11): 5075–87.

Théry, Manuel et al. 2006. "Cell Distribution of Stress Fibres in Response to the Geometry of the Adhesive Environment." *Cell Motility and the Cytoskeleton* 63(6): 341–55. http://doi.wiley.com/10.1002/cm.20126 (May 12, 2020).

———. 2010. "Micropatterning as a Tool to Decipher Cell Morphogenesis and Functions." *Journal of Cell Science* 123(24): 4201–13.

Tibbitt, Mark W., and Kristi S. Anseth. 2009. "Hydrogels as Extracellular Matrix Mimics for 3D Cell Culture." *Biotechnology and Bioengineering* 103(4): 655–63.

Tsai, Chin Hsiung, and Po Ling Kuo. 2013. "Microfluidic Device with Dual Mechanical Cues for Cell Migration Investigation." In *Proceedings of the Annual International Conference of the IEEE Engineering in Medicine and Biology Society, EMBS*, Conf Proc IEEE Eng Med Biol Soc, 842–45.

Tsunenaga, Makoto et al. 1994. "Growth and Differentiation Properties of Normal and Transformed Human Keratinocytes in Organotypic Culture." *Japanese Journal of Cancer Research* 85(3): 238–44.

Ulich, Thomas R. et al. 1994. "Keratinocyte Growth Factor Is a Growth Factor for Type II Pneumocytes in Vivo." *Journal of Clinical Investigation* 93(3): 1298–1306.

Varone, Antonio et al. 2014. "Endogenous Two-Photon Fluorescence Imaging Elucidates Metabolic Changes Related to Enhanced Glycolysis and Glutamine Consumption in Precancerous Epithelial Tissues." *Cancer Research* 74(11): 3067–75.

Velve-Casquillas, Guilhem, Maël Le Berre, Matthieu Piel, and Phong T. Tran. 2010. "Microfluidic Tools for Cell Biological Research." *Nano Today* 5(1): 28–47.

Verheijen, Bert M. 2019. "Modeling Brain Somatic Mosaicism With Cerebral Organoids, Including a Note on Mutant Microglia." *Frontiers in Molecular Neuroscience* 12.

Vining, Kyle H., and David J. Mooney. 2017. "Mechanical Forces Direct Stem Cell Behaviour in Development and Regeneration." *Nature Reviews Molecular Cell Biology* 18(12): 728–42.

Vogt, Angela Katrin et al. 2004. "Impact of Micropatterned Surfaces on Neuronal Polarity." *Journal of Neuroscience Methods* 134(2): 191–98.

Wan, Hao, and Heyu Yin. 2018. "Tunable and Quantitative Serial Dilution on Multi-Channel Miniaturized Microfluidic Electrochemical Platform." *Sensors and Actuators, B: Chemical* 274: 682–88.

Wang, Jieru et al. 2007a. "Differentiated Human Alveolar Epithelial Cells and Reversibility of Their Phenotype in Vitro." *American Journal of Respiratory Cell and Molecular Biology* 36(6): 661–68.

———. 2007b. "Differentiated Human Alveolar Epithelial Cells and Reversibility of Their Phenotype in Vitro." *American Journal of Respiratory Cell and Molecular Biology* 36(6): 661–68.

———. 2009. "Differentiated Human Alveolar Type II Cells Secrete Antiviral IL-29 (IFN-Λ1) in Response to Influenza A Infection." *The Journal of Immunology* 182(3): 1296–1304.

Wang, Shuo et al. 2019. "Micro-/Nano-Scales Direct Cell Behavior on Biomaterial Surfaces." *Molecules* 24(1).

Wang, Xinlong et al. 2016. "Discriminating the Independent Influence of Cell Adhesion and Spreading Area on Stem Cell Fate Determination Using Micropatterned Surfaces." *Scientific Reports* 6(1): 1–13.

WARD, H. E., and T. E. NICHOLAS. 1984. "ALVEOLAR TYPE I AND TYPE II CELLS." *Australian and New Zealand Journal of Medicine* 14: 731–34. http://doi.wiley.com/10.1111/j.1445-5994.1984.tb04343.x (May 14, 2020).

Warrick, Jay W., William L. Murphy, and David J. Beebe. 2008. "Screening the Cellular Microenvironment: A Role for Microfluidics." *IEEE Reviews in Biomedical Engineering* 1(1): 75–93.

Waters, Christopher M., Esra Roan, and Daniel Navajas. 2012a. "Mechanobiology in Lung Epithelial Cells: Measurements, Perturbations, and Responses." *Comprehensive Physiology* 2(1): 1–29.

Waters, Christopher M, Esra Roan, and Daniel Navajas. 2012b. "Mechanobiology in Lung Epithelial Cells: Measurements, Perturbations, and Responses." *Comprehensive Physiology* 2(1): 1–29. http://www.ncbi.nlm.nih.gov/pubmed/23728969 (February 2, 2019).

Weaver, Timothy E., Cheng Lun Na, and Mildred Stahlman. 2002. "Biogenesis of Lamellar Bodies, Lysosome-Related Organelles Involved in Storage and Secretion of Pulmonary Surfactant." *Seminars in Cell and Developmental Biology* 13(4): 263–70.

Wei, Peng et al. 2019. "Transforming Growth Factor (TGF)-B1-Induced MiR-133a Inhibits Myofibroblast Differentiation and Pulmonary Fibrosis." *Cell Death and Disease* 10(9): 1–17.

Welf, Erik S., and Jason M. Haugh. 2011. "Signaling Pathways That Control Cell Migration: Models and Analysis." *Wiley Interdisciplinary Reviews: Systems Biology and Medicine* 3(2): 231–40.

White, Eric S. 2015. "Lung Extracellular Matrix and Fibroblast Function." In *Annals of the American Thoracic Society*, American Thoracic Society, S30–33.

Wijeratne, Subhashinee S.K., Susan L. Cuppett, and Vicky Schlegel. 2005. "Hydrogen Peroxide Induced Oxidative Stress Damage and Antioxidant Enzyme Response in Caco-2 Human Colon Cells." *Journal of Agricultural and Food Chemistry* 53(22): 8768–74.

Wong, Tzyy-Yue et al. 2019. "Closer to Nature Through Dynamic Culture Systems." *Cells* 8(9): 942.

Wu, J. et al. 2018. "Characterization of Air-Liquid Interface Culture of A549 Alveolar Epithelial Cells." *Brazilian Journal of Medical and Biological Research* 51(2).

Wu, Qirui et al. 2020. "Organ-on-a-Chip: Recent Breakthroughs and Future Prospects." *BioMedical Engineering Online* 19(1): 1–19.

Wu, Xia et al. 2018. "Precision-Cut Human Liver Slice Cultures as an Immunological Platform." *Journal of Immunological Methods* 455: 71–79.

Wu, Xiaofang et al. 2011. "Human Bronchial Epithelial Cells Differentiate to 3D Glandular Acini on Basement Membrane Matrix." *American Journal of Respiratory Cell and Molecular Biology* 44(6): 914–21. http://www.ncbi.nlm.nih.gov/pubmed/20724555 (May 12, 2020).

Xavier da Silveira dos Santos, Aline, and Prisca Liberali. 2019. "From Single Cells to Tissue Self-Organization." *FEBS Journal* 286(8): 1495–1513.

Xiao, Zhengtao, Ziwei Dai, and Jason W. Locasale. 2019. "Metabolic Landscape of the Tumor Microenvironment at Single Cell Resolution." *Nature Communications* 10(1).

Xing, Hai-Yan et al. 2015. "The Cytoprotective Effect of Hyperoside against Oxidative Stress Is Mediated by the Nrf2-ARE Signaling Pathway through GSK-3β Inactivation" ed. John Calvert. *PLOS ONE* 10(12): e0145183. https://dx.plos.org/10.1371/journal.pone.0145183 (May 14, 2020).

Yan, Yuanwei, Julie Bejoy, Mark Marzano, and Yan Li. 2019. "The Use of Pluripotent Stem Cell-Derived Organoids to Study Extracellular Matrix Development during Neural Degeneration." *Cells* 8(3): 242.

Yang, Yong, Kai Wang, Xiaosong Gu, and Kam W. Leong. 2017. "Biophysical Regulation of Cell Behavior—Cross Talk between Substrate Stiffness and Nanotopography." *Engineering* 3(1): 36–54.

Yin, Xiaolei et al. 2016. "Engineering Stem Cell Organoids." *Cell Stem Cell* 18(1): 25–38.

Yonchuk, John G. et al. 2017. "Characterization of the Potent, Selective Nrf2 Activator, 3-(Pyridin-3-Ylsulfonyl)-5-(Trifluoromethyl)-2H-Chromen-2-One, in Cellular and in Vivo Models of Pulmonary Oxidative Stress." *Journal of Pharmacology and Experimental Therapeutics* 363(1): 114–25.

Yu, Weiliang et al. 2014. "A Microfluidic-Based Multi-Shear Device for Investigating the Effects of Low Fluid-Induced Stresses on Osteoblasts." *PLoS ONE* 9(2).

Yuan, Tingting et al. 2018. "Fgf10 Signaling in Lung Development, Homeostasis, Disease, and Repair After Injury." *Frontiers in Genetics* 9.

Zemans, Rachel L., and Michael A. Matthay. 2004. "Bench-to-Bedside Review: The Role of the Alveolar Epithelium in the Resolution of Pulmonary Edema in Acute Lung Injury." *Critical Care* 8(6): 469–77. http://ccforum.biomedcentral.com/articles/10.1186/cc2906 (May 17, 2020).

Zhang, Xunli, Huabing Yin, Jon M. Cooper, and Stephen J. Haswell. 2008. "Characterization of Cellular Chemical Dynamics Using Combined Microfluidic and Raman Techniques." *Analytical and Bioanalytical Chemistry* 390(3): 833–40.

Zhao, Cunlu, Zhengwei Ge, and Chun Yang. 2017. "Microfluidic Techniques for Analytes Concentration." *Micromachines* 8(1).

Zhao, Hailin, Shiori Eguchi, Azeem Alam, and Daqing Ma. 2017. "The Role of Nuclear Factor-Erythroid 2 Related Factor 2 (Nrf-2) in the Protection against Lung Injury." *American Journal of Physiology - Lung Cellular and Molecular Physiology* 312(2): L155–62.

Zhao, Hui et al. 2019. "Sphere-forming Assay vs. Organoid Culture: Determining Long-term Stemness and the Chemoresistant Capacity of Primary Colorectal Cancer Cells." *International Journal of Oncology* 54(3): 893–904.

Zhao, Lan, Min Yee, and Michael A. O'Reilly. 2013. "Transdifferentiation of Alveolar Epithelial Type II to Type I Cells Is Controlled by Opposing TGF-β and BMP Signaling." *American Journal of Physiology - Lung Cellular and Molecular Physiology* 305(6).

Zhao, Wenjie, Haiping Zhao, Mingxiao Li, and Chengjun Huang. 2020. "Microfluidic Devices for Neutrophil Chemotaxis Studies." *Journal of Translational Medicine* 18(1).

Zheng, Xiaoyang et al. 2008. "Proteomic Analysis for the Assessment of Different Lots of Fetal Bovine Serum as a Raw Material for Cell Culture. Part IV. Application of Proteomics to the Manufacture of Biological Drugs." *Biotechnology Progress* 22(5): 1294–1300. http://doi.wiley.com/10.1021/bp060121o (May 12, 2020).

Zhou, Jinwen, Amanda Vera Ellis, and Nicolas Hans Voelcker. 2010. "Recent Developments in PDMS Surface Modification for Microfluidic Devices." *Electrophoresis* 31(1): 2–16.

Zhou, Yong et al. 2018. "Extracellular Matrix in Lung Development, Homeostasis and Disease." *Matrix Biology* 73: 77–104.

Zhu, Chenghao et al. 2018. "Increased Cardiomyocyte Alignment and Intracellular Calcium Transients Using Micropatterned and Drug-Releasing Poly(Glycerol Sebacate) Elastomers." *ACS Biomaterials Science and Engineering* 4(7): 2494–2504.

Ziyad, Safiyyah, and M. Luisa Iruela-Arispe. 2011. "Molecular Mechanisms of Tumor Angiogenesis." *Genes and Cancer* 2(12): 1085–96.

6. PUBLICATIONS

"A novel Organ-Chip system emulates three-dimensional architecture of the human epithelia and the mechanical forces acting on it."
Varone Antonio, Nguyen Ke Justin, Leng Lian, Barrile Riccardo, Sliz Josiah, Lucchesi Carolina, Wen Norman, Gravanis Achille, Hamilton A. Geraldine, Karalis Katia and Hinojosa D .Christopher
Biomaterials 2021 June 06th

A Micro-Engineered Airway Lung-Chip Models Key Features of Viral-Induced Exacerbation of Asthma
Janna C Nawroth, Carolina Lucchesi, Deion Cheng, Abhishek Shukla, Justin Ngyuen, Tanvi Shroff, **Antonio Varone**, Katia Karalis, Hyun-Hee Lee, Stephen Alves, Geraldine A Hamilton, Michael Salmon, Remi Villenave
American Journal of Respiratory Cell and Molecular Biology 2020 Jan 24th

Mapping metabolic changes by noninvasive, multiparametric, high-resolution imaging using endogenous contrast
Zhiyi Liu, Dimitra Pouli, Alonzo Carlo, **Antonio Varone**, Sevasti Karaliota, Kyle P. Quinn, Karl Münger, Katia P. Karalis, and Irene Georgakoudi
Science Advances 2018 Mar 07th.

Unraveling the origins of endogenous optical metabolic changes using a multi-parametric approach
Irene Georgakoudi, Zhiyi Liu, Dimitra Pouli, Carlo Alonzo, **Antonio Varone**, Sevasti Karaliota, Kyle P. Quinn, Karl Münger, and Katia P. Karalis
Biophotonics Congress: Biomedical Optics Congress 2018 (Microscopy/Translational/Brain/OTS), OSA Technical Digest (Optical Society of America, 2018), paper JTh1A.1.

Severe Asthma on-Chip: a novel platform enables study of viral-induced exacerbations in asthma and drug response In Vitro
Remi Villenave, Carol Lucchesi, Hyun-Hee Lee, Justin Nguyen, **Antonio Varone**, Katia Karalis, Stephen Alves, Michael Salmon, Geraldine Hamilton
European Respiratory Journal 2017 Dec 06th.

"Non-Invasive Characterization of Metabolic Drug Effects on Breast Cancer Cell Spheroids Using Two-Photon Excited Fluorescence Microscopy"
Z. Liu, E. Dhimolea, **A. Varone**, C. S. Mitsiades, and I. Georgakoudi
Optical Society of America, 2017, paper OmM4D.2.

A microfluidic lung small airway-on-a-chip enables analysis of human lung inflammation and therapeutic responses *in vitro*
Kambez H. Benam, Remi Villenave, Carolina Lucchesi, **Antonio Varone**, Cedric Hubeau, Hyun-Hee Lee, Michael Salmon, Steve Alves, Thomas C. Ferrante, James Weaver, Geraldine Hamilton, Tony Bahinski, and Donald E. Ingber
Nature Methods 2015 Dec 15th

Modeling COPD, asthma in a human small airway-on-a-chip
Remi Villenave, Kambez H. Benam, Carolina Lucchesi, **Antonio Varone**, Hyun-Hee Lee, Stephen E. Alves, Michael Salmon, Thomas C. Ferrante, James C. Weaver, Geraldine A. Hamilton, Anthony Bahinski, and Donald E. Ingber
Science Daily 2015 Dec 8th

Non-invasive assessment of mitochondrial organization in three-dimensional tissues reveals significant changes associated with cancer development
Joanna Xylas, **Antonio Varone**, Kyle P. Quinn, Margaret E. McLaughlin-Drubin, Hong-Thao Thieu, Maria L. Garcia-Moliner, Karl Münger, Irene Georgakoudi
International Journal of Cancer 2015 Jan 15th

Bioengineered Silk Gene Delivery System for Nuclear Targeting
Sezin Yigit, Olena Tokareva, **Antonio Varone**, Irene Georgakoudi, David L., Kaplan
Macromolecular Bioscience 2014 Sep 30th

Endogenous two-photon fluorescence imaging can elucidate metabolic changes related to enhanced glycolysis and glutamine consumption in epithelial tissues
Antonio Varone, Joanna Xylas, Kyle P. Quinn, Dimitra Pouli, Gautham Sridharan, Margaret E. McLaughlin-Drubin, Carlo Alonzo, Kyongbum Lee, Karl Münger, Irene Georgakoudi
Cancer Research 2014 Mar 31st

Enhanced Intracellular siRNA Delivery Using Bioreducible Lipid-like Nanoparticles
Ming Wang, Kyle Alberti, **Antonio Varone**, Dimitri Pouli, Irene Georgakoudi, Qiaobing Xu
Advanced Healthcare Materials 2014 Feb 20th

Label-free assessment of mitochondrial organization in three-dimensional tissues
Irene Georgakoudi, Dimitra Pouli, **Antonio Varone**, Joanna Xylas, Kyle Quinn, Margaret McLaughlin-Drubin, and Karl Munger
Frontiers in Optics 2014

Quantitative optical biomarkers for non-invasive detection of cancerous transformation in live, 3D squamous epithelia
Dimitra Pouli; Antonio Varone; Joanna Xylas; Kyle P. Quinn; Martin Hunter; Irene Georgakoudi; Margaret E. McLaughlin-Drubin; Karl Munger
Presented in 2014 40th Annual Northeast Bioengineering Conference (NEBEC), and published on IEEE Xplore: 2014 Dec 04th